Two-phase flow processes with dynamic effects in porous media – parameter estimation and simulation

Von der Fakultät Bau- und Umweltingenieurwissenschaften der Universität Stuttgart
zur Erlangung der Würde eines Doktors der
Ingenieurwissenschaften (Dr.-Ing.) genehmigte Abhandlung

Vorgelegt von

Sabine Manthey

aus Rheda-Wiedenbrück

Hauptberichter:	Prof. Dr.-Ing. Rainer Helmig
Mitberichter:	Prof. S. Majid Hassanizadeh, Ph.D.
Tag der mündlichen Prüfung:	17. Februar 2006

Institut für Wasserbau der Universität Stuttgart

2006

Heft 157

Two-phase flow processes with dynamic effects in porous media - parameter estimation and simulation

von
Dr.-Ing.
Sabine Manthey

Eigenverlag des Instituts für Wasserbau der Universität Stuttgart

D93 Two-phase flow processes with dynamic effects in porous media – parameter estimation and simulation

Manthey, Sabine:

Two-phase flow processes with dynamic effects in porous media – parameter estimation and simulation / von Sabine Manthey. Institut für Wasserbau, Universität Stuttgart. - Stuttgart: Inst. für Wasserbau der Univ., 2006

(Mitteilungen / Institut für Wasserbau, Universität Stuttgart ; H. 157)
Zugel.: Stuttgart, Univ., Diss., 2006
ISBN 3-9337 61-61-1
NE: Institut für Wasserbau < Stuttgart >: Mitteilungen

Herausgegeben 2006 vom Eigenverlag des Instituts für Wasserbau
Druck: Sprint-Druck, Stuttgart

Danksagung

Die vorliegende Arbeit ist zum großen Teil während meiner Tätigkeit am Institut für Wasserbau, Lehrstuhl für Hydromechanik und Hydrosystemmodellierung als wissenschaftliche Mitarbeiterin entstanden. In dieser Zeit habe ich unter anderem das Teilprojekt C des DFG-Projekt MUSKAT – MUltiSKAlenTransport bearbeitet. Diese Dissertation wäre nicht ohne die Unterstützung der folgenden Personen möglich gewesen.

Als erstes möchte ich Prof. Rainer Helmig für die Übernahme des Hauptberichts danken. Außerdem möchte ich mich für die Diskussionen, Anregungen und die Freiheiten, die ich bei der Arbeit hatte, bei ihm bedanken. Er hat es verstanden, mich auch in schwierigen Phasen meiner Dissertation immer zu motivieren.

Ein Teil der vorliegenden Arbeit ist an der TU Delft, Niederlande bei Prof. Majid Hassanizadeh entstanden. Der halbjährige Aufenthalt wurde durch ein Stipendium der TU Delft ermöglicht. Ich möchte Prof. Hassanizadeh für die Übernahme des Zweitberichts sowie für die zahlreichen und intensiven Diskussionen über dynamische Effekte danken.

Des weiteren gebührt ein besonderer Dank allen meine Kolleginnen und Kollegen am Lehrstuhl für Hydromechanik und Hydrosystemmodellierung. Die tolle Atmosphäre in der Arbeitsgruppe hat für Spaß bei der Arbeit gesorgt. Insbesondere möchte ich die fachliche Unterstützung von Andreas Bielinski, Hartmut Eichel, Insa Neuweiler, Ulrich Ölmann und Alexandros Papafotiou, der seine Masterarbeit bei mir geschrieben hat, erwähnen. Prudence Lawday möchte ich für die Korrektur des Englischen danken.

Besonders erwähnen möchte ich auch die Mitarbeiterinnen und Mitarbeiter von Prof. Hassanizadeh, vor allem Cas Berentsen, Simona Bottero und Twan Gielen, mit welchen ich viele Stunden über dynamische Effekte diskutiert habe.
An dieser Stelle möchte ich auch Prof. Helge Dahle, Universität Bergen, Norwegen für seine Anregungen und den Austausch über porenskalige Prozesse danken.

Mein besonderer Dank gilt meinen Eltern, die mich immer in allen Lebenssituationen unterstützt haben.

Wenn der Frust bei der Arbeit besonders groß war oder wenn Teilerfolge zu feiern waren, haben mir meine Freundinnen (insbesondere Katrin mit Sauna und Andrea mit Telefonaten) und meine Schwester immer beigestanden. Ein Dank geht auch an Tim und Lina, die mich immer wieder daran erinnert haben, dass es im Leben wichtigeres als die Arbeit gibt.

Zum Schluss möchte ich meinem Freund Marcus für seine Unterstützung und seine Geduld in den letzten Jahren herzlichst danken.

"Der Zweifel ist der Beginn der Wissenschaft. Wer nichts anzweifelt, prüft nichts. Wer nichts prüft, entdeckt nichts. Wer nichts entdeckt, ist blind und bleibt blind."

Teilhard de Chardin (1881-1955), frz. Theologe, Paläontologe u. Philosoph

Contents

List of Figures

List of Tables

Notation

The following table shows the symbols used in this thesis. Local notations are explained in the text.
Vectors and matrices are written in bold type.
Averaged values are marked with <>.

Symbol	Definition	Dimension
Greek Letters:		
α^{VG}	Van Genuchten, 1980 parameter	[1/Pa]
α_S	STAUFFER scaling parameter	[-]
γ	interfacial tension	[N m]
Γ	boundary	[-]
δ	KRONECKER-delta	[-]
Δt	time step	[s]
ε	residuum	[-]
ε_S	equilibrium criterion for saturation	[-]
ε_P	equilibrium criterion for pressure	[Pa]
η_i	set of all neighboring nodes of node i	[-]
θ	contact angle	[°]
θ_e	static contact angle	[°]
θ_d	dynamic contact angle	[°]
ι	MUALEM, 1976 parameter in $k_{r\alpha}(S_\alpha)$	[-]
λ	BROOKS & COREY parameter	[-]
λ_α	mobility of phase α	[m s/kg]
μ	dynamic fluid viscosity	[Pa s]
ρ	density	[kg/m^3]
τ	damping coeffeficient	[Pa s]
τ_B	coefficient after BARENBLATT	[s]
τ_*	coefficient after BOURGEAT & PANFILOV	[-]
τ_{HG}	coefficient after HASSANIZADEH & GRAY	[Pa s]
τ_K	coefficient after KALAYDJIAN	[Pa s]
τ_S	coefficient after STAUFFER	[Pa s]
ϕ	porosity	[-]
φ	subcontrol volume face	[m,m^2]

Symbol	Definition	Dimension
$\psi_{\alpha i}$	total potential of phase α at node i	[-]
ω	parameter ratio after BOURGEAT & PANFILOV	[-]
Latin Letters:		
a	interfacial area per volume	[1/m]
A	surface area	[m^2]
b_i	control volume or box for node i	[m^2,m^3]
∂_{b_i}	boundary of box b_i	[-]
e_i	set of elements connected to node i	[-]
g	vector of gravitational acceleration $(0, 0, -g)^T$	[m/s^2]
g	scalar gravitational acceleration	[m/s^2]
h	piezometric head	[m]
$\mathbf{K}$	tensor of (intrinsic) permeability	[m^2]
K	scalar intrinsic permeability	[m^2]
k	hydraulic conductivity	[m/s]
k_r	relative permeability	[-]
M	viscosity ratio μ_w/μ_n	[-]
$\mathbf{n}$	outer normal vector of ∂G	[-]
N_i	ansatz functions functions for node i	[-]
P	pressure	[Pa]
P_c	capillary pressure	[Pa]
P_d	entry pressure for the $P_c(S_w)$ relationship after BROOKS & COREY	[Pa]
q	source or sink	[1/s]
Q	volumetric flux	[m^3/s]
r	radius	[m]
s	sensitivity	
S	saturation	[-]
$S_{\alpha r}$	residual saturation of phase α	[-]
S_e	effective saturation of the wetting phase	[-]
t	time	[s]
T	temperature	[K]
$\mathbf{v}$	vector of DARCY velocity	[m/s]
v	DARCY velocity	[m/s]
v_s	seepage velocity	[m/s]
V	volume	[m^3]
$\lvert b_i \rvert$	volume for the box associated with node i	[m^3]
V_f	volume fraction	[-]
W_i	weighting function for node i	[-]

Symbol	Definition	Dimension
z	elevation head	[m]
z_i	geodetic height of node i	[m]

Subscripts:

α	phase, either wetting (w) or non-wetting (n)
β	phase, either wetting (w) or non-wetting (n)
c	characteristic quantity
f	fine
h	higher
l	lower
n	non-wetting phase (e.g. oil, gas)
p	pore
s	solid phase
w	wetting phase (e.g. water)

Superscripts:

~	approximation
d	dynamic
e	equilibrium
n	time step
B	boundary
L	lower
S	grid-volume weighted average
T	top
V	phase-volume weighted average

Abstract

The constitutive relationships applied for two-phase flow processes on the local and macroscale might be influenced by dynamic and hysteretic effects. This study contributes to the understanding of dynamic effects in the capillary pressure-saturation relationship on the local scale and macroscale as well as giving an assessment as to when these effects might need to be taken into account for the evaluation of two-phase flow processes.
In a general form, the rate-dependent $P_c(S_w)$ relationship as analysed here can be given as

$$P_n - P_w - P_c^e(S_w) = P_c^d - P_c^e(S_w) = -\tau \frac{\partial S_w}{\partial t} .$$

This extended $P_c(S_w)$ relationship is examined in this study under three aspects.
In order to identify flow regimes where dynamic effects might be of importance, a dimensional analysis of the two-phase balance equations being closed with the extended $P_c(S_w)$ relationship is carried out. In the dimensionless equations the well-known capillary and gravitational number, Ca and Gr, evolve. Moreover, the new dimensionless number Dy appears as a factor. Dy quantifies the ratio of the 'dynamic capillary force' to the viscous force. Relating Dy to Ca or Gr yields DyC, the ratio of the dynamic to the capillary equilibrium force, and DyG, the ratio of the dynamic capillary to the gravitational force. Assuming the coefficient τ as a constant, the influence of the dynamic capillary force decreases with increasing characteristic length scale in relation to the equilibrium capillary, viscous or gravitational force. Moreover, with increasing transient flow velocity, the dynamic capillary force gains in importance. On the basis of simulations, the front width of the invading phase was found to be an appropriate interpretation of the characteristic length scale.
For the interpretation of the dimensionless numbers the magnitude of the coefficient τ was assumed to be known. One part of this study deals with the determination of this coefficient on the basis of primary drainage laboratory experiments performed by GeoDelft, The Netherlands and numerical experiments. Using the laboratory experiments τ was calculated to vary between $\tau = 11.0\,\mathrm{kPa\,s}$ and $\tau = 154.7\,\mathrm{kPa\,s}$ depending on the water saturation for a sand with $K = 3.06 \cdot 10^{-12}\,\mathrm{m^2}$ and $P_d = 5587\,\mathrm{Pa}$. The coefficient increases with decreasing water saturation. A linear relation for $\tau(S_w)$ yielded satisfying results for a regression. For the determination of τ using numerical experiments first homogeneous domains were considered in order to test the averaging approach. The coefficient τ was then found to scale proportionally to the porosity, the (saturation-weighted average) viscosity, and the squared averaging length, as well as inversely proportional to the intrinsic permeability. Pa-

rameters that describe the equilibrium $P_c(S_w)$ relationship have a minor influence on the coefficient τ. The empirical formula for the coefficient τ by STAUFFER, 1978 could not be confirmed on the basis of the numerical experiments. The dependence of τ on the averaging length poses a problem as its magnitude is thus not clearly bounded, making it impossible to define an REV. As a consequence, either the averaging length should relate to a bounded property (e.g. the inverse of the distance of a characteristic pressure drop) or the averaging of the phase pressures as applied in this study has to be reconsidered. Moreover two heterogeneous domains were studied, one being a simple pattern of two fine sand lenses in a coarse sand and the other a spatially-correlated random field. An influence resulting from the simple heterogeneity pattern on the coefficient is only noticeable in case the fine sand lenses are drained. The heterogeneity stemming from the spatially-correlated random field does not affect the magnitude of the coefficient. Probably, the continuous distribution of the parameters ensures that the average behaviour dominates.
Finally, the impact on the numerical solution of the balance equations being closed with an extended $P_c(S_w)$ relationship is assessed with simulations of imbibition processes. The dimensionless numbers Dy and DyC can be consulted to assess an impact on the solution. The front width should be applied as the characteristic length scale when calculating these numbers. In the simulation of imbibition examples, it is observed that for a dominance of the dynamic capillary over the viscous force, the rate of change of saturation is dampened and thus a retardation effect with respect to the cumulative mass occurs. Locally, accelerating and slowing down of the displacement can flatten a front in comparison to a reference case. Moreover, for a high influx of wetting phase a process reversal from imbibition to drainage and back occurred. If additionally the equilibrium capillary forces are diminished, oscillations in the solution might occur for a large viscosity ratio. A sensitivity analysis has revealed that neither the integral cumulative mass nor local measures of the saturation possess a sufficient sensitivity w.r.t. the coefficient τ when compared to the other model parameters. It is therefore suggested, that for an inverse parameter identification on the basis of laboratory experiments, all parameters of the traditional two-phase flow model should be determined independently first before quantifying the coefficient on the basis of an additional experiment, which should be specifically designed for the determination of the coefficient. This procedure assumes, that neither the residual saturations nor the relative permeabilities depend on the dynamics of the flow process.

Zusammenfassung

Einleitung

Das Verständnis und die Vorhersage von Strömungsprozessen zweier mobiler Fluidphasen (Zweiphasensystem) in einem porösen Medium spielen wichtige Rollen für bestimmte Umweltfragestellungen oder technische Applikationen. In der ungesättigten Bodenzone dient die Vorhersage der Verteilungen und Durchflussmengen von Wasser und Bodenluft als Basis für die Modellierung des Transports von in Wasser gelösten Stoffen, wie z.B. der Verlagerung von Pestiziden oder Schwermetallen. Des Weiteren müssen Strömungsprozesse in der ungesättigten Zone quantifiziert werden, um die Grundwasserneubildung zu beschreiben. Neben Bodenwasser und -luft können auch Grundwasser und mit Wasser nicht mischbare Kontaminanten, wie z.B. organische Lösungsmittel, ein Zweiphasensystem im Untergrund bilden. Für die Entwicklung und Anwendung von Sanierungstechniken müssen Zweiphasenprozesse grundlegend verstanden werden. Aus den oben genannten Gründen sind Prozesse in den letzten Jahrzehnten intensiv untersucht worden, nicht nur in den Ingenieurwissenschaften, sondern auch in der Bodenphysik und der Hydrogeologie (siehe z.B. CHARBENEAU, 2000 [24]). Technische Anwendungen sind z.B. Strömungsprozesse durch Filter oder die Infiltration von Tinte in Papier (siehe MIDDENDORF, 2000 [79]). Die oben aufgezeigten Fragestellungen können durch ein Modellkonzept beschrieben werden, das in der Regel auf einem nicht deformierbaren porösen Medium und zwei inkompressiblen, nichtmischbaren Fluidphasen beruht.

Die aufgezeigten Anwendungen beziehen sich auf unterschiedliche räumliche Skalen. Die vorliegende Arbeit konzentriert sich auf einen Skalenbereich mit typischen Längen von 0.01 m bis 10 m, hier bezeichnet als lokale Skala bis Makroskala. Schon für die lokale Skala ist, beruhend auf dem REV-Konzept nach BEAR, 1972 [10], ein Mittelungsprozess über die Volumina der Fluidphasen und der Feststoffphase durchzuführen. Die Modelle zur Beschreibung von Zweiphasenprozessen basieren auf den Massen- und Impulserhaltungsgleichungen (erweitertes DARCY Gesetz) für die beiden Fluidphasen. Sie werden mit den konstitutiven Beziehungen, welche die Interaktion zwischen den Fluiden und dem porösen Medium beschreiben, komplementiert. Eine der konstitutiven Beziehungen quantifiziert das Verhältnis zwischen den Volumen-gemittelten Verteilungen der Fluide – den Sättigungen bei einer gegebenen Differenz zwischen den Phasendrücken – dem Kapillardruck. Die Bestimmung der sogenannten Kapillardruck-Sättigungsbeziehung $P_c(S_w)$ basiert traditionell auf der Annahme von Gleichgewichtsbedingungen. Diese liegen bei einer statischen Verteilung der Fluide oder stationären Strömungsprozessen vor. Verschiedene Arbeiten haben in der Vergangenheit das Verhalten der Modelle zur Beschreibung

von transienten Zweiphasenprozessen, in denen die so bestimmte $P_c(S_w)$ Funktion einging, kritisch diskutiert. In diesem Rahmen sind zwei Probleme identifiziert worden:

- Die Beziehung zwischen P_c und S_w kann unter transienten Bedingungen nicht unbedingt als eindeutig vorausgesetzt werden.
- Bestimmte transiente Prozesse können mit den traditionellen Modellen nicht reproduziert werden.

Um den Einfluss transienter Bedingungen auf die $P_c(S_w)$ Beziehung zu illustrieren, wird ein Beispiel aus der Arbeit von TOPP ET AL., 1967 [109] herangezogen. Die Autoren haben im Labor die Hauptdränagekurven für einen sandigen Boden unter quasi-statischen, stationären und transienten Bedingungen gemessen (siehe Abb. 1). Während die unter quasi-statischen oder stationären Bedingungen bestimmten $P_c(S_w)$ Beziehungen kaum voneinander abweichen, treten bei der unter transienten Bedingungen gemessenen Beziehung deutlich höhere Kapillardrücke bei einer gegebenen Sättigung auf. Ähnliche Effekte sind auch für Imbibitionsprozesse beobachtet worden. Der unter statischen oder stationären Bedingungen gemessene Kapillardruck wird im Folgenden Gleichgewichtskapillardruck P_c^e, der unter transienten Bedingungen bestimmte dynamischer Kapillardruck P_c^d genannt. Die Abhängigkeit der $P_c(S_w)$ Funktion von den Flussbedingungen wird hier als dynamischer Effekt aufgefasst. Ein Experiment zur Bestimmung von $P_c^e(S_w)$ wird als Gleichgewichtexperiment, das für die Bestimmung von $P_c^d(S_w)$ als dynamisches Experiment bezeichnet.
Der funktionale Zusammenhang zwischen Kapillardruck und Sättigung kann somit auch unter Vernachlässigung von Hystereseeffekten nicht immer als eindeutig betrachtet werden. Dies sollte bei Labormessungen von $P_c(S_w)$ Beziehungen oder bei der Anwendung der Funktion in numerischen Simulationen transienter Zweiphasenprozesse berücksichtigt werden.

In den letzten Jahrzehnten haben theoretische Arbeiten von HASSANIZADEH & GRAY, 1990 [55], HASSANIZADEH & GRAY, 1993 [56], oder KALAYDJIAN, 1987[67] sowie ein empirischer Ansatz von STAUFFER, 1978 [108] alternative Ansätze zur Behandlung der $P_c(S_w)$ Beziehung auf der lokalen Skala gezeigt. Die Autoren schlagen vor, die Differenz zwischen dem dynamischen und dem Gleichgewicht-Kapillardruck bei einer bestimmten Sättigung als linear abhängig von der Sättigungsrate aufzufassen, nach

$$P_c^d - P_c^e(S_w) = -\tau \frac{\partial S_w}{\partial t} \,. \tag{1}$$

In Glg. (1) quantifiziert die Proportionalitätskonstante τ die Steigung der linearen Beziehung. Die bisherigen Untersuchungen weisen darauf hin, dass τ von der Wassersättigung und von der Struktur des porösen Mediums abhängt. Im Folgenden wird τ allgemein als Koeffizient bezeichnet. Der dynamische Kapillardruck entspricht dem Gleichgewichtskapillardruck nach Glg. (1) nur unter statischen oder

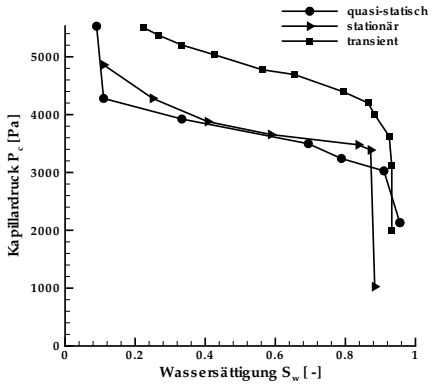

Abb. 1: Illustrierung von dynamischen Effekten in der $P_c(S_w)$ Beziehung basierend auf experimentellen Ergebnissen von TOPP ET AL., 1967 [109]

stationären Bedingungen, wenn die Ableitung der Sättigung nach der Zeit gegen Null geht. Der Ausgleich zwischen den Kapillardrücken erfolgt in Abhängigkeit der Sättigungsrate und der Größe des Koeffizienten τ. Die Funktion in Glg. (1) wird hier als erweiterte $P_c(S_w)$ Beziehung aufgefasst.
Beim Auftreten hoher Änderungsraten der Sättigung sollten demzufolge dynamische Effekte in der $P_c(S_w)$ Beziehung berücksichtigt werden. Hohe Änderungsraten der Sättigung treten z.B. bei der Infiltration von Regenwasser in einen trockenen Boden auf. NIEBER ET AL., 2005 [84] zeigen für einen derartigen Prozess, dass das Verhalten von Schwerkraft getriebenen Instabilitäten beschrieben werden kann, wenn die erweiterte $P_c(S_w)$ Beziehung anstelle der traditionellen Beziehung im Modell eingebunden wird. Des Weiteren können dynamische Effekte in porösen Medien von Bedeutung sein, die einen hohen τ-Wert besitzen. Die Größe des Koeffizienten τ in Abhängigkeit des porösen Mediums und Fluidsystems stellt eine wichtige Frage dieser Arbeit dar.
Obwohl der Einfluss transienter Strömungsbedingungen auf die $P_c(S_w)$ Funktion seit Jahrzehnten aus Laborexperimenten bekannt ist, wurden die theoretischen Arbeiten dazu erst in den letzten Jahren intensiviert. Dennoch besteht Forschungsbedarf, da es weiterhin offene Fragen bezüglich des Einflusses von dynamischen Effekten auf Zweiphasenströmungsprozesse in porösen Medien auf der lokalen Skala und Makroskala gibt:

- Die erhöhte Komplexität des Modells und die Notwendigkeit, einen zusätzlichen Parameter zu bestimmen, können nur gerechtfertigt werden, wenn Prozesse identifiziert werden können, bei denen dynamische Effekte eine signifikante Rolle spielen.

- Die empirische Formel von STAUFFER, 1978 [108] für den Koeffizienten τ, welche auf Laborexperimenten mit vier Sanden beruht, und die dimensionslo-

se Gruppierung von DAHLE ET AL., 2005 [30] basierend auf einem Kapillarbündelmodell, muss für weitere poröse Medien und Fluidsysteme sowie weitere Ansätze zur Bestimmung des Koeffizienten verifiziert werden.

- Im Rahmen einer Analyse eines 'multi-step outflow' Experiments sind Unzulänglichkeiten in den traditionellen Modellen aufgezeigt worden. Die Simulation des Experiments, basierend auf den herkömmlichen Zweiphasenmodellen und konstitutiven Beziehungen, reproduziert nicht das im Experiment beobachtete Relaxationsverhalten. Weder eine Parametervariation noch die Einbeziehung von Heterogenitäten konnten erfolgreich die experimentell gemessenen Ergebnisse wiedergeben. Die Identifikation der Einflüsse aus der erweiterten $P_c(S_w)$ Funktion auf Simulationsergebnisse stellt einen Schwerpunkt dieser Arbeit dar. Unter anderem soll festgestellt werden, ob die Berücksichtigung der erweiterten Beziehung immer in einer Verzögerung der Strömungsprozesse resultiert.

Dimensionsanalyse

Um die Relevanz dynamischer Effekte abzuschätzen, wird zunächst eine Dimensionsanalyse auf Grundlage der Zweiphasenerhaltungsgleichungen durchgeführt. Nach Einführung der dimensionslosen und charakteristischen Größen, in Analogie zu den Arbeiten von HILFER, 1996 [61], HILFER & ØREN, 1996 [62] und ANTON & HILFER, 1999 [1], und der Wahl des Drucks der benetzenden Phase, P_w, sowie der Sättigung der nicht-benetzenden Phase, S_n, als Primärvariablen, kann die Erhaltungsgleichung für die nicht-benetzende Phase,

$$\phi \frac{\partial S_n}{\partial \widehat{t}} = \widehat{\nabla} \cdot \{ k_{rn}(S_n) \frac{\mu_w}{\mu_n} [\frac{K P_{cc}}{\mu_w u_c l_c} (\widehat{\nabla} \widehat{P_w} + \widehat{\nabla} \widehat{P_c}) + \frac{\mu_w}{\mu_n} \frac{K\tau}{\phi \mu_w l_c^2} \widehat{\nabla} \frac{\partial S_n}{\partial \widehat{t}} - \frac{\rho_n}{\rho_w} \frac{\rho_w g K}{\mu_w u_c} \widehat{\nabla} \widehat{z}] \} \,, \quad (2)$$

formuliert werden. Die Erhaltungsgleichung der benetzenden Phase ändert sich durch die Berücksichtigung der erweiterten Beziehung im Vergleich zum traditionellen Ansatz nicht. Neben den schon bekannten dimensionslosen Zahlen, der Kapillarzahl Ca und der Gravitationszahl Gr, kann nun die 'dynamische Zahl' Dy nach

$$\mathrm{Dy} = \frac{\text{dynamischer Einfluss}}{\text{viskoser Einfluss}} = \frac{K\tau}{\phi \mu_w l_c^2} \quad (3)$$

definiert werden. Wenn Zähler und Nenner mit der Inversen einer charakteristischen Zeit erweitert werden, erhält man ein Kräfteverhältnis. Das Verhältnis der bisher eingeführten Zahlen liefert außerdem

$$\mathrm{DyC} = \frac{\mathrm{Dy}}{\mathrm{Ca}^{-1}} = \frac{K\tau}{\phi \mu_w l_c^2} \frac{\mu_w u_c l_c}{K P_{cc}} = \frac{u_c \tau}{\phi P_{cc} l_c} = \frac{\text{dynamischer Einfluss}}{\text{Gleichgewichts-Kapillareinfluss}} \,, \quad (4)$$

und

$$DyG = \frac{\mathrm{Dy}}{\mathrm{Gr}} = \frac{K\tau}{\phi \mu_w l_c^2} \frac{\mu_w u_c}{\rho_w g K} = \frac{\tau u_c}{\phi l_c^2 \rho_w g} = \frac{\text{dynamischer Einfluss}}{\text{Gravitationseinfluss}} \,. \quad (5)$$

Unter der Annahme, dass der Koeffizient τ als Konstante angesehen werden kann, nimmt die Bedeutung von dynamischen Einflüssen mit zunehmender charakteristischer Länge im Vergleich zu den Gleichgewichtskapillarkräften ab. Das Gleiche gilt für das Verhältnis zu den viskosen Kräften oder den Schwerkraftseinflüssen.
Auf der Basis von Simulationen konnte die Frontbreite eines Infiltrationsprozesses als geeignete Interpretation der charakteristischen Länge bestimmt werden. Der Einfluss der dynamischen Effekte nimmt mit zunehmender typischer transienter Fließgeschwindigkeit zu. Bei der Anwendung der dimensionslosen Zahlen ist zu berücksichtigen, dass für die betrachteten Längenskalen ein REV vorliegen muss. Zur Berechnung der dimensionslosen Zahlen muss unter anderem der Wert des Koeffizienten τ für das betrachtete poröse Medium bekannt sein.

Bestimmung des Koeffizienten τ

Auf der Basis von Laborexperimenten und numerischen Simulationen mit dem Zweiphasenmodul von MUFTE-UG werden nun die Terme der erweiterten $P_c(S_w)$ Beziehung nach Glg. (1) bestimmt. Diese Daten bilden die Grundlage für die Berechnung des Koeffizient τ.
Auf der Basis von drei Dränage-Laborexperimenten mit unterschiedlichen Randbedingungen (durchgeführt von GeoDelft, Niederlande) mit einem Sand ($K = 3.06 \cdot 10^{-12}\,\mathrm{m}^2$, $P_d = 5587\,\mathrm{Pa}$) konnte eine inverse proportionale Beziehung des Koeffizienten τ zur Wassersättigung festgestellt werden. Die τ-Werte betragen zwischen $\tau = 11.0\,\mathrm{kPa\,s}$ und $\tau = 154.7\,\mathrm{kPa\,s}$.
Mit Glg. (1) wird eine lineare Beziehung zwischen Kapillardruckdifferenz und Sättigungsänderungsrate angenommen. Diese Annahme wird hier überprüft. Es werden Regressionen durchgeführt, die einen y-Achsenabschnitt ungleich Null zulassen. Die Größe des y-Achsenabschnitts wird als Maß für die Abweichung von der linearen Beziehung interpretiert. Basierend auf den Ergebnissen aus den Dränierungsexperimenten besteht eine nicht-lineare Beziehung zwischen Kapillardruckdifferenz und Sättigungsänderungsrate bei hohen Wassersättigungen. Für eine abschließende Aussage zur Identifizierung der Beziehung sind weitere Messungen notwendig.
Für einen Vergleich mit Ergebnissen von KALAYDJIAN, 1992 [68] wird der Koeffizient τ unabängig für jedes der drei Experimente bestimmt. Die so erhaltenen τ-Werte unterscheiden sich um ein bis zwei Größenordnungen von denen die KALAYDJIAN, 1992 für Imbibitionsexperimente mit einem Kalkstein bestimmt hat. Die höheren Werte bei KALAYDJIAN, 1992 können auf eine Prozessabhängigkeit deuten, da er ein Imbibitionsexperiment verwendet hat. Aber auch Abhängigkeiten von weiteren Parametern, die sich in den hier verglichenen Experimenten unterscheiden, sind denkbar. Diese müssen in weiteren unabhängigen Laboruntersuchungen quantifiziert werden. Hier ist noch zu erwähnen, dass bei der Bestimmung von τ für jedes der drei Experimente eine Abhängigkeit des Koeffizienten von den Randbedingungen auftritt. Mit abnehmenden (transienten) Strömungsgeschwindigkeiten nimmt der Koeffizient τ bei gegebener Wassersättigung zu. Aus diesem Trend resultiert allerdings, dass der Koeffizient ein Maximum bei kapillar-dominierten Prozessen annehmen würde. Dies steht im Gegensatz zu der Annahme, dass unter derarti-

gen Bedingungen dynamische Effekte von untergeordneter Bedeutung sind. Deshalb sollte der Koeffizient auf der Grundlage mehrerer dynamischer Experimente oder mit einem für inverse Parameteridentifikation ausgelegtem Laborexperiment (siehe O'CARROLL ET AL., 2005 [86]) bestimmt werden.

Zusätzlich zu der Auswertung von Laborexperimenten sind 'numerische Experimente' durchgeführt worden. Der Koeffizient kann so für weitere poröse Medien mit einem im Vergleich zu Laborexperimenten geringeren Zeitaufwand bestimmt werden. Darauf aufbauend wird untersucht, ob dynamische Effekte auch für den Übergang von der lokalen Skala zur Makroskala identifiziert werden können.
Da die $P_c^e(S_w)$ -Funktion ein Term der erweiterten Beziehung ist, wird zunächst deren Bestimmung durch ein numerisches Experiment für eine einfache Struktur, zwei Feinsandlinsen eingebettet in einen Grobsand, vorgestellt. In diesem Experiment wird der am Rand vorgegebene Kapillardruck stufenweise erhöht. Vor jeder weiteren Erhöhung werden die Phasendrücke und Sättigungen über das Gebiet gemittelt, um so ein Datenpaar $P_c - S_w$ zu erhalten. Der Ansatz zur Mittelung der Phasedrücke, deren Differenz dann den gemittelten Kapillardruck ergibt, kann somit überprüft werden. Wenn der mit dem Phasenvolumen gewichtete mittlere Phasendruck in die gemittelte $P_c(S_w)$ Beziehung eingeht, kann eine gute Übereinstimmung mit einem analytischen Ansatz erzielt werden (siehe Abb. 2, links). Das arithmetische Mittel der Phasendrücke ergibt bei der Verwendung der Parametrisierung der $P_c(S_w)$ Beziehung nach BROOKS & COREY, 1964 [19] einen zu hohen Kapillardruck solange die Feinsandlinsen noch voll wassergesättigt sind. Dann tragen diese Teile des Gebietes zum mittleren Druck der nicht-benetzenden Phase bei, obwohl deren Sättigung dort Null ist. Wird für die gemittelte $P_c(S_w)$ Beziehung der durch die Randbedingungen vorgegebene Kapillardruck zusammen mit der gemittelten Sättigung verwendet, können Unterschiede zum gemittelten Kapillardruck festgestellt werden. Der gemittelte Kapillardruck kann höher sein als der Randkapillardruck. Diese Differenz geht auf den Aufstau von nicht-benetzender Phase auf den Linsen zurück. Sie geht gegen Null für geringe Druckgradienten in den Phasen. Zum anderen lassen sich größere Abweichungen bei hohen Randkapillardrücken beobachten. Obwohl die Kriterien zur Einschätzung der Stationarität erfüllt sind, bleibt der gemittelte Kapillardruck geringer als der Randkapillardruck. Die Höhe der Stationaritätskriterien ($^{\Delta<P_w>}/_{\Delta t} < \varepsilon_p$ und $^{\Delta<S_n>}/_{\Delta t} < \varepsilon_S$) entscheidet über die Abweichung und somit über die Höhe der Residualsättigung der benetzenden Phase (siehe Abb. 2, rechts). Werden noch strengere Kriterien angelegt, resultiert dies in unakzeptabel langen Rechenzeiten. Die Anwendung eines numerischen Modells ist demzufolge nicht so effizient wie z.B. die von Perkolationsmodellen. Diese beruhen aber auf der Annahme des kapillaren Gleichgewichts. Deshalb können mit dem Modell keine viskosen Einflüsse auf die gemittelte $P_c(S_w)$ Beziehung untersucht werden.
Als weiterer Schritt werden numerische Experimente zur Identifizierung der dynamischen $P_c(S_w)$ Beziehung vorgestellt. Im Gegensatz zu den stationären Experimenten wird hier der Randkapillardruck innerhalb des ersten Zeitschritts um einen

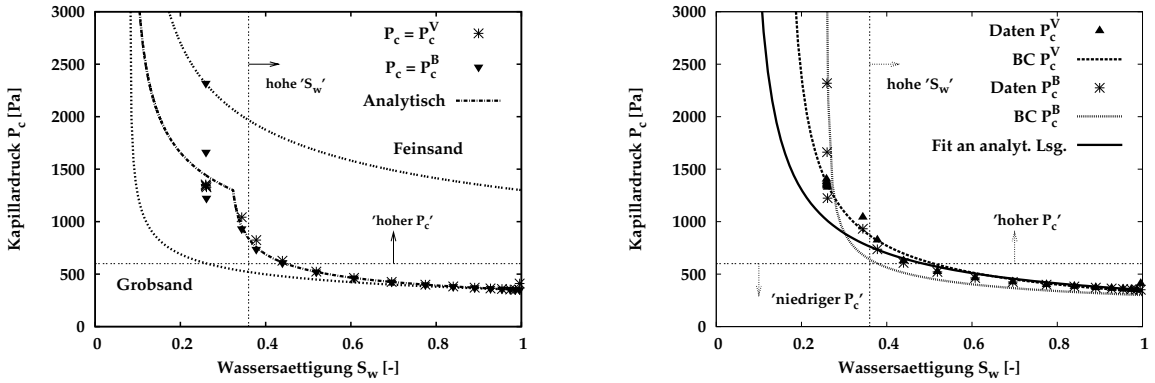

Abb. 2: $< P_c^V > (< S_w >)$ und $P_c^B (< S_w >)$ Beziehungen für das numerische Dränageexperiment mit einer einfachen Heterogenitätsstruktur (links) und Regressionen basierend auf der BROOKS & COREY Parametrisierung (rechts)

signifikanten Betrag erhöht. Nach jedem Zeitschritt werden die Phasendrücke und Sättigungen gemittelt, um einen kontinuierlichen Verlauf der $P_c^d(S_w)$ Funktion zu halten. Zunächst werden homogene Systeme untersucht, um dann im Folgenden zwischen dem Einfluss von Heterogenitäten und dem Einfluss der Randbedingungen, des Mittelungsvolumens und den Eigenschaften des porösen Mediums und der Fluidparameter zu unterscheiden. Ein dynamischer Effekt in der $P_c(S_w)$ -Beziehung kann nur festgestellt werden, wenn gemittelte Phasendrücke, im Gegensatz zu einem diskreten Wert z.B. an einem Knoten, in die $P_c^d(S_w)$ Beziehung eingehen. Der Koeffizient τ verhält sich proportional zur Porosität, zur (mit der Sättigung gewichteten, gemittelten) Viskosität und dem Quadrat der Mittelungslänge. Des Weiteren besteht eine inverse Proportionalität zur intrinsischen Permeabilität. Diese Beziehungen gelten allerdings nur für Viskositätsverhältnisse μ_w/μ_n von eins und kleiner eins bei mittleren Wassersättigungen von $S_{wr} << S_w < 1.0$ (siehe Abb. 3 und 4). Mit diesen Ergebnissen lässt sich die dimensionslose Zahl

$$N_D = \frac{\tau K}{\phi \mu l^2} \tag{6}$$

von DAHLE ET AL., 2005 [30], in dem l eine typische Länge des Mittelungsvolumen ist, nachvollziehen. Diese Autoren bestimmen den Koeffizienten τ auf der Grundlage eines Kapillarbündelmodells und stellen fest, dass N_D bei mittleren Sättigungen ungefähr eins beträgt. Die Parameter, welche in die Parametrisierung der $P_c(S_w)$ -Beziehung eingehen, haben nur einen geringen Einfluss auf die Größe des in numerischen Experimenten bestimmten Koeffizienten. Diese Ergebnisse stehen im Gegensatz zu der von STAUFFER, 1978 [108] vorgeschlagenen Gleichung (3.2) zur Bestimmung von τ, nach der der Koeffizient z.B. positiv mit dem Eindringdruck korreliert.
Wenn der Koeffizient wie hier bestimmt, positiv mit dem Quadrat der Mittelungslänge korreliert, ist seine Größe nicht klar begrenzt. Demzufolge kann kein

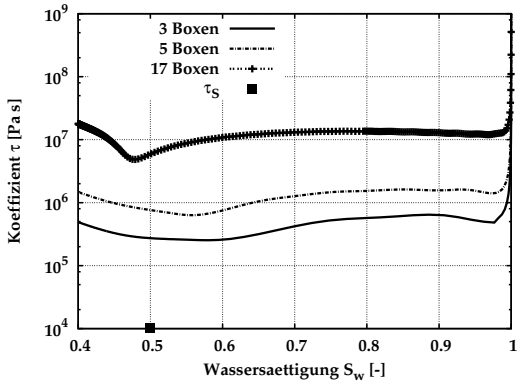

Abb. 3: $\tau(S_w)$ für verschiedene Mittelungsvolumen und kalkuliert nach Glg. (3.2)

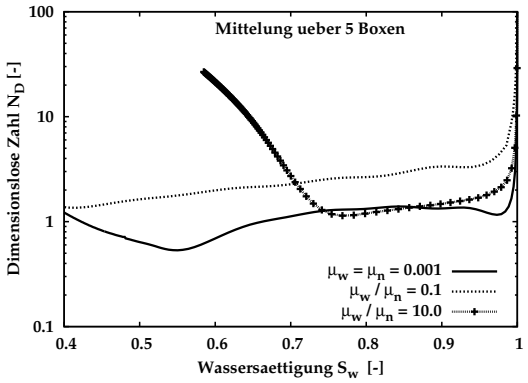

Abb. 4: Die dimensionslose Zahl $N_D(S_w)$ basierend auf der sättigungsgewichteten gemittelten Viskosität für drei Viskositätsverhältnisse (rechts)

REV bestimmt werden. Demzufolge muss entweder die Mittelungslänge auf eine beschränkte Größe bezogen werden (z.B. die Inverse der Distanz des typischen Druckabfalls). Oder aber die Mittelung der Phasedrücke muss überdacht werden.

Für das oben beschriebene heterogene System kann ein signifikanter Einfluss auf den Koeffizienten τ erst bei der Dränage der Feinsandlinsen festgestellt werden. Werden Heterogenitäten basierend auf einem räumlich-korrelierten Zufallsfeld in die Simulationen einbezogen, kann kein Einfluss der Heterogenitäten auf $\tau(S_w)$ festgestellt werden. Anscheinend bewirkt die kontinuierliche Verteilung der Parameter, dass das mittlere Verhalten des Systems dominiert. Wenn man die räumlich-korrelierten Zufallsfelder von Eindringdruck und intrinsischer Permeabilität als subskalige Heterogenitäten auffasst, brauchen diese Verteilungen nicht berücksichtigt werden, wenn der Koeffizient τ basierend auf numerischen Experimenten bestimmt werden soll. Anzumerken ist, dass dynamische Effekte auf Grundlage von Homogenisierungstheorien identifizierbar sind (BOURGEAT & PANFILOV, 1998 [16], LEWANDOWSKA ET AL., 2004, 2005 [75, 76]). Allerdings müssen bestimmte Annahmen erfüllt sein, wie beispielsweise eine klare Skalenseparation der kleinskaligen Heterogenität im Verhältnis zu der Systemabmessung. Außerdem muss das Verhältnis der Parameter der feinen und groben Heterogenitäten bestimmten Anforderungen genügen.

Simulationen

Im letzten Teil der Arbeit wird die Anwendung eines numerischen Modells vorgestellt, mit dem die Zweiphasenerhaltungsgleichungen unter Einbeziehung einer erweiterten Kapillardruck-Sättigungsbeziehung gelöst werden. Basierend auf den beschriebenen Quantifizierungen des Koeffizienten geht τ nicht nur als Konstante sondern auch als Funktion der Sättigung (linear oder quadratisch) in die Simulationen ein.

Unter der Annahme, dass ein Laborexperiment für die Bestimmung des Koeffizienten τ notwendig ist, wird zunächst eine Sensitivitätsanalyse durchgeführt. Es zeigt sich, dass die Sensitivität der kumulativen Masse der benetzenden Phase im System $M_{\mathrm{w}}^{\mathrm{c}}(t)$, einer somit integralen Größe, als auch der Sättigung $S_{\mathrm{n}}(\mathbf{x}, \mathbf{t})$, in Bezug auf den Koeffizienten τ kleiner ist als gegenüber den anderen getesteten Parametern. Es wird daher vorgeschlagen, mindestens zwei unterschiedliche Arten von Laborexperimenten durchzuführen: eine Art zur unabhängigen Bestimmung der traditionell in die Zweiphasengleichungen eingehenden Parameter, und eine andere Art von Experiment ausschließlich zur Bestimmung des Koeffizienten. Diese Herangehensweise setzt voraus, dass weder die Restsättigungen noch die relativen Permeabilitäten von der Dynamik der Prozesse abhängen.
Die dimensionslosen Zahlen Dy und DyC können, unter Verwendung der Frontweite als charakteristischer Länge, zur Einschätzung des Einflusses der erweiterten Kapillardruck-Sättigungsbeziehung auf die Lösung herangezogen werden. Wenn die dynamischen die viskosen, aber nicht die Gleichgewichtskapillareinflüsse dominieren, kann ein Dämpfungseffekt im Verlauf der kumulativen Masse über die Zeit beobachtet werden (siehe Abb. 6.4). In Bezug auf die Infiltrationsfront können Bereiche identifiziert werden, die schneller bzw. langsamer als der Referenzfall reagieren, bei dem das traditionelle Modell mit einer eindeutigen $P_{\mathrm{c}}(S_{\mathrm{w}})$ Beziehung verwendet wurde. Bei der Anwendung einer Neumann-Randbedingung kann eine Prozessumkehr von Imbibition zu Dränage und zurück beobachtet werden (siehe Abb. 6.12). Wenn die dynamischen Einflüsse zusätzlich zu den viskosen auch die Gleichgewichtskapillar-Einflüsse dominieren, können bei einem hohen Viskositätsverhältnis $\mu_{\mathrm{w}}/\mu_{\mathrm{n}}$ Oszillationen in der Lösung auftreten. Generell kann bei den vorliegenden partiellen Differentialgleichungen mit Oszillationen gerechnet werden, wenn bestimmte Parameterverhältnisse auftreten (persönliche Kommunikation H. v. Duijn, TU Eindhoven, Niederlande).
Zusammenfassend kann festgehalten werden, dass ein Einfluss auf die Lösung nur bei hohen Änderungsraten der Sättigung und hohen Koeffizienten τ auftritt. Die dimensionslosen Zahlen Dy und DyC können eine Einschätzung geben, ob die Lösung beeinflusst wird. Zusätzlich muss das Viskositätsverhältnis berücksichtigt werden.

Ausblick

Die Abhängigkeit des auf der Grundlage numerischer Experimente bestimmten Koeffizienten τ vom Mittelungsvolumen ist ein noch nicht gelöstes Problem. Eine wichtige offene Forschungsfrage stellt deshalb die Mittelung der Phasendrücke dar. Die Skalenabhängigkeit des Koeffizienten ist auch in Laborexperimenten noch nicht untersucht worden.
Will man die für ein heterogenes Gebiet bestimmten τ-Werte anwenden, müssen auch andere Parameter und konstitutive Beziehungen gemittelt werden. Während z.B. für die Mittelung der intrinsischen Permeabilität Ansätze existieren, ist die Mittelung der relativen Permeabilitäten unter transienten Bedingungen Gegenstand von Forschungsarbeiten. Nur eine konsistente Mittelung würde den Vergleich zu Laborexperimenten oder homogenen Referenzfällen ermöglichen.

Des Weiteren sollte eine detaillierter Analyse des Einflusses der erweiterten $P_c(S_w)$ - Beziehung auf die Ergebnisse von numerischen Simulationen durchgeführt werden. Die hier vorgestellte Diskretisierung kann außerdem nicht auf heterogene Gebiete angewendet werden, da der Gradient der Änderungsrate der Sättigung bestimmt werden muss. Die Sättigung kann aber an der Grenzfläche von Heterogenitäten unstetig sein. Um diese Grenzflächen korrekt abzubilden, sollte eine Bedingung, ähnlich der von DE NEEF, 2000 [35] vorgeschlagenen Behandlung von Grenzflächen zur korrekten Abbildung des Eindringdrucks, gefunden werden.
Allgemein betrachtet, beeinflussen sowohl dynamische als auch hysteretische Effekte die konstitutiven Beziehungen, welche für die Beschreibung von Zweiphasenprozessen auf der lokalen Skala und der Makroskala angewendet werden. Die Prozesse, die zu solchen Effekten führen und ihre Interaktion sind noch nicht vollständig analysiert. Dies erschwert die Identifikation der auf den verschiedenen räumlichen und zeitlichen Skalen relevanten Prozesse.
Diese Arbeit leistet zum einen einen Beitrag zum Verständnis dynamischer Effekte in Kapillardruck-Sättigungsbeziehungen für die lokale Skala und die Makroskala. Zum anderen gibt sie eine Einschätzung, für welche Zweiphasenprozesse diese Effekte berücksichtigt werden sollen.

1 Introduction

1.1 Motivation

The understanding and prediction of the flow processes of two immiscible fluids in a non-deformable porous medium play an important role in subsurface or in technical applications. In the unsaturated zone of the subsurface, the prediction of the distribution and fluxes of water and gas (air) serves as a basis for the modelling of contaminant transport, such as the displacement of pesticides or heavy metals. Flow processes in the unsaturated zone also need to be quantified in order to calculate groundwater recharge. Moreover, groundwater and a non-aqueous phase liquid (NAPL) contaminant such as an organic solvent form a two-phase system in the subsurface. For the development and application of remediation measures, two-phase flow needs to be understood profoundly. Two-phase flow processes have thus been studied intensively not only in engineering but also in soil physics and hydrogeology over recent decades (e.g. CHARBENEAU, 2000 [24]). Apart from applications related to subsurface hydrosystems, two-phase flow problems are encountered in technical applications, e.g. the movement of two fluids through a filter or the infiltration of ink into paper (see MIDDENDORF, 2000 [79]).
The applications just described are linked to different spatial scales. In general, the smallest scale considered is the pore scale (see Fig. 1.1), where the occurrence of a fluid or the solid matrix is clearly defined for each point in space. An averaging process marks the transition to a larger scale, here denoted local scale. Yet another scale transition leads to the macroscale. This thesis focuses on two-phase flow processes on the local scale and the macroscale, though pore scale processes might be consulted for physical interpretations. Currently, the models on these scales describing two-phase flow consist of the mass balance equations for both phases, including the extended DARCY's law for the calculation of the fluids' velocities, and constitutive relationships that capture the interaction between the fluids and the porous medium in an averaged sense. One of them quantifies the relation of the volumetric fractions of the fluid phases – the saturations – at a given difference between the phase pressures – the capillary pressure – related to an averaging volume. Since the beginning of the last century, many studies have dealt with determining the capillary pressure-saturation relationship $P_c(S_w)$ with either laboratory experiments, analytical approaches or numerical techniques. Traditionally, the determination of the relationship was performed on the assumption of a quasi-static distribution of the fluids or a steady-state where the saturations do not change in time. Several studies have examined the performance of the traditional two-phase flow theory in describing transient flow conditions. Researchers have found various shortcomings when ap-

plying the existing models. Two major issues have thus occurred, non-uniqueness in the $P_c(S_w)$ relationship and the inability to simulate certain two-phase flow behaviour under transient conditions.

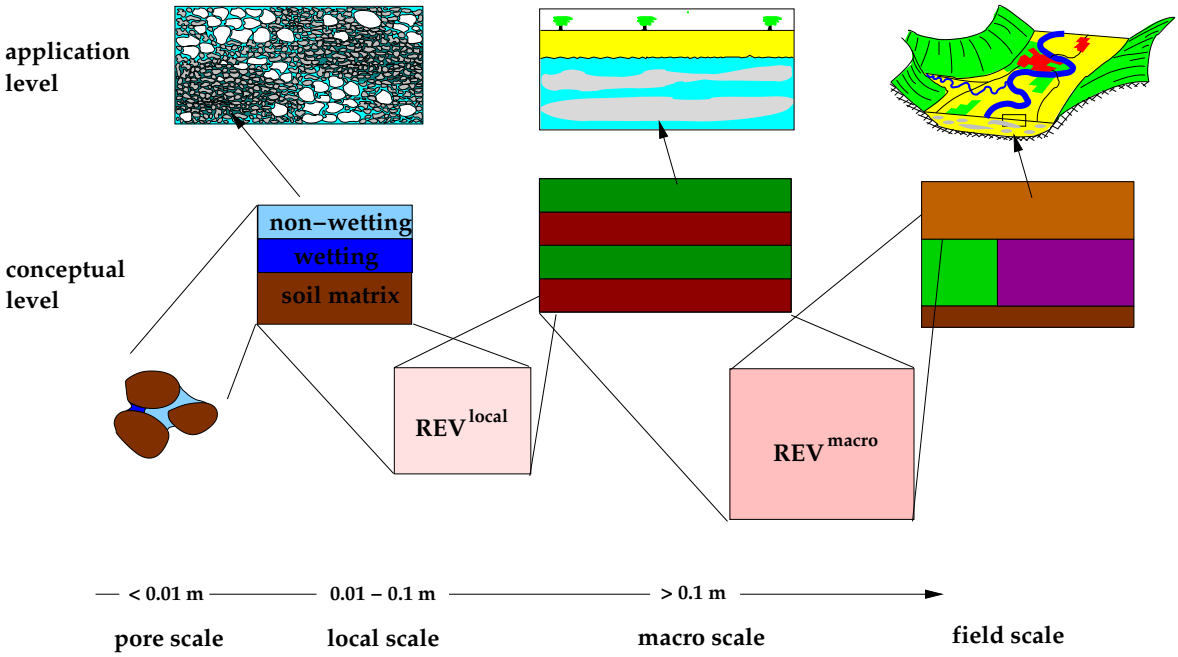

Figure 1.1: Depiction of spatial scales (in parts from KOBUS, 1995 [70])

To illustrate the non-uniqueness in the $P_c(S_w)$ relationship an example from TOPP ET AL., 1967 [109], who measured $P_c(S_w)$ relationships in the laboratory under quasi-static, steady-state and transient flow conditions, is presented (see Fig. 1.2). The $P_c(S_w)$ data measured under stationary conditions (quasi-static or steady-state) differ only slightly. In contrast, the capillary pressure from the transient experiment at a given saturation is higher than the one from the other two experiments. Consequently, the relationship between saturation and capillary pressure cannot be regarded as unique. The effect has been observed both under drainage (e.g. gas displaces water) as well as imbibition (e.g. water displaces oil) conditions. The non-uniqueness needs to be taken into account when the $P_c(S_w)$ relationship is measured in the laboratory, or when this constitutive relationship is applied in the simulation of two-phase flow, e.g. to assess remediation techniques.
In recent decades, theoretical studies carried out by HASSANIZADEH & GRAY, 1990 [55], HASSANIZADEH & GRAY, 1993 [56], or KALAYDJIAN, 1987[67], as well as the empirical approach of STAUFFER, 1978 [108] have produced new aspects to two-phase flow theories. One important aspect relates to the treatment of capillary pressure-saturation relationships. In summary, these authors propose that the difference between the capillary pressure prevailing under transient conditions, denoted here dynamic capillary pressure P_c^d, and the one determined under quasi-static or steady-state conditions (in the following denoted equilibrium capillary

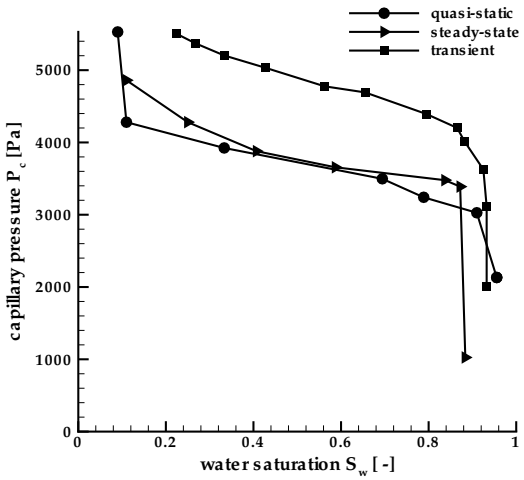

Figure 1.2: Illustration of dynamic effects in the $P_c(S_w)$ relationship using experimental results from TOPP ET AL., 1967 [109]

pressure P_c^e) at a given water saturation can be linearly related to the rate of change of water saturation

$$P_c^d - P_c^e(S_w) = -\tau \frac{\partial S_w}{\partial t} , \tag{1.1}$$

where τ denotes a coefficient quantifying the slope of the relationship. According to Eqn. (1.1), the dynamic capillary pressure equals the equilibrium one only under static or steady-state conditions, when the rate of change of saturation diminishes to zero. Under transient conditions, this convergence may not be reached instantaneously but depending on the rate of change of saturation and the magnitude of the coefficient τ. This rate dependence is denoted here 'dynamic effect'. The relation given in Eqn. (1.1) is termed the extended $P_c(S_w)$ relationship.
Concerning the application scenarios described above, the extended $P_c(S_w)$ relationship needs to be taken into account only for cases where high rates of change of saturation occur or where the porous media possess a large coefficient τ. High saturation rates might be encountered for example when water infiltrates into an initially dry subsurface after heavy rain-fall. The magnitude of the coefficient for a given porous medium and fluid system is one of the questions tackled in this thesis.
Related to the inability of the traditional two-phase flow models to reproduce certain transient flow behaviour, the investigations of NIEBER ET AL., 2005 [84] should be mentioned, who applied the extended $P_c(S_w)$ relationship and were thus able to enhance the modelling of fingering observed in gravity-driven flow. DICARLO, 2005 apply an extended $P_c(S_w)$ relationship to model the saturation-overshoot observed at the tip of fingers but cannot reproduce the overshoot well with this model. O'CARROLL ET AL., 2005 [86] were able to improve the simulation of a multi-step

outflow experiment with water-oil including the extended $P_c(S_w)$ relationship in comparison to simulations on the basis of the traditional assumptions.
Although the influence of transient flow processes on the $P_c(S_w)$ relationship has been examined sporadically over several decades, only recently have investigations intensified. Several open questions pertain to the impact of dynamic effects on two-phase flow in porous media on the local scale to the macroscale.

- The increased model complexity and determination of an additional parameter can only be justified if flow processes can be identified where dynamic effects play a crucial role and thus need to be taken into account in simulations.

- The empirical formula of STAUFFER, 1978 [108] for the coefficient τ on the basis of laboratory experiments with four different sands and a water-air fluid system, as well as the dimensionless grouping introduced by DAHLE ET AL., 2005 [30] on the basis of a bundle of capillary tubes model should be verified for additional porous media or fluid systems and different approaches to the determination of the coefficient.

- My attention was first drawn to dynamic effects in the $P_c(S_w)$ relationship during the analysis of a multi-step outflow experiment performed by researchers at the Universität Heidelberg (see VOGEL ET AL., 1999 [116]). The simulation of the experiments using the standard two-phase flow model could not reproduce relaxation characteristics detected in parts of the measured outflow. Neither parameter variations nor the inclusion of heterogeneity in the simulations resulted in the reproduction of the relaxation behaviour (for details see App. A). Dynamic effects in the $P_c(S_w)$ relationship could not be precluded in the experiment, thus my attention resulted in the analysis of these effects. The impact on simulation results when the extended $P_c(S_w)$ relationship is applied in the balance equations (instead of the traditional $P_c(S_w)$ relationship) needs to be examined. Amongst other issues, the question whether the inclusion of the extended $P_c(S_w)$ relationship results in a retardation of the flow processes needs to be investigated.

1.2 Goals and structure of the thesis

Resulting from the motivation, the goals of this thesis can be summarised as follows.

1. One goal of this thesis is to identify the importance of forces due to dynamic effects in the $P_c(S_w)$ relationship in relation to (equilibrium) capillary, viscous and gravitational forces on the basis of a dimensional analysis of the balance equations closed with the extended $P_c(S_w)$ relationship. The evolving dimensionless numbers should give an indication as to when dynamic effects dominate in two-phase systems.

2. A further aim is to quantify the coefficient τ with different approaches and to analyse these approaches. The determination of the coefficient is based on laboratory experiments performed by GeoDelft, The Netherlands and on simulations which mimic laboratory experiments. Possible dependences of the coefficient τ on the water saturation, on porous media properties, on fluid properties, or on the averaging length scale need to be investigated. Moreover, the validity of the linear relation between capillary pressure difference and rate of change of saturation should be tested.

3. The impact on simulation results stemming from the extended $P_c(S_w)$ relationship should be assessed for different porous media/fluid systems and magnitudes of the coefficient for varying boundary conditions. With a sensitivity analysis, appropriate boundary conditions and to be measured magnitudes should be identified if the coefficient were to be determined by an inverse parameter estimation.

The thesis is structured as follows. In Ch. 2, the physical-mathematical model of two-phase flow in porous media on the local scale and macroscale is described. In Ch. 3 laboratory investigations from the literature which examine dynamic effects in the $P_c(S_w)$ relationship are analysed with a view to reasons why these effects might occur. Models with which the non-uniqueness in the $P_c(S_w)$ relation due to the rate-dependence can be resolved are introduced in Secs. 3.3 to 3.5 and a general form of an extended $P_c(S_w)$ relationship is chosen for further investigation.
On the basis of the local scale conservation equations including the extended $P_c(S_w)$ relationship, a dimensional analysis is carried out, which yields dimensionless numbers quantifying the ratio between forces due to the dynamic effects with respect to the equilibrium capillary, viscous or gravity forces. These numbers facilitate an assessment of the dominating forces for a process given the porous media parameters are known (see Sec. 3.6). The dimensionless numbers help to find parameter combinations for the simulations in Ch. 6. These combinations should ensure a dominance of dynamic forces.
For the simulation of two-phase flow processes, a numerical model is required. The spatial and temporal discretisation is first set up, applying the traditional and secondly the extended $P_c(S_w)$ relationship to close the system of the two-phase balance equations (see Ch. 4).
Calculation of the dimensionless numbers or simulations including the extended $P_c(S_w)$ relationship require a knowledge of the coefficient τ. In Ch. 5 various approaches are tested for the determination of the coefficient. The laboratory data from GeoDelft, The Netherlands, serve to quantify the coefficient τ as a function of the water saturation and to test the linearity of the extended $P_c(S_w)$ relationship (see Sec. 5.3). Furthermore, simulations mimicking laboratory experiments described in Sec. 5.4 are applied to specify the coefficient as a function of water saturation, porous media and fluid properties. A dependence on the length scale is discussed. The determination of the coefficient with numerical experiments is based on the assumption that local scale heterogeneity can introduce dynamic effects in addition to the

ones arising when upscaling from the pore to the local scale as shown by e.g. HASSANIZADEH & GRAY, 1990 [55]. A second assumption is that in the observed flow processes the dynamic effects dominate.
Simulations on the basis of the balance equations including the extended $P_c(S_w)$ relationship are presented in Ch. 6. Assuming known model parameters including the coefficient τ, the resulting dimensionless numbers are calculated for the simulations in order to test whether they assess an impact on simulation results correctly. Three different simulations serve to assess the effect on the results in comparison to simulations on the basis of the traditional $P_c(S_w)$ relationship. Besides the porous media properties, the boundary conditions are varied to yield different magnitudes of the dimensionless numbers.
On the basis of a summary of the findings, conclusions are drawn and an outlook on subsequent work is given in Ch. 7.

2 Physical-mathematical model of two-phase flow

In this thesis, the flow processes of two immiscible fluids in a rigid porous medium at isothermal conditions are examined. First, an overview of the conceptual model and definitions pertaining to this field of research are given. The conceptual model needs to be expressed in the form of a mathematical model. With this mathematical model, the flow of two fluid phases in a porous medium can be assessed at a scale where DARCY's law holds. First, the scale definitions and the appertaining REV concept are introduced.

2.1 Conceptual model and definition of system properties

To progress from one spatial scale to a higher one, an averaging procedure is required. A scale transition is closely related to the concept of the Representative Elementary Volume (REV) after BEAR, 1972 [10]. This concept assumes that the fluctuations of an averaged parameter are negligible for a length l [126], with

$$d << l << L, \tag{2.1}$$

where d represents a length scale of the pore scale and L represents a larger scale where again fluctuations in the averaged parameter might occur (see Fig. 2.1). Over the length l the average of the variable considered does not change with an altering averaging volume. It is assumed that one REV can be found for different parameters.
The first scale transition considered here is the one from the pore scale to the local scale (see Fig. 1.1). Consequently, a volume including a pore space and the fluids distributed therein needs to be found on the pore scale, such that, by averaging over given quantities, effective parameters can be allocated to that volume on the local scale. If for example the volume of the two fluids is averaged over this volume on the pore scale, a new variable – the saturation – evolves on the local scale. As a consequence, the occurrence of one phase can no longer be defined for a point in space, but all phases can theoretically occur at that point. Moving to a yet larger scale, here denoted the macroscale, porous media with different effective parameters on the local scale might need to be taken into account. Averaging over these might introduce new characteristics on the macroscale, such as a direction dependent relative permeability-saturation relationship (see e.g., BRAUN, 2005 [18]).

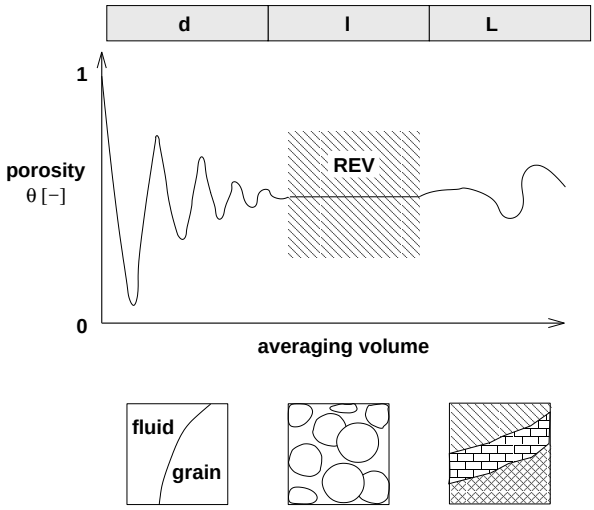

Figure 2.1: REV concept after BEAR, 1972 [10]

This thesis focuses on the local scale and the macroscale, though the scale transition from pore to local scale is also considered to some extent for physical explanations. While the local scale can be related to the laboratory column scale, the macroscale can be linked to laboratory bench scale.

2.1.1 Phase properties

On the pore scale, a **phase** can be defined as a volume of a substance bounded by an area. Within this volume, no jumps in the chemical composition and physical properties such as the density occur. Its boundary is characterised by an interface. On the local scale, the interfaces are no longer resolved, a phase is then quantified by a volume or volume fraction.
In the framework of this study, three phases are distinguished, namely gaseous, liquid, and solid phases.
In the following, the concept of fluid mechanics is adopted, which assumes that all matter can be divided into fluids and solids. In contrast to a fluid, a solid can resist shear stress by a static deformation. A fluid will deform or move continuously as long as shear stress is applied. Liquids and gases can thus both be categorised as fluid phases.
Depending on the thermodynamic state of a system consisting of more than one phase, phase transitions such as evaporation or crystallisation might occur. In the context of this thesis, phase transitions will not be taken into account.

A **porous medium** consists of a solid phase possessing void space, which can be occupied by one or more fluids. The void space is usually named pore space. The pores need to be connected to enable the flow of a fluid phase. The ratio of the

volume of the pores V_p to the averaging volume V_{av} quantifies the porosity

$$\phi = \frac{V_p}{V_{av}} = \frac{V_p}{V_p + V_{solid}}. \tag{2.2}$$

For natural soils, the porosity usually ranges between $\phi = 0.35$ and $\phi = 0.5$ [23].
The solid phase is considered rigid. It will not be counted as a phase when the term 'two-phase' is employed. This term refers here to a porous medium occupied by two immiscible fluid phases.

The **density** of a phase ρ [ML^{-3}] is defined by the ratio of its mass m to the volume V it occupies. The density depends on temperature and pressure, though for most liquids the pressure dependence may be neglected. In this thesis also any density dependence of the gas phase is not taken into account. As only isothermal conditions are considered here, dependence of the fluid density on temperature is not an issue.

The **dynamic viscosity** of a fluid phase μ [$ML^{-1}T^{-1}$] is caused by intermolecular attractive forces, e.g. VAN DER VAALS forces, which impede the displacement of molecules. The dynamic viscosity can be interpreted as proportional to the force required to move a fluid layer of 1 m^2 and 1 m thickness parallel to a boundary layer with a velocity of 1.0 m/s. The dynamic viscosity of a fluid with a constant chemical composition depends on temperature and on pressure. For the scope of this thesis, these dependences are assumed not to play a role.
Tab. 2.1 lists the densities and viscosities of the fluids employed in this thesis. Perchlorethylen (PCE) is a dense non-aqueous phase liquid (DNAPL) that has a higher density than water.

Table 2.1: Fluid parameters for water, gas (air) and Perchlorethylen (PCE) as applied in this study

	density ρ [kg/m^3]	dynamic viscosity μ [$kg/(m\,s)$]
water	1000	0.001
gas (air)	1.8836	$1.65 \cdot 10^{-5}$
PCE	1630	$0.9 \cdot 10^{-3}$

Two phases are bounded by an interface, where forces act which are usually denoted **interfacial tension**. In fluids, cohesion forces, caused e.g. by VAN DER WAALS forces, work between the molecules of the fluid. Especially in water, these forces are strong due to the dipole character of the molecule. Cohesion forces act uniformly within a liquid phase, whereas at the surface of the phase the forces are only effective parallel and perpendicular to the surface. This results in a force which is directed into the phase. To reduce this force, a fluid phase aims at minimising its surface area. The interfacial tension $\gamma_{1,2}$ [MT^{-2}] between phase 1 and 2 relates the

work W required to minimise the surface to the change in surface area $A_{1,2}$ between the phases

$$\gamma_{1,2} = \frac{\partial W}{\partial A_{1,2}}. \tag{2.3}$$

The interfacial tension is thus a measure of the cohesive energy acting on the interface between two phases.
In addition to the cohesion forces, adhesion forces, which are also induced by VAN DER WAALS forces, act between different fluids or fluids and solids. The adhesion forces result in interfacial tension as well.
The interfacial tension depends primarily on the chemical composition of the phases and the temperature. In Section 2.2.1 further dependencies are discussed.

2.1.2 Thermodynamic equilibrium

A system that cannot exchange energy or matter with its surroundings is in thermodynamic equilibrium when its properties do not change with respect to time. Thermodynamic equilibrium can be divided into thermal, chemical, electrical, and mechanical equilibrium. Only the latter is of interest here as exclusively isothermal systems with phases of a constant chemical composition each are considered.
Mechanical equilibrium prevails if the pressure over an interface between two phases is constant, as for example over the boundary between a lake and the atmosphere. However, in a porous medium due to the interfacial tensions, a pressure difference between the two fluid phases exists, namely the capillary pressure (see Sec. 2.2.1). Consequently, the capillary pressure needs to be included in the balancing of the pressures. Then, as long as the pressure of the non-wetting phase equals the capillary pressure plus the wetting phase pressure, the system is in mechanical equilibrium.
In the context of this thesis, 'equilibrium' is defined according to the problems under consideration, although it might not agree with other theories [11]. For a two-phase system in a porous medium, two equilibrium states are distinguished. At **static** equilibrium, the fluid phases do not flow. In addition, at a **steady-state** equilibrium, a fluid phase flows due to a pressure gradient within the phase but the divergence of the flow field and the source/sink term equal zero. Time-dependent flow processes are termed **transient** or **dynamic** processes. In all cases, local mechanical equilibrium is assumed to hold as long as dynamic effects in the capillary pressure-saturation relationship are not taken into account (compare Ch. 3).

2.2 Constitutive relationships

Constitutive relationships are employed on the local scale and higher scales in order to relate a secondary variable, such as the capillary pressure or the relative permeability, to a primary variable, the saturation.

2.2.1 Capillary pressure - saturation relationship

Because this thesis focuses on dynamic effects in two-phase flow, not only the traditional approach to capillarity on the local scale assuming equilibrium conditions but also the influence of transient flow conditions are illustrated. Preceding the local scale definitions, capillarity on the pore scale is described, as pore scale processes might be consulted to explain effects observed in the local scale quantities.

2.2.1.1 Capillarity on the pore scale

Static equilibrium conditions For the static configuration of two fluid phases and a solid phase (e.g. a droplet of water on glass in a gas), three interfacial tensions $\gamma_{\alpha\beta}$ drag on the interfaces (see Fig. 2.2, left). The three phases meet at the contact line (see Fig. 2.2, right). At the interface between the fluids and the solid, an angle develops in relation to the magnitude of the cohesion and adhesion forces. This **static contact angle** θ_e measures the angle between the tangent at the fluid-fluid interface at the contact line and the solid. On the basis of the static contact angle, the wetting ability of a fluid is determined as follows:

- $\theta_e = 0 \quad \rightarrow$ completely wetting
- $0 < \theta_e < 90° \quad \rightarrow$ partially wetting
- $\theta_e > 90° \quad \rightarrow$ non-wetting

In the cases considered here, water is always assumed to be the wetting phase with a contact angle that equals zero.
In a two-phase system, three interfacial tensions act, namely between the solid and the non-wetting phase γ_{sn}, between the non-wetting phase and the wetting phase γ_{wn}, and between the wetting phase and the solid γ_{sw} (see Fig. 2.2, left).

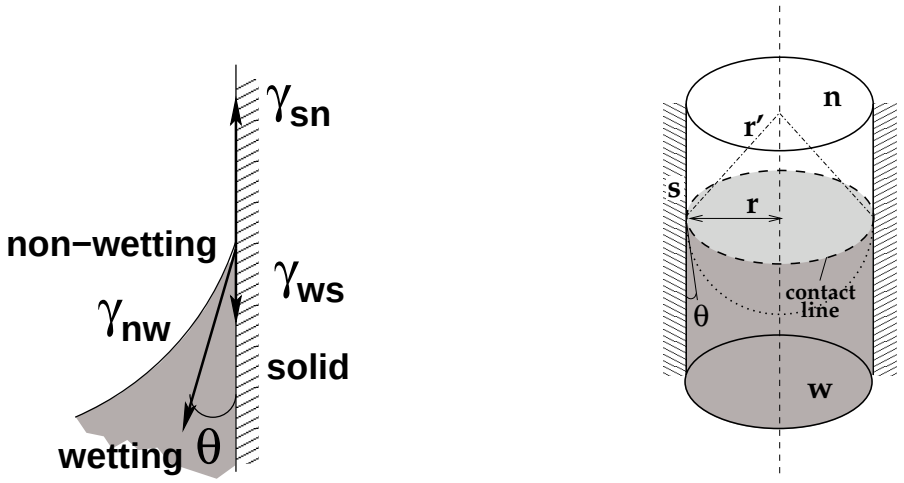

Figure 2.2: Illustration of YOUNG'S equation (left) and capillary pressure in a cylindrical tube (right)

On the basis of YOUNG'S equation [130]

$$\gamma_{wn} \cos\theta_s = \gamma_{sn} - \gamma_{sw} \ , \tag{2.4}$$

the equilibrium of forces parallel to the solid phase boundary can be assessed if gravity can be neglected. Forces perpendicular to the solid phase boundary, acting in the horizontal for a configuration as depicted in Fig. 2.2, left, are not examined here, and are considered negligible.
As indicated in Fig. 2.2, left, the interface between fluid phases can be curved. The curved shape indicates that a pressure difference between the pressure of the non-wetting phase P_n and the pressure of the wetting phase P_w exists, otherwise the interface would be planar. LAPLACE, 1806 [73] relates the difference in the pressures to the interfacial tension and the principal radii of curvature R_1 and R_2

$$\begin{aligned} P_n - P_w &= \gamma_{wn} \left(\frac{1}{R_1} + \frac{1}{R_2} \right) \\ &= P_c \ . \end{aligned} \tag{2.5}$$

The difference between the pressure of the non-wetting phase and the wetting phase is denoted the capillary pressure P_c. The principal radii of curvature can be obtained for any curved surface on the basis of two perpendicular planes (of which one must contain the surface normal) and their intersections with the interface [22]. For a (semi-) spherical interface, where $R_1 = R_2$ and $\frac{2}{R} = \frac{1}{R_1} + \frac{1}{R_2}$ Eqn. 2.5 simplifies to

$$P_c = \frac{2\gamma_{wn}}{R} \ . \tag{2.6}$$

The LAPLACE equation can also be derived with an example more closely related to two-phase flow in porous media. A pore can be idealised as a cylindrical tube with a radius r. If for example a glass tube is dipped vertically into water, water flows up the tube up to a given height and rests there. A meniscus between water and air forms (see Fig. 2.2, right)
The weight of the water ($\Pi r^2 h g \rho_w$) hangs on the contact line ($2\Pi r$) with the force ($\gamma_{wn} 2\Pi r$). The capillary rise h_c of the water in the tube can then be computed for a completely wetting water phase ($\theta_e = 0$, radius of curvature equals the radius of the tube) after

$$h_c = \frac{2\gamma_{wn}}{r \rho_w g} \ . \tag{2.7}$$

For partially wetting systems, Eqn. 2.7 can be recasted slightly. In these systems the radius of curvature r' of the interface can be related to the radius of the tube by $r' = \frac{r}{\cos\theta_e}$, which leads to

$$h_c g \rho = \frac{2\gamma_{wn} \cos\theta_s}{r} \ , \tag{2.8}$$

where the first term quantifies the influence of the hydrostatic pressure. The right side of the equation describes the normal drag of the interface.
The magnitude of the static contact angle depends on the chemical composition and the roughness of the solid surface. Moreover, some authors [63, 124] report a history dependence, a static hysteresis in the contact angle. According to these studies, the contact angle differs when established after drainage as compared to imbibition. In a drainage process, the wetting fluid is displaced by the non-wetting fluid whereas in imbibition the wetting fluid displaces the non-wetting.

Transient conditions On the pore scale, the movement of the interface between two fluids characterises transient conditions. YOUNG'S equation (2.4) can be rewritten, assuming that the balance of forces is also valid under transient conditions [15],

$$\gamma_{wn} \cos\theta_d = \gamma_{sn} - \gamma_{sw}, \tag{2.9}$$

where the **dynamic contact angle** θ_d is introduced. In laboratory experiments a deviation of the dynamic from the static contact angle has been observed. Consequently, at least one of the interfacial tensions in Eqn. (2.9) must deviate from its static value. Two phenomena may play a role on the pore scale: dynamic interfacial tension and dynamic contact angle.
Traditionally, the interfacial tension is measured with standard methods which assume that the interfacial tension at the time of the measurement is in thermodynamic equilibrium. However, **dynamic interfacial tension** has been described both in experimental (e.g. by SCHROTH ET AL., 1995 [97]) and in theoretical (e.g. by SHIKHMURZAEV, 1997 [103]) investigations.
Furthermore, a **dynamic contact angle** has been identified on the pore scale. It has been observed, that the dynamic contact angle increases for increasing velocity of the moving contact line during imbibition processes and decreases with increasing velocity in drainage processes. Several authors thus relate the dynamic contact angle to the pore scale capillary number on the basis of a non-linear function: see, for example, BLAKE ET AL.,1999 [15], FERMIGIER & JENFFER, 1991 [41], WEISLOGEL, 1997 [124], ZIMMERMANN, 1986 [132], and ZHOU & SHENG, 1990 [131]. The pore scale capillary number Ca_p quantifies the ratio of viscous to capillary forces

$$Ca_p = \frac{\mu_w v_p}{\gamma_{wn}}, \tag{2.10}$$

where v_p denotes a typical pore scale fluid velocity. Consequently, the dynamic contact angle reflects the influence of viscous forces on the capillary pressure. Moreover, a dependence of the dynamic contact angle on the radius of tube [83], solid surface roughness and heterogeneity of the solid surface [34] have been observed.
However, apart from predicting the trends, a quantitative calculation of the dynamic contact angle behaviour in a porous medium remains difficult for several reasons.

- Because of the complicated measurement of dynamic contact angles mostly only one interface in a simple geometry, such as single tube, is examined at a

time. The application of these findings to the complex geometry of the pore space of porous media has not been studied yet to my knowledge.

- The dynamic contact angle is strongly influenced by the physical and chemical surface properties of the solid, which are not known in detail on the local scale.
- In the imbibition experiments of ZIMMERMANN, 1986 [132] the dynamic contact angle with a pre-wetted solid surface is roughly three times smaller than for a dry solid surface (see also SHIKHMURZAEV,1996 [102]). Consequently, for estimations on the local scale, the wetting history would have to be known beside the wetting order.
- Fluid systems which are of interest here, e.g. water-air or water-DNAPL systems, have not been investigated yet to my knowledge.

Although a quantification of the effects of the dynamic contact angle for the local scale is not possible here, the following aspects deserve attention. In all the studies, the dynamic contact angle decreases in drainage processes and increases in imbibition processes with increasing velocity of the interface movement. On the assumption that

- interfacial tension can be considered constant,
- the radius of a given capillary tube does not change, and
- the LAPLACE equation (2.5) can be applied to transient processes,

the dynamic capillary pressure P_c^d for a cylindrical tube can be assessed with the dynamic contact angle. Following the observations above, P_c^d increases in a drainage process and decreases in an imbibition process with increasing flow velocity of the fluids' interface.

2.2.1.2 Capillarity at the local scale

When the REV concept is adopted and we proceed from the pore scale to the local and higher scales, it is assumed that the structure of the porous medium and the complicated distribution of the fluids does not need to be known in detail but that it can be captured by constitutive relationships. In the context of capillarity, the interaction between the fluid phases and the solid matrix is quantified by relating the wetting phase saturation to the (local scale) capillary pressure. In the following, this constitutive relationship, the **capillary pressure-saturation relationship** $P_c(S_w)$, is described for equilibrium conditions, where no saturation changes in time occur. In Sec. 3, approaches to account for effects from transient flow processes in this relation are introduced.
The traditional approaches quantifying capillarity on the local scale consist either of averaging of the fluids and their pressures, or of empirical approaches, also relating fluid saturation to a local scale capillary pressure. The concept of the relation between fluid saturation and capillary pressure is described by means of the

bundle of capillary tubes model. A finite number of parallel tubes with varying diameter is one of the simplest approximations of a porous medium. If gravity is neglected, the LAPLACE Eqn. (2.5) defines a threshold capillary pressure. Tubes with a radius larger than the radius corresponding to a capillary pressure are filled with non-wetting phase while all others are filled with wetting phase. The saturation (pertaining to this capillary pressure) of one of the fluid phases is defined by the ratio of the volume of that phase present in the tubes V_α to the volume of all the tubes V_t,

$$S_\alpha(\mathbf{x},t) = \frac{V_\alpha}{V_t}\,, \tag{2.11}$$

with the constraint

$$\sum S_\alpha = 1.0 \text{ with } \alpha \in \text{w,n}\,. \tag{2.12}$$

Saturation thus quantifies the ratio of the volume of a fluid averaged over an REV to the void volume averaged over this REV. In a porous medium, the void volume corresponds to the pore space. Here, S_w denotes the saturation of the wetting phase and S_n the saturation of the non-wetting phase. For various capillary pressures, the saturation might be computed, which yields data sets of P_c vs. S_w. In analogy to the pore scale, capillary pressure at the local scale is defined as the pressure difference between the phase pressures

$$P_c = P_n - P_w. \tag{2.13}$$

Obviously, the pore space of most porous media cannot be represented by a bundle of capillary tubes, as for example the tortuosity and connectivity of the pore space need to be accounted for. Nevertheless, the model illustrates how the transition from the pore to the local scale might be achieved.
As described for the pore scale, capillarity on the local scale might also be influenced by the direction of the process, also denoted hysteretic behaviour. Thus, for one porous medium, the $P_c(S_w)$ relationship measured during a drainage process might differ from the one measured during an imbibition process. In the following, the drainage and imbibition cycles usually determined in the laboratory are described.
When a fully water-saturated sample is drained by increasing the capillary pressure starting from 'A' in Fig. 2.3 the **primary drainage** curve is measured.
In most porous media, the water cannot be depleted completely from the porous medium even under high capillary pressures. Conceptually, the water phase under these conditions coats the solid phase with a thin film. In porous media where the wetting phase is completely wetting, the film always remains continuous as long as phase transitions into the non-wetting phase by evaporation can be neglected. If the contact angle of the wetting phase is larger than zero, the wetting phase can become discontinuous and applying a pressure gradient, e.g. through an external reservoir, would thus not reach all the fluid volume. The phase would no longer

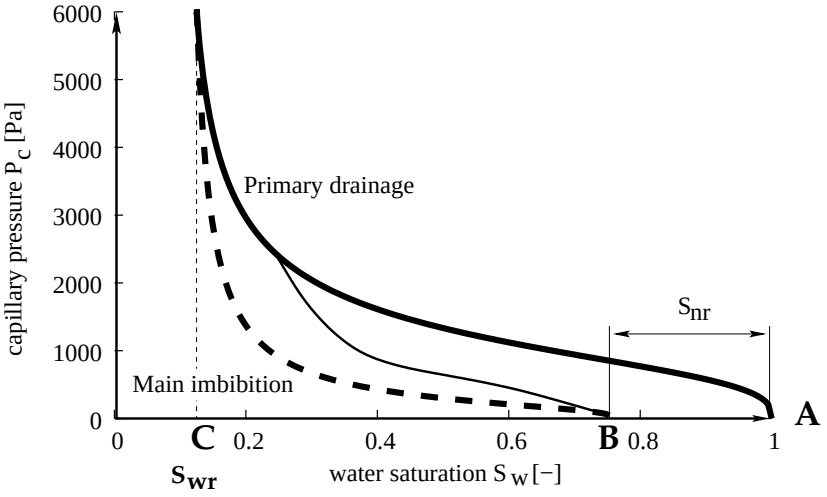

Figure 2.3: Schematic depiction of $P_c(S_w)$ relationships with hysteresis

flow coherently, if at all. The saturation of the wetting phase that cannot be reduced anymore, either because film flow is not considered or because discontinuous wetting phase occurs, is denoted the irreducible or residual wetting phase saturation S_{wr}. For $S_w \leq S_{wr}$, the wetting phase is considered as stagnant.

The following infiltration determines the **main imbibition** curve. Usually, as capillary pressure approaches zero, non-wetting phase is entrapped, e.g. due to snap-off or by-passing (see CHATZIS & DULLIEN, 1983 [25]), two pore scale processes explaining effects in the local scale $P_c(S_w)$ relationship. Thus, at zero capillary pressure, the wetting phase saturation does not reach full saturation (see point 'B' in Fig. 2.3). The volume fraction of non-wetting phase at $P_c = 0$ is denoted entrapped or residual non-wetting phase saturation S_{nr}. From there, the **main drainage** curve can be determined by again increasing the capillary pressure. If the capillary pressure is altered away from the endpoints marked with 'B' and 'C' (irreducible water saturation), the secondary scanning curves are observed.

Apart from the entrapped non-wetting phase, differences in capillary pressure at a given saturation between the drainage and the imbibition curves might be explained by pore scale processes, such as dynamic contact angle phenomena (compare Sec. 2.2.1.1) or the ink bottle effect (MILLER & MILLER, 1956 [80]).

Various approaches to determine data sets of P_c vs. S_w can be applied, e.g. laboratory experiments or theoretical methods. For the simulation of two-phase flow processes, it is desirable to apply an algebraic function relating the capillary pressure to the wetting phase saturation. In principle, data sets, if available, could also be used directly, applying spline functions of different orders to interpolate between the data sets.

In the scope of this thesis, two parametrisations of the equilibrium capillary pressure-saturation relationship are applied: the parametrisation after BROOKS & COREY, 1964 [19] and that after VAN GENUCHTEN, 1980 [114].

BROOKS & COREY, 1964 [19] developed an empirical relationship between the effective water saturation S_e and capillary pressure after

$$P_c(S_e) = P_d \, S_e^{-\frac{1}{\lambda}}, \tag{2.14}$$

$$\text{with } S_e = \frac{S_w - S_{wr}}{1 - S_{wr} - S_{nr}} \quad . \tag{2.15}$$

Their relationship is often applied to simulate primary drainage processes as it explicitly considers the entry pressure. The entry pressure P_d [Pa] relates to the radius and thus the capillary pressure of the largest accessible pore at which the non-wetting phase first infiltrates the porous medium. With the parameter λ [-], the pore size distribution might be assessed in a qualitative manner. For a large λ (usually $\lambda > 2.0$), the pore size distribution can be expected to be narrow, whereas the pore size distribution is broad for a small λ parameter.

The residual wetting phase saturation S_{wr} was originally derived as the wetting phase saturation which can be fitted to a straight line in a log-scale plot of the capillary pressure-effective water saturation plot.

COREY & BROOKS warn against over-interpreting the parameters in a physical sense, as they were originally derived as empirical fitting parameters [28]. The Fig. 2.4, left depicts two $P_c(S_w)$ relationships that were computed with their parametrisation.

In the VAN GENUCHTEN parametrisation

$$P_c(S_e) = \frac{1}{\alpha}(S_e^{-\frac{1}{m}} - 1)^{\frac{1}{n}} \, , \tag{2.16}$$

three parameters are employed to calculate the functional relationship between capillary pressure and the effective water saturation as defined by Eqn. (2.15). The parameter α [1/Pa] can be related to the inverse capillary pressure at a medium effective water saturation ($S_e = 0.5$). In the VAN GENUCHTEN model, the largest pore of the porous medium theoretically possesses an infinite radius whereas, in the BROOKS & COREY model, the radius of the largest accessible pore can be related to the entry pressure. The VAN GENUCHTEN parametrisation has the advantage that it is continuous for all water saturations.

The parameters n [-] and m [-] can be interpreted as relating to the pore size distribution. For uniform pore size distributions, the parameter n is small. In the literature the VAN GENUCHTEN n varies between smaller than one and sometimes larger than ten. Often, the VAN GENUCHTEN m is derived from the n after $m = 1 - 1/n$, as this leads to a closed-form expression for the relative permeability-saturation relationship after MUALEM, 1976 [82] (see Section 2.2.2). The right Fig. 2.4 depicts two $P_c(S_w)$ relationships that were calculated with the parametrisation after VAN GENUCHTEN.

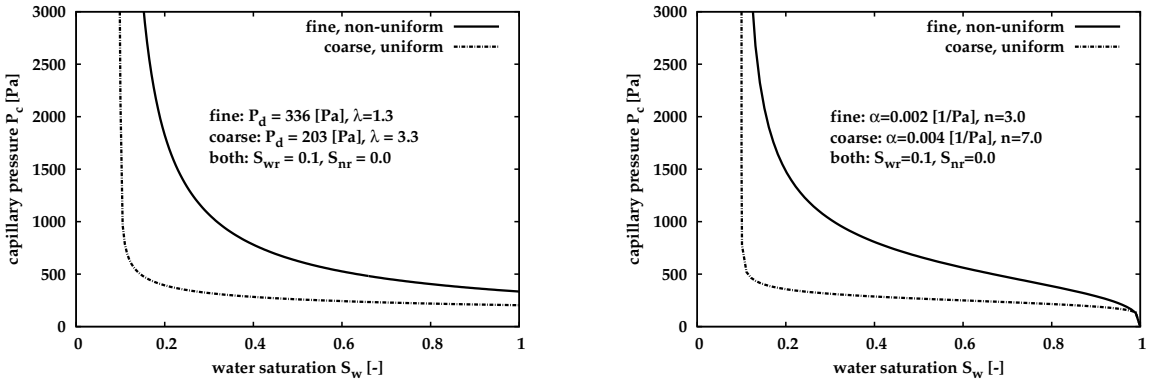

Figure 2.4: Parametrisation of the equilibrium $P_c(S_w)$ relationship after BROOKS & COREY, 1964 [19] (left) and VAN GENUCHTEN, 1980 [114] (right)

2.2.2 Relative permeability-saturation relationship

When two phases fill a porous medium, they influence the flow behaviour of one another because each occupies parts of the pore space which is then not available for the other phase. If the saturation of the wetting phase is for example reduced from full to partial saturation, the effective permeability for the wetting phase is decreased as well. The effective permeability for a phase K_α [L^2] is defined as the product of the intrinsic permeability [L^2] and the relative permeability of phase α

$$K_\alpha(S_\alpha) = K\, k_{r\alpha}(S_\alpha), \tag{2.17}$$

where the effective and the intrinsic permeability are treated as scalar functions, but could be tensors for an anisotropic porous medium [18]. While the intrinsic permeability is independent of the fluid saturation or the fluid properties, the relative permeability depends on it. Consequently, in most local scale applications, the $k_{r\alpha}(S_\alpha)$ relationships depend on the $P_c(S_w)$ relationship.
The two approaches presented here are based on the bundle of capillary tubes model. While BURDINE, 1953 [21] considered a model where the radii of the tubes vary only perpendicular to the flow direction, MUALEM, 1976 [82] derived the relative permeabilities for the extension of the bundle of capillary tubes model by CHILDS & COLLIS-GEORG, 1950 [26], where the radii additionally vary in the flow direction.
Originally, the following models were derived with no specific parametrisation of the $P_c(S_w)$ relationship in mind. Traditionally, the approach of BURDINE is mostly coupled to the parametrisation of the $P_c(S_w)$ relationship of BROOKS & COREY, 1964 [19]. The relative permeability for the wetting phase is then

$$k_{rw} = S_e^{\frac{2+3\lambda}{\lambda}}\,, \tag{2.18}$$

and for the non-wetting phase

$$k_{rn} = (1 - S_e)^2 (1 - S_e^{\frac{2+\lambda}{\lambda}})\,. \tag{2.19}$$

The progression of the relative permeability-saturation relationships is shown in Fig. 2.5 for the parameters applied to calculate the $P_c(S_w)$ relationship after BROOKS & COREY in Fig. 2.4. The curves illustrate that the relative permeability for the wetting phase decreases faster at high S_w compared to the decrease in k_{rn} for high S_n. This effect results from the wetting order. The non-wetting phase predominantly occupies the large pores whereas water retreats to the small pores.
VAN GENUCHTEN, 1980 [114] applied his $P_c(S_w)$ relationship to the model of MUALEM. He defines an analytical expression for the relative permeability for the wetting phase

$$k_{rw} = S_e^{\iota}[1-(1-S_e^{\frac{1}{m}})^m]^2, \tag{2.20}$$

and for the non-wetting phase

$$k_{rn} = (1-S_e)^{\iota}[1-S_e^{\frac{1}{m}}]^{2m}, \tag{2.21}$$

where the parameter ι is supposed to quantify a part of the tortuosity. For many soils $\iota = 0.5$ is a good estimate, thus this value is applied in all simulations here. The parameter m can be deduced from the n parameter of the $P_c(S_w)$ parametrisation after $m = 1.0 - 1.0/n$. The exponent ι was determined to equal $\iota = 0.5$ with 45 samples by MUALEM, 1976. In MUFTE-UG this value for ι is applied as default for the $k_{r\alpha}(S_\alpha)$ relationships, but may be varied as for example done in App. A.
Fig. 2.5 depicts the curve progression of the VAN GENUCHTEN / MUALEM model for the wetting and the non-wetting phase.

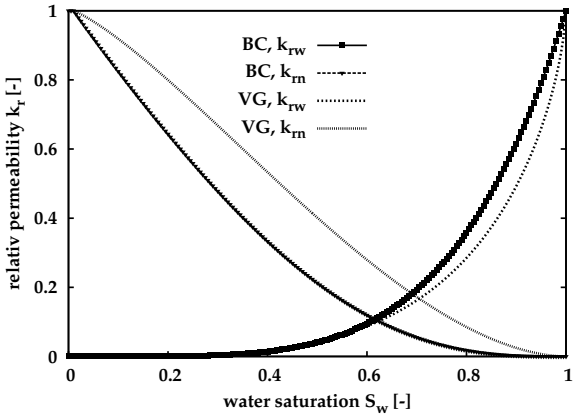

Figure 2.5: Parametrisations of the $k_{r\alpha}(S_\alpha)$ relationships after MUALEM, 1976 [82] and VAN GENUCHTEN,1980, and BURDINE, 1953 [21] and BROOKS & COREY, 1966 [20], parameters as given for the porous medium 'fine' in Fig. 2.4

Both models are sometimes applied independently of the $P_c(S_w)$ relationship when for example for an inverse problem the parameters for the constitutive relationships are fitted independently.

2.3 Conservation equations

In this thesis, the common approach to modelling two-phase flow in a porous medium on the local scale is adopted, where the mass conservation equation of a phase is solved. For the velocity of a phase, DARCY's law [31] is applied. In the following, first DARCY's law is introduced for a single phase, and then its extended form for two fluid phases. At the end of this section the mass conservation equations for two fluid phases are introduced.

2.3.1 DARCY's law for a single phase

In 1856, HENRY DARCY [31] published experimental results from which he defined the famous DARCY law, which is still applied today. On the basis of one-dimensional laboratory experiments on columns filled with fine sand and water as a fluid, DARCY discovered that the volumetric discharge Q [L^3T^{-1}] over the cross-sectional area of the column A [L^2] is determined by a linear law, relating the hydraulic conductivity k [LT^{-1}] to the difference in hydraulic head h [L] between two measurement points

$$Q = -Ak\frac{\Delta h}{\Delta l} \,. \tag{2.22}$$

The hydraulic head consists of two parts, the pressure head $^{p}/_{\rho\, g}$ and the elevation head z, which quantifies the potential energy per unit weight of fluid measured from a given reference point. Defining the ratio of Q to A as the DARCY velocity v and extending the approach to three dimensions gives the general DARCY equation

$$\mathbf{v} = -\mathbf{k}\nabla h \,, \tag{2.23}$$

where ∇ denotes the Nabla operator yielding the spatial gradient of the scalar function h. The hydraulic conductivity is considered a tensor; anisotropic properties of porous media can thus be taken into account. The hydraulic conductivity depends not only on the porous matrix but also on the fluid properties of a fluid α

$$\mathbf{k}_\alpha = \frac{\rho_\alpha g}{\mu_\alpha}\mathbf{K} \,. \tag{2.24}$$

The intrinsic permeability tensor $\mathbf{K}$ quantifies the inverse of the resistance of the porous matrix to the flow.
DARCY'S thus can be expressed more generally for single phase flow as

$$\mathbf{v}_\alpha = -\mathbf{k}_\alpha \nabla h_\alpha \,. \tag{2.25}$$

The validity of the DARCY equation is restricted to slow flow regimes. The REYNOLDS number

$$Re = \frac{v_s l \rho_\alpha}{\mu_\alpha} \,, \tag{2.26}$$

which quantifies the ratio of inertial to viscous forces, should not exceed one to ten, if the mean grain diameter of the porous medium is chosen for the characteristic length l (BEAR, 1972 [10]). In the REYNOLDS number the seepage velocity v_s is employed, which can be related to the DARCY velocity by $v = \phi\, v_s$. For larger REYNOLDS numbers, the linearity of the DARCY equation may no longer hold, and additional quadratic terms might need to be considered.

2.3.2 Two-phase flow

DARCY originally derived his law for a single-phase fluid system. Later on, an extension of the DARCY law (2.22) to multiphase systems was proposed based on experimental evidence (SCHEIDEGGER, 1974 [96]),

$$\mathbf{v}_\alpha = -\frac{k_{r\alpha}(S_\alpha)}{\mu_\alpha}\mathbf{K}\nabla(P_\alpha - \rho_\alpha g z)\,, \tag{2.27}$$

where $\mathbf{v}_\alpha$ denotes the DARCY velocity of phase α and $k_{r\alpha}$ the relative permeability of phase α depending on its saturation S_α. The concept of relative permeability is described in Section 2.2.2. The ratio of the relative permeability to the viscosity of the phase is often summarised as its mobility

$$\lambda_\alpha = \frac{k_{r\alpha}(S_\alpha)}{\mu_\alpha}. \tag{2.28}$$

2.3.3 Mass conservation

For the mathematical description of two-phase flow, the conservation of mass is of interest.
For a constant control volume in time and space, the mass balance of a fluid α over the volume G is given in differential form (valid in G) as

$$\frac{\partial \phi_\alpha \rho_\alpha}{\partial t} + \nabla\cdot\{\phi_\alpha \rho_\alpha \mathbf{v}_{s\alpha}\} - \rho_\alpha q_\alpha = 0\,, \tag{2.29}$$

where ϕ_α denotes the volume fraction of the pore space filled with fluid α, and $\rho_\alpha q_\alpha$ quantifies sources or sinks. Considering the definition of the saturation given in Eqn. (2.11), the effective porosity ϕ_α can be decomposed to $\phi_\alpha = S_\alpha \phi$. In addition, the average (often also defined as seepage) velocity $\mathbf{v}_{s\alpha}$ of a phase is related to the DARCY velocity $\mathbf{v}_\alpha$ by the effective porosity after $\mathbf{v}_\alpha = \mathbf{v}_{s\alpha}\phi_\alpha$. With these definitions, Eqn. (2.29) can be expressed as

$$\frac{\partial S_\alpha \phi \rho_\alpha}{\partial t} + \nabla\cdot\{\rho_\alpha \mathbf{v}_\alpha\} - \rho_\alpha q_\alpha = 0. \tag{2.30}$$

The time derivative in the accumulation term for the wetting phase can be reduced to part 1 of Eqn. (2.31) because the fluid phase and the porous medium are assumed

to be incompressible (Part 2 and 3 of Eqn. (2.31))

$$\frac{\partial S_\alpha \phi \rho_\alpha}{\partial t} = \overbrace{\phi \rho_\alpha \frac{\partial S_\alpha}{\partial t}}^{\text{Part 1}} + \overbrace{S_\alpha \phi \frac{\partial \rho_\alpha}{\partial t}}^{\text{Part 2}} + \overbrace{S_\alpha \rho_\alpha \frac{\partial \phi}{\partial t}}^{\text{Part 3}}. \tag{2.31}$$

For the non-wetting phase, compressibility may be taken into account. Inserting the extended DARCY's law after Eqn. (2.27) into the mass balance equation (2.30) for each phase leads to the continuity equation for the wetting phase

$$\phi \rho_\mathrm{w} \frac{\partial S_\mathrm{w}}{\partial t} - \nabla \cdot \{\rho_\mathrm{w} \lambda_\mathrm{w} \mathbf{K} \nabla (P_\mathrm{w} - \rho_\mathrm{w} g z)\} - \rho_\mathrm{w} q_\mathrm{w} = 0 \tag{2.32}$$

and the non-wetting phase

$$\phi \frac{\partial \rho_\mathrm{n} S_\mathrm{n}}{\partial t} - \nabla \cdot \{\rho_\mathrm{n} \lambda_\mathrm{n} \mathbf{K} \nabla (P_\mathrm{n} - \rho_\mathrm{n} g z)\} - \rho_\mathrm{n} q_\mathrm{n} = 0. \tag{2.33}$$

The two equations (2.32) and (2.33) are strongly coupled through the relative permeability-saturation relationships. The system of two equations with the four unknowns $S_\mathrm{w}, P_\mathrm{w}, S_\mathrm{n}, P_\mathrm{n}$ can be closed by the additional constraints for the sum of the saturations

$$S_\mathrm{w} + S_\mathrm{n} = 1.0\,, \tag{2.34}$$

and the traditional approach of defining capillary pressure as the difference between the phase pressures

$$P_\mathrm{c} \;=\; P_\mathrm{n} - P_\mathrm{w} \qquad \text{with} \quad P_\mathrm{c} = P_\mathrm{c}(S_\mathrm{w}), \tag{2.35}$$

where the capillary pressure is assumed to be a unique function of the water saturation. Consequently, the four primary variables can be reduced to two, e.g. the saturation of the non-wetting phase and the pressure of the wetting phase, which results in the balance equation for the wetting phase

$$-\phi \rho_\mathrm{w} \frac{\partial S_\mathrm{n}}{\partial t} - \nabla \cdot \{\rho_\mathrm{w} \lambda_\mathrm{w} \mathbf{K} \nabla (P_\mathrm{w} - \rho_\mathrm{w} g z)\} - \rho_\mathrm{w} q_\mathrm{w} = 0 \tag{2.36}$$

and the non-wetting phase

$$\phi \frac{\partial \rho_\mathrm{n} S_\mathrm{n}}{\partial t} - \nabla \cdot \{\rho_\mathrm{n} \lambda_\mathrm{n} \mathbf{K} \nabla (P_\mathrm{w} + P_\mathrm{c} - \rho_\mathrm{n} g z)\} - \rho_\mathrm{n} q_\mathrm{n} = 0\,. \tag{2.37}$$

The following assumptions are inherent to the balance equations (2.32) and (2.33) including DARCY's law [4]:

- Any inertial effects may be ignored for slow moving fluids (laminar flow).

- The momentum transfer by viscous shear is considered to be negligible; this is especially true for water-air systems with a high viscosity difference. Here, it is assumed that this holds for water-NAPL systems with low viscosity differences as well.
- Strictly speaking, the constitutive relationships between water saturation, capillary pressure and relative permeability are only valid for static or steady-state conditions.
- Gravity as the only external force acts in the vertical direction.
- Only NEWTONIAN fluids are considered, for which the velocity gradient is directly proportional to the shear stress.

It is assumed here that the DARCY law accounting for the flow velocity of a phase holds on all scales larger than the pore scale.
The conservation equations yielded by the mathematical model will be solved numerically and thus need to be discretised in space and time (see Ch. 4).

3 Framework: The extended capillary pressure-saturation relationship

In applications of two-phase flow on the local scale and the macroscale, a constitutive relationship between fluid saturation and capillary pressure is commonly employed. However, many studies in recent decades have shown non-uniqueness in the $P_c(S_w)$ relationship, which can either be attributed to a direction dependence (hysteresis, compare Sec. 2.2.1) or to a rate dependence, e.g. the rate of change of saturation or capillary pressure. Rate dependence is here considered and thus denoted as a dynamic effect.
In this chapter, laboratory and theoretical studies analysing dynamic effects in the local scale $P_c(S_w)$ relationship are reviewed. Non-uniqueness in the relative permeability-saturation relationship (see e.g. [40, 69, 93, 108, 110, 129]) is not studied. An extended $P_c(S_w)$ model, with which the non-uniqueness from rate dependence is overcome, is further investigated. With a dimensionless analysis the relevant scales and flow processes, where dynamic effects might be of importance are identified on the basis of the chosen model.

3.1 Introduction

To facilitate the comparison of various laboratory and theoretical studies, some definitions are introduced which will be applied in the subsequent chapters.
As described in Sec. 2.2.1, the equilibrium $P_c^e(S_w)$ relationship (see Fig. 3.1, left) can be determined for a two-phase system if saturation does not change in time. In order to determine such a relationship, an 'equilibrium experiment' can be employed, where only small changes of the boundary capillary pressure are applied to induce a saturation change (see Fig. 3.1, right). For example, in the pressure-cell experiment described in more detail in Sec. 5.3, the experiment to determine the equilibrium primary drainage $P_c^e(S_w)$ relationship starts with a fully water-saturated sample. Capillary pressure is increased at one boundary by a small augmentation of the pressure of an incompressible non-wetting phase (e.g. PCE), inducing an infiltration of this phase into the sample. While the side boundaries are closed, the opposite boundary allows an exfiltration of the water phase. The data sets of P_c and S_w (e.g. from point measurements) are determined once equilibrium conditions are attained. For the pressure-cell experiment this implies static conditions. In other set-ups, e.g. the flow-through cell (see Sec. 5.2), equilibrium conditions are reached at steady-state.
A dynamic $P_c^d(S_w)$ relationship is derived from a two-phase system where the rate

of change of saturation does not equal zero. In a '**dynamic experiment**', a high rate of change as well as a large change of pressure at the boundary induce a saturation change, and P_c as well as S_w are monitored and then plotted continuously (see Fig. 3.1, left).
Thus, for a given porous medium, one equilibrium and (in theory) an infinite number of dynamic $P_c(S_w)$ relationships can be established. As will be shown here, depending on the boundary conditions, a dynamic $P_c^d(S_w)$ relationship might differ from the equilibrium one. Thus, a non-uniqueness in the relation between capillary pressure and saturation evolves. Models which resolve this non-uniqueness are called extended capillary pressure-saturation relationships here.

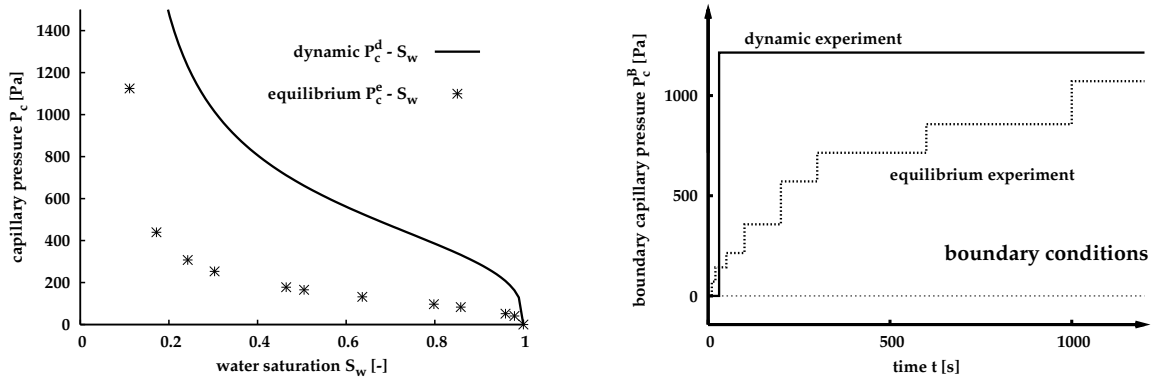

Figure 3.1: Illustration of equilibrium and dynamic $P_c(S_w)$ relationships (left) and the pertaining boundary conditions (right)

3.2 Review of laboratory studies

In this section, an overview of laboratory studies examining dynamic effects in the local-scale $P_c(S_w)$ relationship is given.
HASSANIZADEH ET AL., 2002 [52] amply review the literature on laboratory work. Some of the findings are repeated here for completeness, and the review is extended in some parts. Finally, more recent experimental investigations are addressed.
HASSANIZADEH ET AL., 2002 [52] summarise laboratory experiments aimed at examining dynamic effects in the $P_c(S_w)$ relationship by MOKADY & LOW, 1964 [81], WATSON, 1965 [120], DAVIDSON ET AL., 1966, [33], TOPP ET AL., 1967 [109], WATSON & WHISLER, 1968 [122], SMILES ET AL., 1971 [106], VACHAUD ET AL., 1972 [113], ELZEFTAWY & MANSELL, 1975 [40], STAUFFER, 1978 [108], WANA-ETYEM, 1982 [118], and KALAYDJIAN, 1992 [68]. Moreover, the authors cite literature, where the non-uniqueness of the $P_c(S_w)$ relationship is examined with respect to parameter identification, as in NÜTZMANN ET AL., 1994 [85], DURNER ET AL., 1996 [36], HOLLENBECK & JENSEN, 1998 [64], PLAGGE, 1999 [93], SCHULTZE ET AL., 1999 [100], and WILDENSCHILD ET AL., 2001 [129]. Only KALAYDJIAN, 1992 [68] used

water and oil, whereas all the other authors mentioned employed water and gas (air).
In summary, the overview of HASSANIZADEH ET AL., 2002 [52] yields the following findings:

1. Several authors performed experiments to determine the equilibrium (static and / or steady-state) as well as the dynamic $P_c(S_w)$ relationship with the same porous medium. They observed that the dynamic capillary pressure P_c^d exceeded the equilibrium one for drainage at a given saturation S_w [40, 64, 85, 106, 108, 109, 113, 118, 122, 129]. For imbibition, the dynamic P_c^d was found to be smaller than the equilibrium one [68, 106, 118] at a given saturation.

2. SMILES ET AL., 1972 as well as WANA-ETYEM, 1982 note that, for imbibition, the difference between the dynamic and equilibrium capillary pressure is smaller than for drainage.

3. WANA-ETYEM, 1982 [118] as well as WILDENSCHILD ET AL., 2001 [129] state that the deviation of the dynamic to the equilibrium $P_c(S_w)$ is not as pronounced for fine as for coarse porous media. In contrast, STAUFFER, 1978 [108] proposes that the dynamic effect (or, to be more precise, a coefficient in the extended $P_c(S_w)$ relationship) is inversely proportional to the permeability of the porous medium.

4. MOKADY & LOW, 1964 [81], and WATSON, 1965 [120] did not find a non-uniqueness in the $P_c(S_w)$ relationship.

In addition to the studies cited by HASSANIZADEH ET AL., 2002 [52], other studies are reviewed here. Although WATSON & WHISLER, 1968 [122] found pronounced dynamic effects in the $P_c(S_w)$ relationship, WATSON, 1968 [121] states that the dynamic $P_c^d(S_w)$ was based on the assumption that the gas pressure equals atmospheric pressure during the whole experiments. They disproved this assumption by additional measurements of the gas pressure, which was less than atmospheric pressure. Correcting the dynamic $P_c(S_w)$ relationship accordingly diminishes the dynamic effect pronouncedly.
VACHAUD ET AL., 1973 [112] examine the effects of gas pressure on the equilibrium and dynamic $P_c(S_w)$ relationship for a heterogeneous column with closed or perforated column walls consisting of two fine sand layers enclosing a coarse sand layer. The $P_c(S_w)$ relation of the coarse sand is measured, first assuming the gas pressure always equals atmospheric pressure and secondly applying the gas pressure measured within the sample. The authors chose two different types of experiment, one applying a constant flux at one boundary, and the other a drainage experiment where a gravity-induced flux prevailed. The findings of VACHAUD ET AL., 1973 [112] can be summarised as follows:

- For the constant flux experiment with closed walls, the P_c measurement that related to atmospheric pressure showed a change in capillary pressure although

no saturation change occurred. Measuring P_c that related to the gas pressure within the sample as well as both capillary pressure measurements of the constant flux experiment in the perforated column showed that changes in capillary pressure and saturation coincided. The discrepancy was also not observable for a smaller influx of water. The authors argue that at high influx rates the water front reaches the interface between the upper fine sand layer and the underlying coarse sand almost at full water saturation. Thus, the pore gas is compressed ahead of the front in the large pores of the coarse sand, where the capillary pressure but not the saturation thus changes.

- The $P_c(S_w)$ relationships measured for the gravity drainage showed a dynamic effect only if the closed-wall column and the measurement of $P_c(S_w)$ with atmospheric P_n are considered. Water can only drain from the coarse sand if the entry pressure of the fine sand is overcome and if gas can replace water. For the closed-wall column the first criterion is fulfilled before the second, whereas they are reached simultaneously for the open-wall column.

The work of STAUFFER, 1977, 1978 [107, 108] is mentioned here in some detail, as he not only performed laboratory experiments but also came up with an extended $P_c(S_w)$ relationship. He examined one-dimensional vertical drainage processes in three fine sand columns with water and gas (air) as fluids. Quasi steady-state experiments yielded the equilibrium and transient experiments the dynamic $P_c(S_w)$ relationship. STAUFFER measured the capillary pressure with a tensiometer, confirming with additional measurements that the gas pressure always remained at atmospheric pressure and the tensiometer thus yielded $P_c = -P_w$, where the atmospheric pressure is set to zero. STAUFFER finds a difference between the equilibrium and dynamic capillary pressure especially at high water saturations. In search of a functional relationship to account for the non-uniqueness he plotted the difference between the dynamic and the quasi steady-state capillary pressure as a function of a) the rate of change of saturation and b) the rate of change of capillary pressure. While the relationship in the first case seemed to be linear, it appeared to be non-linear in the second case. STAUFFER chose to concentrate on the linear dependence, proposing the empirical relationship

$$P_c^d - P_c^e(S_w) = -\tau_S \frac{\partial S_w}{\partial t}, \tag{3.1}$$

with the coefficient τ_S defined by

$$\tau_S = \frac{\alpha_S \mu_w \phi}{K\lambda} \left(\frac{P_d}{\rho_w g} \right)^2, \tag{3.2}$$

where $\alpha_S = 0.1$ denotes a constant scaling parameter. The coefficient τ_S can thus be calculated for a given porous medium and wetting fluid. The τ_S values of the fine sands examined by STAUFFER vary between $\tau_S = 2.7 \cdot 10^4$ Pa s and $\tau_S = 7.7 \cdot 10^4$ Pa s.

WEITZ ET AL., 1987 [125] determined experimentally dynamic capillary pressure as a function of the flow velocity for an imbibition process with water and oil in a porous medium, measuring the phase pressures continuously. At high flow velocities, P_c changes its sign due to an increase of the contact angle above 90°. They suggest

$$P_c(v) = \frac{\gamma_{wn}}{r}\left(-1 + S\,\mathrm{Ca}_p^b\right) , \tag{3.3}$$

where r denotes a mean pore radius of the porous medium, S a constant, Ca_p the pore scale capillary number as given in Eqn. (2.10), and b is a fitting parameter. In contrast to the studies mentioned in Sec. 2.2.1, where the contact angle is related to the pore scale capillary number for dynamic experiments with one glass tube, the authors here have applied a porous medium and tried to measure the phase pressures. Introducing for example the interfacial tension or a mean pore radius, they apply pore scale parameters to describe dynamic effects in a local scale capillary pressure.

HWANG & POWERS, 2003 [65] performed multi-step outflow experiments in a pressure-cell with three sets of boundary conditions for the same sample of a sandy soil, increasing the number of pressure steps as well as the time to allow equilibration of the sample. On the basis of an inverse parameter estimation employing a two-phase flow code, the authors observe a better confidence interval for the parameters derived from experiments applying a large number of pressure steps and allowing enough time for equilibration than for regressions on the basis of experiments with fewer and thus higher pressure steps and less time for equilibration. The authors attribute the difference in confidence to the narrow pore size distribution. In comparison to the slow experiment, the data from the fast experiment might lack information from medium water saturations where the $P_c(S_w)$ relationship is narrow.

TSAKIROGLOU ET AL., 2003 [110] performed transient displacement experiments with paraffin oil ($\mu_n = 0.026\,\mathrm{Pa\,s}$) and water on a transparent glass-etched planar pore-network. They obtained $P_c(S_w)$ and $k_{r\alpha}(S_\alpha)$ relationships on the basis of an inverse modelling approach with the traditional local-scale balance equations for two phases. The larger the capillary number, the higher was the dynamic P_c^d compared to the $P_c^e(S_w)$ determined at a low capillary number.

Many authors give physical explanations for the occurrence of dynamic effects. FRIEDMAN, 1999 [43] and WILDENSCHILD ET AL., 2001 [129] summarise the literature, like HASSANIZADEH ET AL., 2002 [52]. The summaries are reproduced here including additional remarks and the findings are categorised by pore and local scale effects, processes pertaining to imbibition or drainage and reasons relating to the experimental set-up.

On the **pore scale** the dynamic contact angle is often given as one reason for dynamic effects in a capillary tube, as already described in Section 2.2.1. The dynamic contact angle decreases with increasing drainage flow velocity and increases with increasing imbibition flow velocity. Consequently, a higher capillary pressure for drainage and

a lower capillary pressure for imbibition results compared to the equilibrium one. It should be noted, however, that for small contact angles as measured for water-air with respect to glass ($\theta_e < 20^\circ$ [132]), the effect on the drainage P_c is expected to be small [98]. Additionally, dynamic surface tension as described in Section 2.2.1 can play a role on the pore scale. Both effects can influence the dynamic capillary pressure in imbibition as well as drainage processes.
For **drainage** processes on the local scale, the continuity of the water phase might be questioned for dynamic processes.

- At high water saturations, large pores might drain fast and thus might cut off small pores when responding to a sudden capillary pressure increase (STAUFFER, 1977 [107]). VACHAUD ET AL., 1972 [113] observed increasing irreducible water saturations as well as augmenting deviations from the equilibrium $P_c^e(S_w)$ for large as compared to small rates of change in the boundary capillary pressure. For small pores to be hydraulically isolated, either the water phase needs to be discontinuous or an evolving film is too thin to facilitate measurable water flow. In both cases, the relative permeability of the water phase would be significantly reduced. In contrast, WILDENSCHILD ET AL., 2001 [129] state the relative permeability of the water phase to be higher in dynamic experiments at high water saturations than the values determined from equilibrium experiments. For decreasing water saturation a cross-over is observed and the dynamic k_{rw} is then less than the equilibrium one.

- At low water saturations, the water phase might become discontinuous if the contact angle is larger than zero (compare Sec. 2.2.1) and form pendular rings at the contacts between the grains of the porous medium. POULOVASSILIS, 1974 [94], TOPP ET AL., 1967 [109], and WANA-ETYEM, 1982 [118] argue that the size and redistribution of pendular rings depends on the rate of change of drainage and thus influences the $P_c(S_w)$ relationship.

For **imbibition**, the following processes have been identified:

- BARENBLATT ET AL., 2002 [7] argue that the non-sequential filling of the pores by the wetting fluid may cause dynamic effects. If water imbibes a pore at a higher capillary pressure than the YOUNG (2.4) and LAPLACE (2.5) equations predict, the dynamic P_c would be smaller at a given water saturation.

- Moreover, in imbibition processes, fingering due to the spatial pore size distribution can result in air entrapment, and thus an increase in the residual non-wetting phase compared to the equilibrium $P_c(S_w)$ relationship. Consequently, at a given saturation a lower capillary pressures for the dynamic case as opposed to the equilibrium one can be observed (e.g. DAVIDSON, 1966 [33]). This assumes that the entrapped non-wetting phase does not contribute to the capillary pressure or that within the entrapped phase the same pressure prevails as in the continuous non-wetting phase. Increasing air entrapment results in a larger residual non-wetting phase saturation S_{nr} in the $P_c(S_w)$ relationship.

Related to the **experimental set-up** and problems of inverse parameter identification the following aspects deserve attention:

- Water can be drained only if air can imbibe the porous media at the same time. If air access is limited, water cannot be drained effectively, resulting in higher water saturation under dynamic conditions. DAVIDSON, 1966 [33], ELRICK, 1963 [39], ELZEFTAWY & MANSELL, 1975 [40], SCHULTZE ET AL., 1999 [100], and VACHAUD ET AL., 1973 [112] describe problems of air availability. Especially, VACHAUD ET AL., 1973 [112] and SCHULTZE ET AL., 1999 [100] point out, that the dynamic effect in the $P_c(S_w)$ relationship is not pronounced if the drainage experiment is conducted with a column possessing perforated walls. VACHAUD ET AL., 1972 [113] report diminishing dynamic effects for decreasing initial water saturations.

- Capillary pressure in unsaturated flow is often derived from tensiometer measurements assuming that the air pressure equals atmospheric pressure. Several authors have shown for homogeneous as well as for heterogeneous porous media, that this assumption might not always hold (e.g. KNEALE, 1985 [69], SCHULTZE ET AL., 1999 [100], and WATSON, 1968 [121]). In contrast, SMILES ET AL., 1971 [106], STAUFFER, 1977 [107], and TOPP ET AL., 1967 [109] found P_n to equal atmospheric pressure during all of their experiments. These seemingly opposing results might be explained by a discontinuity of the air phase. Air pressure measurements might reach only the continuous part of the air phase, which can be at atmospheric pressure (SCHULTZE ET AL., 1999 [100]). However, in discontinuous parts of the air phase this might not be the case.

- Based on inverse parameter identification, the calculated equilibrium and dynamic $P_c(S_w)$ relations might differ for the same porous medium. Both NÜTZMANN ET AL., 1994 [85], and WILDENSCHILD ET AL., 2001 [129] argue that at least some part of the seemingly dynamic effects could be attributed to a lack of data for the $P_c(S_w)$ relationship if sudden pressure drops are applied to uniform porous media. In these kinds of medium, small capillary pressure changes can result in large saturation changes.

Moreover, SCHULTZE ET AL., 1999 [100] give thermodynamic energy changes due to a local reorganisation of water as one reason for dynamic effects.

In summary, measured or inversely determined capillary pressure-saturation relationships might be influenced by

- boundary conditions (and thus the rate of change of saturation or capillary pressure),
- sub-scale heterogeneity and resulting entrapment of the non-wetting phase, and
- the experimental set-up.

While the influence of the experimental set-up should be carefully assessed and a dependence of the $P_c(S_w)$ on it avoided, the impact of the first two items will also occur in the field or in the case of large pressure gradients, in technical applications. Not all the processes leading to dynamic effects in the $P_c(S_w)$ relationship can be quantified precisely as especially the pore scale processes are difficult to access. Nevertheless, these effects are observed and we need to deal with them on the local and higher scales. Thus, it is one aim of this study to examine the impact of including these effects on the flow behaviour on the local scale. If the parameters for an extended $P_c(S_w)$ relationship, like the parameter τ_S in STAUFFER's equation (see Eqn. (3.1)), can be determined, simulations including this extended $P_c(S_w)$ relationship can elucidate its influence on the simulated flow at the local scale.

3.3 Overview of theoretical studies

In this section, theoretical studies where dynamic effects in the $P_c(S_w)$ relationship play a role are presented. Whereas the first experimental studies analysing dynamic effects in the $P_c(S_w)$ relationship were performed in the 1960s (e.g. [81, 120]), the theoretical investigations appear about two decades later. In most of the laboratory work, the experiments were performed for water-air systems in sedimentary porous media, with a view to applications in soil or agricultural science. There, mostly the RICHARDS equation [95] is applied which assumes an infinite mobility of the gas phase. Only STAUFFER, 1978 [108] proposed an empirical model for capturing dynamic effects in water-gas flow. Most of the theoretical investigations presented here are concerned with two-phase flow as encountered in oil reservoir engineering, where predominantly water-oil fluid systems occur.
KALAYDJIAN, 1987 [67] sets up macroscopic balance equations of mass, momentum, energy and entropy for two incompressible, immiscible fluid phases and their interface as well as phenomenological equations on the basis of the theory of irreversible thermodynamic processes. Expressed here in terms of the wetting phase for a rigid porous medium, KALAYDJIAN, 1987 [67] proposes the relation

$$P_n - P_w - \frac{2}{R}\gamma_{wn} = -\tau_K \phi \frac{\partial S_w}{\partial t} \tag{3.4}$$

where R denotes the radius of a half-spherical interface between the wetting and the non-wetting phase. Thus, the model assumes a circular The left hand side can be interpreted as the difference between dynamic capillary pressure $P_c^d = P_n - P_w$ and the equilibrium capillary pressure, here $P_c^e = \frac{2}{R}\gamma_{wn}$. This difference is a function of the rate of change of saturation, multiplied by the porosity and the coefficient τ_K [$ML^{-1}T^{-1}$]. KALAYDJIAN, 1992 argues that the right-hand side can be seen as a measure for the distance from equilibrium. Thus, for large rates of change of saturation the system under consideration is far from equilibrium, while for example for very small saturation rates the system would be close to equilibrium. Also, a porous

medium possessing a large τ_K would be more prone to experience non-equilibrium effects than one with a small value. KALAYDJIAN, 1992 [68] performed laboratory experiments in order to gain insight into Eqn. (3.4) and to quantify the coefficient τ_K (see Sec. 3.2).

BARENBLATT and co-workers set up their model with BARENBLATT & GILMAN, 1987 [6], and further develop it in BARENBLATT ET AL., 1997 [5] as well as BARENBLATT ET AL., 2002 [7]. The authors develop a model for describing non-equilibrium effects for water-oil displacement or spontaneous countercurrent imbibition processes such as are often encountered in reservoir engineering. The authors argue that during these flow processes the fluids do not necessarily occupy the pores that they would occupy at an equilibrium state. To illustrate this point, during an imbibition process the water phase might infiltrate a pore that has a larger radius than the LAPLACE Eqn. (2.5) would predict for the prevailing capillary pressure. Then a redistribution process would take place. As long as the process time of the imbibition is on a much larger time scale than the redistribution time, these effects do not need to be taken into account. However, if for example at the front both time scales are of the same order of magnitude, BARENBLATT ET AL., 2002 suggest taking non-equilibrium effects into account.

While assuming that the equilibrium constitutive relationships still hold and can be measured for a given porous medium, the authors propose that they should not be evaluated at the actual wetting phase saturation occuring in the system but at an apparent saturation η. This implies that a value of η exists for which for example $k_{rw}(\eta)$ equals the non-equilibrium relative permeability of the water phase. Similarly, the relative permeability for the non-wetting phase and the $P_c(S_w)$ relationship can be treated. The apparent saturation η can be interpreted as the saturation at a given time in the future. Consequently, for an imbibition process the apparent wetting phase saturation would be higher than (or equal to) the actual saturation. It is assumed that η does not differ for all three constitutive relationships.

BARENBLATT ET AL., 2002 [7] suggest an empirical relation between the apparent and the actual saturation S_w

$$\eta - S_w = \tau_B \frac{\partial S_w}{\partial t} \,, \tag{3.5}$$

where τ_B [T] denotes a constant redistribution time. Thus, the adjustment between the apparent saturation and the actual saturation depends on the rate of change of saturation.

The authors then describe the mathematical model, the conservation equations for two phases, where the saturation formulation is applied for incompressible and immiscible fluids (compare HELMIG, 1997 [59]).

BOURGEAT & PANFILOV, 1998 [16] apply the homogenisation theory to upscale two-phase conservation equations for mass including the extended DARCY's law for a porous medium with periodic heterogeneities. These authors thus start the averaging on the local scale and do not scale up from pore scale equations. In contrast to the two models just presented, these authors take heterogeneity on the local scale

into account. The heterogeneity pattern consists of a coarse background material with embedded fine lenses. For the limit, when the ratio ε of the small scale length l (comprising of one cell with a fine lense embedded in the coarse sand) to the large scale L (the system length) approaches zero, upscaled balance equations can be derived for the periodic medium by formal asymptotic expansion. One of the relations BOURGEAT & PANFILOV, 1998 obtain is given by

$$\mathrm{Pe}^{-1} P_c^{\mathrm{co}}(S_w^{\mathrm{co}}) - P_c^{\mathrm{fi}}(S_w^{\mathrm{fi}}) = -\tau_*(S_w^{\mathrm{fi}}) \frac{\partial S_w^{\mathrm{co}}}{\partial t_*} \,, \tag{3.6}$$

where co marks quantities from the coarse, fi from the fine material and $t_* = {}^{t}/_{t_c}$ denotes a dimensionless time that is scaled by a characteristic time $t_c = {}^{(\phi^{\mathrm{co}} \mu_n L^2)}/_{(K^{\mathrm{co}} \Delta P)}$. The relation is multiplied by the inverse of the PECLET number Pe, defined as the ratio of the viscous pressure drop ΔP to a typical equilibrium capillary pressure of the fine material. BOURGEAT & PANFILOV, 1998 interpret τ_* as a capillary relaxation time being a function of the saturation in the fine material, and thus the mobilities of the two phases within the fine material and the ratios of the two permeabilities and porosities as well as on the expansion parameter ε. For spherical lenses, they obtain an explicit formula for the capillary relaxation time. For unit viscosities and $k_{rw}(S_w) = S_w^2$ and $k_{rn}(S_n) = S_n^3$, the function τ_* has a minimum at $S_w \sim 0.4$ and tends to infinity at $S_w \to 1.0$ and $S_w \to 0$. The authors explain that, during an imbibition process, counter-current flow will occur when the wetting phase infiltrates the fine lenses. When either of the phases is at a very low saturation, its relative permeability is also small, which makes the flow processes very slow and thus lets the capillary relaxation time tend to infinity. The model by BOURGEAT & PANFILOV, 1998 will not be pursued in the following as it is restricted to a porous medium with periodic heterogeneities, and the focus here is on porous media which might be homogeneous on the local scale.

Dynamic effects are often described in relation to relaxation processes, as for example BARENBLATT and co-workers have done. Their coefficient τ_B thus possesses the unit of time. A different approach to taking relaxation processes into account is double porosity or double continua models. For these models, it is assumed that the considered domain consists of two porous media with properties which differ distinctly. Conceptually, if such a domain were drained, the connected coarse parts would drain first and subsequently the fine parts would drain, indicating two different time scales. The interaction between the two parts needs to be described by exchange terms. Double porosity or double continua models are commonly applied to represent fractured porous media, but are also used in soil physics in an attempt to capture relaxation effects, cf. SIMUNEK ET AL., 2001 [105]. LEWANDOWSKA ET AL., 2004, 2005 [75, 76] apply a homogenisation theory for a double porosity approach and can also reproduce relaxation effects with the upscaled model.

This thesis focusses on dynamic effects in the $P_c(S_w)$ relationship without making assumptions about the heterogeneity of the porous medium. Approaches that use the homogenisation theories are thus not analysed. The model of BARENBLATT has already been examined intensively. It also includes dynamic effects in the relative

permeability, which are beyond the scope of this thesis.
In the following section, the investigations of HASSANIZADEH AND GRAY, 1990, 1993 [55, 56] are described in some detail. Their model is then compared to those of STAUFFER, 1978 [108] and KALAYDJIAN, 1992 [68] (see Sec. 3.5).

3.4 The extended $P_c(S_w)$ relationship after HASSANIZADEH & GRAY

In a series of papers, HASSANIZADEH & GRAY, 1979, 1979A [53, 54] HASSANIZADEH, 1986 [51], and GRAY & HASSANIZADEH, 1989 [48] derive local scale balance equations for two fluid phases, the solid phase and the interfaces between them from microscopic balance laws by volume averaging. In contrast to the conceptual model introduced in Ch. 2, in which interfaces between the fluids are not taken into account on the local scale, the interfaces are here also considered on the local scale. The balance equations include the conservation of mass, momentum, energy and entropy. HASSANIZADEH & GRAY, 1990 [55] define constitutive relationships on the local scale to close the large system of equations. They choose the independent, primary variables, and determine constitutive relationships for the dependent variables while keeping in mind that the structure evolving from the interfaces should also be captured on the local scale. Each of the dependent variables could depend on the independent variables. The authors then apply the COLEMAN & NOLL [27] method to diminish the dependencies. This method defines the restrictions on the constitutive relationships resulting from the postulation that neither the conservation law nor the second law of thermodynamics must be violated. The second law of thermodynamics, the entropy inequality, prescribes that the entropy production of reversible processes should be zero and the one of irreversible processes larger that zero. The authors state that the product of the material time derivative of the water saturation $\dot{S_w}$ and the difference between the phase pressures to the capillary pressure contributes to the entropy production if

$$-\dot{S_w}[P_n - P_w - P_c] \geq 0\,. \tag{3.7}$$

As a first approach, the authors suggest using the linearised relation

$$\dot{S_w} = -\frac{1}{\tau_{HG}}[P_n - P_w - P_c]\,. \tag{3.8}$$

The coefficient τ [$ML^{-1}T^{-1}$] now introduced needs to be non-negative to satisfy the entropy inequality. The authors suggest that it might be a function of

$$\tau_{HG} = f(\rho_\alpha,\, \phi,\, S_w,\, a_{wn},\, \rho_{IF},\, T)\,, \tag{3.9}$$

where a_{wn} denotes the interfacial area between the two fluid phases, and ρ_{IF} a mass allocated to this interface. Considering the requirement that τ is non-negative, the entropy inequality is satisfied if

$$P_n - P_w - P_c^e > 0 \wedge \dot{S_w} < 0 \quad \text{or} \quad P_n - P_w - P_c^e < 0 \wedge \dot{S_w} > 0\,. \tag{3.10}$$

The relationship between the saturation rate and the difference in pressures is illustrated in Fig. 3.2. As stated in Eqn. 3.10, the entropy inequality is only fulfilled if the product of the rate of change of saturation and the capillary pressure difference is not negative (indicated by the projected areas marked 'drainage' and 'imbibition' in Fig. 3.2, left).
The material time derivate as defined by HASSANIZADEH & GRAY, 1990 can be reduced to the partial time derivative for a non-deforming porous medium (HASSANIZADEH ET AL., 2002 [52]). Eqn. (3.8) thus simplifies to

$$P_{\mathrm{n}} - P_{\mathrm{w}} - P_{\mathrm{c}}^{\mathrm{e}} = -\tau_{\mathrm{HG}} \frac{\partial S_{\mathrm{w}}}{\partial t} \,. \tag{3.11}$$

If the phase pressure difference is denoted the dynamic capillary pressure and the equilibrium capillary pressure is interpreted as a function of wetting phase saturation, the equation can be expressed as

$$P_{\mathrm{c}}^{\mathrm{d}} - P_{\mathrm{c}}^{\mathrm{e}}(S_{\mathrm{w}}) = -\tau_{\mathrm{HG}} \frac{\partial S_{\mathrm{w}}}{\partial t} \,, \tag{3.12}$$

where it is assumed that the equilibrium capillary pressure depends only on the water saturation. In the following, Eqn. (3.12) is compared to the other models presented in Sec. 3.3 and arising questions are posed.

3.5 Open questions related to the extended $P_{\mathrm{c}}(S_{\mathrm{w}})$ relationship

In Sec. 3.2 to Sec. 3.4, various models for capturing dynamic effects in the local-scale $P_{\mathrm{c}}(S_{\mathrm{w}})$ relationship are described. Although the empirical model by STAUFFER, 1978 [108] and the theoretical models by KALAYDJIAN, 1987 [67] and HASSANIZADEH & GRAY, 1990 [55] differ in some respects, they also show similarities.
On the assumption that the dynamic capillary pressure as applied by STAUFFER, 1978 can be interpreted as the pressure difference between the phase pressures (under equilibrium and dynamic conditions), the relation proposed by STAUFFER, 1978 as given in Eqn. (3.1) resembles that proposed by HASSANIZADEH & GRAY, 1990 as given in Eqn. 3.13 for a non-deformable solid phase. The same holds for the relation suggested by KALAYDJIAN, 1987 [67] as given in Eqn. (3.4) (assuming for example that $\tau_{\mathrm{HG}} = \tau_{\mathrm{K}} \cdot \phi$), although KALAYDJIAN restricts the definition of the equilibrium capillary pressure to spherical interfaces between the two fluid phases. The approaches differ in their definition of the (upscaled) phase pressures. Yet they all define a difference between a dynamic and an equilibrium capillary pressure as a linear function of the rate of change of saturation, all introducing a coefficient with the units $[\mathrm{ML}^{-1}\mathrm{T}^{-1}]$.
In the following, the general definition of the extended capillary pressure saturation relationship

$$P_{\mathrm{n}} - P_{\mathrm{w}} - P_{\mathrm{c}}^{\mathrm{e}}(S_{\mathrm{w}}) = P_{\mathrm{c}}^{\mathrm{d}} - P_{\mathrm{c}}^{\mathrm{e}}(S_{\mathrm{w}}) = -\tau \frac{\partial S_{\mathrm{w}}}{\partial t} \tag{3.13}$$

is applied for the analysis of dynamic effects on the local to macro scale in homogeneous or heterogeneous porous media. For the coefficient τ it is assumed that

$$\tau = \tau(S_w) \tag{3.14}$$

The difference between the dynamic and the equilibrium capillary pressure ΔP_c will also be denoted difference in capillary pressure here. The term 'rate of change of saturation' can be abbreviated to saturation rate. For illustration, the extended $P_c(S_w)$ relationship is plotted for drainage conditions for a constant τ value (see Fig. 3.2). For imbibition, it is expected that the dynamic capillary pressure at a selected saturation remains smaller than the equilibrium capillary pressure, otherwise Eqn. (3.10) would be violated. The extended $P_c(S_w)$ relationship predicts that the

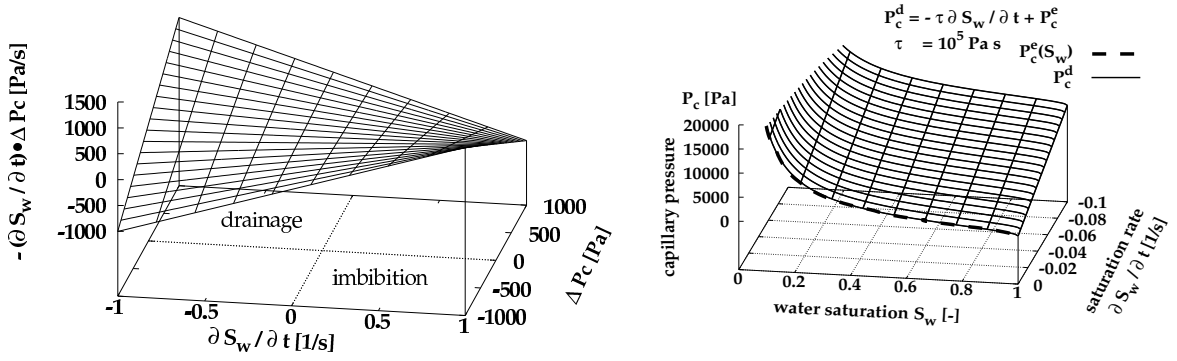

Figure 3.2: Plots of the 'entropy inequality' for the extended $P_c(S_w)$ relationship (left) and of the linearised, extended $P_c(S_w)$ relationship (right) with $\Delta P_c = P_c^d - P_c^e$

equilibration of the pressure difference between the phase pressures and the equilibrium capillary pressure depends on the rate of change of saturation. The coefficient τ can be interpreted as a measure how fast this equilibration takes place (considering a constant saturation rate), keeping in mind that it has the units $[ML^{-1}T^{-1}]$ and not the ones of a time. If the saturation rate is small, only a small deviation of the dynamic from the equilibrium capillary pressure is expected. Thus, in the limit of capillary-dominated flow, the consideration of an extended $P_c(S_w)$ relationship should be obsolete. Generally speaking, it is assumed that a process is damped more strongly for a larger coefficient than for a small coefficient. The magnitude of the coefficient is expected to depend on porous medium and fluid properties and the saturation, but other functional forms such as a dependence on the rate of change of saturation might also be possible.
The following aspects of the extended $P_c(S_w)$ relationship require analysis. The investigation into the relationship is carried out following the assumptions that isothermal conditions prevail and that the porous medium behaves rigidly (compare Ch. 2).

1. Can scales or processes be identified where the extended relationship needs to be taken into account? As the balance equations including the extended

relationship are more difficult to solve compared to applying the traditional closure condition after Eqn. 2.35 and an additional parameter needs to be determined, it is desirable if the applications were limited.

2. Does the linearisation of the term in the entropy inequality hold? HASSANIZADEH & GRAY, 1990 linearised the term, assuming that a linearisation is admissible for conditions near enough to equilibrium. However, they mention that this assumption needs to be verified by experiments.

3. How can one determine the magnitude of the coefficient τ and possible dependences? There are several studies which attempt to quantify it either in laboratory experiments or based on numerical approaches; these are described in Sec. 5.1. HASSANIZADEH & GRAY, 1990 suggest that τ might for example be a function of the wetting phase saturation or the fluid density. However, they do not define the functional relationship. STAUFFER has suggested an empirical formula, with which the coefficient for a given porous medium (and a water-gas fluid system) might be calculated on the basis of the properties of water, the porous medium and the BROOKS & COREY parameters for the equilibrium $P_c(S_w)$ relationship. Up to now, STAUFFER's formula has not been verified.

4. If the extended $P_c(S_w)$ relationship is applied to close the two-phase balance equations instead of the traditional, unique $P_c(S_w)$ relationship, how does this effect the results of simulations?

Within this thesis, some of these questions are addressed. By means of a dimensional analysis, relevant scales and processes are identified, for which the extended relationship should be considered in simulations. Moreover, the magnitude of the coefficient is determined on the basis of laboratory and numerical experiments applying the two-phase module of MUFTE-UG. The results also offer insight into the admissibility of the linearisation. Finally, simulations including the extended relationship are presented and analysed.

3.6 Dimensional analysis

In order to assess the dominating forces within a two-phase system, a dimensional analysis can be employed. For a dimensional analysis with the two-phase balance equations including the DARCY law and the traditional $P_c(S_w)$ relationship (see Eqn. (2.35)), the investigations of HILFER, 1996 [61], HILFER & ØREN, 1996 [62] and ANTON & HILFER, 1999 [1] can be consulted. Here, a dimensionlal analysis is performed applying the extended $P_c(S_w)$ relationship after Eqn. (3.13) to close the system of balance equations for a homogeneous porous medium and two fluid phases. Making the balance equations dimensionless allows the definition of dimensionless numbers. In addition to the traditional ones as for example described by HILFER

& ØREN, 1996, a new number appears, with which the influence of dynamic effects can be evaluated. On the basis of chosen examples, dimensionless ratios are calculated and interpreted.

To start with, the primary variables are chosen, i.e. the pressure of the wetting phase P_w and the saturation of the non-wetting phase S_n (compare Sec. 2.3.2). The requirement that the sum of the saturations should equal one (see Eqn. (2.12)) and the extended $P_c(S_w)$ relationship are applied to close the balance equations. This leads to the balance equation for an incompressible non-wetting phase

$$\phi \frac{\partial S_n}{\partial t} = \nabla \cdot \left\{ \frac{k_{rn}(S_n)}{\mu_n} K (\nabla [P_w + P_c + \tau \frac{\partial S_n}{\partial t}] - \rho_n g \nabla z) \right\} , \tag{3.15}$$

where the source/sink term is zero and the coefficient τ is assumed to be constant. As the balance equation for the wetting phase is not altered by the application of the extended $P_c(S_w)$ relationship, it will be neglected in the following. To rewrite Eqn. (3.15) in dimensionless form the definitions

$$\widehat{z} = \frac{z}{l_c} , \tag{3.16}$$

$$\widehat{\nabla} = \nabla l_c , \tag{3.17}$$

$$\widehat{t} = \frac{t}{t_c} , \tag{3.18}$$

$$\widehat{P_w} = \frac{P_w}{P_{cc}} , \quad \text{and} \tag{3.19}$$

$$\widehat{P_c} = \frac{P_c}{P_{cc}} . \tag{3.20}$$

are introduced, where t_c is a characteristic time and l_c a characteristic length. Note that the characteristic length is introduced in order to non-dimensionalise the spatial derivatives, e.g. the gradients in the balance equation. Thus, an interpretation of the characteristic length scale should relate for example to a distance over which a characteristic pressure drop occurs. Characteristic time and length are assumed to relate through the characteristic velocity through $u_c = \phi l_c / t_c$. The characteristic time scale thus relates to the advective processes. Note, that by linking these three characteristic magnitudes only two of them can be considered as independent.

The phase pressure and the capillary pressure are normalised with the characteristic capillary pressure P_{cc}, which can for example be derived from the mid-point of the equilibrium $P_c(S_w)$ relationship [1]. Alternatively, the entry pressure of the equilibrium $P_c(S_w)$ relationship after BROOKS & COREY can be chosen [17]. A hat marks the dimensionless quantities. With the definitions given in Eqn. (3.16) to Eqn. (3.20) Eqn. (3.15) can be expressed as

$$\frac{\partial S_n}{\partial \widehat{t}} = \widehat{\nabla} \cdot \{ k_{rn}(S_n) \frac{\mu_w}{\mu_n} [\frac{K P_{cc}}{\mu_w u_c l_c} (\widehat{\nabla} \widehat{P_w} + \widehat{\nabla} \widehat{P_c}) + \frac{K \tau}{\phi \mu_w l_c^2} \widehat{\nabla} \frac{\partial S_n}{\partial \widehat{t}} - \frac{\rho_n}{\rho_w} \frac{\rho_w g K}{\mu_w u_c} \widehat{\nabla} \widehat{z}] \} . \tag{3.21}$$

The (traditional) dimensionless numbers can now be defined as

$$\mathrm{Ca} = \frac{\mu_\mathrm{w} u_\mathrm{c} l_\mathrm{c}}{K P_\mathrm{cc}} = \frac{\text{viscous forces}}{\text{capillary forces}}, \quad \text{and} \tag{3.22}$$

$$\mathrm{Gr} = \frac{\rho_\mathrm{w} g K}{\mu_\mathrm{w} u_\mathrm{c}} = \frac{\text{gravitational force}}{\text{viscous force}}\,, \tag{3.23}$$

where Ca denotes the capillary and Gr the gravity number. While the enumerator and denominator of the capillary number have the units of a force, in the gravity number they have force per length. Additionally, a new dimensionless number appears for the second term on the right-hand side, namely the dynamic number

$$\mathrm{Dy} = \frac{\text{dynamic capillary force}}{\text{viscous force}} = \frac{K\tau}{\phi \mu_\mathrm{w} l_\mathrm{c}^2}\,. \tag{3.24}$$

In the dynamic number, the units MLT^{-1} in the enumerator and denominator need to be extended by the inverse of time in order to yield the units of a force.
According to Eqn. (3.24), the dynamic number Dy does not depend on the characteristic velocity. This is contrary to the assumption that dynamic effects should not play a role for very slow processes independent of the fluids and the porous medium. The characteristic flow velocity might however be reintroduced into the equation by applying $l_\mathrm{c} = {u_\mathrm{c} t_\mathrm{c}}/{\phi}$.
Now, the dimensionless balance equation can be formulated as

$$\frac{\partial S_\mathrm{n}}{\partial \widehat{t}} = \widehat{\nabla} \cdot \{ k_\mathrm{rn}(S_\mathrm{n}) \frac{\mu_\mathrm{w}}{\mu_\mathrm{n}} (\mathrm{Ca}^{-1} (\widehat{\nabla} \widehat{P_\mathrm{w}} + \widehat{\nabla} \widehat{P_\mathrm{c}}) + \mathrm{Dy} \widehat{\nabla} \frac{\partial S_\mathrm{n}}{\partial \widehat{t}} - \frac{\rho_\mathrm{n}}{\rho_\mathrm{w}} \mathrm{Gr} \widehat{\nabla} \widehat{z}) \}\,. \tag{3.25}$$

Further insight can be gained by relating the various dimensionless numbers. Thus, for example, defining the ratio of the dynamic number to the inverse of the capillary number yields the dimensionless number DyC

$$\mathrm{DyC} = \frac{Dy}{Ca^{-1}} = \frac{K\tau}{\phi \mu_\mathrm{w} l_\mathrm{c}^2} \frac{\mu_\mathrm{w} u_\mathrm{c} l_\mathrm{c}}{K P_\mathrm{cc}} = \frac{u_\mathrm{c} \tau}{P_\mathrm{cc} l_\mathrm{c} \phi} = \frac{\text{dynamic capillary force}}{\text{equilibrium capillary force}}\,, \tag{3.26}$$

which is interpreted as the ratio of influences stemming from dynamic capillary effects in the numerator to the equilibrium capillary influence in the denominator. The units in the ratio of FL^{-1} quantify a force per length. The numerator and the denominator would have to be extended by a characteristic length in order to obtain a force only. Nevertheless, the term force will be applied in the following related to the terms in the ratio of DyC.
If the characteristic velocity u_c in Eqn. (3.26) is replaced by $u_\mathrm{c} = {\phi l_\mathrm{c}}/{t_\mathrm{c}}$, DyC becomes

$$\mathrm{DyC} = \frac{\tau}{t_\mathrm{c} P_\mathrm{cc}}\,. \tag{3.27}$$

With this reformulation, one may conclude that the influence from the dynamic effects is large for small time scales or small equilibrium capillary pressures. In the

limit of no capillary forces ($P_{cc} \to 0$), the dimensionless number DyC tends to infinity. In the balance equation (3.15), the second term of the advective right hand side vanishes, but the dynamic term remains. An interpretation of the resulting balance equation is difficult, as the derivation of the extended $P_c(S_w)$ relationship relies on the presence of capillary forces. To overcome this problem, τ can be interpreted as a function of capillary pressure decreasing to zero when capillary pressure is zero.
The ratio of the dynamic number Dy to the gravitational number Gr results in

$$DyG = \frac{Dy}{Gr} = \frac{K\tau}{\phi\mu_w l_c^2} \frac{\mu_w u_c}{\rho_w g K} = \frac{\tau u_c}{\phi l_c^2 \rho_w g} = \frac{\text{dynamic capillary force}}{\text{gravitational force}} , \tag{3.28}$$

where again a ratio of force per length is defined. Similar to the number Dy, the ratio of the forces would be scale-independent if the coefficient τ scaled with length squared.
In the following, calculations of the new dimensionless numbers Dy, DyC and DyG for different porous media help to assess at which characteristic lengths or flow velocities dynamic effects need to be considered. For this analysis, it is assumed that the soil parameters like the permeability and the porosity are known and constant for a given porous medium. The τ values for three different porous media are calculated using Eqn (3.2) proposed by STAUFFER, 1977 [107] (see Tab. 3.1), which assumes that the coefficient τ is a soil property independent of length scale, saturation or rate of change of saturation. The STAUFFER formula introduces a correlation between the permeability, the equilibrium capillary pressure (here $P_d = P_{cc}$), and the coefficient τ. Substitution of Eqn. (3.2) in Eqn. (3.24) results in a relationship for Dy that is independent of permeability

$$\mathrm{Dy} = \frac{\alpha_S}{\lambda l^2} \left(\frac{P_d}{\rho_w g}\right)^2 . \tag{3.29}$$

This equation implies, if all other parameters remain constant, that for fine porous media with a high entry pressure dynamic effects are important. This is a consequence that still needs to be verified.
When the values of τ given in Tab. 3.1 are compared, it is striking that magnitudes vary over five orders of magnitude. Such a behaviour is not observed in any of the other parameters. Whether these ranges in τ are realistic needs to be verified experimentally.
In the following, it is assumed that an equilibrium of forces is attained at a ratio equalling one. With an extension all numbers could have the unit of a force but the extension would cancel out.
In Tab. 3.1, the characteristic flow velocity u_c at the balance of equilibrium and dynamic effects DyC = 1 at a characteristic length of one metre as well as the magnitude of the dynamic number Dy for a characteristic length of 0.1 m are given for different porous media; the parameters such as permeability and porosity are taken from the literature.
The balance of equilibrium and dynamic forces (DyC = 1) is attained at $u = 0.23\,\mathrm{m/s}$ for the coarse sand CS, a velocity that is not usually observed in two-phase flow in

the unsaturated zone or groundwater remediation. However, in technical applications such as paper production, high flow velocities may be attained. For the porous media, where τ is derived on the basis of Eqn. (3.2), trends can be determined from the analysis: the finer the porous medium, the smaller the characteristic velocity u_c at which dynamic and viscous forces balance each other. If the coefficient τ is determined independently by a laboratory experiment, this trend is not necessarily confirmed. For Sand 1, the permeability equals that of CS, but Dy is four orders of magnitude higher than for CS.

Fig. 3.3 illustrates the behaviour of the dimensionless numbers Dy and DyC for Sand 1 and Zeijen sand ZS with varying characteristic length and a characteristic velocity of $u_c = 10^{-5}\,\mathrm{m/s}$ (for the parameters K and τ see Tab. 3.1, $P_{cc} = P_d$). It is again assumed that the properties of the homogeneous porous media are known and constant on all length scales.

The dimensionless number Dy quantifies the ratio of dynamic to viscous forces. Thus, as Dy decreases with increasing length, the viscous effect dominates the dynamic capillary effect. This observation agrees with field-scale applications, where in particular reservoir engineers neglect capillary forces and in particular dynamic terms. As an exception, the works of BARENBLATT ET AL. [6, 5] and SILIN & PATZEK, 2004 [104] are cited, who not only take capillary effects into account but do also introduce a non-equilibrium term.

The dimensionless number DyC relates the influence of the dynamic to the equilibrium capillary effects. For decreasing values of DyC, the equilibrium influence gains importance (see Fig. 3.3). For Sand 1 the balance of these two effects is attained at a length scale of $l = 0.2\,\mathrm{m}$; for the Zeijen sand, the length is about two orders of magnitude smaller. In general, on small length scales dynamic effects might dominate the capillary equilibrium force rather than on large length scales.

Similar to the number DyC, the dimensionless number DyG shows that the influence of the dynamic capillary force decreases with the characteristic length scale in relation to the gravitational force (see Fig. 3.4).

As mentioned before, the characteristic length can be interpreted in different ways,

Table 3.1: Porous media parameters and values for Dy and u_c

Soil	K [m^2]	ϕ [-]	P_d [Pa] ($= P_{cc}$)	λ [-]	τ^- [Pa s]	u_c [m/s] DyC = 1, $l_c = 1\,\mathrm{m}$	Dy $l_c = 0.1\,\mathrm{m}$
CS	$5.66 \cdot 10^{-11}$	0.32	1370	5.83	$1.89 \cdot 10^{3}$	0.23	0.03
Sand 1	$5.66 \cdot 10^{-11}$	-	2317	-	$2.71 \cdot 10^{7}$	$4.63 \cdot 10^{-5}$	283.0
ZS	$3.06 \cdot 10^{-12}$	0.35	5587	6.11	$6.07 \cdot 10^{5}$	$9.78 \cdot 10^{-3}$	0.17
Silt	$5.16 \cdot 10^{-13}$	0.49	9412	0.56	$1.56 \cdot 10^{8}$	$2.96 \cdot 10^{-5}$	16.40

$^-$: Values determined after Eqn. (3.2) except for Sand 1,

Parameter for CS from URSINO & GIMMI, 2004 [111], for Sand 1 from TOPP ET AL., 1967 [109], for ZS from HASSANIZADEH ET AL., 2005 [57], for silt from VAN GENUCHTEN ET AL., 1999 [115]

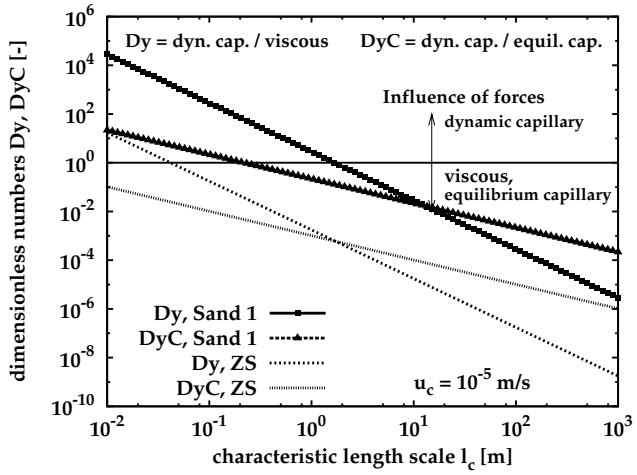

Figure 3.3: Dimensionless numbers Dy and DyC as functions of the characteristic length scale for the Zeijen sand ZS and Sand 1 (see Tab. 3.1)

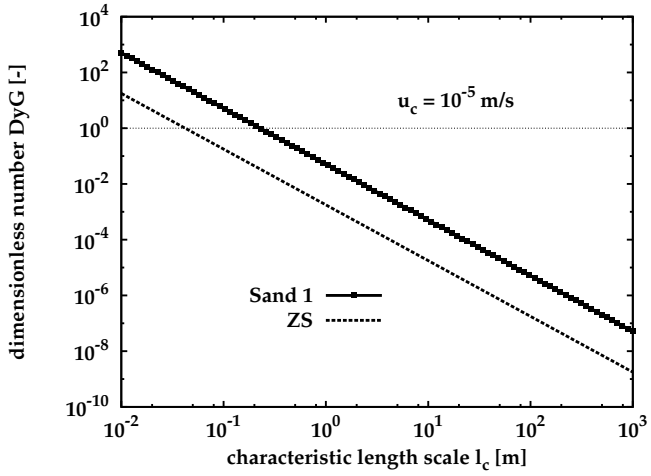

Figure 3.4: Dimensionless number DyG as a function of the characteristic length scale for Zeijen sand ZS and Sand 1 (see Tab. 3.1)

e.g as

- the system length,
- the characteristic length of a process, e.g. a front width,
- for numerical simulations, the grid size, or,
- for laboratory measurements, a measurement scale.

If the characteristic length is interpreted as the system length the influence of dynamic effects is important on small length scales with respect to viscous, equilibrium

capillary and gravitational effects (see Figs. 3.3 and 3.4). For length scales much smaller than $l_c = 0.01\,\mathrm{m}$, the validity of the underlying DARCY law (see Eqn. (2.22)) might be questioned for the sands under consideration, because it is applicable at scales larger than the pore scale. Interpreting the characteristic length as the system length gives an upper bound set by the dimensions of a reservoir or a watershed, scales where the porous system is clearly heterogeneous. However, the dimensional analysis is based on a system of equations for homogeneous systems.
If, on the other hand, the characteristic length scale is related to a process, e.g. the front of an imbibition process, the upper bound of the characteristic length is represented by the largest width of a front. For the lower bound, an REV again needs to be establishable, because the front is otherwise reduced to the pore-scale interface between the two phases. For an assessment of the influence of the effects in simulations, the grid size could be employed also. However, refining the grid for a simulation does not imply an alternation of the influence of the different effects but rather a better approximation of the solution as numerical diffusion is reduced. However, at the moment it can not be excluded that a coarsening of the grid might necessitate to include dynamic effects on the coarse grid. This aspect requires further analysis and is not part of of this thesis. The simulation results presented in Sec. 6 serve to analyse the question how the characteristic length scale could be interpreted.
Now, a constant characteristic length scale is chosen and the characteristic flow velocity in DyC is varied. In order to assess the importance of dynamic effects, this characteristic flow velocity needs to represent a flow velocity from a transient process. At a steady state, dynamic effects do not play a role as the rate of change of saturation then equals zero. For illustration, calculated DyC is plotted for the parameters of the coarse sand CS and the Zeijen sand ZS (see Fig. 3.5).

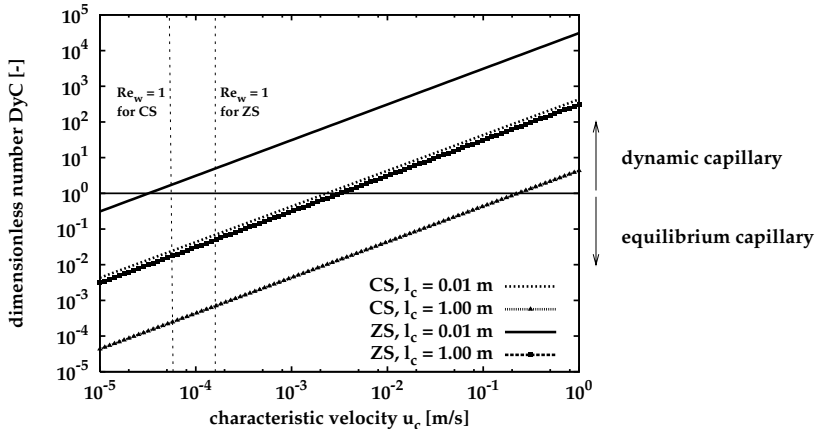

Figure 3.5: Dimensionless number DyC as a function of the characteristic flow velocity for the coarse sand CS and the Zeijen sand ZS (see Tab. 3.1)

For increasing flow velocities, the dynamic capillary force gain importance in relation to the equilibrium capillary force. As an example, for the coarse sand CS,

the balance between dynamic and equilibrium capillary effects for $l_c = 0.01\,\mathrm{m}$ is attained at a characteristic flow velocity of approximately $u_c = 2 \cdot 10^{-3}\,\mathrm{m/s}$. For the Zeijen sand, the flow velocity at balance is approximately two orders of magnitude smaller for the same characteristic length.
The applicability of DARCY's law might be endangered at high flow velocities, as the linear relation of flux to head gradient can change to non-linear (compare Section 2.3.1). As a measure, the REYNOLDS number (see Eqn. 2.26) is employed, which should not exceed one (to ten) for DARCY's law to hold. The characteristic flow velocity u_c can be related to the characteristic seepage velocity v_{cs} applied in the REYNOLDS number through $v_{cs} = u_c/\phi$. As the dimensionless numbers are defined related to the wetting phase properties, the wetting phase parameters are employed for the computation of the REYNOLDS number. The REYNOLDS number Re_w indicates that, for porous media with mean grain diameters of $d_{50} = 0.006\,\mathrm{m}$ (coarse sand), the seepage velocity should not exceed $v_s = 0.001\,\mathrm{m/s}$, while for $d_{50} = 0.0002\,\mathrm{m}$ (coarse silt), it should remain smaller than $v_s = 0.1\,\mathrm{m/s}$. For reference, $\mathrm{Re_w} = 1$ is indicated in Fig. 3.5 for both sands. Apparently, for the Zeijen sand ZS, the range of velocities where dynamic capillary forces dominate (DyC < 1) and the DARCY law holds, is small. For the coarse sand, the equilibrium capillary force dominates throughout the whole range of the applicability of DARCY'S law.
In Sec. 6, simulations are run to which different magnitudes of the dimensionless numbers pertain in order to assess the impact of the extended $P_c(S_w)$ relation on simulation results. In two of the examples, the dynamic forces exceed the capillary equilibrium but not the viscous ones.
The conclusions from the dimensional analysis can be summarised as follows:

- From the dimensional analysis of the two-phase balance equations on the local scale including an extended $P_c(S_w)$ relationship, a new dimensionless number Dy evolves, which quantifies the ratio of dynamic to viscous influences. Division of Dy by the inverse of the capillary number Ca and the gravitational number Gr yields DyC, the ratio of dynamic to equilibrium capillary forces, and DyG, the ratio of dynamic capillary to gravitational effects.

- On the assumption that the coefficient τ is a constant the importance of dynamic effects diminishes with increasing length scale with relation to equilibrium capillary, viscous and gravitational effects. If the characteristic length scale is assumed to be the system length, dynamic effects might play a role especially in laboratory experiments (e.g. for parameter identification) and small scale applications (e.g. filters) where large rates of change of saturation occur.

- The influence of the dynamic forces increases with increasing characteristic flow velocity from a transient process.

- The range in which the dynamic effects might play a role is limited by at least two factors,

- the smallest length scale possible for establishling an REV for the balance equations and the properties of the porous medium and
- the maximum flow velocity where the REYNOLDS number does not exceed one (to ten).

In most applications concerning subsurface hydrosystems, the REYNOLDS number does not exceed this limit.

In brief, the influence of dynamic effects declines with increasing length scale (of either the system or the front width) and decreasing flow velocity on the assumption that τ is a constant. As mentioned before, this observation agrees with field-scale applications, where especially reservoir engineers neglect capillary forces and thus do not distinguish between equlibrium and dynamic capillary effects.
The dimensionless analysis is based on the assumption that the coefficient τ is a constant. HASSANIZADEH & GRAY, 1993 have argued that τ might depend on the saturation, the rate of change of saturation and other properties of the porous media. For a dependence on the saturation, a characteristic value of τ could then be employed, similar to the definition of the characteristic equilibrium capillary pressure. The same holds for a given range of saturation rates. Inclusion of these effects might shift the values for τ, but the principal behaviour of the numbers would not be altered.
A more important issue is the question whether the coefficient τ scales with length scale. DAHLE ET AL., 2005 [30] propose that τ scales with length squared for a large range of water saturations. Consequently, the ratios of the dynamic capillary force to the viscous and gravitational ones do not depend on the length scale, as l^2 then cancels out and only the constant part of τ remains in the equations. If this relation is inserted into Eqn. 3.27, the dynamic capillary force still increases with length scale in comparison to the equilibrium capillary effects then constant over all length scales. Relating τ instead of the system length to a front width, as suggested by DAHLE ET AL., 2005 [30], also raises questions. If the coefficient scales directly with length squared, it is then large for a broad front width and small for steep fronts. This introduces a dependence on the flow process assuming that steep fronts are encountered in processes with high flow velocities and broad fronts are related to small flow velocities. Additionally, having a large coefficient for slow processes violates the assumption that in the limit of capillary dominated flow dynamic effects do not need to be taken into account. Questions related to the dependence of τ on the length scale will be taken up again in Ch. 5.

4 Numerical model of two-phase flow

In Sec. 2.3.2, the mathematical model for describing the conservation of mass and momentum for two fluid phases assuming a rigid, incompressible porous medium is introduced. The two balance equations are coupled through the relative permeability-saturation relationships and the additional constraints for the saturations (see Eqn. (2.34)) and the capillary pressure (see Eqn. (2.35)). The resulting system of highly non-linear partial differential equations can only be solved analytically for simple cases, e.g. the Buckley-Leverett problem where displacement neglecting capillary pressure is treated [42]. Thus, the equations are approximated by numerical methods (discretisation in space and time). The evolving algebraic equations can then be tackled with efficient and fast solvers.

4.1 The simulation programme MUFTE-UG

Simulations carried out for this thesis employ the simulator MUFTE-UG (MUltiphase Flow Transport and Energy model on Unstructured Grids). MUFTE-UG consists of two parts, one providing the implementation of the spatial discretisation of the balance equations, the constitutive relationships as well as the problem descriptions (MUFTE), and the second providing the means for solving partial differential equations on complex geometries in two and three dimensions, possibly on unstructured grids. In the framework of this thesis, only two-dimensional domains with structured grids are applied.
The spatial and the temporal discretisation as well as the solvers applied here will be described in Sec. 4.2.
The solvers implemented in UG, the geometric and algebraic data structures, the grid management, visualisation and parallelisation options as well as a theoretical background to these methods are described in detail by BASTIAN, 1999 [8]. Assessments of the different discretisation approaches and the solving routine can be found in BASTIAN & HELMIG, 1999 [9], or HELMIG & HUBER, 1998 [60].

4.2 Spatial and temporal discretisation of the two-phase conservation equations

In Sec. 2.3.2, the conservation equations of mass including DARCY's law for two fluids, given in Eqns. (2.32) and (2.33), as well as the additional constraints after

Eqns. (2.34) and (2.35) are introduced. These continuous functions need to be discretised in space and time in order to solve them. First, the spatial discretisation applying the traditional closure assumption that $P_c = P_n - P_w = P_c(S_w)$ is outlined. In Sec. 4.3, the discretisation for the closure with the extended $P_c(S_w)$ relationship as given in Eqn. 3.13 is presented. For the discretisation of the balance equations, they are first of all expressed in the integral form,

$$\int_\Omega \phi \frac{\partial}{\partial t}(S_\alpha \rho_\alpha) \mathrm{d}V = \int_\Omega \nabla \cdot [\rho_\alpha \lambda_\alpha \mathbf{K} \nabla (P_\alpha - \rho_\alpha g z)] \mathrm{d}V + \int_\Omega \rho_\alpha q_\alpha \mathrm{d}V \,, \tag{4.1}$$

over the domain Ω, that can be chosen freely.
The domain, for which the two balance equations should be solved is discretised by m number of elements $E = \{e_1, ..., e_m\}$ possessing i numbers of vertices $V = \{v_1, ..., v_i\}$. In the following, the grid made up of these elements and vertices is denoted the Finite Element (FE) or primary mesh. At the boundary of the domain Γ, either Dirichlet ($\Gamma_{\alpha,D}$) or Neumann ($\Gamma_{\alpha,N}$) boundary conditions can be prescribed for the phase α.
On the basis of the primary mesh, a secondary, Finite Volume (FV) mesh is constructed by connecting an element's centre of gravity to the midpoint of the element edges (see Fig. 4.1). Thus, around each vertex v_i, a control volume can be defined, which is called a box, described by b_i. The intersection of an element with a box is denoted sub-control volume. Its boundary can be subdivided into two sub-control volume faces. The whole boundary of a box is denoted ∂_{b_i}. The spatial discretisation presented is denoted sub-domain collocation control volume method or, more simply, BOX method.

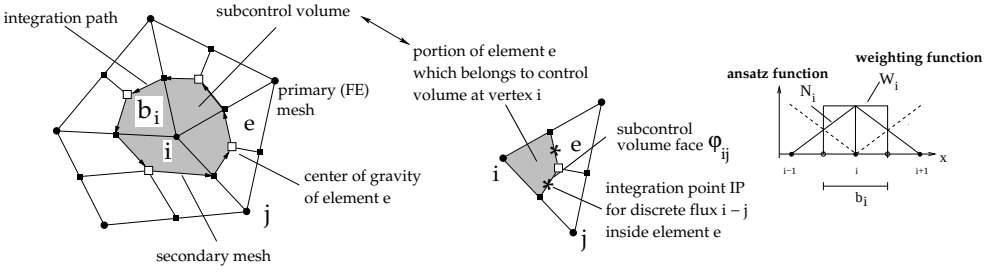

Figure 4.1: Primary (FE) mesh and construction of the secondary mesh as well as the basis and ansatz functions (after [59, 8])

Introducing a numerical scheme implies that the primary variables P_α and S_α are approximated by ansatz functions N_j. Within the BOX scheme, these are common C^0 Lagrangian polynomials, meaning they are piecewise linear and continuous, but not continuously differentiable. For example the wetting phase pressure P_w, the approximated quantity $\tilde{P_w}$ can be calculated after

$$\tilde{P_w} \approx \sum_j P_{wj} N_j \,, \tag{4.2}$$

and its gradient after

$$\nabla \tilde{P_{\mathrm{w}}} \approx \sum_{j \in \eta_j} (P_{\mathrm{w}j} - P_{\mathrm{w}i}) \nabla N_j \,, \tag{4.3}$$

where η_i is the set of neighbouring vertices of vertex i. The ansatz function N_j is defined by

$$N_j(\mathbf{x}_k) = \begin{cases} 1 & \text{for} \quad j = k \\ 0 & \text{for} \quad j \neq k \,. \end{cases} \tag{4.4}$$

Consequently, the primary variables are no longer a function of space.
The approximation of the primary variables effects that the balance equations cannot be solved exactly any more, e.g. the terms on the left-hand side of Eqn. (4.1) no longer equal zero but a residuum ε, which should be weighted such that it is zero on average over the domain. To this end, the position-dependent weighting functions $W_i(\mathbf{x})$ are introduced. If one considers the principle of orthogonality, these should be chosen such that

$$\int_{\Omega} W_i \, \varepsilon \, \mathrm{d}V = 0 \quad \text{for} \quad i = 1, 2, ..., n_{\mathrm{nodes}} \,, \tag{4.5}$$

where n_{nodes} denotes the total number of nodes. For the BOX scheme the weighting functions W_i are defined as piecewise constant with

$$W_i(\mathbf{x}) = \begin{cases} 1, & \text{if} \quad \mathbf{x} \in b_i \\ 0, & \text{if} \quad \mathbf{x} \notin b_i \,. \end{cases} \tag{4.6}$$

Including these definitions, Eqn. (4.1) can thus be expressed as (suppressing the time derivate)

$$\begin{aligned} &\overbrace{\int_{\Omega} W_i \phi \sum_{j \in \eta_i} (S_\alpha \rho_\alpha)_j N_j \mathrm{d}\Omega}^{\text{Term M}} \\ &- \overbrace{\int_{\Omega} W_i \nabla \cdot [\rho_\alpha \lambda_\alpha \mathbf{K} \{ \sum_{j \in \eta_i} (P_{\alpha j} - P_{\alpha i}) - \rho_{\alpha ij} g \sum_{j \in \eta_i} (z_j - z_i) \} \nabla N_j] \mathrm{d}\Omega}^{\text{Term A}} \\ &- \overbrace{\int_{\Omega} W_i \rho_\alpha q_\alpha \mathrm{d}\Omega}^{\text{Term Q}} \; = \; 0 \,, \end{aligned} \tag{4.7}$$

where z_i denotes the z-coordinate of vertex i, and $\rho_{\alpha,ij}$ describes the density of phase α arithmetically averaged between the vertices i and j. In the following, the treatment of the different terms in Eqn. (4.7) within the BOX discretisation is explained.

The accumulation term 'Term M' and the source/sink term 'Term Q' are approximated by applying the mid-point rule. Thus, the accumulation term can be calculated after (again omitting the time derivative)

$$\int_{\Omega} W_i \phi \Big(\sum_{j \in \eta_i} (S_\alpha \rho_\alpha)_j \Big) N_j \mathrm{d}\Omega = \phi (S_\alpha \rho_\alpha)_i |b_i| \,, \tag{4.8}$$

and, similarly, the source/sink term after

$$\int_{\Omega} W_i \rho_\alpha q_\alpha \mathrm{d}\Omega = (\rho_\alpha q_\alpha)_i |b_i| \,, \tag{4.9}$$

where $|b_i|$ denotes the volume of box b_i. This procedure corresponds to the mass lumping technique in Finite Element methods.
Before the flux term 'Term A' is explained, the total potential $\Psi_{\alpha i}$ is introduced

$$\Psi_{\alpha i} \;=\; \Big(\sum_{j \in \eta_i} P_{\alpha i} - \rho_{\alpha i} g \sum_{j \in \eta_i} z_i \Big) \,. \tag{4.10}$$

The second order in space within the volume integral of the flux term can be reduced to a first order by applying the product rule of differentiation, having summarised the flux term to $\int_{\Omega} W_i \nabla \cdot \mathbf{F} \mathrm{d}V$

$$\int_{\Omega} \nabla \cdot (W_i \mathbf{F}) \mathrm{d}\Omega = \int_{\Omega} \nabla W_i \mathbf{F} \mathrm{d}\Omega + \int_{\Omega} W_i \nabla \cdot \mathbf{F} \mathrm{d}\Omega \tag{4.11}$$

which is equal to

$$\int_{\Omega} W_i \nabla \cdot \mathbf{F} \mathrm{d}\Omega = \int_{\Omega} \nabla \cdot (W_i \mathbf{F}) \mathrm{d}\Omega - \int_{\Omega} \nabla W_i \mathbf{F} \mathrm{d}\Omega \tag{4.12}$$

where the first term on the right-hand side becomes zero for the chosen weighting functions W_i. Applying the GREEN-GAUSS integral theorem allows the volume integral to be conveyed to a boundary integral

$$\int_{\Omega} \nabla \cdot (W_i \mathbf{F}) \mathrm{d}V = \oint_{\Gamma} W_i \mathbf{F} \cdot \mathbf{n} \mathrm{d}\Gamma \,, \tag{4.13}$$

where $\mathbf{n}$ denotes the outer unit normal vector. Thus, 'Term A' can be expressed as

$$\int_{\Omega} W_i \nabla \cdot [\rho_\alpha \lambda_\alpha \mathbf{K} (\Psi_{\alpha j} - \Psi_{\alpha i}) \nabla N_j] \mathrm{d}\Omega = \oint_{\partial b_i} W_i \rho_\alpha \lambda_\alpha \mathbf{K} \Psi_{\alpha i j} \nabla N_j \cdot \mathbf{n} \, \mathrm{d}\Gamma_{b_i} \tag{4.14}$$

with

$$\Psi_{\alpha i j} \;=\; \Big(\sum_{j \in \eta_i} (P_{\alpha j} - P_{\alpha i}) - \rho_{\alpha i j} g \sum_{j \in \eta_i} (z_j - z_i) \Big) \,, \tag{4.15}$$

where $\Psi_{\alpha,ij}$ denotes the difference in the total potential between the vertices i and j. Within the BOX scheme, the internal fluxes are evaluated at the mid-point of a sub-control volume face φ at the integration point IP (see Fig. 4.1) and then weighted on that face. Thus, the integration over the flux term of one box can be approximated by

$$F_i := \sum_{l \in e_i} \sum_{j \in \eta_i} (\rho_\alpha \lambda_\alpha)_{ij} \Psi_{\alpha ij} \nabla N_j \cdot \mathbf{n} \varphi_{ij}^{el} \,. \tag{4.16}$$

It has not yet been specified how the product of the density ρ_α times the mobility λ_α is to be treated. An upstream weighting technique is applied here, which stabilises the solution and hinders the infiltration of non-wetting phase into a part of the domain with high entry pressure for sufficiently refined grids [66]. The upstream direction is defined by

$$(\rho_\alpha \lambda_\alpha)_{ij}^{\text{ups}} = \begin{cases} (\rho_\alpha \lambda_\alpha)_i & \text{if} \quad (\Psi_{\alpha j} - \Psi_{\alpha i}) \geq 0 \\ (\rho_\alpha \lambda_\alpha)_j & \text{if} \quad (\Psi_{\alpha j} - \Psi_{\alpha i}) < 0 \,, \end{cases} \tag{4.17}$$

describing a fully upwinding scheme.
Choosing the pressure of the wetting phase and the saturation of the non-wetting phase as the two primary variables to be solved for, and closing the system accordingly with Eqns. (2.34) and (2.35), the balance equations can thus be expressed as

$$\begin{aligned} g_{\alpha,i}(P_{\text{w},i}; S_{\text{n},i}) := {} & (-1)\delta^{\alpha,\text{w}} \phi (S_\alpha \rho_\alpha)_i |b_i| \\ & - \sum_{l \in e_i} \sum_{j \in \eta_i} (\rho_\alpha \lambda_\alpha)_{ij}^{\text{ups}} \mathbf{K} (\Psi_{\alpha j} - \Psi_{\alpha i}) \nabla N_j \cdot \mathbf{n} \varphi_{ij}^{el} \\ & - (\rho_\alpha q_\alpha)_i |b_i| - m_{\alpha i} \end{aligned} \tag{4.18}$$

with

$$\Psi_{\alpha i} = P_{\text{w},i} + \delta^{\alpha,n} P_{\text{c},i} - \rho_{\alpha i} g z_i \,. \tag{4.19}$$

The term $m_{\alpha i}$ quantifies the flux over the boundary in case $\partial b_i \cap \Gamma_{\alpha,N}$.
The flux over the sub-control volume face of $b_i \cap b_j$ from box b_i into box b_j equals the opposite flux from box b_i to $b_i \cap b_j$. The method thus conserves mass locally.
For the evolving discretised system of equations, appropriate boundary conditions have to be defined. In the context of this thesis, only DIRICHLET or NEUMANN boundary conditions are applied.
The just described coupled, highly non-linear equations need to be discretised in time as well. For the temporal discretisation, a one step method, a fully implicit Euler scheme is applied, which can be stated in general for a time-dependent variable u as

$$\frac{\partial u}{\partial t} \approx \frac{u^{n+1} - u^n}{\Delta t} \quad \text{with} \quad \Delta t = t^{n+1} - t^n \,. \tag{4.20}$$

The balance equations already spatially discretised thus become

$$
\begin{aligned}
g_{\alpha,i}(P_{\mathrm{w},i};S_{\mathrm{n},i}) := {} & (-1)\delta^{\alpha,\mathrm{w}}\frac{\phi}{\Delta t}((S_\alpha\rho_\alpha)_i^{n+1}-(S_\alpha\rho_\alpha)_i^{n})|b_i| \\
& - \sum_{l\in e_i}\sum_{j\in\eta_i}(\rho_\alpha\lambda_\alpha)_{ij}^{\mathrm{ups},n+1}\mathbf{K}(\Psi_{\alpha j}^{n+1}-\Psi_{\alpha i}^{n+1})\nabla N_j\mathbf{n}\varphi_{i,j}^{e_l} \\
& - (\rho_\alpha q_\alpha)_i^{n+1}|b_i| - (m_{\alpha i})^{n+1}\,. \qquad (4.21)
\end{aligned}
$$

HELMIG, 1997 [59] and BASTIAN & HELMIG , 1999 [9] have shown that the implicit Euler scheme is unconditionally stable for arbitrary time steps. Numerical diffusion might be introduced by this temporal discretisation [58], which the algorithm in MUFTE-UG attempts to diminish by a time step control. The time step is adapted automatically within the solving algorithm based on the performance of the damped, inexact NEWTON scheme to solve the non-linear, algebraic system of equations. The inexactness refers to the approximated solution of the linearised system of equations evolving in the NEWTON algorithm. The damping is employed to facilitate global convergence. To determine the damping factor a line search is utilised. The number of line searches may influence the time stepping. If the damping factor can be calculated within the first line search, the time step is multiplied by a factor. If, on the other hand, the damping factor cannot be determined after a given number of line searches (usually four to six), the time step is reduced applying the factor *dtred*.

For the time stepping algorithm, the size of the first, the maximum and the minimum time step can be defined. If convergence cannot be achieved for the smallest time step, a simulation is aborted.

The NEWTON algorithm requires starting values for the unknowns. To obtain a good guess a multi-grid algorithm is employed as a pre conditioner [50]. Beginning on the coarsest level, the solution of the previous time step on the coarsest level is taken as the initial guess. The solution on the coarsest grid is then prolongated to the next finer level to provide an initial guess. This procedure is repeated up to the finest level, and then the solution is restricted again cycling through the levels up to the coarsest level. The procedure is called a V-cycle. LANG, 2001 [72] describes the realisation of the multi-grid data structure in MUFTE-UG in detail.

The linear system of equations evolving in the NEWTON scheme is treated with an incomplete LU decomposition (as a pre- and post-smoother), and then solved with a stabilised bi-conjugate gradient algorithm.

For a detailed overview of the solvers implemented in UG, BASTIAN, 1999 [8] can be consulted.

4.3 Inclusion of the extended capillary pressure-saturation relationship in the mathematical-numerical model

So far, the two-phase balance equations have been closed by the saturation identity after Eqn. (2.34) and applying a unique relationship between capillary pressure and water saturation (see Eqn. (2.35)). Instead of this traditional approach, the extended $P_c(S_w)$ relationship (see Eqn. 3.13) is chosen now to close the system of equations. It is assumed that the linearisation of the relation holds, and that the coefficient τ may be a function of the water saturation as observed in experiments (see Sec. 5.3).
As in Sec. 4.2 the pressure of the wetting and the saturation of the non-wetting phase are selected as primary variables. The application of Eqn. 3.13 allows that the gradient of the pressure of the non-wetting phase can be expressed as

$$\nabla P_n = \nabla \left(P_w + P_c + \tau \frac{\partial S_n}{\partial t} \right) ,$$

or, as the gradient of the sum equals the sum of the gradients,

$$\nabla P_n = \nabla P_w + \nabla P_c + \nabla \tau \frac{\partial S_n}{\partial t} . \tag{4.22}$$

The new additional term is thus a mixed second-order term.
The balance equation for the wetting phase is not affected by this alternative closure of the system, while the balance equation for the non-wetting phase given in Eqn. (2.33) in the integral form changes to

$$\begin{aligned} \int_\Omega \phi \frac{\partial \rho_n S_n}{\partial t} d\Omega \; = \; & \int_\Omega \nabla \cdot \left[\rho_n \lambda_n \mathbf{K} \{ \nabla P_w + \nabla P_c + \nabla \tau \frac{\partial S_n}{\partial t} - \rho_n g \nabla z \} \right] d\Omega \\ & + \int_\Omega \rho_n q_n d\Omega . \end{aligned} \tag{4.23}$$

As a consequence now a mixed third order term has to be treated.
With the chain rule of differentiation the new term might be expressed as

$$\nabla \tau \frac{\partial S_n}{\partial t} = \tau \frac{\partial}{\partial t} \frac{\partial S_n}{\partial x} + \frac{\partial S_n}{\partial t} \frac{\partial}{\partial x} \tau , \tag{4.24}$$

This illustrates that the gradient of the water saturation appears (in the first term on the right hand side). As the water saturation might be discontinuous at the interface of heterogeneities its gradient cannot be determined at such an interface. The second term on the right hand side vanishes for a constant τ coefficient.
Introducing the weighting functions W_i after Eqn. (4.6) and the linear ansatz functions N_j after Eqn. (4.4) to approximate the variables as described in Sec. 4.2 as well

as discretising the equation in time applying the fully implicit Euler scheme after Eqn. 4.20 as described in Sec. 4.2 leads to

$$\begin{aligned}
&\int_\Omega W_i \frac{\phi}{\Delta t}[(\rho_n S_n)_i^{n+1} - (\rho_n S_n)_i)^n \sum_{j\in\eta_i} N_j] \mathrm{d}G \\
&= \oint_\Gamma W_i (\rho_n \lambda_n)_{ij}^{\mathrm{ups},n+1} \mathbf{K} \sum_{j\in\eta_i} [(P_{w\,i} + P_{c\,i} - \rho_n g z_i)^{n+1} + \frac{\tau}{\Delta t}(S_{n,i}^{n+1} - S_{n,i}^n)] \nabla N_j \cdot \mathbf{n} \mathrm{d}\Gamma \\
&+ \int_\Omega W_i (\rho_n q_n)_i^{n+1} \mathrm{d}\Omega \,. \qquad (4.25)
\end{aligned}$$

Eqn. (4.25) will be handled in two ways: first, the new term will be treated together with the accumulation term and secondly, it will remain in the flux term. Both approaches were implemented.
In MUFTE-UG the discretised equations are multiplied by the time step rather than divided by the time step as this might lead to the division by very small numbers. Consequently, with Eqn. (4.21) as a basis Eqn. (4.25) can be expressed as

$$\begin{aligned}
&\frac{\phi}{\Delta t}((\rho_n S_n)_i^{n+1} - (\rho_n S_n)_i^n)|b_i| \\
&- \frac{1}{\Delta t} \sum_{l\in e_i} \sum_{j\in\eta_i} (\rho_n \lambda_n)_{ij}^{n+1} \mathbf{K}\tau (S_{n,i}^{n+1} - S_{n,i}^n) \nabla N_i \cdot \mathbf{n} \varphi_{i,j}^{e_l} \\
&= A + Q + m_{n,i}^{n+1} \,, \qquad (4.26)
\end{aligned}$$

where A equals the flux and Q the source/sink term as defined by Eqn. (4.21). The additional term would still be treated as a flux term, perhaps also using the upstream mobility. In contrast to the handling of the flux term in Eqn. (4.21) an upwinding scheme is not applied to the newly evolved boundary integral. The accumulation term is thus recast as

$$\begin{aligned}
&\frac{1}{\Delta t}\{\phi((\rho_n S_n)_i^{n+1} - \sum_{l\in e_i} \sum_{j\in\eta_i} (\rho_n \lambda_n)_{ij}^{n+1} \mathbf{K}\tau S_{ni}^{n+1} \nabla N_j \cdot \mathbf{n} \varphi_{ij}^{e_l} \\
&- (\rho_n S_n)_i^n)|b_i| - \sum_{l\in e_i} \sum_{j\in\eta_i} (\rho_n \lambda_n)_{ij}^n \mathbf{K}\tau S_{ni}^n \nabla N_j \cdot \mathbf{n} \varphi_{ij}^{e_l}\} \\
&= A + Q + m_{n,i}^{n+1} \,, \qquad (4.27)
\end{aligned}$$

As the gradient of the saturation – a possibly discontinuous variable in heterogeneous domains – occurs in the formulation it can strictly speaking only be applied to homogeneous domains, unless an additional interface condition is found to satisfy the extended $P_c(S_w)$ relationship at the interface.
In the second approach, the additional term $\nabla\tau^{\Delta S_n/\Delta t}$ remains within the flux term. The balance equation can be described by

$$\begin{aligned}
&\frac{\phi}{\Delta t}((\rho_n S_n)_i^{n+1} - (\rho_n S_n)_i^n)|b_i| \\
&= \sum_{l\in e_i} \sum_{j\in\eta_i} (\rho_n \lambda_n)_{ij}^{\mathrm{ups},n+1} \mathbf{K}\{\Psi_{nij}^{n+1} + \tau \frac{S_{ni}^{n+1} - S_{ni}^n}{\Delta t}\} \nabla N_j \cdot \mathbf{n} \varphi_{i,j}^{e_l} + Q + m_{ni}^{n+1} \,. \qquad (4.28)
\end{aligned}$$

In contrast to the first implementation the additional term is now included in the upwinding scheme of the flux term. Comparing simulations for the first and second implementation did not show detectable differences in the results. Thus, the inclusion in the upwinding scheme is maintained.
To this end, the saturation of the time steps $S_{\mathrm{n}}^{n}, S_{\mathrm{n}}^{n+1}$ as well as t^{n}, t^{n+1} are saved after each time step and made available at the next time step. The solution S_{n}^{n+1} is assumed to be a good initial guess to compute the saturation rate at the next time step. During the solving routine, the values are updated after each successful NEWTON iteration.
Simulations based on the first approach were compared to simulations with the second approach and a difference in the cumulative mass over time (see Eqn. 6.1) could not be detected. However, with the first approach problems occurred if the coefficient τ exceeded a certain magnitude in combination with unfavourable initial and boundary conditions. Thus, the simulations presented in Ch. 6 are based on the second approach.

5 Determination of the coefficient τ in the extended $P_c(S_w)$ relationship

In this chapter, laboratory and numerical experiments are presented, on the basis of which the coefficient τ in the extended $P_c(S_w)$ relationship relationship (compare Sec. 3.5) is calculated.
A short literature review introduces various approaches to determining the τ coefficient. Subsequently, a laboratory experiment from GeoDelft, The Netherlands serves to quantify the coefficient and analyse its dependence on the water saturation. Then numerical experiments applying MUFTE-UG (see Sec. 4.1) provide a basis for assessing whether the coefficient can be identified on the local scale and macroscale. Thus, the coefficient τ is determined by two approaches, namely laboratory and numerical experiments. It is not the aim of this thesis to examine dynamic effects in the relative permeability-saturation relationship. For a complete upscaling approach, this constitutive relationship also needs to be determined under equilibrium and dynamic conditions in order to apply the upscaled parameters in a large-scale simulation. However, this lies beyond the scope of this thesis and is a topic of further investigations.

5.1 Literature review

In Section 3.2, studies examining dynamic effects in the local scale $P_c(S_w)$ relationship were presented. Except for the work of STAUFFER, 1978, these studies do not attempt to derive a functional form to handle the non-uniqueness or to test existing models. Here, methodical and laboratory studies that calculate the coefficient τ are introduced. Results of KALAYDJIAN, 1992 [68] are compared to the results from the GeoDelft experiments in Sec. 5.3.
HASSANIZADEH ET AL., 2002 [52] calculate τ on the basis of experimental data from the literature. For water-gas (air) fluid systems, its values range between $\tau = 3 \cdot 10^4$ Pa s and $\tau = 5 \cdot 10^7$ Pa s for various sands and drainage processes.
TSAKIROGLOU ET AL., 2003 [110] perform transient displacement experiments with paraffin oil ($\mu_n = 0.026$ Pa s) and water on a transparent glass etched 2D pore-network (0.134 m $\cdot$ 0.10 m). They obtain $P_c^e(S_w)$ and $P_c^d(S_w)$ relationships from an inverse modelling approach with the traditional local-scale balance equations for two phases (see Sec. 2.3.2). The determination of the coefficient τ after HASSANIZADEH & GRAY, 1993 for each of the experiments results in a slight dependence of τ on the water saturation. However, a pronounced dependence on the boundary condi-

tions and thus the dominating forces is observed. For a fast process, the coefficient amounts to $\tau = 1.56 \cdot 10^6$ Pa s and for a slow process to $\tau = 6.73 \cdot 10^7$ Pa s, thus, the values differ by appr. an order of magnitude. For capillary-dominated flow, the τ values are higher than for viscous dominated flow. The authors offer the following interpretation. If τ is a damping coefficient, it can be interpreted as a measure of the time required to establish equilibrium. For fast processes with large flow velocities (large capillary number Ca (3.22)) this time is small and for slow processes (small capillary number) it is high. On the assumption that the flow velocity is positively correlated to the rate of change of saturation, this interpretation suggests that the coefficient might be a function of the rate of change of saturation.
This interpretation contradicts the assumption that for slow processes, the deviation from the equilibrium $P_c(S_w)$ relationship should be small, and thus an extended $P_c(S_w)$ relationship would not be required when simulating the flow process. It should also be noted that the coefficient τ has the units of pressure times time, and not of time. The relation to the velocity of the process can be interpreted as a dependence of τ on the rate of change of saturation. Whether this is the case is still an open question.
Methodical studies comprise pore-scale models, ranging from bundle of capillary tubes to three-dimensional pore-network models, which are applied to upscale equilibrium and dynamic $P_c(S_w)$ relationships from the pore scale to the local scale.
DAHLE ET AL., 2005 [30] calculate the flow of two immiscible fluids through a bundle of capillary tubes applying the WASHBURN [119] equation with a constant contact angle. They undertake a volume-averaging of the phase pressures and phase volumes over the length of the tubes (~ 0.001 m) and find that the difference in the phase pressures in the transient case does not equal the equilibrium capillary pressure calculated after the LAPLACE equation. The dynamic P_c^d for drainage exceeds the equilibrium P_c for a given upscaled saturation. The authors determine the coefficient τ as a function of water saturation with values ranging between ~ 250 Pa s and ~ 400 Pa s. DAHLE ET AL., 2005 introduce the dimensionless grouping N_D as defined by

$$N_D = \frac{\tau K}{\phi \mu l^2} , \tag{5.1}$$

where l is a characteristic associated length scale, as for example the averaging length scale, and calculate it for given water saturations for a given variance of the tube-diameter distribution. They find that τ scales with the square of the length for medium to high water saturations (see Fig. 5.1). This would imply that $\tau = \tau^* l^2$, where τ^* is a constant value. The authors note that rather than relating τ to the length scale of the system, the averaging and thus the coefficient should be related to a typical process length, e.g. the front width. Then the magnitude of τ would be bounded.
GIELEN ET AL., 2004 [45] and GIELEN ET AL., 2005 [46] apply dynamic pore-network models to examine dynamic effects in the upscaled $P_c(S_w)$ relationship, also using volume averaging for the pressures and the fluids. In the dynamic numerical

experiments, the interfaces between the fluids are tracked with time. The authors also assume a constant contact angle. They show that, in drainage, the dynamic P_c^d exceeds the equilibrium P_c^e for a given saturation. The calculated coefficient τ is a function of the water saturation from a pore network with the dimensions $0.006\,m \cdot 0.006\,m \cdot 0.008\,m$ (see Fig. 5.2); its values are about one to two orders of magnitudes larger than the ones stated by DAHLE ET AL., 2005 [30]. The increase can probably be related to the increase of the averaging length scale, as both authors apply similar conservation equations and the same averaging approach.

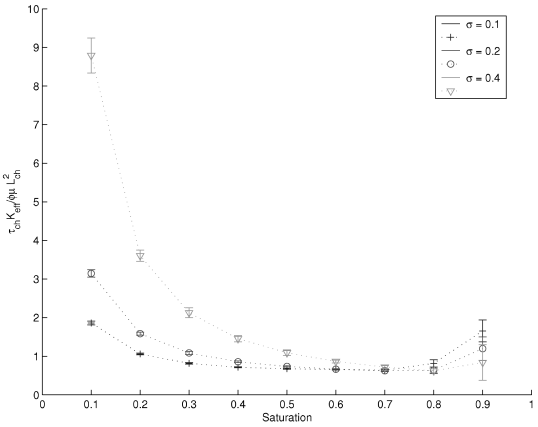

Figure 5.1: The dimensionless grouping $N_D(S_w)$ for varying pore size distributions σ as determined from a bundle of capillary tubes model by DAHLE ET AL., 2005 [30]

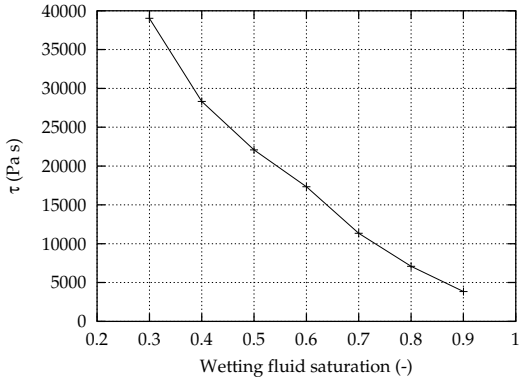

Figure 5.2: $\tau(S_w)$ as determined from a dynamic pore-network model from GIELEN ET AL., 2004 [45]

Tab. 5.1 lists values for the coefficient τ from the literature mentioned here and compares them where possible to the τ values calculated after the formula of STAUFFER, 1978 [108] given in Eqn. (3.2). If the required parameters could not be derived directly from the publication, values are either assumed or calculated from available data, e.g. the permeability from the mean pore size. The values thus derived for the coefficient τ_S after STAUFFER, 1978 differ in all the cases by orders of magnitudes from the experimentally determined ones. Two aspects need to be mentioned. First, in all the three publications, the viscosity ratios of the fluids do not resemble the water-air system for which STAUFFER, 1978 derived the formula. All viscosities of the non-wetting fluids exceed the ones of air by approx. two orders of magnitude. Secondly, in the approaches followed by DAHLE ET AL., 2005 [30] and GIELEN ET AL., 2005, an averaging of phase pressures and saturations is performed, which introduces a dependence of the coefficient τ on the averaging length scale. This is in contrast to STAUFFER's formula, which does not proclaim a dependence on the length scale. Even though the term $(P_d/\rho_w g)^2$ can be intepreted as a length, it relates to a capillary height (compare Eqn. (2.7)), which is limited by the smallest and the largest pore occuring in a porous medium and not by a system length scale. While

the differing viscosity ratios can explain the difference to the coefficients determined after STAUFFER (which makes its application to water-oil fluid systems questionable), the second issue of the length scale dependence will have to be investigated in more detail. The question will be discussed again at the end of this chapter, when numerical experiments on the local scale are applied to determine the coefficient.

Table 5.1: Magnitudes of the coefficient τ taken from the literature for various porous media and fluid systems

Ref.	min. τ [Pa s]	max. τ [Pa s]	τ_S[Pa s]	Assumed parameters		
				K [m^2]	P_d [Pa]	BC λ
1.*	$3\cdot10^4$	$5\cdot10^7$				
2.	$3\cdot10^4$	$5\cdot10^7$	$7.95\cdot10^2$		526.8	6.27
3.	$2.5\cdot10^2$	$4\cdot10^2$	$5.4\cdot10^6$	$4.8\cdot10^{-12}$	10^4	6.0
4.	$4\cdot10^3$	$4\cdot10^4$	$2.3\cdot10^5$	$5.0\cdot10^{-12}$	4100	6.0
5.	0	$5.9\cdot10^5$	$6.4\cdot10^6$	$5.7\cdot10^{-12}$	3800	0.161

* both values for a water-gas system, all others water-oil, data from 1. HASSANIZADEH ET AL., 2002, 2. TSAKIROGLOU ET AL., 2003, 3. DAHLE ET AL., 2005, 4. GIELEN ET AL., 2004 and 5. OUNG ET AL., 2005 [89] assuming that τ is given there in [kPa s] and permeability in [m/s] in their tables

Before the laboratory experiments aimed at determining the coefficient τ for a water-oil system in a sand are presented, procedures are introduced which are required to determine the terms in the extended $P_c(S_w)$ relationship. As the coefficient τ is not only derived from laboratory data but also calculated from numerical experiments, the domains and boundary conditions for these experiments are introduced additionally.

5.2 Procedure for determining the equilibrium and dynamic $P_c(S_w)$ relationships

In the preceding section, the investigations of DAHLE ET AL., 2005 [30] and GIELEN ET AL., 2005 were presented. These authors perform numerical experiments on the pore scale and determine the coefficient τ for the local scale on the basis of volume-averaged phase pressures and averaged phase volumes. A similar approach is followed in this investigation. On the assumption that local scale heterogeneity might introduce additional dynamic effects on the macroscale, numerical experiments are performed, applying the balance equations for two phases on the local scale introduced in Sec. 2.3 and their discretisation (see Ch. 4).
It should be stressed that no rigorous upscaling procedure is followed here. While HASSANIZADEH & GRAY, 1990 [55] as well as KALAYDJIAN, 1987 [67] have derived the extended $P_c(S_w)$ relationship scaling up from the pore to the local scale, BOURGEAT & PANFILOV, 1998 [16] as well as LEWANDOWSKA ET AL., 2005 [76]

have shown by applying a homogenisation theory that dynamic effects can arise on the macroscale (see Sec. 3.3). This approach requires the existence of periodic heterogeneities and a clear separation of the small to the large scale. Here, a simple, discrete pattern and a random, spatially correlated heterogeneity pattern will be examined and the terms entering into the extended $P_c(S_w)$ relationship as described in Sec. 3.5 are determined from the numerical experiments by undertaking a volume averaging of the phase pressures and arithmetically averaging the saturations.
For the determination of the coefficient τ, the equilibrium and dynamic $P_c(S_w)$ relationships as well as the rate of change of saturation are required. To obtain the equilibrium $P_c^e(S_w)$ relationship, either a percolation model is applied or numerical experiments are carried out, applying boundary condition combinations, which mimic laboratory experiments. The dynamic $P_c^d(S_w)$ and the saturation rate are determined on the basis of numerical experiments only. These dynamic numerical experiments also mimic laboratory experiments.
On the basis of the small τ values derived from pore-network models (see Sec. 5.1) and simulations including the extended $P_c(S_w)$ relationship (see Ch. 6), it is assumed that local-scale dynamic effects can be neglected in the numerical experiments as the inclusion of τ with a small magnitude does not have an influence on the solution. This approach analyses whether dynamic effects can be observed on the macroscale for a system with negligible dynamic effects on the pore scale.

5.2.1 Boundary and initial conditions

In the numerical experiments the boundary conditions of two kinds of laboratory experiment, a pressure-cell set-up and a flow-through experiment, are mimicked, both inducing primary drainage processes.
In the **flow-through** set-up, the domain is initially fully water-saturated. Gravity is neglected. In each phase, a pressure difference ΔP_α from the top to the lower boundary is prescribed (see Fig. 5.3). Additionally, at the boundaries, a difference between the phase pressures results in a boundary capillary pressure. At both side boundaries, no-flux conditions prevent an exfiltration of either phase. For homogeneous domains, this choice of boundary conditions results in one-dimensional processes.
To determine the $P_c(S_w)$ relationships, the capillary pressures at the top and lower boundary are augmented by an increase of the non-wetting phase pressure, while the pressure of the wetting phase at the boundaries remains constant throughout the whole numerical experiment.
In order to identify the equilibrium (quasi steady-state) $P_c^e(S_w)$ relationship, the capillary pressure at the top and lower boundary is augmented stepwise (see Fig. 3.1, right), inducing the non-wetting phase to infiltrate into the domain from the top according to the pressure gradient within the phase. As the capillary pressure is increased simultaneously at both boundaries, counter-current flow might occur after the capillary pressure augmentation. However, the pressure difference within each phase from the top to the bottom boundary ensures that, at steady state, no counter-current flow can be noticed.

For the calculation of a dynamic $P_c^d(S_w)$ relationship, the pressure of the non-wetting phase is increased at $t > 0$ to a large value within the first time step. The main problem arising with this kind of boundary conditions in the dynamic experiment is that counter-current flow occurs near the boundaries. Furthermore, the high increase in capillary pressure results in a fast decrease of the wetting phase saturation and thus its relative permeability. Thus, the remaining wetting phase is entrapped within the domain. Nevertheless, this kind of boundary condition was chosen to determine the equilibrium $P_c^e(S_w)$ and thus a few aspects are demonstrated with it for the dynamic case as well.

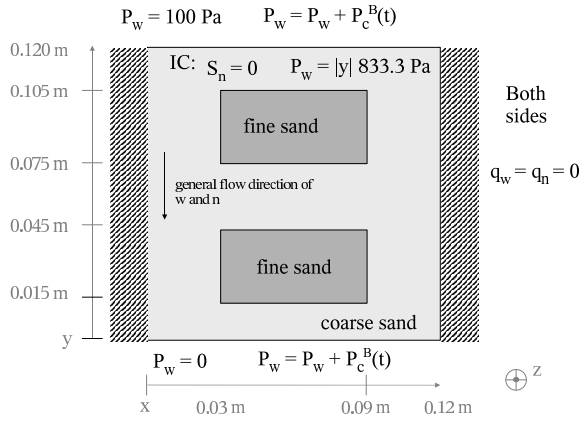

Figure 5.3: Initial and boundary conditions for the flow-through set-up with exemplary values ($|y|$ denotes the unit-less value of y)

As an alternative to the flow-through cell, the **pressure-cell** experimental set-up is chosen to calculate dynamic $P_c^d(S_w)$ relationships (see Fig. 5.4). Again, gravity is neglected except for the simulation of the GeoDelft experiments (see Sec. 5.4.1). The domain is initially fully water-saturated and a constant pressure in the water phase is prescribed. The pressure of the non-wetting phase is increased for $t > 0$ to a large value at the top boundary, while for the wetting phase a no-flux boundary condition is applied there. At the lower boundary, the non-wetting phase cannot leave the domain and, for the wetting phase pressure, a constant value is assumed. At both sides, no-flux boundary conditions are applied for both phases.

5.2.2 The heterogeneous domains

Two kinds of heterogeneous domain will be applied within this study, a simple heterogeneity pattern of two fine sand lenses embedded in a coarse sand (see Fig. 5.5, left) and a continuous heterogeneity pattern on the basis of a geostatistical approach (see Fig. 5.5, right).
ATAIE-ASHTIANI ET AL.,2001 [3] identified the simple heterogeneity as an REV within a periodically heterogeneous medium. Following the study of DAS ET AL.,

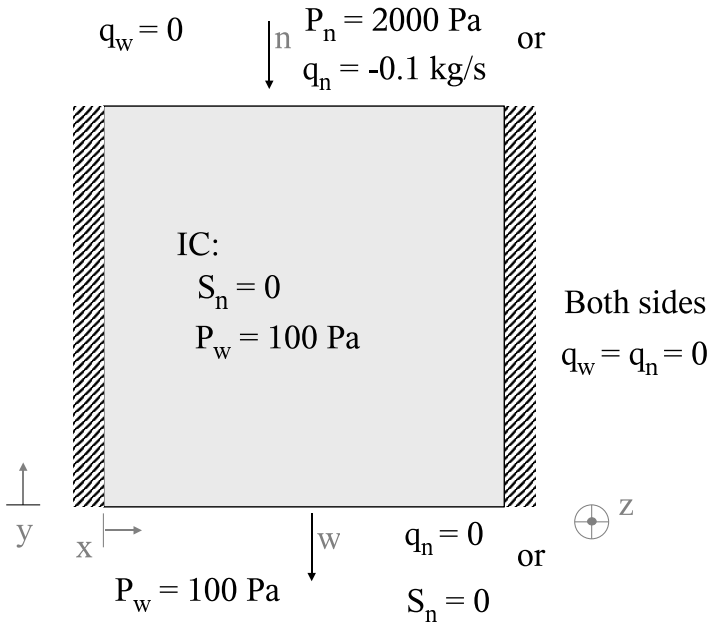

Figure 5.4: Initial and boundary conditions for the pressure-cell set-up with exemplary values

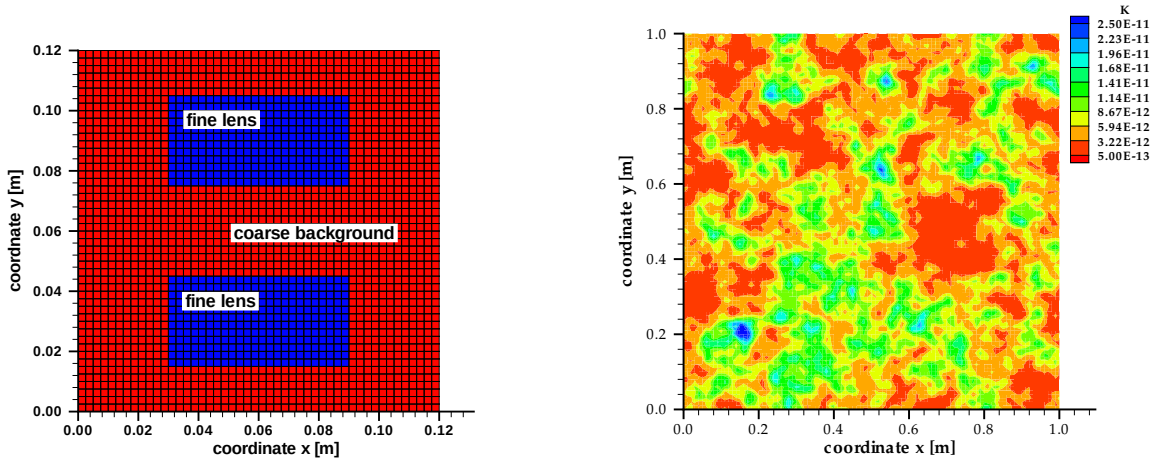

Figure 5.5: Heterogeneous 2D domain (left) and isotropic intrinsic permeability field (right)

2004 [32] the domain is extended here from $\Delta x = \Delta y = 0.10\,\mathrm{m}$ to $\Delta x = \Delta y = 0.12\,\mathrm{m}$. The parameters of the coarse and fine sand are similar to those given by ATAIE-ASHTIANI ET AL., 2002 [2], who chose to parameterise the $P_c(S_w)$ relationship with the approach of BROOKS & COREY (BC) and the relative permeabilities with the BROOKS & COREY and BURDINE functions (see Tab. 5.2).

Table 5.2: Properties of the examined porous media (sand, coarse and fine sand), for the random field the mean values are given

	sand	coarse sand	fine sand
porosity ϕ [-]	0.4	0.4	0.4
intrinsic permeability K [m^2]	$5.11 \cdot 10^{-12}$	$5.0 \cdot 10^{-9}$	$5.0 \cdot 10^{-12}$
entry pressure P_d [Pa]	500	350	1000
psd index λ [-]	2.0	3.0	3.0
irreducible water saturation S_wr [-]	0.05	0.08	0.1
residual DNAPL saturation S_nr [-]	0.0	0.0	0.0
$\omega_k = \frac{\min K}{\max K}$	0.027	0.001	
$\omega_c = \frac{\min P_\mathrm{d}}{\max P_\mathrm{d}}$	0.164	0.35	
variance σ^2 of $\ln K$ distribution	0.5		
correlation length [m]	0.05		

The random heterogeneity field of one by one metre was generated on the basis of an approach by DYKAAR & KITANIDIS, 1992 [38] with an isotropic exponential covariance function. As the grid is made up of 1012 nodes, one correlation length of 0.005 m is covered by five nodes, resulting in twenty correlation lengths in the x- as well as the y-direction.
Additional heterogeneity is introduced by accounting for a distribution of entry pressures, while all the other BROOKS & COREY parameters remain the same. The entry pressure of a given node i is assumed to correlate to the permeability according to the LEVERETT approach given by

$$P_{\mathrm{d}i} = P_\mathrm{d}^\mathrm{ref} \sqrt{\frac{K^\mathrm{ref}}{K_i}} \,, \tag{5.2}$$

where the superscript 'ref' denotes the arithmetic mean values of entry pressure and intrinsic permeability.

5.2.3 Averaging of saturation and pressure

On the assumption of a discrete distribution of phase pressures, for example from a simulation, is given, the average pressure of a phase may be calculated in two ways, the phase-volume weighted arithmetic mean

$$< P_\alpha^\mathrm{V} > = \frac{\sum_i^m P_{\alpha i} V_{\alpha i}}{\sum_i^m V_{\alpha i}} \quad \text{with} \quad V_{\alpha i} = S_{\alpha i} \phi_i V_{\mathrm{SCV}i} \,, \tag{5.3}$$

or the sub-control volume weighted arithmetic mean

$$< P_\alpha^S > = \sum_i^m P_{\alpha i} w_i \quad \text{with} \quad w_i = \frac{V_{SCVi}}{V_{dom}} , \tag{5.4}$$

where V_{SCV} denotes the volume of a sub-control volume from the spatial discretisation (see Sec. 4.2), V_{dom} the volume of the averaging domain and m the number of sub-control volumes belonging to the averaging domain. Averaged quantities will be marked with $<>$ in the following.
The average capillary pressures result from

$$< P_c^V > = < P_n^V > - < P_w^V > , \tag{5.5}$$

or

$$< P_c^S > = < P_n^S > - < P_w^S > \ . \tag{5.6}$$

The sub-control volume weighted arithmetic mean yields the average saturations $< S_\alpha >$ after

$$< S_\alpha > = \frac{\sum_i^m V_{SCVi} S_{\alpha i}}{\sum_i^m V_{SCVi}} . \tag{5.7}$$

For the averaging process, either the complete domain or only parts of the domain are considered. If the complete domain is taken into account, the averaging is performed during the numerical simulations. During the solving algorithm, the system of equations is set up by a loop over all elements, and for each element by a loop over its sub-control volumes (see Ch. 4). The averaging routine follows this procedure at the finest multi-grid level after each time step. In Eqns. (5.3), (5.4) and (5.7), m then equals the total number of sub-control volumes.
If only parts of the domain are taken into account, the averaging is based on output files with the nodal values of the primary and secondary variables at each node. For the BOX method, the nodal values are related to the BOX belonging to that node. Thus, for the rectangular domains with structured grids as applied here the averaging can be performed for a given variable e after:

```
1
2       for (i = 0; i < NUMBER\_OF\_NODES; i++)
3         {
4        if (CORNERNODE)
5           {
6             e_av = e_av + e[i]*0.25;
7             number_cornernodes = number_cornernodes + 0.25;
8           {
9        if (BOUNDARYNODE)
```

```
10          {
11            e\_av = e\_av + e[i]*0.5;
12            number_boundarynodes = number_boundarynodes + 0.5;
13          }
14       if (INNERNODE)
15          {
16            e_av = e_av + e[i];
17            number\_innernodes = number\_innernodes + 1.0;
18          }
19      }
20
21      weighting = number_cornernodes + number_boundarynodes + number_innernodes;
22      e_av = e_av/weighting;
23
```

5.2.4 Determination of the extended $P_c(S_w)$ relationship

For the extended $P_c(S_w)$ relationship, the equilibrium and at least one dynamic $P_c(S_w)$ relationship as well as the rate of change of saturation need to be determined. Then a linear regression using $\Delta P_c(\Delta S_w/\Delta t)$ yields the coefficient τ, which quantifies the slope of the function. HASSANIZADEH & GRAY, 1990 argue that the coefficient might be a function of the water saturation; the regression is thus performed at selected saturations.

Obtaining the equilibrium $P_c(S_w)$ relationship: BRAUN, 2000 [17] gives an overview of upscaling methods aimed at determining constitutive relationships in two-phase flow. One of the methods is based on the assumption of capillary equilibrium (e.g GREEN ET AL., 1996 [49], PICKUP & STEPHEN, 2000 [92]). Resulting from this assumption a reduction of variables is achieved, which facilitates the application of a percolation model. The equilibrium $P_c(S_w)$ relationship is thus calculated following a percolation model approach for a given spatial heterogeneity distribution. The distribution consists of n numbers of cells characterised by local $P_c(S_w)$ relationships which can be specified for example by BROOKS & COREY parameters. Furthermore, the volume fractions w belonging to the cells need to be given if a node-centred approach is followed. An arithmetically weighted average water saturation $< S_w >$ can be determined for a distribution for i numbers of increments in the capillary pressure (following for example a geometric series) after

$$< S_w > (P_{c,i}) = \frac{\sum_n S_{w,n}(P_{c,i}) w_n}{\sum_n w_n} , \tag{5.8}$$

applying for instance the inverse $P_c(S_w)$ relationship after BROOKS & COREY, 1964 [19]

$$S_w(P_c) = \begin{cases} S_{wr} + (1 - S_{wr} - S_{nr}) \frac{P_c}{P_d}^{-\lambda} & \text{if} \quad P_c > P_d \\ 1.0 \quad \text{if} \quad P_c \leq P_d \, . \end{cases} \tag{5.9}$$

Note that, in this fashion, hysteresis effects such as an entrapped non-wetting phase cannot be represented as a connection to the boundary is assumed for each porous medium cell. However, only primary drainage processes are examined here, so accessibility does not play a role as long as the (local) wetting phase saturation exceeds the residual saturation S_{wr} prescribed by the local $P_{\mathrm{c}}(S_{\mathrm{w}})$ relationship, which ensures that the relative permeability k_{rw} exceeds zero.
For the spatially correlated random field, the $P_{\mathrm{c}}(S_{\mathrm{w}})$ relationships are derived from the distribution of permeabilities, using them to scale the entry pressures after Eqn. 5.2, while all other BROOKS & COREY parameters remain the reference values (see Tab. 5.2). The average equilibrium $P_{\mathrm{c}}(S_{\mathrm{w}})$ relationships (see Fig. C.1) possess a smaller entry pressure compared to the reference curve. The minimum entry pressure for the scaled field amounts to 212 Pa. For water saturations $S_{\mathrm{wr}} < S_{\mathrm{w}} < 0.6$, the average curves are steeper than the reference $P_{\mathrm{c}}(S_{\mathrm{w}})$ relationship.
The application of a percolation model is one approach to determining the equilibrium $P_{\mathrm{c}}(S_{\mathrm{w}})$ relationship. In order to test the capillary equilibrium assumption, the equilibrium $P_{\mathrm{c}}(S_{\mathrm{w}})$ relationship could also be calculated on the basis of numerical experiments as for example done by ATAIE-ASHTIANI ET AL., 2002 [2]. Their procedure is repeated here for the simple heterogeneity pattern and the results will be compared.

Determination of the dynamic $P_{\mathrm{c}}(S_{\mathrm{w}})$ relationship: The dynamic $P_{\mathrm{c}}(S_{\mathrm{w}})$ relationships are determined on the basis of numerical experiments applying the initial and boundary conditions described in Sec. 5.2.1 and the averaging procedures described in Sec.5.2.3.
The difference between equilibrium and dynamic capillary pressure ΔP_{c} as defined by

$$\Delta P_{\mathrm{c}} = P_{\mathrm{c}}^{\mathrm{d}} - P_{\mathrm{c}}^{\mathrm{e}}(S_{\mathrm{w}}) = (P_{\mathrm{n}} - P_{\mathrm{w}}) - P_{\mathrm{c}}^{\mathrm{e}}(S_{\mathrm{w}}), \tag{5.10}$$

can be determined from the the equilibrium and the dynamic $P_{\mathrm{c}}(S_{\mathrm{w}})$ relationships for a given water saturation (see Fig. 5.6).

Determination of the rate of change of saturation: The rate of change of saturation for a given time step or measurement point at the time step n is approximated in the manner of a central difference scheme on the basis of the average saturation after

$$\frac{\partial S_{\mathrm{w}}}{\partial t} \approx \left(\frac{\Delta < S_{\mathrm{w}} >}{\Delta t} \right)^n = \frac{< S_{\mathrm{w}} >^{n+1} - < S_{\mathrm{w}} >^{n-1}}{t^{n+1} - t^{n-1}} \quad \text{for} \quad 1 < n < N\,, \tag{5.11}$$

where N is the total number of time steps in the simulations or number of the measurements in the laboratory experiments.
In order to obtain the magnitudes of the capillary pressure difference or saturation rate at the target saturations, values are linearly interpolated

$$y = y_{\mathrm{l}} + \frac{x - x_{\mathrm{l}}}{x_{\mathrm{h}} - x_{\mathrm{l}}} (y_{\mathrm{h}} - y_{\mathrm{l}})\,, \tag{5.12}$$

where y can be substituted by the rate of change of saturation or capillary pressure difference and x by the water saturation.

Determination of the coefficient τ: The extended $P_c(S_w)$ relationship is a linear relation between the capillary pressure difference and the rate of change of saturation (see Eqn. (3.13) and Fig. 5.6) running through the origin. Thus, at zero saturation rate, the pressure difference should also equal zero (see 'regression for τ_0' in Fig. 5.7). Clearly, it makes sense from a physical point of view that at equilibrium the difference between the phase pressures should be zero. However, it still might be the case that the relation between ΔP_c and $^{\Delta S_w}/_{\Delta t}$ is nonlinear for some range of saturation rates. An indication that the linearity does not hold for the whole range of saturation rates is, if a fitted linear relation does not run through the origin (see 'regression for τ_b' in Fig. 5.7). The magnitude of the y-axis intercept can be interpreted as a measure for the deviation from the linear case. For the data displayed in Fig. 5.7, a non-linear relation is called for at small saturation rates in order to force the relation $\Delta P_c(^{\Delta S_w}/_{\Delta t})$ to go through the origin. DAHLE ET AL., 2005 [30], who applied a bundle of capillary tubes model, have suggested a quadratic relation for small saturation rates.
Two formulas are thus considered for the calculation of the τ coefficient, the one defined by Eqn. (3.13) (denoting the coefficient τ_0 in the following) and the other allowing for a y-axis intercept, here denoted b (and denoting the coefficient τ_b in the following).

$$\Delta P_c = b - \tau_b \frac{\Delta S_w}{\Delta t} , \tag{5.13}$$

where possibly

$$\tau_b = \tau_b(S_w). \tag{5.14}$$

With this procedure, the linearity of the relationship between capillary pressure difference and saturation rate can be tested, assuming that $b \neq 0$ indicates a non-linear relationship at least for a range of saturation rates.
In order to perform the linear regression, at least two data sets of $\Delta P_c(^{\Delta S_w}/_{\Delta t})$ are required if measurement errors can be neglected. If the exact nature of the possibly occurring non-linearity is to be analysed a lot more data points are be required, which should cover a large range of saturation rates.
As mentioned before, the coefficient τ is determined for given water saturations. Thus, it can additionally be determined if the coefficient depends on the water saturation and if so how. No assumption is made about the relation a priori; it might be linear or non-linear.
If the regression is performed on the basis of laboratory data, errors in the dependent variable are taken into account. For data from numerical experiments, errors, e.g. at $S_w \rightarrow 1.0$ stemming from the discretisation length [77], are considered negligible.

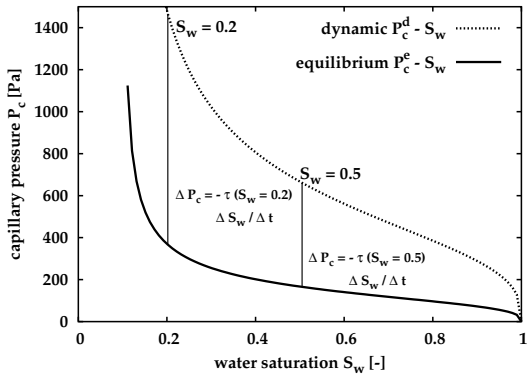

Figure 5.6: The extended $P_c(S_w)$ relationship for a projection on the S_w vs. P_c plane

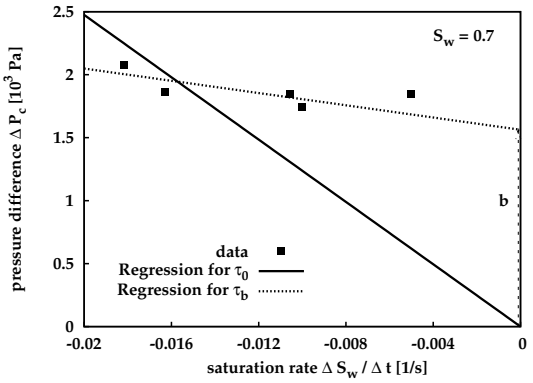

Figure 5.7: Regressed functions for the determination of τ in the extended $P_c(S_w)$ relationship

5.3 Applying laboratory experiments from GeoDelft, The Netherlands

The results of primary drainage experiments performed at GeoDelft Laboratories in Delft, The Netherlands, serve to determine the coefficient τ in the extended capillary pressure-saturation relationship after HASSANIZADEH & GRAY, 1990 [55]. For a description of the experimental set-up and the experiments performed by GeoDelft, Appendix B can be consulted.

5.3.1 Determination of the dynamic $P_c(S_w)$ and the rate of change of saturation

In laboratory experiments GeoDelft determined the equilibrium and three dynamic primary drainage $P_c(S_w)$ relationships of a natural Dutch sand, the Zeijen sand (HASSANIZADEH ET AL., 2005 [57]). A description of the experimental set-up can be found in App. B. In the drainage experiments, a DNAPL, Perchlorethylen (PCE), as the non-wetting phase displaced water as the wetting phase. Both phase pressures were measured continuously at opposite sides of the sand sample over an area of approx. $2.83 \cdot 10^{-5}\,\mathrm{m}^2$ each. These pressures are considered here as local pressures as opposed to average pressures. It is assumed that gravity influences can be neglected for the 0.03 m high column and that thus a linear run of the pressures over the sample can be presumed. Moreover, on the assumption that the flow process is mainly one-dimensional, the difference between the phase pressures measured at the middle of the sample yields the capillary pressure. The water saturation in the column is derived from the water pressure measurements in the lower reservoir. For the dynamic experiment, it is then corrected to represent a local measurement by shifting the measurement in time in order to let the first change in capillary pressure

coincide with the saturation change.
The measured dynamic $P_c(S_w)$ relationships applying non-wetting phase pressures in the upper reservoir of $P_n^T = 16\,\text{kPa}, 20\,\text{kPa}, 25\,\text{kPa}$ differ pronouncedly from the equilibrium $P_c(S_w)$ relationship (see Fig. 5.8, left). On the basis of the experimental data, the difference between the equilibrium and dynamic capillary pressure for a given saturation can be plotted as a function of the rate of change of saturation occurring at that saturation. As three dynamic experiments are performed, three data sets can be obtained for each saturation.
To take equilibrium capillary pressures between the measured data sets into account, the BROOKS & COREY $P_c(S_w)$ relationship (see Eqn. (2.14)) is fitted to the data pairs of the equilibrium primary drainage $P_c^e(S_w)$ relationship (see Fig. 5.8, left). The equilibrium $P_c(S_w)$ relationship thus calculated is assumed to be correct. The difference between the dynamic to the equilibrium capillary pressure at water saturations $S_w > 0.5$ are plotted in the right Fig. 5.8.

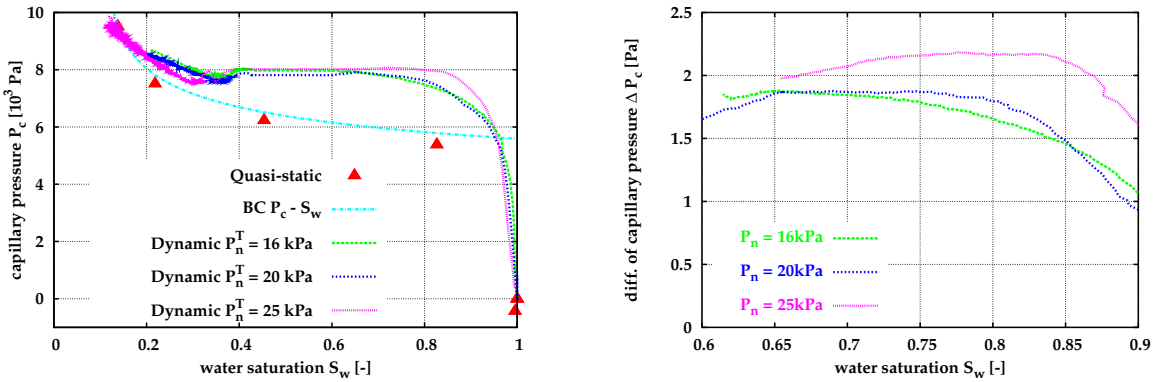

Figure 5.8: Equilibrium (quasi-static) and dynamic primary drainage $P_c(S_w)$ relationships, applying $P_n^T = 16, 20, 25\,\text{kPa}$ for the Zeijen sand (left) and their difference (right)

The rate of change of saturation is calculated on the basis of Eqn. (5.11), where n enumerates the saturation measurements and N the total number of measurements. The saturation rates thus determined show oscillations due to the noise in the measurements (see Fig. 5.9). Consequently, a smoothed saturation rate $< s >$ is determined, employing a moving median as given by

$$< s >^l = MM(s^{l-a}, ..., s^{l+a}) \quad \text{for} \quad a < l < N - a\,, \tag{5.15}$$

where N represents the number of original data s and a the (then to be sorted) range of data to be taken into account. The moving median is chosen, because it is less sensitive to outliers in the original data than the moving mean. On the basis of Eqn. (5.15), the moving median for the rate of change of saturation of each of the three experiments is calculated. As examples the smoothed saturation rates for $P_n^T = 16\,\text{kPa}$ are plotted here (see Fig. 5.10). The smoothed saturation rate derived from the moving median of eleven data sets is applied in the calculations of the material coefficient.

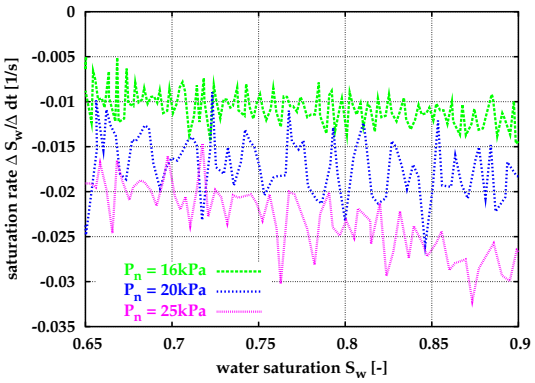

Figure 5.9: Rate of change of saturation as a function of the water saturation for the drainage GeoDelft experiments

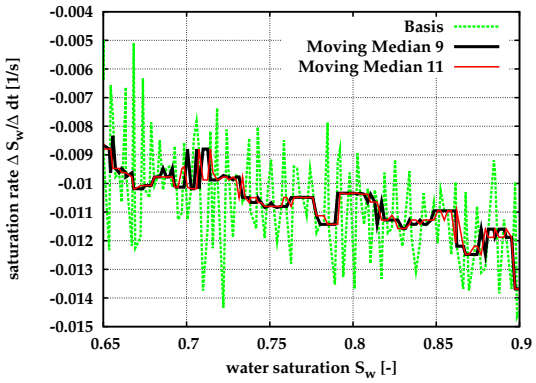

Figure 5.10: Smoothed rate of change of saturation (applying a moving median of nine or eleven data sets) as a function of saturation for $P_n^T = 16\,\mathrm{kPa}$

The three $^{\Delta S_w}/_{\Delta t}(S_w)$ functions show little dependence on the saturation, but a clear difference depending on the applied pressure P_n in the upper reservoir. As expected, for higher pressure, higher rates of change of saturation can be observed.

5.3.2 Regression to calculate τ

The chosen regression algorithm does not allow for an error in the independent variable. To take into account errors both in the rate of change of saturation as well as in the difference of the capillary pressures, regressions are performed, using either of them as the dependent variable. For the rate of change of saturation, the error was assessed on the basis of the oscillations to $0.005\,{}^1/_s$, while for the difference $\Delta P_c = P_n - P_w$ GeoDelft gives an error of 0.25 kPa for all measurements.
On the basis of the calculated data, regressions applying a least-squares Marquardt-Levenberg algorithm are performed for water saturations larger than $S_w > 0.6$, a saturation which corresponds to a time in the experiments when the front has not yet reached the lower boundary (membrane). In the following, the linear relationship as given by Eqn. (3.13) and Eqn. (5.14) allowing for a y-axis intercept are fitted to three data sets applying varying independent variables x and dependent variables y, namely

1. $x = {}^{\Delta S_w}/_{\Delta t}$ after Eqn. (5.11) and $y = \Delta P_c$ (case 1),
2. $x = \Delta P_c$ and $y = {}^{\Delta S_w}/_{\Delta t}$ after Eqn. (5.11) (case 2), and
3. $x = \Delta P_c$ and $y = {}^{\Delta S_w}/_{\Delta t}$ as resulting from the averaging with a moving median after Eqn. (5.15) (case 3).

Fig. C.2 to Fig. C.4 in App. B show the data sets and the resulting functions, whose coefficients are listed in Tab. C in the Appendix to give the exact magnitudes of the resulting τ and b values.

The regressions on the basis of Eqn. (3.13) yield τ_0 values varying from $\tau_0 = 65.4\,\mathrm{kPa\,s}$ to $\tau_0 = 143.5\,\mathrm{kPa\,s}$ depending on the water saturation and the case (see Fig. 5.11, left, and Figs. C.5 to C.7 in App. B). DAHLE ET AL., 2005 [30] as well as GIELEN ET AL., 2004 [45] also report that τ is a function of the water saturation from pore scale calculations with a bundle of capillary tubes and a pore-network model respectively. The differences between the τ_0 values of case 1 and 2 result from the differing errors in ΔP_c and and $^{\Delta S_w}/_{\Delta t}$. The smoothed saturation rate effects a smoothing of $\tau_0(S_w)$ (case 3). While the $\tau_0(S_w)$ data of cases 1 and 2 show a maximum at $S_w = 0.75$ and indicate a quadratic $\tau_0(Sw)$ relation, $\tau_0(S_w)$ from the smoothed saturation rate (case 3) indicates a linear trend, inversely proportionally to the water saturation. The error in the determined τ_0 values ranges from 10.5 % to 18.7 %, again depending on the saturation and the case.
The regression on the basis of Eqn. (5.14) yields τ_b values between $\tau_b = 11.0\,\mathrm{kPa\,s}$ and $\tau_b = 154.7\,\mathrm{kPa\,s}$ depending on the water saturation and the data sets (see Fig. 5.11, right and Figs. C.2 to C.4). The differences between the τ_b values of case 1 and 2 are more pronounced than the ones of the $\tau_0(S_w)$ data. This might be attributed to the fact that the confidence in the τ_b values is in general worse than in the τ_0 values. For τ_b the errors range between zero and 146.5 %, depending on the saturation and the case. The $\tau_b(S_w)$ data of cases 1 and 2 possess a minimum at $S_w = 0.75$ and show a parabolic shape, whereas the $\tau_b(S_w)$ data of case 3 suggests a linear relationship with τ_b behaving directly proportional to the water saturation (see Fig. 5.11, right).

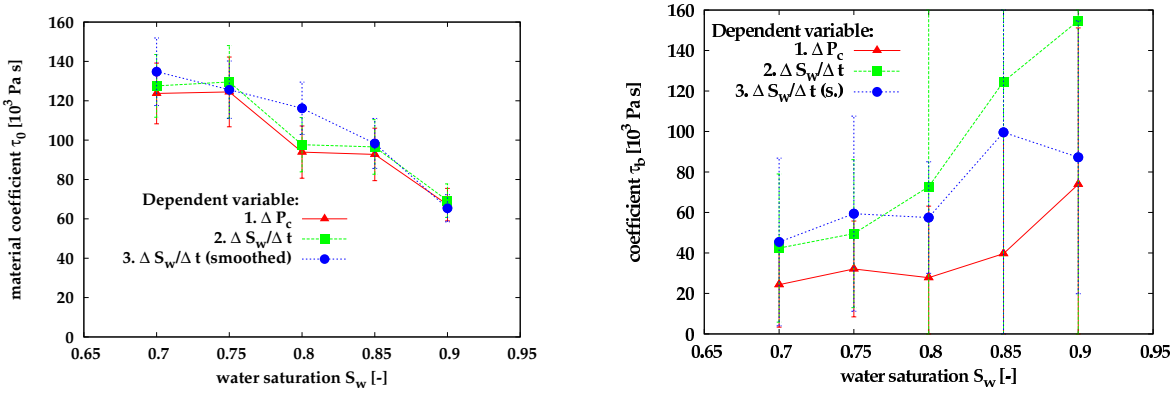

Figure 5.11: Comparison of $\tau_0(S_w)$ (left) and $\tau_b(S_w)$ (right) for varying dependent variables in the regression routine

The y-axis intersect b varies between $b = -1.57\,\mathrm{kPa}$ and $b = 1.56\,\mathrm{kPa}$ (see Fig. 5.12, left). With increasing saturation, the values for b decrease for all three data sets. The highest b values result from the regression to the data of case 1, the lowest are observed for case 2. With increasing water saturation, the confidence in the b values diminishes for all three data sets. For water saturations of $S_w = 0.85$ and $S_w = 0.9$, the b value could thus possibly also equal zero. If the value of b is interpreted as a measure for the deviation from the linear relation $\Delta P_c(^{\Delta S_w}/_{\Delta t})$, then this deviation depends on the water saturation. For medium water saturation, the deviation is

expected to be larger than for high water saturations, where the absolute values of and the confidence in b decrease.
In addition, the difference in the τ values ($\tau_0 - \tau_b$) for each saturation (see Fig. 5.12, right) can be consulted to validate the linearity of Eqn. (3.13). The differences in τ depend on the water saturation for each of the three cases. Also, for all cases, the difference is positive for medium water saturations and negative for high water saturations, thereby showing the same trend as the $b(S_w)$ data which are obviously correlated.
The differences in the coefficient τ for a given water saturation also imply either that the linear approximation is not valid at all or that it is only valid for a range of saturation rates. In the experiments, the norm of the rates of change of saturation at the chosen water saturations does not decrease below $0.009\,1/s$. Thus, one can only assume, that the relationship between the rate of change of saturation and the difference in capillary pressure is non-linear at low rates of change of saturation. DAHLE ET AL., 2005 [30] suggest a quadratic relation for this range on the basis o: computations of τ with a bundle of capillary tubes. In contrast, GIELEN, 2005 [46] does not find a y-axis intercept unequal to zero on the basis of pore-network simulations.

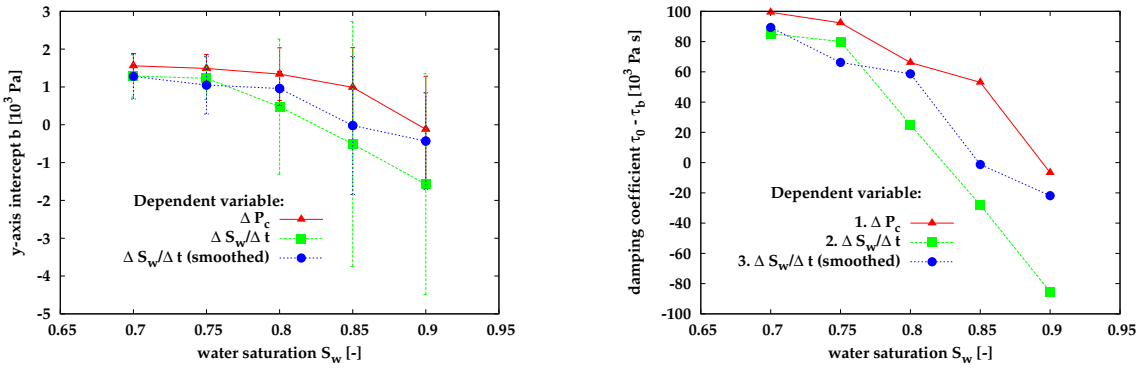

Figure 5.12: Values of b (left) and the difference $\tau_0 - \tau_b$ (right) for varying dependent variables in the regression routine

5.3.3 The coefficient τ as a function of water saturation

The determined τ values indicate the coefficient to be a function of the water saturation. Thus quadratic and linear functions are fitted to $\tau(S_w)$ of case 3 (see Fig. 5.13, for regressions to data base 1 and 2 see also Figs. C.5 to C.8) again applying a least-squares Marquardt-Levenberg algorithm. The b-values of the regressions with Eqn. (5.14) are not taken into account. Obviously, with increasing degrees of freedom the deviations from data to regressed function decrease.
The trends in the $\tau_0(S_w)$ and $\tau_b(S_w)$ functions show opposing trends for both the linear and the quadratic approximation. Whereas for $\tau_0(S_w)$ the quadratic function has

a maximum, $\tau_b(S_w)$ shows a minimum. Regarding the linear fitting function, $\tau_0(S_w)$ decreases with increasing water saturation (negative slope), while $\tau_b(S_w)$ increases (positive slope). CARROLL ET AL., 2005 [86] found a good agreement between simulation and data of a multi-step outflow experiment for a linear $\tau(S_w)$ function with negative slope as opposed to applying τ as a constant. The slope of the function is calculated here amount to 317 kPa for the $\tau_0(S_w)$ data.

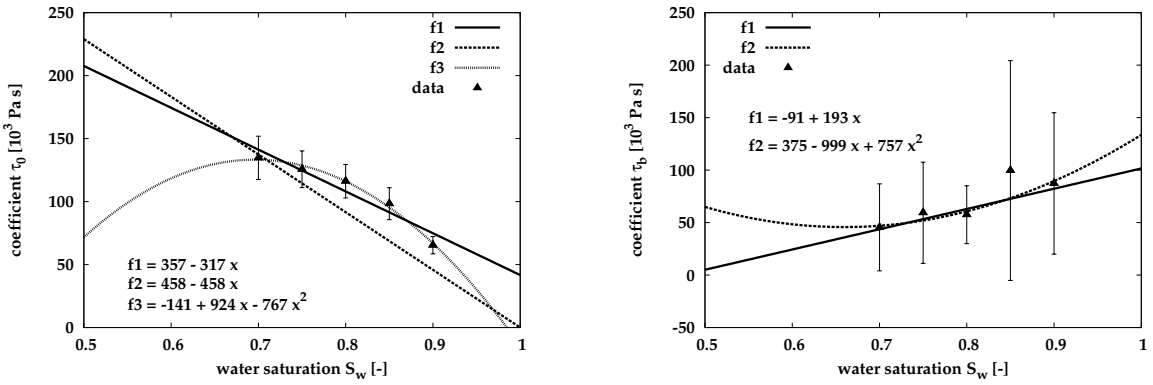

Figure 5.13: $\tau_0(S_w)$ (left) and $\tau_b(S_w)$ (right) from regression to (smoothed) experimental data with the inverse of Eqn. (3.13)

5.3.4 Comparison to the investigation of KALAYDJIAN, 1992

In the following, the study of KALAYDJIAN, 1992 [68] is consulted for a comparison of results despite some differences in the experimental procedure and the samples applied. KALAYDJIAN, 1992 determines τ coefficients on the basis of equilibrium and dynamic main imbibition experiments with a limestone sample. In the experiments employing a sample of 0.222 m height, water displaces an oil phase with a dynamic viscosity of $\mu_n = 1.49\,\mathrm{Pa\,s}$ and a density of $\rho_n = 1032.4\,\mathrm{kg/m^3}$, while the density of the aqueous phase is stated as $\rho_w = 757.5\,\mathrm{kg/m^3}$. To determine the equilibrium capillary pressure-saturation relationship, the author applied a low influx of $2.055 \cdot 10^{-10}\,\mathrm{m^3/s}$ of oil. A medium influx of $1.389 \cdot 10^{-9}\,\mathrm{m^3/s}$ as well as a high influx of $4.167 \cdot 10^{-9}\,\mathrm{m^3/s}$ were used for the determination of the dynamic $P_c^d(S_w)$ relationship. Both phase pressures and the water saturation were measured locally. For imbibition processes, the dynamic capillary pressure is expected to be smaller than the equilibrium one at a given water saturation; which is confirmed by the experimental results of KALAYDJIAN, 1992.
KALAYDJIAN performed regressions applying Eqn. (3.4) (compare Secs. 3.3 and 3.5). In contrast to the approach taken here, where for each saturation the data sets $\Delta P_c(\Delta S_w/\Delta t)$ of three experiments are applied to calculate τ, KALAYDJIAN, 1992 fits the function to the $\Delta P_c(\Delta S_w/\Delta t)$ data at a given (effective) saturation for each one of the two dynamic experiments. Thus, he implicitly assumes that the linear relationship running through the origin holds and that τ is a function of the influx or of the

capillary number. The τ values thus determined range between $\tau \approx 5.4 \cdot 10^5$ Pa s and $\tau \approx 2.9 \cdot 10^6$ Pa s (see Fig. 5.14) depending on the reduced water saturation and the influx. For water saturations of $S_e > 0.7$, the τ values gained from the high influx exceed those from the low influx, whereas the opposite holds for smaller water saturations. For the medium inflow rate the τ values show a maximum, while for the high rate a minimum can be observed.

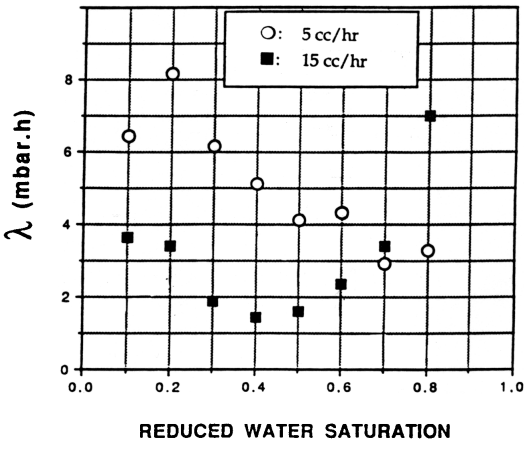

Figure 5.14: $\tau_K(S_e)$ as given in KALAYDJIAN, 1992 [68], where λ[mbar h] $\approx 3.6 \cdot 10^5 \tau$[Pa s]

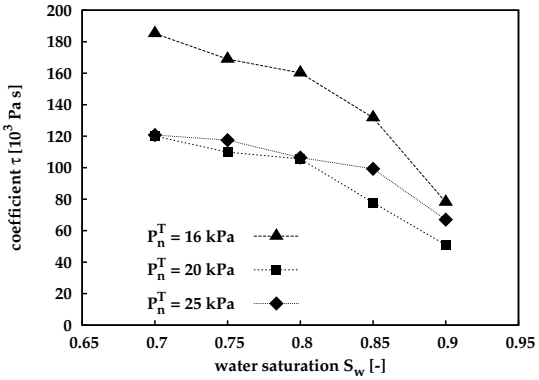

Figure 5.15: $\tau(S_w)$ as determined by regression to the data from each of the GeoDelft experiments

To facilitate a comparison to the data of KALAYDJIAN, 1992, the coefficient τ is also determined with the GeoDelft data depending on the water saturation for each experiment. All three resulting $\tau(S_w)$ data sets behave inversely proportionally to the water saturation (see Fig. 5.15). While the $\tau(S_w)$ data differ slightly for dynamic experiments applying $P_n^T = 20$ kPa or $P_n^T = 25$ kPa, the magnitudes of $\tau(S_w, P_n^T = 16\,\text{kPa})$ are larger compared to the other two especially at medium water saturations. The data of KALAYDJIAN, 1992 show the same behaviour (see Fig. 5.14); τ of a medium influx is higher than that of the high influx rate. Moreover, compared to the $\tau(S_w)$ data calculated on the basis of all three GeoDelft experiments, the $\tau(Sw)$ values determined for the individual experiments show higher maximum values of $\tau(S_w)$ especially at medium water saturations. Differences in $\tau(S_w)$ from each of the experiments again indicate that the linear function between ΔP_c and $\Delta S_w/\Delta t$ might not hold for the whole range of saturation rates. Also, the data suggest that the deviations are higher for medium than for high water saturations.
Regarding the magnitude of KALAYDJIAN's τ values, they exceed the ones determined here by approximately one to two orders of magnitude. Differences in the coefficient from the GeoDelft data and KALAYDJIAN, 1992 might be explained by differences in

- the porous medium properties,
- fluid properties,

- and a process-direction dependence.

The sample employed by KALAYDJIAN, 1992 had an intrinsic permeability of $K = 1.61 \cdot 10^{-13}\,\mathrm{m}^2$, which is about one order of magnitude less than the permeability of the Zeijen sand. In addition, the viscosity of the non-wetting phase differs in the two experiments. According to the formula proposed by STAUFFER, 1978 [108], the coefficient scales inversely with the permeability and directly with the viscosity. However, this formula was set up for a water-gas system and thus might not be applicable to water-oil systems. Nevertheless, the inverse proportionality to the permeability could be confirmed by the data.
Moreover, while KALAYDJIAN, 1992 determined the coefficient τ for a main imbibition process, GeoDelft performed primary drainage experiments. It is possible, that the τ values show a process-dependent behaviour, that it to say they could differ from imbibition to drainage.

5.3.5 Summary of the results from laboratory experiments

In this section, the coefficient τ from the extended $P_c(S_w)$ relationship is determined on the basis of experimental data of GeoDelft, The Netherlands. The results are compared to data of KALAYDJIAN, 1992 [68]. The following conclusions can be drawn:

- The values determined for the coefficient τ range between 11.0 kPa s and 154.7 kPa s depending on the water saturation and on whether a y-axis intercept is accounted for or not. On the basis of the smoothed data of the rate of change of saturation, an inversely proportional linear relationship of the coefficient on the water saturation seems appropriate.

- Testing the linearity of the extended $P_c(S_w)$ relationship suggests that it might not hold for the whole range of saturation rates. As only a limited range of saturation rates occurred in the experiments, the magnitude of the deviation from linear at low rates of change of saturation should be a matter of further research. Moreover, this effect might depend on the water saturation. For high water saturations the confidence in the linearity is larger than at low water saturations. One explanation of the higher confidence at high water saturations might be that the relative measurement error of the saturation is smaller at high saturations.

- The comparison of the data to results of KALAYDJIAN, 1992 [68] shows deviations of one to two orders of magnitude in the τ coefficients. It is thus argued that τ is sensitive (either) to the intrinsic permeability, the fluid properties and / or the process. STAUFFER, 1978 [108] suggests a proportional behaviour of τ to the water viscosity and an inverse proportionality to the permeability. The comparision to KALAYDJIAN, 1992 seems to confirm the inverse relation to the intrinsic permeability. A hysteretic behaviour of τ needs to be investigated further.

- Following the regression approach taken by KALAYDJIAN, 1992 [68], who obtained τ values depending on the applied influx, the coefficient has to be treated as a function of for example the rate of change of saturation for all ranges of the saturation rate. While this might be the case, it does not make sense that τ should increase with decreasing flux. In the limit of capillary dominated flow, τ would then reach a maximum or tend to infinity. However, it is assumed here that for capillary dominated flow, the equilibration between the difference in phase pressure and the equilibrium capillary pressure is given at all times and that thus an extended $P_c(S_w)$ relationship does not need to be taken into account. It is therefore suggested either to perform the fitting on the basis of several dynamic experiments or to use a different experimental set-up and to determine τ by inverse parameter identification (see CARROL ET AL., 2006).

In Section 5.4, the τ values from the experimental data are compared to values calculated from the simulation of the experiments.

5.4 Numerical experiments applying MUFTE-UG

Laboratory experiments have the advantage displaying the characteristics of a flow process while no or only few assumptions need to be made. However, restricted measurement facilities (e.g. their resolution in space and time) and the time input for the more advanced observations in two-phase flow (like the determination of an equilibrium $P_c(S_w)$ relationship) limit the possibilities of laboratory experiments. In contrast, numerical experiments applying a simulator like MUFTE_UG usually enable us to perform parameter studies or sensitivity analysis for a large number of examples in a short time. However, when such a model is set up, assumptions need to be made for the underlying physical-mathematical model, which restricts the applicability.
In the following, the advantages of numerical models are exploited to determine the coefficient τ on the local scale to macroscale, while assuming that pore scale dynamic effects can be neglected. HASSANIZADEH & GRAY, 1990 [55] well as by KALAYDJIAN, 1987 [67] obtained their extended $P_c(S_w)$ relationship within an upscaling procedure from the pore to the local scale. It is assumed here that heterogeneity on the local scale may introduce additional dynamic effects when averaging to the macroscale.
Various numerical experiments mimicking laboratory experiments are performed. Equilibrium numerical experiments yield an upscaled equilibrium $P_c^e(S_w)$ relationship. On the basis of dynamic numerical experiments dynamic $P_c(S_w)$ relationships as well as the rate of change of saturation are calculated. The simulation of a laboratory experiment serves to examine the nature and the magnitude of the pore scale effects that are not captured with the traditional two-phase flow model. The averaging of pressure or saturation as described in Sec. 5.2.3 is first tested with equilibrium numerical experiments for the simple heterogeneity pattern

using a comparison to a percolation model approach assuming capillary equilibrium. Then the averaging is applied in dynamic numerical experiments in order to analyse whether dynamic effects in an averaged $P_c(S_w)$ relationship can be observed.

5.4.1 Simulation of laboratory experiments

In Sec. 5.3, data from laboratory experiments performed at GeoDelft Laboratories, The Netherlands, are applied to determine the coefficient τ. Here, the simulations of the experiments are described. On the basis of the simulations, the coefficient τ is determined and its values are compared to the ones derived from the laboratory experiments.
In the simulations applying MUFTE-UG (see Sec. 4.1), the two-phase balance equations (2.36) and (2.37) are solved, where, for the closure of the system, the unique relation for the capillary pressure after Eqn. (2.35) is applied.

Domain, boundary and initial conditions The 0.03 m by 0.05 m domain of the simulations (see Fig. 5.16) corresponds to the experimental set-up of membranes plus their holders and the sand sample as described in App. B. The grid has a regular spacing of $\Delta z = 0.0025$ m in the z-direction. The membranes and membrane holders either for the top (TM) or for the bottom (BM) of the sand sample are considered together respectively and are represented by equivalent properties (see Tab. 5.3).
From the three dynamic drainage laboratory experiments described in Sec. 5.3, the experiment applying a non-wetting phase pressure of $P_n^T = 20$ kPa in the upper reservoir is selected for the simulations. The sand sample and the BM are initially fully water-saturated; thus, a hydrostatic pressure distribution can be prescribed for the wetting phase pressure.
In the TM, the non-wetting phase (PCE) saturation initially equals $S_n = 0.99$. The non-wetting phase saturation needs to be slightly less than one for numerical reasons. Choosing P_w and S_n as primary variables implies that at the relative permeability of the wetting phase equals zero $S_n = 1.0$. Thus, the flux term in the balance equation for the wetting phase becomes zero. In addition, the capillary pressure in the $P_c(S_w)$ relationship goes to infinity for $S_w \to S_{wr}$, which causes numerical problems.
The non-wetting phase pressure at the top boundary equals $P_n^T = 20$ kPa. For the wetting phase, a no-flux boundary is imposed at the top as the hydrophobic membrane prevents water to exfiltrate. At the bottom boundary, a constant water pressure of $P_w = 0.49$ kPa (corresponding to a pressure head of the water phase of 0.04 m) and a no-flow condition for the non-wetting phase are imposed. As MUFTE-UG only allows for two- and not one-dimensional domains, no-flow boundaries are imposed on both sides of the domain for both fluid phases. Instead of the DIRICHLET boundary condition at the lower boundary for the water phase, a free flow boundary condition was also tested, where a NEUMANN boundary condition is given without specifying the flux. The flux is then computed within each time step, which

requires a DIRICHLET boundary condition for the non-wetting phase ($S_n = 0$). The differences in the cumulative outflow over time from both simulations are negligible. The DIRICHLET boundary condition is consequently considered a good approximation.
Fig. 5.17 shows the water saturation at selected times from the simulation.

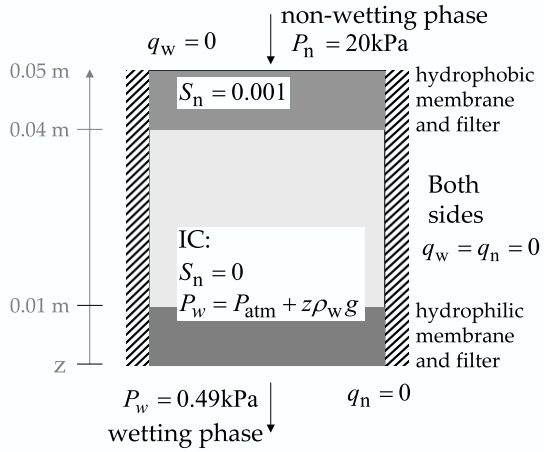

Figure 5.16: Initial and boundary conditions for the simulation of the laboratory dynamic primary drainage experiment

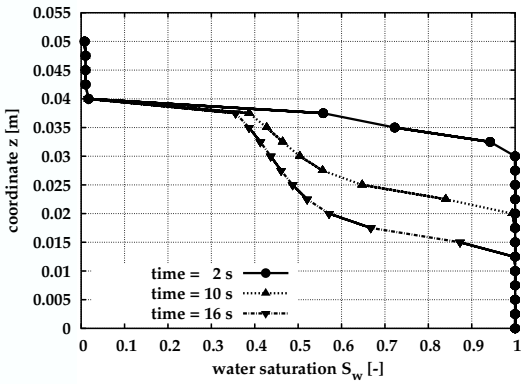

Figure 5.17: $S_w(z)$ from the simulation of the laboratory experiment by GeoDelft at selected times

Properties: Tab. 5.3 lists the properties of the Zeijen sand, and the membranes plus membrane holders TM and BM. For the BC parameters of the $P_c(S_w)$ relationships for the membranes, reasonable values are assumed for the numerical simulations. In order to mimic the different properties of the TM and BM, the hydrophilic BM is assigned a high BC entry pressure of $P_d = 20$ kPa, while the hydrophobic TM is

Table 5.3: Parameters for the Zeijen sand (ZS), the hydrophobic top membrane including the holder (TM) and the hydrophilic bottom membrane including the holder (BM)

Parameter	ZS	TM	BM
Porosity Φ [-]	0.35	0.4	0.45
Intrinsic permeability K [m^2]	$3.06 \cdot 10^{-12}$	$3.1 \cdot 10^{-12}$	$3.06 \cdot 10^{-13}$
BC entry pressure P_d [kPa]	5.587	1.0	20.0
BC pore volume distribution index λ [-]	6.11	2.0	2.0
Irreducible water saturation S_{wr} [-]	0.104	0.0	0.0
Residual DNAPL saturation S_{nr} [-]	0.0	0.2	0.0

assigned a comparatively low BC entry pressure of $P_d = 1\,\text{kPa}$ and an initial DNAPL saturation of $S_n = 0.99$. As only primary drainage with an infiltration of the non-wetting phase starting from the top is simulated, the upper filter is represented sufficiently. If an imbibition process were to be simulated, the properties would have to be reconsidered.

Local and average variables: Corresponding to the laboratory experiment, the local capillary pressure $P_c(z = 0.025\,\text{m})$ is tracked with time. Local capillary pressure from the numerical experiments here corresponds to the capillary pressure at one node in a grid with a spacing in the z-direction of $0.0025\,\text{m}$. In addition, the average water saturation $< S_w >$ after Eqn. (5.7) as well as the average phase-volume-weighted pressures $< P_w^V >$ and $< P_n^V >$ after Eqn. (5.3) are calculated for the end of each time step. Eqn. (5.5) then yields the average capillary pressure $< P_c >$ for that step. Averaging includes only the part of the domain from $0.01\,\text{m}$ to $0.04\,\text{m}$, which represents the sand sample.
The average water saturation changes as soon as the non-wetting phase pressure is increased at the upper boundary at the beginning of the experiment. In comparison to the experiment, the average water saturation changes faster in the simulation (see Fig. 5.18, left). In Fig. 5.18, right, the local capillary pressure measurement vs. time from the experiment is compared to the local capillary pressure from the simulation. The large deviation at the beginning can be attributed to the application of the BROOKS & COREY model for the equilibrium $P_c(S_w)$ relationship. At full water saturation the capillary pressure then equals the entry pressure and not zero. Both pressures $P_c(t)$ only begin to alter at $t \approx 6\,\text{s}$, when the non-wetting phase front reaches the middle of the sample. The P_c measured in the laboratory then increases to a maximum of $\approx 8\,\text{kPa}$ at $t = 25\,\text{s}$ and slightly decreases again afterwards. Clearly, the behaviour of the P_c in the laboratory experiment is not represented by the local P_c from the simulation, which reaches a maximum of $\approx 6.7\,\text{kPa}$ at $t = 25\,\text{s}$ and then remains more or less constant during the considered time range. The differences in the local capillary pressure between experiment to simulation can be attributed to pore-scale dynamic effects which are not represented in the unique $P_c(S_w)$ relationship applied in the simulations.
Thus, the rate of change of saturation as a function of time (see Fig. 5.19, left) of the simulation is also about 50 % higher (regarding absolute values) than that of the experiment. Plotting the saturation rate over time clearly shows the influence of the lower membrane in the simulation. As soon as the non-wetting phase front reaches the bottom membrane, the rate of change of saturation decreases. This happens earlier than in the experiment (see Fig. 5.18, left)

Comparison of capillary pressure-saturation relationships from experiment and simulation: As in Sec. 5.3, only water saturations higher than $S_w > 0.6$ will be considered for the analysis, because at approximately that saturation the non-wetting front reaches the lower membrane. Then the influence of the boundary conditions

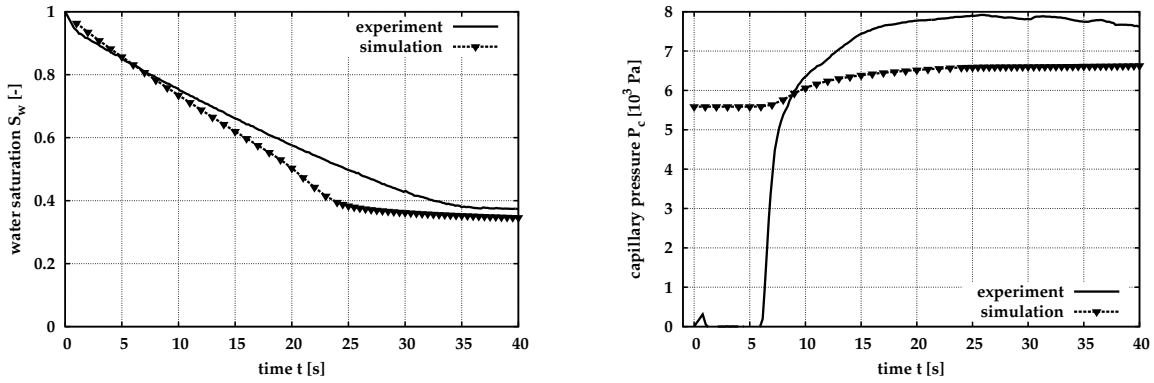

Figure 5.18: $< S_\mathrm{w} > (t)$ (left) and $P_\mathrm{c}(z = 0.025\,\mathrm{m}, t)$ (right) for laboratory experiment and simulation

becomes pronounced, which is to be avoided. It is presumed here, that parameters determined in laboratory experiments or by upscaling approaches should not depend on boundary conditions as such a dependence would restrict their applications to cases where the same boundary conditions prevail.
Measured and simulated dynamic $P_\mathrm{c}^\mathrm{d}(S_\mathrm{w})$ relationships differ from each other (see Fig. 5.19, right).

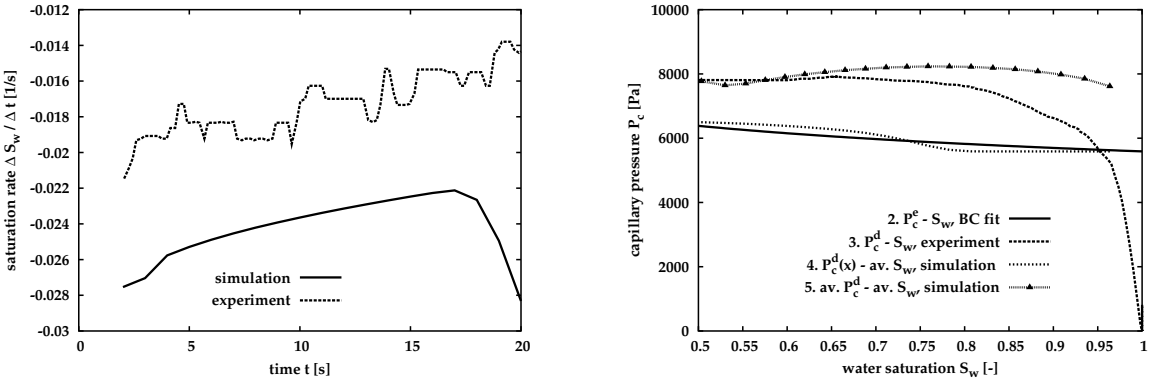

Figure 5.19: $P_\mathrm{c}^\mathrm{e}(S_\mathrm{w})$ and $P_\mathrm{c}^\mathrm{d}(S_\mathrm{w})$ relationships from the laboratory experiment and simulation with $P_\mathrm{n}^\mathrm{T} = 20\,\mathrm{kPa}$

First, the simulated $P_\mathrm{c}^\mathrm{d}(S_\mathrm{w})$ using the local $P_\mathrm{c}^\mathrm{d}(z = 0.025\,\mathrm{m})$ and average water saturation $< S_\mathrm{w} >$ (curve 3 in Fig. 5.19, right) is compared to the measured $P_\mathrm{c}^\mathrm{d}(S_\mathrm{w})$ relationship (curve 3). The capillary pressure at a given water saturation of curve 3 is higher than the measured dynamic $P_\mathrm{c}^\mathrm{d}(S_\mathrm{w})$ relationship (curve 2 in Fig. 5.19, right) for $S_\mathrm{w} \to 1.0$, where in the simulation the influence of the chosen parametrisation of the $P_\mathrm{c}^\mathrm{e}(S_\mathrm{w})$ with the approach after BROOKS & COREY (BC) becomes apparent. Before the non-wetting front reaches the middle of the domain, the local capillary pressure equals the entry pressure. For water saturations smaller

than $\approx S_w < 0.95$, the simulated $P_c^d(z)$ is pronouncedly smaller than the measured one. What is more, for water saturations of $S_w > 0.75$, the capillary pressure of the simulated dynamic $P_c^d(S_w)$ is smaller than the equilibrium $P_c^e(S_w)$ after BROOKS & COREY being applied in the simulations. This is contrary to the expectation that, in a drainage experiment, the difference between the dynamic and equilibrium capillary pressure should always be positive. The negative difference in $P_c^d - P_c^e$ and the difference to the measured $P_c^d(S_w)$ relationship indicate that

- dynamic effects of the pore scale are not represented in the mathematical-physical model underlying the simulation, where the traditional, unique relationship between capillary pressure and saturation is assumed to hold, and
- the averaged phase pressure represents the pressure measurement of the selective phase pressure transducers better than the pressure of one node.

Secondly, for a given water saturation, the simulated $P_c^d(S_w)$ using the average $< P_c^V >$ and average water saturation (curve 4 in Fig. 5.19, right) exceeds the measured dynamic $P_c^d(S_w)$ curve at high water saturations. At medium water saturations curve 4 approaches the measured dynamic $P_c^d(S_w)$ relation.
When the traditional $P_c(S_w)$ relationship and not an extended one is applied, pore-scale dynamic effects are neglected in the simulations. A difference between the dynamic and the equilibrium capillary pressure arises solely due to the volume-averaging of the phase pressures.

Determination of the coefficient τ: On the basis of curve 4, the equilibrium $P_c(S_w)$ relationship after BROOKS & COREY and the simulated saturation rate (see Eqn. (5.11)), values of τ are calculated as a function of water saturation (see Fig. 5.20), applying the linear relationship given in Eqn. (3.13). Testing the linearity of the relationship is not an issue in this section. In contrast to the experimentally determined τ values described in Sec. 5.3, the magnitude of τ from the simulations appears not to depend on the water saturation. However, the τ values from the simulations are of the same order of magnitude as those from the experiment if one keeps in mind the confidence interval of the τ values. Strictly speaking, the τ values from the simulation should only be compared to those gained from the laboratory experiment when $P_n^T = 20\,\text{kPa}$ at the top is applied (see 'exp., 20kPa only' in Fig. 5.20). These differ from the τ gained from regressions to three data sets per saturation ('exp., b = 0') for medium but not for high water saturations.

Influence of the membranes: The influence of the membranes is tested for the dynamic drainage case applying a non-wetting phase pressure of $P_n^T = 16\,\text{kPa}$ at the top boundary. One simulation is carried out in which the membranes and filters are accounted for (the domain is thus 0.05 m high (see Fig. 5.16). Averaging the pressures and the water saturation is carried out over the sample only, namely from 0.01 m to 0.04 m. In the second simulation, the membranes are disregarded, the domain thus only has an extension in the z-direction of 0.03 m. Fig. 5.21 displays the resulting

$\tau(S_w)$ functions, which are derived on the basis of average dynamic capillary pressure and water saturation. Clearly, the representation of the membranes influences the magnitude of the $\tau(S_w)$ functions. If the simulation is carried out with the membranes, the τ values at a given saturation are higher than the ones derived from a simulation without the membranes.
While at water saturations of approx. $S_w > 0.7$, the difference between $\tau(S_w)$ data including the membranes and the $\tau(S_w)$ data excluding the membranes is constant, the membranes influence also the trend in the curves for lower saturation. For $\tau(S_w)$ from the numerical experiment including the membranes, the magnitude of the coefficient τ increases with decreasing water saturation; the opposite trend is observable in $\tau(S_w)$ resulting from simulations without considering the membranes.

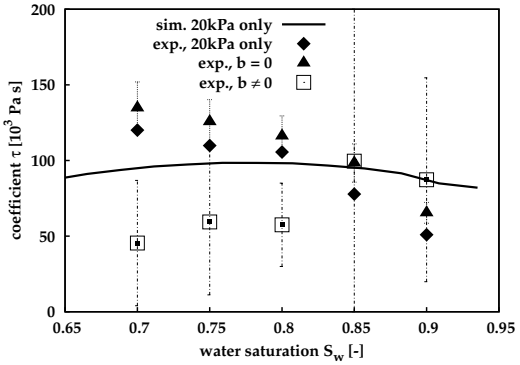

Figure 5.20: $\tau(S_w)$ on the basis of laboratory experiment ($P_c(z)(S_w)$) and simulation ($< P_c > (< S_w >)$)

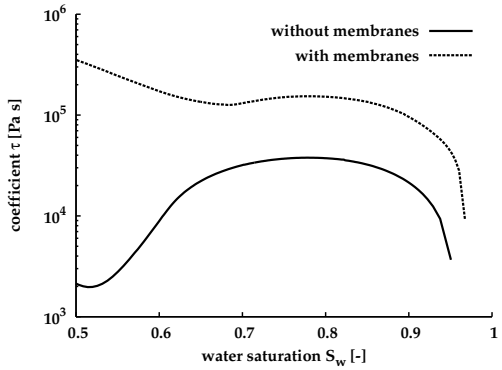

Figure 5.21: Comparison of $\tau(S_w)$ from simulations of the dynamic drainage laboratory experiment ($P_n^T = 16\,\text{kPa}$) including and excluding membranes

Obviously, pore-scale dynamic effects are neglected in the simulations and the $\tau(S_w)$ relations are based on average $< P_c^V >$ and $< S_w >$ values. In a local measurement of phase pressures and saturation, the effect might be less pronounced. Nevertheless, these effects should be taken into account when laboratory or numerical experiments are performed with a view to determining the coefficient τ.
In this section, the experimental data of the dynamic primary drainage experiment applying a non-wetting phase pressure of $P_n^T = 20\,\text{kPa}$ at the top is compared to simulation results. Besides the temporal development of water saturation and capillary pressure, the capillary pressure-saturation relationships and the calculated coefficients are analysed. The results may be summarised as follows:

- Applying a unique $P_c(S_w)$ relationship in the simulations over-predicts the rate of change of saturation, while the local dynamic P_c is underestimated. In the simulations the unique, equilibrium $P_c(S_w)$ is assumed to hold locally; thus, only this relation can be derived from a local plot of $S_w - P_c$. Both deviations to the laboratory data can be attributed to pore-scale dynamic effects which are not represented in the model.

- The $P_c^d(S_w)$ relationship (for $P_n = 20\,\text{kPa}$ that is based on the simulation differs from the experimentally determined ones. For the $P_c^d(z)$-S_w relationship this can be attributed to the assumption of a unique $P_c(S_w)$ relationship in the simulation. For the average $< P_c^d > (< S_w >)$ relationship, the difference to the experimentally determined $P_c(S_w)$ relationship is less pronounced than for the local $P_c^d(z)$-S_w relationship. The difference between the two $P_c^d(S_w)$ relationships from the simulation results from the averaging of the phase pressures. At one node one prescribes in the model that the difference in the phase pressures equals the capillary pressure; the further away from the node, the larger the deviation to the applied parametrisation of the $P_c(S_w)$ might be.

- Despite the differences in the rate of change of saturation and the dynamic capillary pressure, the magnitude of the coefficient τ compares well to the experimental ones when the average $< P_c^V > (< S_w >)$ relationship is applied to determine τ.

5.4.2 Equilibrium $P_c(S_w)$ relationship for a simple heterogeneity pattern

As shown in the previous section, both the equilibrium and the dynamic $P_c(S_w)$ relationship are required for the determination of the coefficient τ. The difference between the dynamic and the equilibrium capillary pressure at a given saturation can only be assessed accurately if the equilibrium $P_c(S_w)$ relationship is determined correctly. For the estimation of τ on the basis of numerical experiments with heterogeneous domains (see Sec. 5.4.4), it is necessary to specify the equilibrium $P_c(S_w)$ relationship for these domains. As described in Sec. 5.2, various approaches can be applied on the macroscale to determine equilibrium $P_c(S_w)$ relationships. On the basis of a two-dimensional simple heterogeneity pattern, the approach of assuming a capillary equilibrium is compared here to the more general approach by ATAIE-ASHTIANI ET AL., 2001, 2002 [3, 2] and DAS ET AL., 2004 [32], who employ a numerical model to mimic a laboratory flow-through cell experiment for the determination of the quasi steady-state $P_c(S_w)$ relationship. As outlined in Sec. 2.1.1, (quasi) steady-state conditions are considered here as equilibrium as opposed to transient conditions.
The equilibrium $P_c(S_w)$ relationship is calculated for a two-dimensional simple heterogeneity pattern of a coarse sand with two embedded fine sand lenses (see Fig. 5.5). First, an analytical formula for computing the equilibrium $P_c(S_w)$ applying the assumptions of capillary equilibrium is applied for the simple heterogeneity. Then (quasi) steady-state $P_c(S_w)$ relationships are derived from numerical drainage experiments. Thus, the influence of viscous forces resulting from the pressure difference within each phase on the $P_c(S_w)$ relationship in comparison to the $P_c(S_w)$ relation determined for exclusively capillary dominated flow can be shown.

Capillary pressure-saturation relationship applying the assumption of capillary equilibrium: For the simple heterogeneity, where the coarse sand makes up a volume fraction of $V_f = 0.75$, Eqn. 5.8 can be expressed as

$$\overline{S_w}(P_c) = 0.25 \cdot S_w^{fi}(P_c) + 0.75 \cdot S_w^{co} \quad \text{for} \quad S_w^{fi} > S_{wr}^{fi} \quad \text{and} \quad S_w^{co} > S_{wr}^{co}. \tag{5.16}$$

to calculate the equilibrium $P_c(S_w)$ applying the assumption of capillary equilibrium. Here, $S_w^{fi}(P_c)$ denotes the wetting phase saturation of the fine sand and $S_w^{co}(P_c)$ that of the coarse sand at a given capillary pressure, as determined by the inverse $P_c(S_w)$ relationship after BROOKS & COREY (see Eqn. 5.9) for the fine and the coarse sand (see Tab. 5.2 for their properties). As mentioned in Sec. 5.2 this approach does not take accessibility into account. Because the coarse sand as the background material is connected to the boundaries a site-percolation model as employed by BRAUN ET AL., 2005 [18] would yield the same average $P_c(S_w)$ relationship for a drainage process. It should be noted, however, that the solution is only valid for ranges of the capillary pressure where $S_w^{fi} > S_{wr}^{fi}$ and $S_w^{co} > S_{wr}^{co}$ is ensured. These restrictions guarantee that the relative permeability for the wetting phase remains larger than zero in both sands. For the coarse sand at capillary pressures higher than approx. $P_c \sim 3400\,\text{Pa}$ the relative permeability for the wetting phase is zero.

Boundary conditions In a mimic of a laboratory flow-through cell experiment (see Sec. 5.2), the equilibrium $P_c^e(S_w)$ relationship for the simple heterogeneity pattern (see Fig. 5.5, left) is determined. The pressure of the wetting phase (water) varies linearly from the top with $P_w^T = 1000\,\text{Pa}$ to the lower boundary of the domain ($P_w^L = 0$), resulting in a pressure gradient of $\nabla P_w = 8333.33\,\text{Pa/m}$. Gravity is neglected and the atmospheric pressure is assumed to be zero. The non-wetting phase (NAPL) pressure P_n initially equals the wetting phase pressure plus the entry pressure.
The capillary pressure at the boundaries is increased by augmenting the non-wetting phase pressure at the top (index T) and lower (index L) boundary following a geometric series

$$P_n^S(n) = P_w^S + P_c^B(n) = P_w^S + P_d^{co} + \sum_{i=0}^{l=18} 1.5^i \quad \text{with} \quad S \in L, L\,, \tag{5.17}$$

where P_c^B is the boundary capillary pressure. In Eqn. (5.17) the index i denotes the i-th of l number of steps in the boundary condition, n denotes the time step and P_d^{co} the entry pressure of the coarse sand (see Tab. 5.2). The geometric series accounts for two aspects. On the one hand, the entry pressure and the narrow slope of the average $P_c(S_w)$ at high wetting phase saturations are resolved highly. On the other hand, at high capillary pressures, where a large increase in P_c results in small saturation changes, the steps in the induced boundary capillary pressure P_c^B are larger. A maximum boundary capillary pressure of 3304 Pa (for $i = 18$) should ensure that the relative permeability of the coarse sand remains above zero. For larger P_c^B the relative permeability might drop to zero, inhibiting all flow and thus any further saturation changes.

Equilibrium criteria: Before the augmentation of the increment *i* in Eqn. (5.17) equilibrium criteria have to be met. The criteria include two components, which are checked in a post-processing step; the norm of the change of arithmetically averaged non-wetting phase saturation and wetting phase pressure between two subsequent time steps n and n+1 should not exceed the difference 'equil_S' for the saturation and 'equil_P' for the pressure:

```
1     NumberNodes = 0;
2       for (theNode=FIRSTNODE; theNode!= 0; theNode=SUCCESSORNODE)
3       {
4             NumberNodes ++;
5              average_Sn_n+1 += Sn_p1(theNode);
6              average_pw_n+1 += pw_p1(theNode);
7              average_Sn_n += Sn_0(theNode);
8              average_pw_n += pw_0(theNode);
9       }
10
11      average_Sn_n+1 = average_Sn_n+1/NumberNodes;
12      average_pw_n+1 = average_pw_n+1/NumberNodes;
13      average_Sn_n = average_Sn_n/NumberNodes;
14      average_pw_n = average_pw_n/NumberNodes;
15
16      dSnAv = ABS(average_Sn_n+1 - average_Sn_k);
17      dpwAv = ABS(average_pw_n+1 - average_pw_k);
18
19      if ( dSnAv < equil_S  && dpwAv < equil_P)
20      {
21            increment ++;
22      }
```

The averages of pressure and saturation might differ from the averages defined in Eqns. (5.3), (5.4) and (5.7). For a structured grid, the boundary nodes should be weighted differently as only half or one quarter of the volume belonging to a non-boundary node pertains to them. For unstructured grids, the simple averaging might differ distinctly from the volume-weighted average. As only structured grids are applied here and the change in time rather than the magnitude of the saturation or pressure is of interest, this approximation is considered sufficient. The difference 'equil_S' (in the following denoted ε_S) for the saturation is distinguished from the difference 'equil_P' (in the following denoted ε_P) for the pressure, as the values of these variables differ by orders of magnitude. It is assumed that these equilibrium criteria suffice to establish a (quasi) steady state in the simulation. For the comparison of results from various time steps, the averaging of the variables needs to be redone in the post-processing, via a loop over the nodes, where the primary variables are saved for the time steps $n-1, n, n+1$.
With respect to the described numerical drainage experiments, the choice of the average capillary pressure and differing equilibrium criteria for establishing (quasi) steady-state conditions are analysed including a comparison to the analytical solution.

The choice of the average capillary pressure: For the upscaled $P_c(S_w)$ relationship, three capillary pressures can be chosen, namely

- the one derived from the phase-volume weighted average phase pressures $< P_c^V >$ after Eqn. (5.5),
- the one derived from the subcontrol-volume weighted phase pressures $< P_c^S >$ after Eq. (5.6), and
- the boundary capillary pressure P_c^B.

First, quasi steady-state $P_c(S_w)$ relationships on the basis of the average capillary pressures $< P_c^V >$ and $< P_c^S >$ are compared to the analytical solution (see Fig. 5.22).

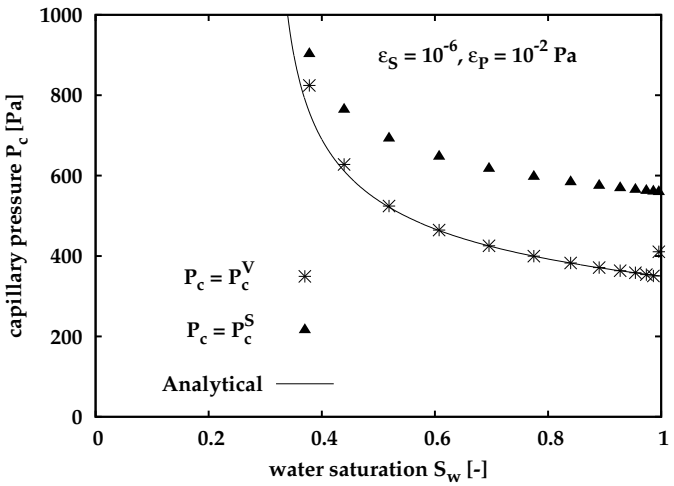

Figure 5.22: Average equilibrium $P_c^e(S_w)$ and analytical $P_c(S_w)$ relationships for simple heterogeneity

For capillary pressures smaller than the entry pressure of the coarse sand P_e^{co}, none of the $P_c(S_w)$ relationships reproduces the analytical solution. At a boundary capillary pressure of $P_c^B = 351\,\text{Pa}$, $< P_c^V > (S_w)$ clearly exceeds $P_c^B(S_w)$. The continuous $< P_c^V > (< S_w >)$ curve at high wetting phase saturations and $< S_w > (t)$ (see Fig. 5.23) illustrate that, at the beginning of the numerical experiment, the average capillary pressure inside the domain does not equal the applied boundary capillary pressure, but is higher. The large capillary pressure at the beginning is a numerical artefact, which does not occur if the first time step is chosen larger. Furthermore, for the small saturation changes at the first increase of boundary capillary pressure by $\Delta P_c^B = 1\,\text{Pa}$, the equilibrium criteria do not suffice to determine quasi steady-state conditions.
For boundary capillary pressures between $P_c^B = 351\,\text{Pa}$ and $P_c^B = 800\,\text{Pa}$, $< P_c^V > (< S_w >)$ reproduces the analytical solution. The $< P_c^S > (< S_w >)$ relation differs at low capillary pressures, when the entry pressure of the fine sand is not yet exceeded. At full water saturation, the non-wetting phase pressure amounts

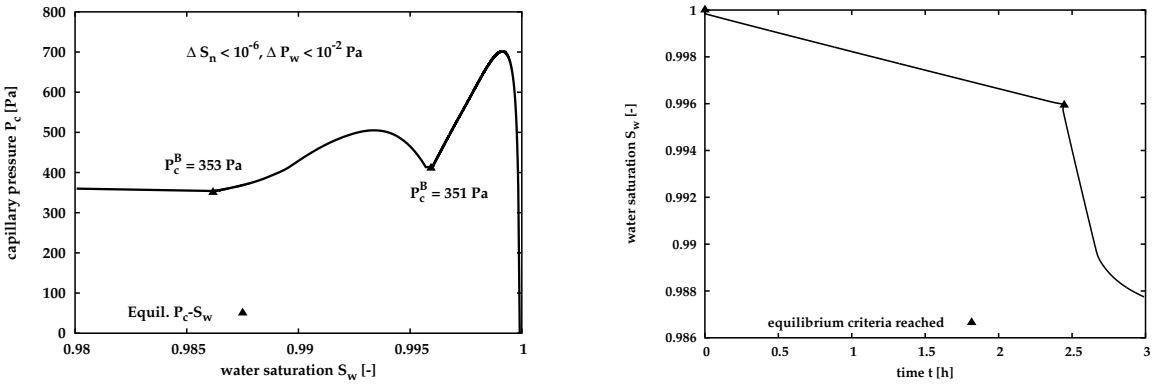

Figure 5.23: Continuous run of $< P_c^V > (< S_w >)$ (left) and $< S_w > (t)$ for the $t < 3\,h$ of simulated time (right) from equilibrium numerical experiment with simple heterogeneity

to $P_n = P_e + P_w$. Thus, the fine sand lenses with $S_n = 0$ contribute to the average of the non-wetting phase pressure $< P_n^S >$. For the volume-weighted phase pressures, the pressure of the non-wetting phase equals zero within the fine sand lenses as the saturation and thus the volume of non-wetting phase are zero. If the average capillary pressure were to be computed as the pressure difference at each node, the $< P_c^S >$ would not change. The $< P_c^V >$ would be smaller than the difference between the averaged phase pressures, as long as the entry pressure of the fine sand is not exceeded. Then, P_c would equal $-P_w$ in these regions.

Consequently, the choice of the average capillary pressure influences the upscaled $P_c(S_w)$ relationship especially at high wetting phase saturations if the approach of BROOKS & COREY is chosen for the parametrisation of the $P_c(S_w)$ relationships in the simulations. On the basis of the capillary pressure $< P_c^S >$, the upscaled entry pressure is overestimated compared to the analytical solution. This holds as long as the entry pressure is not exceeded in all parts of the domain. As the $< P_c^V > (< S_w >)$ relationship compares well to the analytical solution, the phase-volume weighted pressures are chosen to calculate average $P_c(S_w)$ relationships.

The boundary capillary pressure P_c^B may also be chosen for the capillary pressure in the upscaled $P_c(S_w)$ relationship. In laboratory experiments, the capillary pressure is often determined by the pressure difference between the non-wetting phase reservoir and that of the wetting phase reservoir. OUNG & BEZUIJEN, 2003 [88] show that the boundary capillary pressure does not always represent the capillary pressure within a sample. Especially at high capillary pressures, as measured by the difference in pressures in the reservoirs, a deviation from the capillary pressure measured inside the sample by means of selective phase pressure transducers can be observed. By a comparison of the $P_c^B(< S_w >)$ and the $< P_c^V > (< S_w >)$ relationships derived from a numerical drainage experiment for the 2D simple heterogeneity pattern applying the equilibrium conditions $\varepsilon_S = 10^{-6}$ and $\varepsilon_P = 10^{-2}$ Pa, a similar effect can be shown (see Figure 5.24, left).

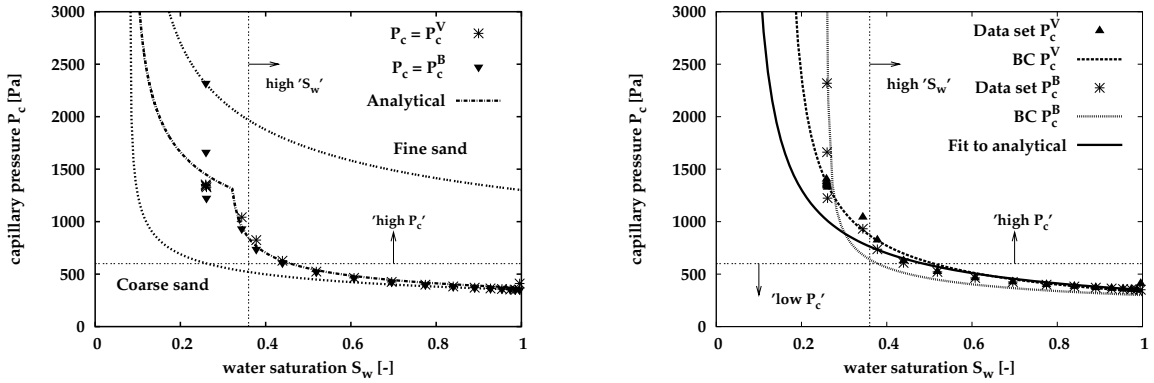

Figure 5.24: $< P_c^V > (< S_w >)$ and $P_c^B(< S_w >)$ relationships for the numerical equilibrium drainage experiment with the simple heterogeneity (left) and regressions using the BROOKS & COREY parametrisation (right)

For low capillary pressures, the $P_c^B(< S_w >)$ and the $< P_c^V > (< S_w >)$ relationships differ only negligibly from the analytical solution. For high capillary pressures, a distinct deviation between $< P_c^V > (< S_w >)$ and $P_c^B(< S_w >)$ evolves. Despite the seemingly strict equilibrium criteria the average capillary pressure inside the domain does not equal the boundary capillary pressure. When the equilibrium criteria, are met at $P_c^B \geq 607\,\text{Pa}$, the boundary capillary pressure is increased further although quasi steady-state conditions are not attained. For $607\,\text{Pa} \leq P_c^B \leq 1224\,\text{Pa}$ the average exceeds the boundary capillary pressure. This difference can be explained by the non-wetting phase pooling up especially on the fine sand lens. The entry pressure P_e^{fi} is not exceeded, thus a pool of NAPL remains on the lens also at quasi steady-state (see Fig. C.10 in App. C). For the applied boundary conditions, the viscous forces do not suffice to mobilise the NAPL pools. A comparison to a $< P_c^V > (< S_w >)$ relationship derived with the same equilibrium criteria but using pressure differences in each phase of $\Delta P_\alpha = 100\,\text{Pa}$ supports this reasoning. For $\Delta P_\alpha = 100\,\text{Pa}$ the analytical solution is reproduced exactly for boundary capillary pressures up to 937 Pa (see Fig. 5.25).

Back to the comparison of the average $P_c(S_w)$ relationships (see Fig. 5.24, left): it should be pointed out that at $P_c^B = 1224\,\text{Pa}$ the relative permeability of the wetting phase k_{rw} has decreased by three orders of magnitude compared to $P_c^B = 607\,\text{Pa}$ (see Fig. 5.4.2, left). Due to the small k_{rw} especially at the boundaries, the mobility of the wetting phase at the boundaries dominates its flux. Consequently, the changes in saturation decrease. The equilibrium criteria are met earlier than an adjustment between P_c^B and P_c inside the domain can be attained. In principle, for $k_{rw}^{co} > 0$ this equilibration should be accomplishable within a finite simulation time.

From on the increase of boundary capillary pressure from 2319 Pa to 3304 Pa, the pressure of the wetting phase inside the domain does not decrease monotonically from the top to the lower boundary. At the top boundary, due to an increase of P_w inside the domain a gradient evolves (see Fig. 5.4.2, right). The difference of the

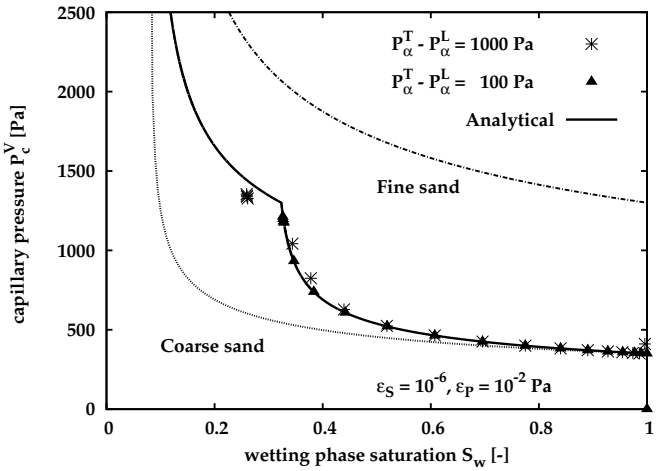

Figure 5.25: $< P_c^V > (< S_w >)$ relationships for phase pressure differences $\Delta P_\alpha = 100\,\text{Pa}$ and $\Delta P_\alpha = 1000\,\text{Pa}$ using the simple heterogeneity, applying the equilibrium criteria $\varepsilon_S = 10^{-6}$ and $\varepsilon_P = 10^{-2}$ in both cases

volume-weighted phase pressure $< P_c^V >$ does not increase significantly more than approx. 1300 Pa though the capillary pressure at the boundary is augmented up to $P_c^B = 3304\,\text{Pa}$.

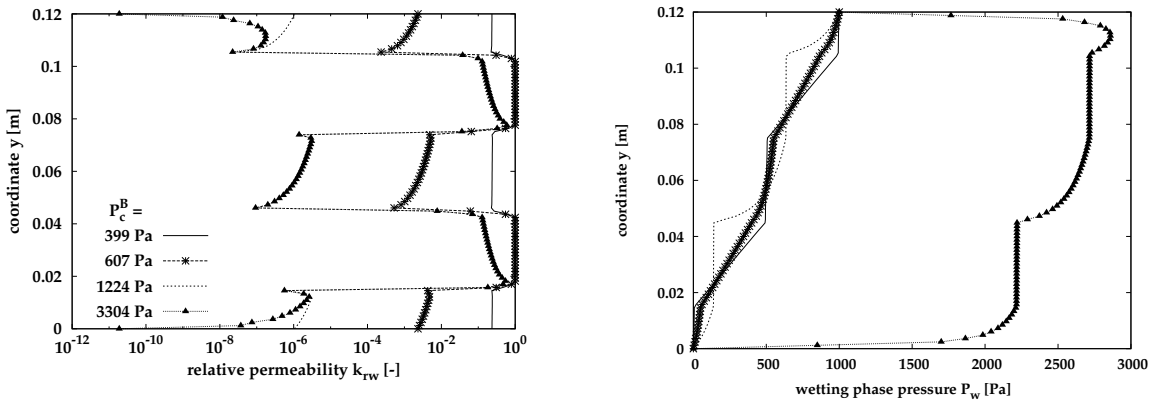

Figure 5.26: Wetting phase relative permeability $k_{\text{rw}}(y)$ (left) and pressure $P_{\text{w}}(y)$ (right) for quasi steady states at four selected boundary capillary pressures (cross-section at $x = 0.06\,\text{m}$, legend for graph $P_{\text{w}}(y)$ given with graph $k_{\text{rw}}(y)$)

Through an increase of the boundary capillary pressure from 932 Pa to 1224 Pa, the entry pressure of the fine sand is exceeded although the boundary capillary pressure is still smaller than the entry pressure of the fine sand. At high capillary pressures, the non-wetting phase pools especially on the top fine sand lens (see wetting phase distribution in Fig. C.10), caused by the pressure difference in the non-wetting phase from the top to the lower boundary. A local pressure increase of P_{n} and thus P_{c}

results. ATAIE-ASHTIANI ET AL.,2002 [2] show this effect, which is less pronounced for a phase pressure difference from the upper to lower boundary of $\Delta P_\alpha = 100\,\text{Pa}$. Consequently, both the $< P_c^V > (< S_w >)$ and the $P_c^B(< S_w >)$ do not reproduce the analytical solution exactly, as the analytical solution is based on the assumption of exclusively capillary dominated flow.

On the basis of the analysis of the numerical drainage experiment, the the chosen equilibrium criteria need to be questioned. In order to avoid plotting data sets derived from transient states the boundary capillary pressure should not be chosen for the determination of a equilibrium $P_c(S_w)$ relationship. Choosing P_c^B might result in an overestimation of the residual water saturation. A regression using the BROOKS & COREY parametrisation, employing a LEVENBERG-MARQUARD algorithm to minimise the residuals, illustrates that $P_c(S_w)$ relations differ distinctly in residual wetting phase saturation (see Fig. 5.24, right). While S_{wr} equals $S_{wr} = 0.152$ for the $< P_c^V > (< S_w >)$ relationship, the regression yields $S_{wr} = 0.259$ for the $P_c^B(< S_w >)$ relationship. In the first case the value overestimates S_{wr} by 50 % and in the second case by more than 250 %, compared to $S_{wr} = 0.070$ resulting from a regression to the analytical solution. The average $P_c(S_w)$ relationships presented by ATAIE-ASHTIANI ET AL., 2002 [2] and DAS ET AL., 2004 for the same 2D heterogeneity pattern with slightly different BC parameters are based on the boundary capillary pressure P_c^B. These authors show that residual wetting phase saturation of the average $P_c(S_w)$ relationship might be larger than S_{wr} of the homogeneous sands. It was shown here that, for high capillary pressures, the boundary capillary pressure P_c^B may not equal the average capillary pressure, presumably because steady-state conditions are not established. As the authors do not state their exact equilibrium criteria, a detailed comparison cannot be carried out.

ATAIE-ASHTIANI ET AL., 2002 [3] state that, for a boundary capillary pressure of $P_c^B = 1500\,\text{Pa}$, the relative permeability $k_{rw}^{co}(S_w)$ equals zero. This would imply that, the saturation could not change for larger boundary capillary pressures, regardless of the pressure difference applied in each phase. This does not agree with their $P_c^B(< S_w >)$ relationship for a pressure difference $\Delta P_\alpha = 100\,\text{Pa}$, where the average saturation clearly changes for $P_c^B > 1500\,\text{Pa}$. ATAIE-ASHTIANI ET AL., 2002 state that regardless of the pressure difference ΔP_α each of the numerical experiments simulated a time of 420 days. Steady-state might thus have been attained more closely in the case of a high ΔP_α as compared to a small ΔP_α because a high pressure difference induces higher fluxes. Following the arguments above, the large residual wetting phase saturation observed by the authors might be explained by the choice of P_c^B for the upscaled $P_c(S_w)$ relationship, rather than the relative permeability k_{rw}^{co} decreasing to zero.

In summary, when average $P_c(S_w)$ relationships are determined from numerical experiments, attention should be given to the equilibrium criteria. If the values for the criteria are chosen too high and only the boundary capillary pressure is applied for the upscaled $P_c(S_w)$, then the difference between P_c^B and $< P_c^V >$ might not be noticed. As a consequence, the residual saturation of the wetting phase might be overestimated compared to an analytical solution applying the assumption of cap-

illary equilibrium.

Influence of the magnitude of the equilibrium criteria: Varying magnitudes of the equilibrium criteria ε_S and ε_P (see paragraph 'Equilibrium criteria' in this section for the definition) serve to test their influence on the upscaled equilibrium $< P_c^V > (< S_w >)$ relationship. None of the $< P_c^V > (< S_w >)$ relations differs significantly from the analytical solution for high water saturations (compare Fig. 5.27). In all the numerical drainage experiments, the boundary capillary pres-

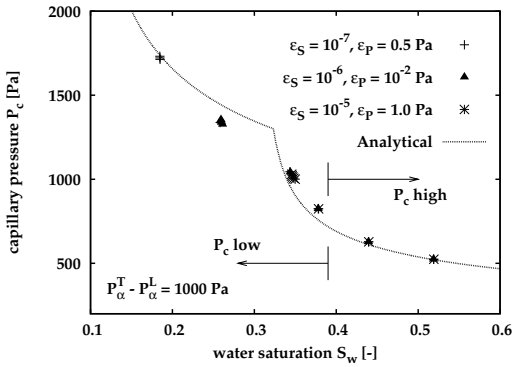

Figure 5.27: Quasi steady-state $< P_c^V > (< S_w >)$ relationships for three sets of equilibrium criteria using the simple heterogeneity ($\Delta P_\alpha = 1000\,\text{Pa}$)

sure is increased up to 3304 Pa as the equilibrium criteria are met. However, in the $< P_c^V > (< S_w >)$ relationships, the capillary pressure does not exceed 1731 Pa. The magnitude of the attained average capillary pressure depends especially on the strictness of the equilibrium criterion for the saturation. For $\varepsilon_S = 10^{-7}$ and $\varepsilon_P = 0.5\,\text{Pa}$, the maximum capillary pressure is higher than for the criteria $\varepsilon_S = 10^{-6}$ and $\varepsilon_P = 10^{-2}\,\text{Pa}$, where ε_P is smaller than in the first case, but ε_S is higher. For the chosen equilibrium criteria, the capillary pressure within the domain is not at equilibrium with respect to the boundary conditions before a new pressure step is taken starting at a boundary capillary pressure of $P_c^B = 607\,\text{Pa}$. For lower P_c^B the average capillary pressure $< P_c^V >$ equals P_c^B (see Eqn. (5.5)), when the equilibrium criteria are met. For the criteria $\varepsilon_S = 10^{-6}$ & $\varepsilon_P = 10^{-2}\,\text{Pa}$, the last three capillary pressures steps ranging from 1223 Pa to 3304 Pa cover a simulated time of 0.05 h, whereas the first part of the numerical experiment comprises 86.06 h of simulated time.
When the equilibrium criteria do not suffice to establish a steady state at high P_c^B the residual wetting phase saturation is overestimated. Consequently, much stricter equilibrium criteria should be chosen to compute the average $P_c(S_w)$ relationship for high capillary pressures. For example, the change of saturation and pressure within one time step should either be normalised or the criteria should be saturation dependent to account for varying magnitudes of the fluxes. In the following, an

equilibrium numerical experiment applying strict equilibrium criteria is analysed with respect to the time stepping behaviour and execution time.

Computation time The simulator MUFTE-UG (see Sec. 4.1) is used here to determine $P_c^e(S_w)$ relationships with numerical experiments. In Sec. 4.2 the algorithm for solving the coupled, highly non-linear balance equations for two-phase flow is described. Within the solution routine, the time step size is automatically adapted within user-set bounds on the basis of the performance of the nonlinear solver, a damped, inexact NEWTON scheme. For the following numerical experiments, the parameters for the NEWTON scheme were set as follows: if convergence is attained within one line search, the time step is doubled. If on the other hand, the line search does not converge within six line searches, the time step is halved.
If in the system of algebraic equations the non-linearities caused by the constitutive relationships become strong, it is more likely that the line search will not converge, resulting in a reduction of the time step.
For a numerical experiment applying the equilibrium criteria $\varepsilon_S = 10^{-10}$ and $\varepsilon_P = 10^{-10}$Pa, the time stepping and thus the execution time for the simulation is analysed in relation to the saturation and pressure changes (compare Tab. 5.4). It should be stressed that a thorough analysis of the execution time as would be required for a benchmark test is not the aim of this study but rather an order of magnitude estimation and comparison to other methods. The simulations were carried out on a PC with an installed memory of 512 MB and a 1.2 GHz processor, running under a Linux system.
In the first experiment, equidistant pressure increments are applied. The boundary capillary pressures of 800 Pa and 1400 Pa are chosen for the analysis. An overview of the number of time steps illustrates that to attain changes in saturation or pressure of less than $\varepsilon_S = 10^{-6}$&$\varepsilon_P = 10^{-4}$ at most 3,234 time steps are required (see Tab. 5.4). To fulfil the final equilibrium criterion, it takes at least another 50,161 time steps. Within these time steps, the average capillary pressure alters by approximately 60 Pa, within a computed time of 5.366 h, which used a computing time of seven days. At the interruption of the numerical experiment, the change of the average saturation still exceeded $\Delta S_n > 10^{-7}$ and the change of the averaged capillary pressure was larger than $\Delta P_w > 10^{-3}$ Pa within one time step.
The large number of time steps correlates to a decrease of the time step size Δt, which can be explained by three reasons. First, the water saturation in the coarse material S_w^{co} approaches residual saturation and thus high derivatives of its $P_c(S_w)$ relationship occur. Secondly, the differences between the saturation in the coarse and the fine sand increase, which causes high gradients in the saturation. Furthermore, for high non-wetting phase saturations the relative permeability for the non-wetting phase becomes highly non-linear (with a local minimum of the derivative).
Strong non-linearities in the system of equations to be solved can affect the convergence behaviour of the solvers (e.g. of the line search). This effect will be analysed in a second example applying the equilibrium conditions $\varepsilon_S = 10^{-6}$ and $\varepsilon_P = 10^{-2}$ Pa

Table 5.4: Equilibrium criteria for the determination of the $P_c^e(S_w)$ relationship in relation to the time steps

	P_c^B 800Pa	P_c^B 1400Pa
1) time steps until $\Delta S_w < 10^{-6}$	145	21
computed time until 1)	0.0393 h	0.0028 h
average time step	0.98 s	0.48 s
2) time steps 1) until $\Delta P_w < 10^{-4}$ Pa	170	3234
computed time 1) until 2)	0.0607 h	0.1060 h
average time step from 1) to 2)	0.94 s	$3.2 \cdot 10^{-5}$ s
time steps from 2) until eq./interrupted	384	50 161
computed time from 2) until eq.	0.1008 h	5.3667 h
average time step from 2) to end	0.674 s	0.378 s

(see Fig. C.11 in App. C). For boundary capillary pressures lower than 737 Pa, the execution time required to fulfil the equilibrium conditions does not exceed $8,863$ s (= 2.45 h). Then, for the boundary capillary pressures 932 Pa and 1224 Pa, the execution time required to reach equilibrium is $17,126$ s (= 4.76 h) and $52,471$ s (= 14.58 h). As shown in Tab. 5.4, the execution time for higher boundary capillary pressures would be higher than observed here, if stricter equilibrium criteria were applied. An analysis of the iterations in linear and nonlinear solvers per time step (see Fig. C.11) clarifies that at the labelled boundary capillary pressures the number of iterations increases dramatically. Simultaneously, the time step sizes decrease. Consequently, w.r.t. execution time, the calculation of an equilibrium $P_c(S_w)$ relationship on the basis of a numerical experiment is not as efficient as a percolation model or, for simple heterogeneity patterns, analytical solutions. However, the alternative approaches assures a capillary equilibrium. Thus, effects such as, for example, the influence of the phase pressure gradient on the equilibrium $P_c(S_w)$ relationship, caused by a pooling of non-wetting phase, as shown by ATAIE-ASHTIANI ET AL.,2002 [2], cannot be captured.

Summary On the basis of numerical drainage experiments using a coarse sand with two embedded fine sand lenses, the choice of the average capillary pressure, the equilibrium criteria to establish (quasi) steady-state conditions, and the time-stepping behaviour were analysed including a comparison to the analytical solution. It was shown that $< P_c^S > (S_w)$ does not reproduce the analytical solution gained on the basis of the capillary equilibrium assumptions because of the applied BC parametrisation for the $P_c(S_w)$ relationships of the coarse and fine sand. In contrast the $< P_c^V > (< S_w >)$ agrees well with the analytical solution for low boundary capillary pressures. It was shown furthermore that choosing P_c^B for the upscaled

$P_c(S_w)$ relationship might conceal that

- the average $< P_c^V >$ might exceed P_c^B due to a pooling of non-wetting phase on the fine sand lens (an effect that is not observed when the boundary phase pressure difference in each phase is $\Delta P_\alpha = 100\,\text{Pa}$ instead of $\Delta P_\alpha = 1000\,\text{Pa}$), and
- for high P_c^B the average capillary pressure remains significantly lower than the boundary capillary pressure, indicating that the applied equilibrium criteria do not suffice to establish a steady state.

Furthermore, the magnitude of the equilibrium criteria influences the upscaled residual wetting phase saturation. The stricter the criteria are set, the smaller residual saturation, but at the same time the computation time increases. When average $P_c(S_w)$ relationships are analysed on the basis of numerical experiments, these aspects should be kept in mind.
With the determination of the equilibrium $P_c(S_w)$ relationship, the foundation for the calculation of the coefficient τ in the extended $P_c(S_w)$ relationship is laid. In the following, dynamic numerical experiments are described, which are performed in order to identify the two missing terms, the dynamic capillary pressure-saturation relationship, and the rate of change of saturation.

5.4.3 The coefficient τ for homogeneous domains

The idea to determine the coefficient τ on the basis of numerical experiments on the local scale results from the assumption that heterogeneities on the local scale might lead to dynamic effects at the macroscale when an averaging procedure is applied similar to the approach by DAHLE ET AL., 2005 [30] or GIELEN ET AL., 2005 [46]. But before this assumption is tested with heterogeneous domains, the averaging approach is examined with a homogeneous domain to distinguish between effects arising from heterogeneities and influences from

- the averaging of the phase pressures,
- the averaging length scale,
- the boundary conditions, and
- porous medium as well as fluid properties.

In the following, these aspects will be analysed successively.

5.4.3.1 The choice of the averaged phase pressure

In Sec. 5.4.2, the choice of the average capillary pressure for the average, equilibrium $P_c^e(S_w)$ relationship was discussed for an equilibrium numerical experiment by comparison to a percolation model approach. The phase-volume weighted phase pressure difference $< P_c^V > = < P_n^V > - < P_w^V >$ applied in the equilibrium $P_c(S_w)$ relationship resulted in the most accurate approximation of an analytically

determined $P_c(S_w)$ relationship. For the dynamic case, a comparison to an analytical approach is lacking. However, $< P_c^V >$ and $< P_c^S >$ from a dynamic numerical experiment are equal to each other for a homogenous domain as no entry pressure variation could cause a deviation to the analytically resulting $P_c(S_w)$ relationship. But for a dynamic experiment with the simple heterogeneity pattern, $< P_c^S >$ will exceed $< P_c^V >$ slightly. The difference is caused as in the computation of the equilibrium $P_c(S_w)$ relationship (see Sec. 5.4.2) by the parametrisation of the equilibrium $P_c(S_w)$ relationships with the BROOKS & COREY relationship. Thus, for the dynamic experiments, the volume-weighted phase pressures and the derived capillary pressure are chosen to enter into the averaged, dynamic $P_c^d(S_w)$ relationship.

5.4.3.2 Aspects resulting from the averaging length scale

For a homogeneous domain, an REV does not need to be determined. In the approach taken here, however, it will be shown that the averaging length scale influences the magnitude of the coefficient τ_0. The impact is examined for two cases, namely

1. averaging over domains of varying dimension $l_x = l_y = 0.03, 0.12, 1.0\,\mathrm{m}$ (while maintaining the same (initial) pressure gradient within each phase of $\Delta P_\alpha = 8333.33\,\mathrm{Pa/m}$) using the boundary conditions specified for the flow-through cell experiment (see Fig. 5.3), and
2. averaging over varying volumes, applying the results of one numerical experiment with the boundary conditions specified for the pressure-cell with $P_n = 10^4\,\mathrm{Pa}$ at the top boundary (see Fig. 5.4).

As the boundary conditions result in one-dimensional flow processes for the homogeneous domain, averaging over increasing volumes is the same as averaging over an increasing number of nodes in the direction of the flow. For the first case, the properties of the coarse sand in Tab. 5.2 are used, in the second case the 'sand' properties also listed in that table apply. The numerical experiments serving as a basis for the averaging were originally applied for different purposes, but are considered sufficient for a comparison of the two averaging approaches. As the porous media properties differ, only a qualitative comparison of the two cases is undertaken in the following.
For the first case 1, two trends can be observed. At a given saturation, the saturation rate increases and the capillary pressure difference $\Delta P_c = P_c^d - P_c^e$ decreases for decreasing domain lengths (see Fig. 5.28, left). The local minimum of ΔP_c at a water saturation of $S_w \simeq 0.95$ for the largest domain vanishes if the first time step is fixed to a larger value, and is thus interpreted as a numerical artefact. The initial time step for this numerical experiment was not changed in order to show this effect. In the second case 2 (averaging over varying volumes), the saturation rates and the differences in the capillary pressure show the same dependence on the averaging length scale (see Fig. 5.28, right). No averaging of the variables is performed if one node only, with an associated grid length of ($\Delta y = 0.025\,\mathrm{m}$), is taken into account. These

values thus can be considered as corresponding to a point or local measurement. The (local) saturation rate exceeds the other ones for a large range of saturations, while the capillary pressure difference ΔP_c equals zero for all water saturations. Obviously, for one box, the prescribed equilibrium $P_c^e(S_w)$ relationship must hold, as dynamic effects are not accounted for in the numerical model. Consequently, the dynamic equals the equilibrium capillary pressure at all times.
In order to obtain a functional dependence between the capillary pressure difference and the saturation rate, a dynamic capillary pressure resulting from averaged phase pressures has to be applied to compute the capillary pressure difference ΔP_c. The length scale dependence of the saturation rate and the capillary pressure difference results in a length scale dependence of the coefficient τ_0, in addition to the dependence on the water saturation (see Fig. 5.29).

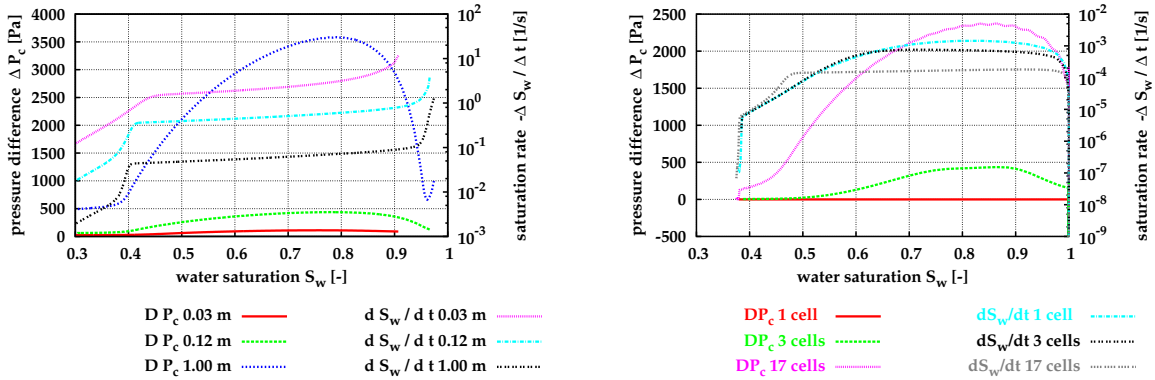

Figure 5.28: ΔP_c (left) and $^{\Delta S_w}/_{\Delta t}$ (right) for domain sizes and varying averaging volumes using the homogeneous reference medium of the geostatistical field (see Tab. 5.2)

For comparison, (at a chosen water saturation of $S_w = 0.5$) the values of τ_S after STAUFFER, 1978 [108] (see Eqn. (3.2)) are plotted additionally. These values remain

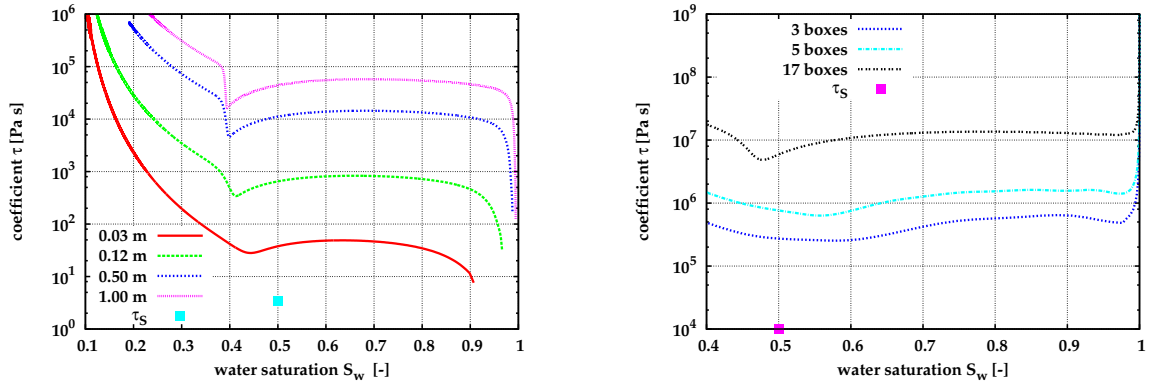

Figure 5.29: $\tau(S_w)$ for varying domain sizes (left) and averaging volumes (right) for the homogeneous reference medium and calculated after Eqn. (3.2)

about one order of magnitude smaller than the smallest τ values from the numerical experiments. The coefficient τ_S depends neither on the length scale nor on the water saturation. The empirical formula was derived for laboratory experiments with a column of $l = 0.6\,\mathrm{m}$; its length scale was thus in the range of the ones regarded here. Whether STAUFFER's formula given in Eqn. (3.2) or the numerically determined values give a correct estimate of the coefficient τ for a given medium will have to be examined in more detail, consulting additional laboratory experiments where point and average phase pressures are also determined.
DAHLE ET AL., 2005 define the dimensionless grouping N_D given in Eqn. (5.1) and show that it approaches unity for medium water saturations (see Fig. 5.1). For the two cases here, a similar behaviour of N_D can be observed for medium water saturations (see Fig. 5.30), though for the first case the curves show a different characteristic. As this effect does not occur in the second approach, it is attributed to the inclusion of the boundary nodes in the averaging and to the applied boundary conditions. As the average water saturation diminishes and approaches the residual water saturation, N_D becomes much larger than one for the example employing varying domain sizes. With the behaviour of $\tau(S_w)$ at small water saturations this trend is expected. It might be argued that, for $N_D = 1$, the coefficient τ scales with

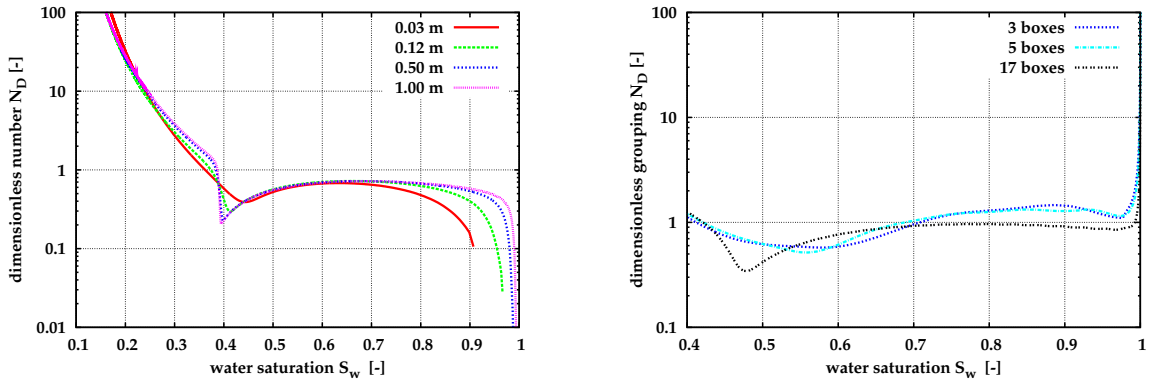

Figure 5.30: Dimensionless grouping N_D for $\tau(S_w)$ derived from numerical experiments with varying domain sizes (left) or averaging lengths (right)

the square of the averaging length. Consequently, it is not possible to define an REV for the determination of the coefficient τ if the averaging length is not bounded.
In flow and transport processes, other parameters have been shown to increase with scale, e.g. the longitudinal dispersion coefficient (see e.g. GELHAR ET AL., 1992 [44] or SCHULZE-MAKUCH, 2005 [101]). However, this scale dependence can be explained by new heterogeneity patterns that appear on the larger scales. The increase of dispersion can be attributed to the appearance of new heterogeneities with increasing length scales. If variance, average and correlation length of a permeability field are constant for varying scales, the determined longitudinal dispersion would not alter in the time limit, on the assumption that a tracer has seen enough correlation lengths.

DAHLE ET AL., 2005 [30] propose linking the determination and thus the magnitude of τ to a typical process length, e.g. the front width. As all other parameters entering into N_D are not process-dependent and consequently remain constant, the coefficient would consequently be large for broad front widths and small for steep fronts. On the assumption that the ratio of capillary and viscous forces influences the front width, and that the front is wide for dominating capillary forces, the coeffcient would be large for capillary dominated flow. Under such flow conditions it is assumed that dynamic effects do not play a role; using a front width to compute τ is thus not considered appropriate.
In addition to checking the behaviour of the averaging length scale, the location of the averaging is also varied (see Fig. C.9). The resulting $\tau_0(S_w)$ data only show negligible differences.
For the time being, the question of how to overcome the length scale dependence is postponed. For the following calculations it is assumed, that a typical length scale can be found and that effects stemming from the boundary conditions etc. can thus be examined for that typical length scale.

5.4.3.3 Influence of the boundary conditions

Three combinations of boundary conditions serve to test their influence on the coefficient τ. First a flow-through set-up (FT) is applied because it proved appropriate to calculate an equilibrium $P_c^e(S_w)$ relationship (see Sec. 5.4.2). For the second and third example the boundary conditions mimic the pressure-cell set-up (see Fig. 5.4). Either a Dirichlet boundary condition (PCDir) or a Neumann boundary condition (PCNeu) are applied at the top to induce the infiltration of the non-wetting phase (see Tab. 5.5). For the PCDir, a no-flow boundary condition is given for the non-wetting phase at the lower boundary, and for the PCNeu a Dirichlet boundary condition ($S_n = 0$).

Table 5.5: Types of dynamic experiments to determine the coefficient τ

Name	porous medium	variations in	averaging over
FT	coarse sand	$P_c^B = \{2,4,7,10\}$ kPa	domain
PCDir	sand	$P_n^T = \{0.5,1,2\}$ kPa	5 boxes
PCNeu	sand	$q_n^T = \{0.01,0.1,1.0\}$ kg/s	5 boxes

For the FT, the pressure difference in each of the phases ΔP_α from one boundary to the other amounts to $\Delta P_\alpha = 100$ Pa, while the boundary capillary pressure P_c^B is varied (see Tab. 5.5). In contrast to the equilibrium experiment, this combination of boundary conditions causes pronounced counter-current flow. The large increase of the boundary capillary pressure at the opposing boundaries causes the non-wetting phase to infiltrate at both boundaries, enclosing the wetting phase. The pressure

of the wetting phase thus develops a maximum in the middle of the domain, causing gradients w.r.t. to the boundaries and thus a flow from the middle towards the boundaries. These are unwanted flow conditions. These numerical experiements will be considered here nevertheless in order to show the influence of the boundary conditions in combination with the averaging over the whole domain. The capillary pressure differences ΔP_c of the dynamic numerical experiments differ, the differences increase with decreasing water saturation (see Fig. 5.31, left, where the results of $P_c^B = 10^4\,\mathrm{Pa}$ are given for easier readability). In contrast, the rates of change of saturation exhibit the same magnitude and the same monotonic trend. The coefficient τ_0 is calculated first for each boundary capillary pressure P_c^B, and then, on the basis of all four experiments, regressions are performed for the data at given water saturations in order to gain τ_0 as well as τ_b (see Fig. 5.31, right).

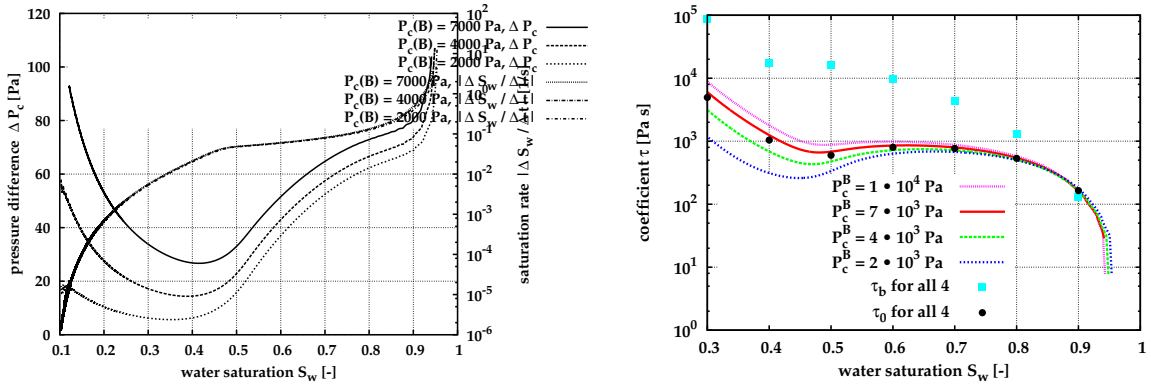

Figure 5.31: ΔP_c and $^{\Delta S_w}/_{\Delta t}$ (left) as well as $\tau(S_w)$ (right) for the coarse sand applying Dirichlet boundary conditions ($P_c^B = 2000, 4000, 7000\,\mathrm{Pa}$ and $\Delta P_\alpha = 100\,\mathrm{Pa}$)

The values of the coefficient τ_0 from each of the experiments range between $\tau_0 \simeq 110\,\mathrm{Pa\,s}$ and $\tau_0 \simeq 9\,\mathrm{kPa\,s}$ for the considered saturation range. With increasing boundary capillary pressure the coefficient also increases at a given saturation. Differences between $\tau_0(S_w)$ from the individual experiments increase with diminishing water saturation. It was assumed that, by applying different boundary capillary pressures, different magnitudes of the saturation rate would also be induced. However, on the assumption that the rate of change of the averaged water saturation is propoportional to the average flow velocity, the flow regimes of the four experiments differ only slightly for large water saturations (see Fig. 5.31, left). Consequently, the differences in the coefficient τ_0 mainly arise because of the dependence of the capillary pressure difference on the boundary conditions. On the further assumption that the similarities in the saturation rates are based on a similar distribution of the wetting fluid inside the domain, the capillary pressure distribution inside the domain should also be similar. The differences in ΔP_c would thus be evoked by including the boundary nodes with the prescibed boundary capillary pressure into the averaging. Consequently, $\tau_0(S_w)$ correlates positively with the boundary capillary pressure, an effect that cannot be observed in the second approach (see below)

where the boundary nodes are not included in the averaging procedure.
In order to test the linearity of the extended $P_c(S_w)$ relationship (compare Sec. 3.5), the coefficient τ is also calculated after Eqns. (3.13) and (5.14) on the basis of all four numerical experiments for selected water saturations. While $\tau_0(S_w)$ obviously show the same trend as $\tau_0(S_w)$ from the individual experiments, the $\tau_b(S_w)$ values are up to one order of magnitude larger for water saturations smaller than $S_w < 0.9$ (see Fig. 5.31, right). Similar to the results from the laboratory experiments (see Sec. 5.3), the deviation from the linear relation running through the origin decreases with increasing water saturations.
In a second approach, where the pressure-cell set-up is mimicked, the boundary capillary pressure is not fixed and the averaging is performed only over parts of the domain corresponding to five adjacent (in the y-direction and consequently flow direction) nodes of the grid. For both the PCDir and the PCNeu numerical experiments, distinct differences in the magnitude of the saturation rate as well as the capillary pressure difference occur (see Fig. 5.32), while the same trends are noticable. In contrast to the FT results, the saturation rate does not show a monotonic behaviour, but from full saturation increases steeply (when the invading front reaches the averaging domain), then remains approx. constant over a range of medium saturations before it decreases again at low water saturation. The saturation rate as well as the difference in capillary pressure behave proportionally to the boundary conditions for PCDir as well as PCNeu.

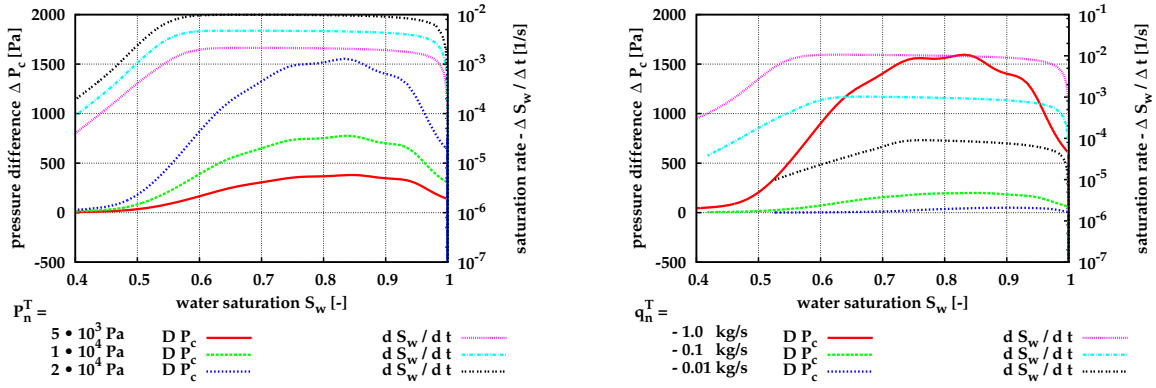

Figure 5.32: $\Delta P_c(S_w)$ and $\Delta S_w/\Delta t(S_w)$ for Dirichlet (left) and Neumann (right) boundary conditions using the homogeneous reference sand

The resulting $\tau_0(S_w)$ functions for each of the numerical experiments of the PCDir behave similarly (see Fig. 5.33, left). If one keeps in mind the log-scale plot, the dependence on the water saturation can be considered negligible, all $\tau_0(S_w)$ values vary around 10^5 Pa s. For a given water saturation, the coefficient might differ depending on the boundary conditions, being larger for small pressures of the non-wetting phase at the top boundary.
The $\tau_0(S_w)$ data of the individual numerical PCNeu experiments (see Fig. 5.33, right) exhibit a dependence on the water saturation which is more pronounced for the low

than for the high inflow rate. Similar to the PCDir experiments, $\tau_0(S_w)$ resulting from a numerical experiment with low saturation rates exceeds that stemming from high saturation rates.

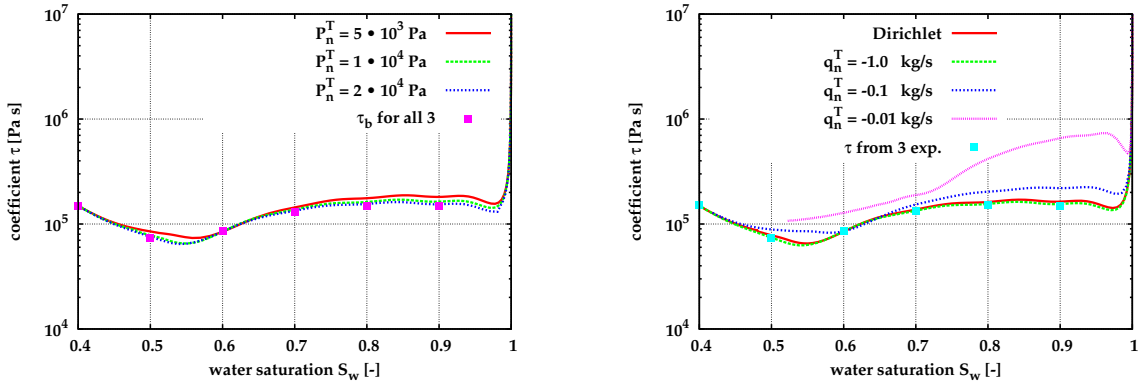

Figure 5.33: $\tau_0(S_w)$ for Dirichlet (left) and Neumann (right) boundary conditions for the homogeneous reference sand

The results from PCDir and PCNeu confirm the findings of KALAYDJIAN, 1992 [68], who determined $\tau_0(S_e)$ for various Neumann boundary conditions and found a negative correlation between the applied influx and the magnitude of the coefficient. However, all these findings are contrary to the expectation that for slow flow processes an extended $P_c(S_w)$ relationship does not need to be taken into account.
A dependence on the boundary conditions is not desirable if the calculated coefficient is to be applied in forward simulations. A further option is to perform a linear regression to the data from all numerical experiments of one type of boundary condition. If Eqn. (5.14) is fitted to data sets from PCDir or PCNeu, the resulting coefficients $\tau_b(S_w)$ follow the values of the numerical experiment with the highest saturation rate (see Fig. 5.33). In contrast to the results from the FT set-up, the magnitude of the y-axis intercept b can be neglected, which confirms the linear relation between saturation rate and capillary pressure difference.

5.4.3.4 Influence of porous medium and fluid properties on the magnitude of the coefficient τ

On the assumptions that

- the phase-volume averaged pressures are the correct choice for the averaging,
- the determination of the coefficient τ can be related to a typical process length, and
- the possible impact of the boundary conditions can be neglected if the same conditions are applied for all comparisions,

then the influence of the porous medium and fluid parameters on the magnitude of τ can be estimated. To this end, the pressure-cell set-up with a length of 1 m is applied.

Tab. 5.6 lists the parameters of the reference case, yielding the cofficient τ_{ref}, as well as the ratio of the varied to the reference parameter. For each of the simulations, only one parameter is varied at a time. Results from the dynamic numerical experiments with a variation of either K, ϕ, P_d, λ are plotted in App. C. For the computation of the capillary pressure difference, the equilibrium $P_c^e(S_w)$ relationship as prescribed by the varied parameters is applied. On the basis of dynamic numerical experiments, the coefficient for the variation cases, τ_{var}, is determined.
The ratio τ_{ref}/τ_{var} is taken to quantify the impact of the parameter on the material coefficient. For a ratio of one, an influence cannot be detected, while ratios unequal to one indicate a dependence of the coefficient on the parameter.
The variation of the entry pressure does not influence on the magnitude of the coefficient as the ratio of τ_{ref}/τ_{var} at the chosen water saturations is approximately one (see Tab. 5.6). For large water saturations, the influence of the pore size distribution index λ on τ is negligible, for saturations of ~ 0.6 the magnitude of τ is increased, for smaller water saturations it is decreased (see Fig. C.12). For the pore size distribution index, no general relation can be defined. As its influence is not pronounced, the index does not need to be taken into account for an approximation of τ. The coefficient behaves inversely proportionally to the intrinsic permeability and directly proportionally to the porosity.

Table 5.6: Parameter variation to test the influence on the coefficient τ

	Reference	Variation $^{Var}/_{Ref}$	τ_{ref}/τ_{var} $S_w = 0.6$	τ_{ref}/τ_{var} $S_w = 0.8$
Porosity ϕ	0.4	0.75	0.75	0.75
Permeability K	$5.11 \cdot 10^{-12}\,m^2$	10.0	0.100	0.100
Entry pressure P_d	500 Pa	2.0	1.00	1.09
Psd index λ	2.0	0.5	1.02	1.15

Moreover, the viscosities of the fluids influence the coefficient depending on the water saturation. The viscosity ratio is defined here as

$$M = \frac{\mu_w}{\mu_n} . \tag{5.18}$$

When cross sections of the water saturation $S_w(y)$ and the capillary pressure $P_c(S_w)$ for three viscosity ratios are compared (see Fig. C.13 in App. C), the front of the non-wetting phase infiltrating into the domain becomes sharper for smaller viscosity ratios. Although a fingering process cannot be detected, the choice of a viscosity ratio of $M > 1$ when neglecting gravity does not fulfil the stability criterion for horizontal displacement defined by LAKE, 1989 [71]. Nevertheless, the example is adhered to in order to investigate the effect of the ratio M on the coefficient.
The magnitude of the viscosity as well as the ratio influence the coefficient (see Fig. 5.34, left). For equal viscosities, the material coefficient scales proportional to the viscosity. For viscosity ratios unequal to one, stability aspects need to be taken

into account (gravity is neglected). As long as the viscosity of the displacing fluid (here the non-wetting fluid) is equal or greater than that of the displaced fluid, N_D calculated with saturation-weighted viscosities

$$\mu(< S_w >) =< S_w > \mu_w + (1.0 - < S_w >)\mu_n \tag{5.19}$$

ranges between 0.5 and three (see Fig. 5.34, right). For the viscosity ratio of ten, N_D is approx. one for average water saturations larger than $< S_w >> 0.7$, but exceeds one by an order of magnitude for smaller saturations. For large viscosity ratios, where the stability criterion is not met, the possible instability is also reflected in the coefficient, for which a scaling with the saturation weighted viscosity can no longer be defined.
The application of a saturation-weighted average viscosity could also be a possible extension of the STAUFFER formula (3.2) to two-phase systems.

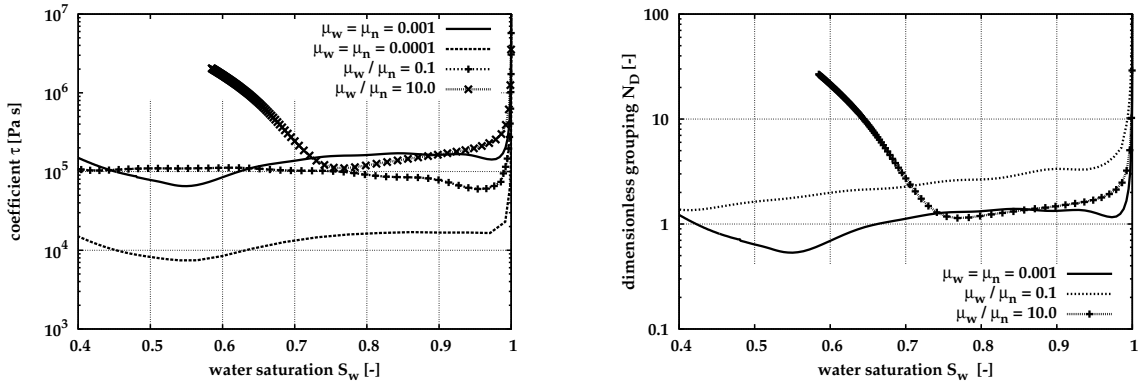

Figure 5.34: $\tau_0(S_w)$ (left) and the dimensionless grouping $N_D(S_w)$ with saturation-weighted average viscosity (right) for three viscosity ratios using the homogeneous reference sand (averaging over five boxes)

Summary: The calculation of the coefficient τ for a homogeneous domain with varying boundary conditions has thrown light on the following aspects:

- A dynamic effect in the $P_c(S_w)$ relationship can only be detected if averaged phase pressures in contrast to a nodal value are applied for the calculation of the dynamic capillary pressure. At one node, the difference in phase pressures is the same as the capillary pressure as prescribed by the mathematical-numerical model, while the rate of change of saturation might be unequal to zero.

- The scaling of the coefficient proportional to

  - the porosity,
  - the (saturation-weighted) viscosity, and

– the squared averaging length,

as well as the inverse proportionality to the intrinsic permeability as suggested by DAHLE ET AL., 2005 [30], who used a bundle of capillary tubes model, are confirmed by numerical experiments on the local scale for viscosity ratios of $M = \mu_w/\mu_n$ of one and smaller and for medium water saturations $S_{wr} << S_w < 1.0$. The parameters from the equilibrium $P_c(S_w)$ relationship only have a minor influence.

- The scaling of the coefficient to the square of the entry pressure as proposed by STAUFFER, 1978 [108] is not confirmed. Moreover, the inverse proportionality to the pore size distribution index λ could not be found on the basis of the numerical experiments.
- If the coefficient τ scales with the square of the averaging length, the magnitude of τ is not clearly bounded and an REV cannot be defined. To overcome this problem, either the averaging length needs to be related to a bounded property or the averaging of the pressures and saturations has to be reviewed. It is assumed here, that a characteristic length scale of a process can be defined, and that this length scale should then be inversely proportional to the distance of the characteristic viscous pressure drop. Consequently, for small gradients the coefficient τ should also be small. A more promising approach seems to be a re-definition of the averaging procedure.
- For the determination of the coefficient the boundary conditions should ensure a uni-directional flow process, thus preventing counter-current flow.
- If the capillary pressure is fixed at the boundaries, the boundary nodes should not be taken into account for the averaging of the variables.
- The magnitude of the coefficient might depend on the boundary conditions and the flow regimes thus induced. For high saturation rates, the magnitude of τ is smaller compared to the one derived from examples with small rates of change of saturation. A similar behaviour is observed by KALAYDJIAN, 1992 [68] in laboratory imbibition experiments. KALAYDJIAN, 1992 [68] argues, that, for viscous dominated flow regimes, the coefficient should be smaller, as the typical process is faster. However, if the coefficient increases with augmenting capillary forces, it would reach a maximum for entirely capillary dominated flow. Capillary dominated flow is assumed for the capillary equilibrium approach (see Sec. 5.4.2), the phase pressure difference should then always be equal to the equilibrium capillary pressure. Thus, the extended $P_c(S_w)$ relationship should be obsolete.

5.4.4 The coefficient τ for heterogeneous domains

Numerical experiments for the determination of the coefficient τ have been performed applying homogeneous domains (see Sec. 5.4.3). Assuming that additional

dynamic effects might arise from heterogeneities, two kinds of two-dimensional heterogeneous domains serve to investigate the influence of heterogeneities on $\tau_0(S_w)$,

1. the simple heterogeneity of two fine sand lenses embedded in a coarse sand, and
2. continuous heterogeneities on the basis of a geostatistical approach (compare Sec. 5.2).

In contrast to the homogeneous domains, the examples here show a two-dimensional flow behaviour. The averaging of the variables thus relates to an area. In order to investigate the behaviour of the coefficient in a general way, it is assumed that the linear relationship running through the origin is a correct approximation.
For the heterogeneous domains two degrees of heterogeneity are considered,

- only the intrinsic permeability differs, and
- the intrinsic permeability plus the entry pressure vary in space.

To quantify heterogeneity often the ratio of the minimum to the maximum value of a given quantity is expressed. In the frame of this thesis two ratios defined by BOURGEAT & PANFILOV, 1998 [16] are applied (though they are used in a framework of periodic heterogeneity patterns), one for the intrinsic permeability ratio

$$\omega_K = \frac{\min K}{\max K} , \tag{5.20}$$

and the second one for the entry pressure ratio

$$\omega_{Pd} = \frac{\min P_d}{\max P_d} . \tag{5.21}$$

The fluid parameters are the ones given in Tab. 2.1. In both cases, the pressure-cell set-up with a Dirichlet boundary condition at the left is chosen. Averaging includes only time steps before the non-wetting phase reaches the lower boundary.

5.4.4.1 Simple heterogeneity pattern

For the simple heterogeneity the non-wetting phase pressure equals $P_n = 2000\,\mathrm{Pa}$ at the left boundary for $t > 0$. In case only the permeability is varied the entry pressure equals $P_d = 500\,\mathrm{Pa}$ in the whole domain. For the entry pressure variation, P_d of the fine material is increased to $P_d = 800\,\mathrm{Pa}$. A smaller difference in entry pressures as compared to the example described in Sec. 5.4.2 facilitates the infiltration of non-wetting phase into the fine lenses. In Fig. C.14 in App. C plots of the final distribution of the wetting phase saturation are shown.
Applying the values from the simple heterogeneity pattern the heterogeneity ratios amount to $\omega_K = 0.1$ and $\omega_{Pd} = 0.625$, thus both being less than one.
For the first case, $\tau_0(S_w)$ is compared to homogeneous reference cases. Averaging is performed over most of the domain ($0.005\,\mathrm{m} \leq y \leq 0.115\,\mathrm{m}$), boundary nodes are

thus excluded. Strictly speaking, the averaging area is smaller than the REV size, however, for the principal investigation done here, possible differences in the results are assumed to be negligible.
The $\tau_0(S_w)$ data might be calculated by a weighted arithmetic average of the homogeneous reference cases for average water saturations larger than ~ 0.63 (see Fig. 5.35, right). At smaller average water saturations, the non-wetting phase has reached the right boundary, an assessment of the behaviour of τ_0 can thus not be given.
In the second case, the variation of the entry pressure influences the capillary pressure difference in comparison to the first case, while the rate of change of saturation only differs slightly at least for the considered saturation range (see Fig. 5.35, left). The run of the curve of $\tau_0(S_w)$ deviates from the first case for medium average water saturations ($< S_w > < 0.7$, see Fig. 5.35, right).

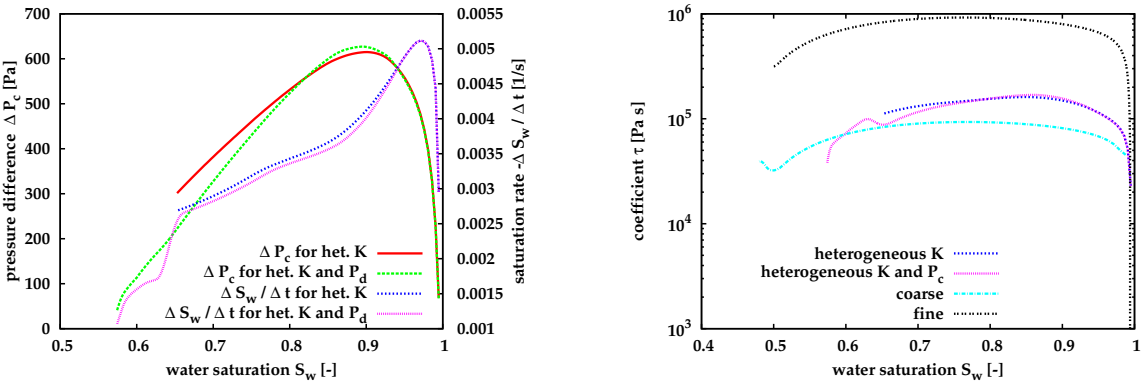

Figure 5.35: $\Delta P_c(S_w)$ and $\Delta S_w/\Delta t(S_w)$ (left) and $\tau_0(S_w)$ (right) for simple heterogeneity

The dimensionless grouping N_D after DAHLE ET AL., 2005 [30] serves to analyse the influence of the heterogeneities. For the heterogeneous case, the permeability is averaged with a weighted arithmetic mean. The same would hold for the porosity, though a porosity variation is not presented here. As a two-dimensional domain and flow process is considered instead of the averaging length squared, the averaging area $\Delta x \Delta y$ is applied, which leads to the dimensionless grouping for a heterogeneous case

$$N_{2D} = \frac{< K > \tau}{< \phi > \mu(< S_w >)\Delta x \Delta y} , \tag{5.22}$$

where again the saturation weighted viscosities are employed. Considering heterogeneity in the permeability only (K in Fig. 5.36), the dimensionless grouping N_{2D} remains close to one for a large range of averaged water saturations. Including also a difference in entry pressure N_{2D} varies around one for water saturations from one to ~ 0.7 (see K and P_d in Fig. 5.36) after which it decreases.
Consequently, it stands to reason that including heterogeneity in the intrinsic permeability can influence the behaviour of the coefficient τ_0 as a function of water

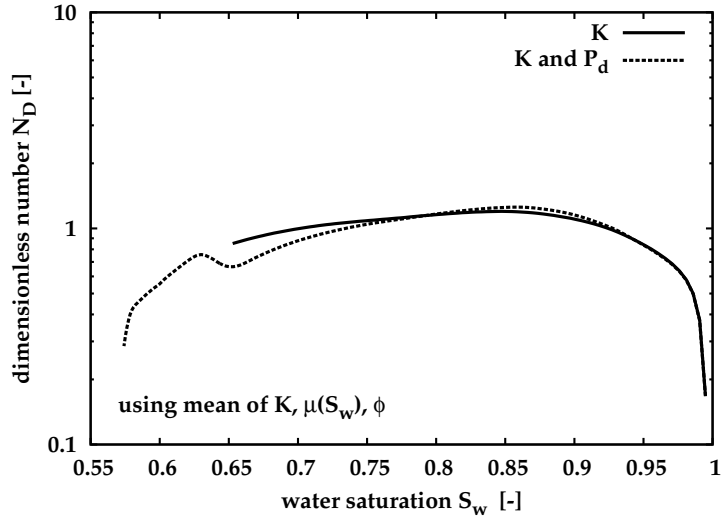

Figure 5.36: Dimensionless grouping N_{2D} for simple heterogeneity with variations in permeability (K) and permeability plus entry pressure (K and P_d)

saturation. Nevertheless, accounting for the heterogeneity when computing the dimensionless grouping N_{2D}, the material coefficient still scales with averaging area, porosity, and average viscosity. If entry pressure variations are included, the scaling might not hold any longer as soon as the fine parts are drained.

5.4.4.2 Spatially correlated random field

For the whole geostatistical heterogeneity field the differences in permeability range from $2.85 \cdot 10^{-11}\,\mathrm{m}^2$ to $7.71 \cdot 10^{-13}\,\mathrm{m}^2$. If the entry pressure is scaled according to Eqn. (5.2) it varies from 212 Pa to 1287 Pa. Choosing the ratios ω_K and ω_{Pd} as defined by Eqns. (5.20) and (5.21) to assess the degree of heterogeneity for the spatially correlated random field, its values of $\omega_K = 0.027$ and $\omega_{Pd} = 0.165$ reveal, that the heterogeneity in permeability as well as entry pressure is more pronounced than in the case of the simple heterogeneity pattern.
For the spatially correlated random field again the boundary conditions of the pressure-cell set-up are applied. The simulations are stopped well before the non-wetting front reaches the right boundary (see Fig. 5.37).
Averaging is performed over the part of the domain that sees the non-wetting front moving through it, that is to say from $y = 0.5\,\mathrm{m}$ to $y = 0.9\,\mathrm{m}$, thus excluding the boundary nodes. It covers twenty correlation lengths in the x- and eight correlation lengths in the y-direction. This is considered sufficient to have an REV keeping in mind the only slight deviations in the equilibrium $P_c(S_w)$ relationships when comparing the one from averaging over the whole domain to the ones from the averaging over a part (see Fig. C.1). The resulting dynamic $P_c(S_w)$ relationships for the homogeneous reference case, for including heterogeneity in the permeability,

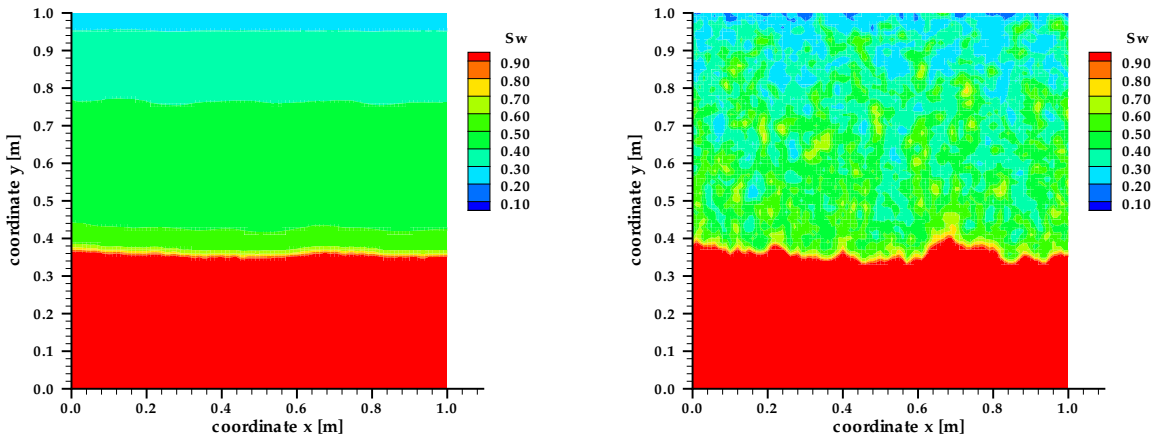

Figure 5.37: Wetting phase distribution at $t = 5 \cdot 10^3$ s for numerical experiment with spatially correlated random field varying only the permeability (left) and varying the permeability plus the entry pressure (right)

and for including heterogeneity in permeability as well as entry pressure distinctly differ from the equilibrium $P_c(S_w)$ relationship (see Fig. 5.38, left). However, they hardly differ from each other. At water saturations near one, the dynamic capillary pressure is negative for all three cases. A plot of the pressures and the water saturation over time reveals that the average non-wetting phase pressure decreases at the beginning of the numerical experiment, especially when the non-wetting phase front enters the averaging area (see Fig. 5.38, right). After that, the average non-wetting phase pressure increases steadily and exceeds the average wetting phase pressure at an average water saturation of $S_w = 0.9875$. The decrease of the non-wetting phase pressure at the beginning can be observed in the other numerical experiments applying the pressure-cell boundary conditions, however, there $< P_n^V >$ exceeds $< P_w^V >$ at all times.

The transition of fully to partially water-saturated conditions also posed problems for the computation of the equilibrium $P_c(S_w)$ relationship when calculating the average capillary pressure (see Sec. 5.4.2). A similar problem arises here. If a large part of the averaging area is fully water saturated, the contribution of the non-wetting phase pressure to the averaged pressure equals zero, as the computation of the averaged pressure is based on a phase-volume weighted approach after Eqn. 5.3. Consequently, the average of the wetting-phase pressure relates to the whole domain, but the one from the non-wetting phase pressure is mainly influenced by the left part of the domain, where the non-wetting phase has infiltrated. The Fig. C.15, right depicts $P_n(y)$ and $P_w(y)$ at $t = 1500$ s. At $y \simeq 0.75$ m the transition of partial to full water saturation occurs. For the lower part of the domain, the non-wetting phase does not contribute to the average capillary pressure as the phase volume-averaged pressure of the non-wetting phase equals zero, and there thus $P_c = -P_w$. In Fig. 5.38

the average phase pressures and wetting phase saturation are plotted as functions of time. Only at $t \simeq 620\,\mathrm{s}$ the average pressure of the non-wetting phase starts to exceed the average wetting phase pressure.

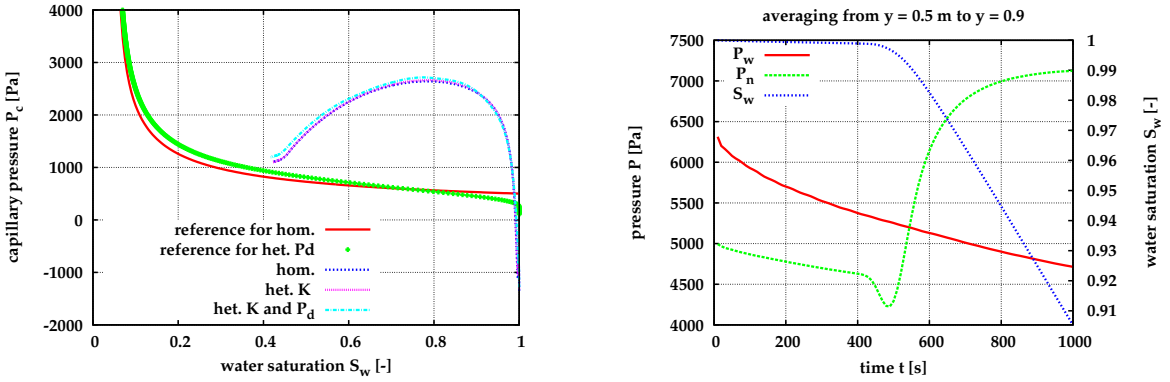

Figure 5.38: Equilibrium and dynamic $P_c(S_w)$ relationships (left) and $P_w(t), P_n(t), S_w(t)$ (right) for spatially correlated random field

The negative capillary pressure at high water saturation is also reflected in the difference of the capillary pressures (see Fig. C.15, left). The difference in capillary pressure from the heterogeneity in permeability and entry pressure differs slightly from the other two cases. The rates of change of saturation more or less equal each other (see Fig. C.15, left).
The $\tau_0(S_w)$ curves of the homogeneous case and the two heterogeneous cases hardly differ (see Fig. 5.39, left). The influence of the decreasing rate of change of saturation is noticeable at an average water saturation of $S_w \sim 0.47$, where the coefficient also changes by almost an order of magnitude.
Following the procedure of the preceding sections, the dimensionless grouping N_{2D} after Eqn. (5.22) is calculated, employing a simple arithmetic mean of the permeabilities for the heterogeneous cases (see Fig. 5.39, right). The $N_{2D}(S_w)$ functions do not vary around one, but remain smaller than one for a large range of the saturation. A similar behaviour has been observed in $N_D(S_w)$ of the homogeneous coarse sand, employing flow-through boundary conditions. In contrast to the flow-through cell, the boundary capillary pressure is not fixed, but the pressure of the non-wetting phase is increased to $P_n = 10^4\,\mathrm{Pa}$ at the left boundary. Thus P_n at the boundary is much larger than for the example of the homogeneous set-up employed for the parameter variation, where $N_D(S_w)$ was equal to one over a large range of saturations.
In **summary**, the following aspects are drawn attention to:

- For the simple heterogeneity pattern an influence on the coefficient τ which might be attributable to the heterogeneity is only noticeable when fine sand lenses are drained.

- In the second example applying a spatially correlated random field, negative capillary pressures at high water saturations are observed. In the example

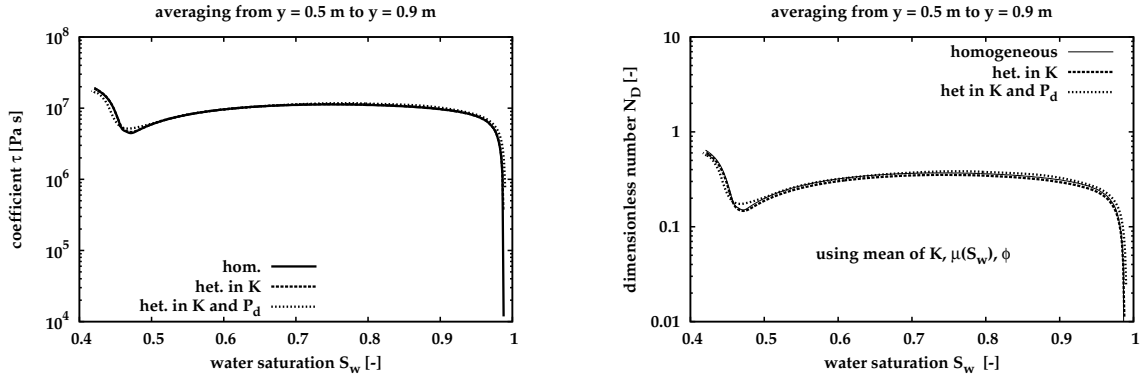

Figure 5.39: $\tau_0(S_w)$ (left) and the grouping N_{2D} (right) for the spatially correlated random field

described in Sec. 5.4.3 negative dynamic P_c values do not occur.

- Moreover, in the second example, due to the high non-wetting phase pressure at the upper boundary, a rapid infiltration of non-wetting phase occurs. As can be seen in Fig. 5.37, S_w decreases distinctly near the upper boundary, which also reduces the relative permeability of the wetting phase. Thus, also in the pressure-cell experiment the influence of the boundary conditions plays a role, even though counter-current flow is prevented by the no-flow boundary condition for the wetting phase at the upper boundary.

- The results from the spatially correlated random field do not show an effect on $\tau(S_w)$ from adding heterogeneity for the considered average saturation range. Although the degree of heterogeneity measured by the ratio of the minimum to the maximum value of K or P_d is larger for the geostatistical case compared to the simple heterogeneity pattern, the influence on $\tau(S_w)$ from including heterogeneity in comparison to homogeneous reference case is less. The continuous distribution of the parameters ensures that for the quantities considered here, the average behaviour of the system dominates.

- Considering the spatially correlated random field of K and P_d as a sub-scale heterogeneity as it might be encountered in the field, sub-scale heterogeneity does not need to be taken into account for the determination of the coefficient τ on the basis of numerical experiments.

In this chapter, the coefficient τ has been determined with several approaches, showing its magnitude to vary distinctly. In the next chapter, simulations are presented, where the extended $P_c(S_w)$ relationship is included in the two-phase balance equations.

6 Simulations with an extended capillary pressure-saturation relationship

In the preceding chapters, a dimensionless analysis and the determination of the coefficient τ in the extended $P_c(S_w)$ relationship were performed. In this chapter, simulations of two-phase flow processes applying the traditional $P_c(S_w)$ relationship are compared to simulations applying the extended $P_c(S_w)$ relationship with magnitudes of the coefficient τ as identified in Ch. 5. The discretisation of the balance equations in space and time is described in Ch. 4. Calculating the dimensionless numbers for the simulations aims at verifying whether they can help in assessing an impact on the solution.

6.1 Introduction

The study of WATSON & WHISLER, 1978 [123] was one of the first where a dynamic $P_c(S_w)$ relationship was applied in a numerical scheme. These authors do not formulate an extended relation between saturation and capillary pressure, but employ differently scaled $P_c(S_w)$ relations depending on the height of the sand column whose drainage they simulate with a Finite Element Code solving the RICHARDS equation [95].
STAUFFER, 1977 [107] simulated a drainage experiment he performed in the laboratory with a fine sand including his extended $P_c(S_w)$ relationship (see Eqn. (3.2)) and, additionally, a dynamic relative permeability-saturation relationship in the RICHARDS equation. He found a better agreement between simulation results and laboratory observations for the simulations including the extended constitutive relationships compared to the traditional approach. In this thesis, only the effect stemming from the extended $P_c(S_w)$ relationship while neglecting dynamic effects in the relative permeabilities will be examined. Thus, a comparison to STAUFFER's results is not attempted.
BELIAEV & HASSANIZADEH, 2001 [12] as well as BELIAEV & SCHOTTING, 2001 [13] adapt the extended $P_c(S_w)$ relationship after HASSANIZADEH & GRAY, 1990 [55] with the inclusion of hysteresis effects using a play-type, and a second order model (PRANDLE-ISHLINSKY) for the history dependent part of the $P_c(S_w)$ relationship. The authors utilise an implicit-explicit time stepping scheme to solve the RICHARDS equation. They compare their solution to an analytical solution of a problem as

given by PHILIP, 1991 [91], which describes an imbibition and drainage process in the same domain, and find a good agreement.
In HASSANIZADEH ET AL., 2002 [52] the extended $P_c(S_w)$ relationship is also included in the RICHARDS equation and a numerical scheme is applied to simulate an imbibition process. This imbibition example will also be analysed here.
In the studies described so far, the extended $P_c(S_w)$ relationship is included in the RICHARDS equation assuming the coefficient τ to be a constant. O'CARROLL ET AL., 2005 [86] employ a Finite Difference scheme for two-phase flow to determine $\tau(S_w)$ from a multi-step drainage laboratory experiment with water and PCE. The inclusion of the extended $P_c(S_w)$ relationship leads to a better fit of the simulation to the measurement of the cumulative outflow of wetting phase as the retardation of the outflow is captured better as opposed to applying a unique $P_c(S_w)$ relationship.
In this thesis, the extended $P_c(S_w)$ relationship after Eqn. (3.12) is employed to close the two-phase balance equations, which are then discretised with a Finite Volume numerical scheme with the primary variables P_w and S_n (see Sec. 4.3). The coefficient τ might be a function of the effective water saturation. In this chapter, simulations of imbibition processes applying this scheme are presented and analysed. The effects of the inclusion of the extended relationship on the solution, denoted in the following extended cases, are compared to reference simulations where a unique relation between capillary pressure and saturation is assumed w.r.t. the following questions.

- How does the distribution of the saturation, the rate of change of saturation as well as its gradient behave for different boundary conditions?
- Does the choice of the relation between the coefficient τ and the effective water saturation influence the simulation results distinctly?
- Do the simulations reflect the assessment of the dominating forces determined by the dimensionless numbers Dy and DyC (as gravity is neglected DyG does not play a role)?
- How do different boundary conditions affect the solution?

Furthermore sensitivity analyses assist to identify appropriate boundary conditions and to be measured parameters with which the coefficient τ might be determined with inverse simulations of laboratory experiments. As the focus of this thesis is on dynamic effects in the $P_c(S_w)$ relationship, dynamic effects in the relative permeabilities are not taken into account.
The impact on the solution is demonstrated with set-ups that differ in the initial and boundary conditions. In all of the examples gravity is neglected. All the combinations of boundary conditions induce an infiltration of the wetting phase into a domain with initially high non-wetting phase saturation. The simulations are run until a steady-state is approximately attained.
For a comparison to the reference cases, where the traditional approach to the $P_c(S_w)$ relationship after Eqn. (2.35) is assumed to hold, two integral measures and three space-dependent quantities are chosen, namely

- the absolute value of the cumulative mass of wetting phase M_w^c in the domain,
- the time until steady-state is approximately reached,
- profiles of the non-wetting phase saturation, and on the basis of a post-processing step,
- profiles of the rate of change of non-wetting phase saturation and its gradient.

The mass of wetting phase inside the domain is computed after each time step by a loop over the sub-control volumes. Then the difference to the initial mass in the domain is computed after

$$M_w^c(t) = M_w(t=0) - M_w(t) \,, \tag{6.1}$$

where $M_w^c(t)$ denotes the cumulative mass of wetting phase. For the considered examples the cumulative mass is negative at all times, thus the absolute value of M_w^c might be plotted over time.
On the basis of the cumulative mass, the time until steady-state is reached approximately is assessed. The difference to $t = 0$ is then denoted as the 'characteristic time scale' t_c. In contrast to the computation of the equilibrium $P_c(S_w)$ relationship, where varying equilibrium criteria are applied, the attainment of a steady state is estimated using a plot of the cumulative outflow. This is considered sufficient as most characteristic time scales from the reference to the simulations including the extended $P_c(S_w)$ differ distinctly.
Moreover, for the one-dimensional flow processes analysed here, the rate of change of saturation and its gradient are approximated by a backward difference scheme for i numbers of nodes in the y-direction for a fixed x-coordinate and and a total number of N time steps according to

$$\begin{aligned}(\Delta S_n/\Delta t)^n(y_i) &= \frac{S_n^n(y_i) - S_n^{n-1}(y_i)}{t^n - t^{n-1}} \\ &= D_s^n(y_i) \quad \text{for} \quad 0 < n < N \,,\end{aligned} \tag{6.2}$$

and

$$\Delta y^{-1}(\Delta S/\Delta t)^n(y_i) = \frac{D_s^n(y_i) - D_s^n(y_{i-1})}{y_i - y_{i-1}} \quad \text{with} \quad y_i > y_{i-1} \,. \tag{6.3}$$

If for the saturation of the non-wetting phase a Dirichlet boundary condition is applied, obviously the rate of change of saturation at this boundary equals zero for all time steps, which also influences the gradient of the rate of change of saturation. These effects are kept in mind when discussing the simulation results. The calculations of D_s and $\Delta y^{-1} D_s$ are performed as a post-processing step applying $S_n(y)$ for each time step. The gradient of the rate of change of saturation appears as an additional term in the conservation equation of the non-wetting phase when the extended $P_c(S_w)$ relationship is applied to close the system of equations (see Sec. 4.3). It is thus chosen for the comparison. It is assumed, that the values derived from the post-processing allow an estimation of the behaviour of these terms as they occur during the simulations.

6.2 First imbibition example

The first simulations presented here follow the example from HASSANIZADEH ET AL., 2002 [52], who apply the RICHARDS equation with an extended $P_c(S_w)$ relationship in simulations of an imbibition process. They compare the wetting phase saturation at given times and report a retardation of the front when the extended $P_c(S_w)$ relationship is taken into account. PAPAFOTIOU, 2004 [90] uses a two-phase flow model also including the extended $P_c(S_w)$ relationship for the simulation of this imbibition process. He mimics the boundary conditions of the just mentioned example by fixing the capillary pressure at the boundaries assuming that at the boundaries the traditional approach to the $P_c(S_w)$ relationship holds. Comparing a reference case with $\tau = 0$ and simulations with a constant coefficient much larger than zero he also observed a retardation of the imbibition process.
Tab. 6.1 lists the porous medium and fluid properties as well as the parameters of the constitutive relationships for the simulations performed here. Although the viscosities correspond to the properties of water and gas (air), the fluid phases are termed wetting and non-wetting phase. Assuming that the gas phase is at atmospheric pressure at the boundaries corresponds to the assumption for the RICHARDS equation [95] that the air pressure is constant. Here, the atmospheric reference pressure equals $P_n = 10^5$ Pa.
The parametrisation of VAN GENUCHTEN is selected for the $P_c(S_w)$ relationship (see Eqn. (2.16)) and the approach after VAN GENUCHTEN / MUALEM for the $k_{r\alpha}(S_\alpha)$ relationships after Eqns. (2.20) and (2.21).

Table 6.1: Fluid and porous medium properties for the first imbibition example

Property	Value
Viscosity wetting phase μ_w	$1.0 \cdot 10^{-3}$ Pa s
Viscosity non-wetting phase μ_n	$1.65 \cdot 10^{-5}$ Pa s
Residual saturation wetting phase S_{wr}	0.277
Residual saturation non-wetting phase S_{nr}	0.0
Porosity ϕ	0.368
Intrinsic permeability K	$9.3985 \cdot 10^{-12}$ m^2
VAN GENUCHTEN α	0.0003414 1/Pa
VAN GENUCHTEN n	2.0

The domain is 0.6 m long and 0.1 m wide (gravity is neglected). Although a one-dimensional problem is solved, a two-dimensional domain needs to be prescribed as MUFTE-UG can only handle 2D or 3D domains. The 2D domain possesses a depth of 1.0 m.
The initial and boundary conditions are equal to the ones employed by PAPAFOTIOU, 2004 [90], who applied Dirichlet pressure boundary conditions for both phases at each end of the domain, which relate to a low capillary pressure at the upper and a high capillary pressure at the lower boundary.

6.2.1 Parameter sensitivity for a preliminary example

In this preliminary investigation it is attempted to analyse the parameter sensitivity of the cumulative mass calculated after Eqn. (6.1) and the water saturation over time at the middle of the domain $S_w(x = 0.3\,\mathrm{m}, t)$ w.r.t. the parameters listed in Tab. 6.1 (except S_{nr} and the viscosities).
The parameter sensitivity s is defined by the partial derivative of a function with respect to this parameter. Usually, parameter sensitivities serve to identify the relevant parameters and their correlations for parameter estimations with inverse methods. Also, sensitivities are evaluated for the design of laboratory experiments. If the parameter sensitivities are calculated in advance of the experiment, it can be determined which quantities should be measured and where, in order to yield high sensitivities with respect to the model parameters. Moreover, it can be assessed if the to be applied initial and boundary conditions allow for high sensitivities of the model parameters and small correlations between them. By this approach it is assumed inherently that the applied physical-mathematical model captures all processes correctly, and that the thus designed experiments can yield measurements for the parameter identification. Obviously, the performance of the laboratory experiment would then have to verify this assumption. Here, calculating sensitivities on the basis of simulations aims at assessing the sensitivities' magnitude of the model parameters for the one-dimensional imbibition example.
The derivative of a function with respect to a parameter p is approximated numerically by

$$s = \frac{\partial f(x,t,p)}{\partial p} \simeq \frac{f(x,t,p+\Delta p) - f(x,t,p)}{\Delta p}\,, \tag{6.4}$$

where Δp is supposed to be a small increment of the parameter, usually one percent of the reference value. For absolute values of the numerator in Eqn. 6.4 smaller than $\varepsilon = 10^{-12}$ the derivative is set to zero. As PAPAFOTIOU, 2004 [90] shows that small variations of the coefficient τ do not have an observable effect on the solution, the parameter is varied from one in the reference case to $\tau = 5 \cdot 10^6\,\mathrm{Pa\,s}$ neglecting any dependence on the water saturation. For a first estimation it is assumed that nonlinearities can be neglected. Furthermore, it is crucial that τ should not depend on the rate of change of saturation as rate-dependent parameters might necessitate a different sensitivity analysis (OSTERMANN, 2005 [87]). In order to ensure that Δp is of a similar order of magnitude to facilitate a comparison between the parameter sensitivities, the logarithm of K, α, τ are applied for the calculation of the sensitivity s.
The reference simulation is performed applying the parameters listed in Tab. 6.1. Then the simulation is repeated six times, each time varying one parameter. Except for τ all parameters are increased by one per cent. In case a parameter for the equilibrium $P_c(S_w)$ relationship is altered, the initial conditions are adapted, assuming that for a given capillary pressure an equilibrium (which might not be known) is established before an experiment starts. The boundary conditions are not changed.

For each time step of the reference case the sensitivity is calculated. The quantities of interest from the solution $(M_{\mathrm{w}}^{\mathrm{c}}(t), S_{\mathrm{w}}(y,t))$ of the simulation applying Δp are linearly interpolated for the given target times as the time stepping is adaptive and might differ.

The parameter sensitivity with respect to the cumulative mass shows that a positive correlation exists in relation to all the parameters of the $P_{\mathrm{c}}(S_{\mathrm{w}})$ relationship and a negative one for the permeability and the porosity (see Fig. 6.1, left). A negative correlation implies that at a given time more wetting phase mass has entered the domain in comparison to the reference case. As Dirichlet boundary conditions are applied, increasing the intrinsic permeability results in larger flow velocities. Augmenting the porosity, does not increase the flow velocities but results in a higher infiltration of mass into the domain.

An increase of the VAN GENUCHTEN parameter α effects a smaller P_{c} at an effective water saturation of $S_{\mathrm{e}} = 0.5$ in the applied equilibrium $P_{\mathrm{c}}(S_{\mathrm{w}})$ relationship. Thus for a given capillary pressure, the water saturation is smaller compared to the $P_{\mathrm{c}}(S_{\mathrm{w}})$ relationship of the reference case. The parameter n alters the $P_{\mathrm{c}}(S_{\mathrm{w}})$ relationship for effective saturations $S_{\mathrm{e}} \neq 0.5$. If n is increased, then the $P_{\mathrm{c}}(S_{\mathrm{w}})$ relationship has a smaller derivative at saturations larger than the residual water saturation. Thus in both cases the imbibition processes are slower compared to the reference case. Also, a higher n results in a flatter slope of the equilibrium $P_{\mathrm{c}}(S_{\mathrm{w}})$ relationship, thus the gradient in capillary pressure is smaller for medium water saturations. An increase of residual water saturation also retards the imbibition process with respect to the reference simulation. The variation of S_{wr} by one per cent results in the highest change in the initial wetting phase saturation, thus the high difference to the reference (compare the sensitivities for $S_{\mathrm{w}}(x,t)$).

The sensitivity of the cumulative mass with respect to the coefficient τ reaches a maximum at $t = 0.1639\,\mathrm{h}$ and decreases then to approx. 10^{-3} towards the end (see zoomed graph in Fig. 6.1, left). Consequently, its sensitivity is by more than two orders of magnitude smaller than the ones of the other parameters. The same holds true when the sensitivity of $S_{\mathrm{w}}(x = 0.3\,\mathrm{m}, t)$ is calculated (see Fig. 6.1, right). The negative values of the sensitivity w.r.t. the coefficient increase monotonically from on $t = 1.4\,\mathrm{h}$ until they reach -0.022 at the end of the simulation. The sensitivities for the other parameters all show an extremum, which the sensitivity for τ does not exhibit.

In comparison to the other varied parameters, the system response is much less sensitive to the parameter τ. Consequently, it might be difficult to determine τ for the given porous medium with an inverse approach even though its sensitivity pattern especially when considering $S_{\mathrm{w}}(x,t)$ differs from the other ones. As the variation of the parameters that enter into the $P_{\mathrm{c}}(S_{\mathrm{w}})$ relationship alter also the equilibrium conditions of a given set-up, in the following, the focus will be on the variation of the permeability compared to the one of the τ coefficient. It is thus inherently assumed, that the parameters for the equilibrium constitutive relationships can be determined independently and that they do not change under varying flow conditions. This might not hold true e.g. for the residual water saturation (see e.g. GIELEN, 2004

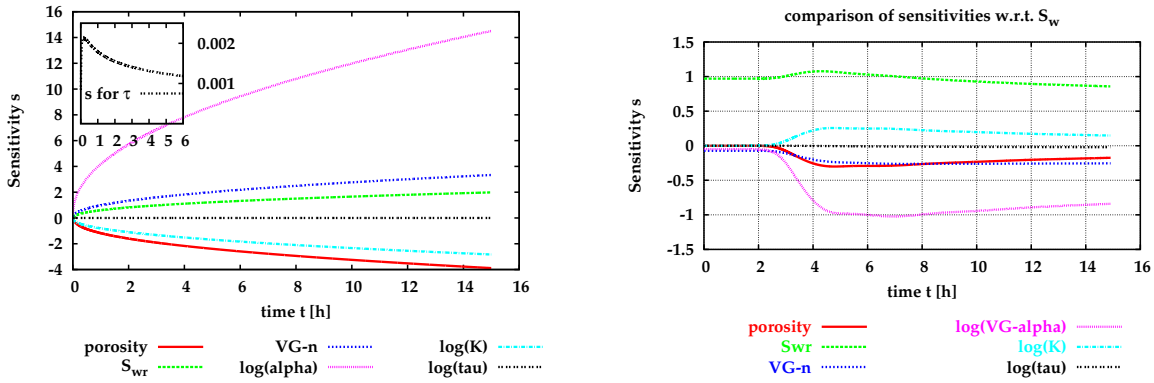

Figure 6.1: Sensitivities of the cumulative mass $M_w^c(t)$ (left) and of $S_w(x = 0.3\,\mathrm{m}, t)$ (right) for preliminary investigation

[45]) or the relative permeabilities (see e.g. [14], [110], [129]).

6.2.2 Simulation results

In the dimensionless analysis (see Sec. 3.6) the influence of the individual terms in the balance equations of two-phase flow is assessed with the help of the ratios of the forces. If for the dimensionless number Dy after Eqn. (3.24), which quantifies the influence of dynamic over viscous effects, the system length is inserted as the characteristic length scale, and $\tau = 5 \cdot 10^6\,\mathrm{Pa\,s}$, the dynamic number with $\mathrm{Dy} = 0.13$ is less than one for the example just described in Sec. 6.2.1. In order to increase the influence from the dynamic term the intrinsic permeability is increased by two orders of magnitude for the following example.
The initial and boundary conditions for the first imbibition example can be seen from Fig. 6.2. In the y-direction the domain is discretised with 40 cells. Initially, a wetting phase pressure of $P_w = 1900\,\mathrm{Pa}$ and a non-wetting phase saturation of $S_n = 0.701$ are applied. For both fluid phases Dirichlet boundary conditions are applied at the opposing ends of the set-up. Assuming that the pressure of the non-wetting phase is mostly constant (similar to the assumption in the RICHARDS equation) the wetting phase pressure equals to $P_n - P_c(98100\,\mathrm{Pa})$ at the lower boundary and to $P_n - P_c(7357.5\,\mathrm{Pa})$ at the upper boundary. This reduction in capillary and increase in wetting phase pressure compared to the initial conditions induces the wetting phase to infiltrate into the domain. The saturation of the non-wetting phase at these boundaries corresponds to $1.0 - S_w(P_c)$.
As described in Sec. 5.3 to Sec. 5.4 the coefficient τ is found to be a function of the water saturation in laboratory as well as numerical experiments. Consequently, the coefficient τ is not only considered a constant but also as a linear or quadratic function of the effective water saturation (see Fig. 6.3).
First, the cumulative mass of wetting-phase for five simulations, which differ in their treatment of the $\tau(S_e)$ relationship, are compared (see Fig. 6.4). The titles in the

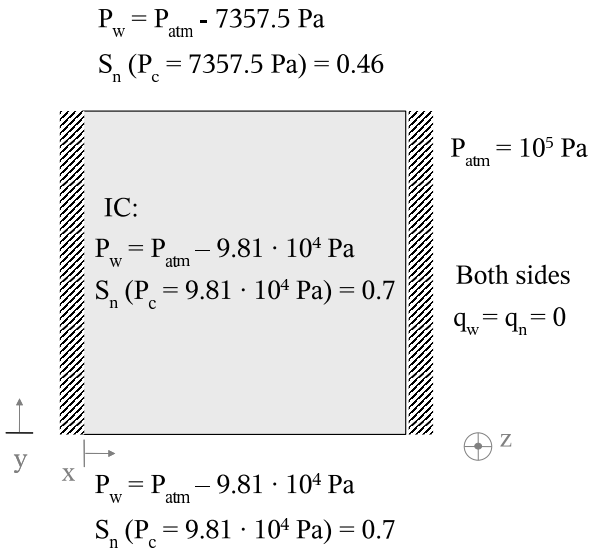

Figure 6.2: Boundary and initial conditions for the first imbibition example

legend correspond to the $\tau(S_e)$ relationships depicted in Fig. 6.3 except for the last curve, which is the result of a simulation applying a constant coefficient $\tau = 10^5$ Pa s. For the simulations where $\tau = 0$, the term referenceïs applied. This numerical experiment illustrates that the coefficient needs exceed a threshold value to influence the simulation results. Considering the extended $P_c(S_w)$ relationship after Eqn. (3.13), and assuming that the rate of change of saturation is less than one, the coefficient needs to be larger than 10^4 Pa s to induce a distinct difference between the pressure difference to the equilibrium capillary pressure, which varies in this example between 7357.5 Pa $< P_c <$ 98100 Pa. In the following, only the cases where the inclusion of the coefficient impacts the solution visibly will be considered.

While the reference case has a characteristic time of $t_c \simeq 1600$ s, the characteristic time of the cases including the extended $P_c(S_w)$ relationship with $\tau(S_e)$ after Fig. 6.3 all amount to approx. $t_c \simeq 2600$ s. Consequently, the inclusion of the extended $P_c(S_w)$ relationship results in all three cases in a retardation of the imbibition process. Comparing the cumulative mass of wetting phase at $t = 1000$ s reveals differences in this quantity depending on the $\tau(S_e)$ function. For the quadratic function the dampening of the process is less pronounced compared to applying a constant coefficient. However, the shape of the curves differ only slightly. The effective water saturation ranges between $0.413 < S_e < 0.970$, where the $\tau(S_e)$ functions differ distinctly compared e.g. to effective saturations smaller than $S_e < 0.2$, however, the impact on the cumulative mass of wetting phase does not reflect these differences.

In addition to these integral measures also the variation of quantities depending on space are considered. As the $M_w^c(t)$ data deviate from each other distinctly at $t = 1000$ s, the non-wetting phase saturation profile at this time is investigated (see Fig. 6.5, left). The transition of $S_n \rightarrow 0.7$ will be denoted the front of the wetting

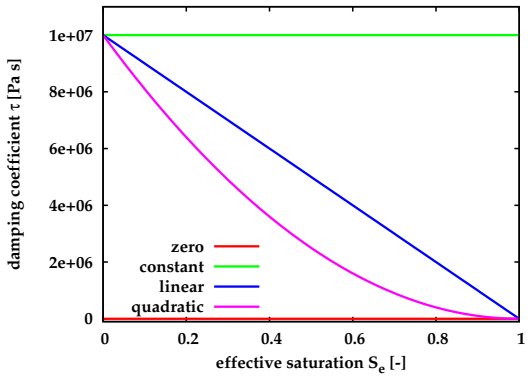

Figure 6.3: Different $\tau(S_e)$ functions as applied in the imbibition examples

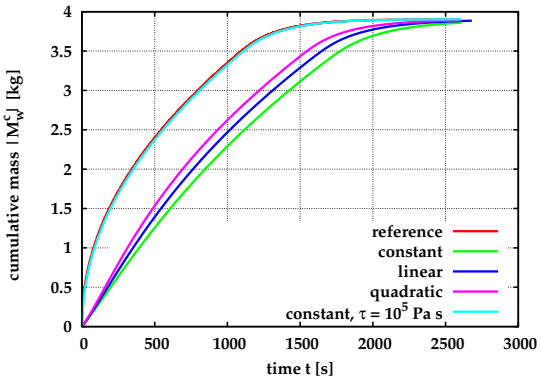

Figure 6.4: Norm of $M_w^c(t)$ from simulations of the first imbibition example applying varying $\tau(S_e)$ relations

phase in the following. Due to the fixed non-wetting phase saturation at the boundary obviously all cases need to have the same $S_n(y = 0.6\,\mathrm{m})$. With the inclusion of τ, the non-wetting phase saturation exhibits a higher gradient in the lower part of the domain compared to the reference case. At the same time less wetting phase has entered the system, thus the front has not advanced as far into the domain as in the reference case. Additionally, the non-wetting phase saturations are compared when the cumulative mass of wetting phase is approximately $|M_w^c| \simeq 2.0\,\mathrm{kg}$ (see Fig. 6.5, right). The inclusion of different $\tau(Se)$ functions influences the profile $S_n(y)$ only slightly if equal viscosities are compared. While the quadratic relation does not alter the profile distinctly, especially the constant coefficient causes a flattening of the front. Keeping in mind that the mass in the system is not exactly the same, it is nevertheless noticeable that at the front the gradient of the saturation profile is steeper for the reference case compared to the other ones. In contrast, near the upper boundary the decrease in S_n is more pronounced for the reference case.

The rate of change of saturation $\Delta S_n/\Delta t$ for this imbibition process is either zero or negative in case S_n decreases (see Fig. 6.6). All $\Delta S_n/\Delta t(y)$ data increase from the top boundary towards the middle of the domain and display a local minimum at the wetting-phase front. Obviously, in absolute terms this minimum corresponds to a maximum change in the saturation with time. The minimum only differs slightly between the cases at a time of $t = 1000\,\mathrm{s}$ (see Fig. 6.6, left). The profiles all have the same shape, but the minimum is less pronounced for the constant coefficient as opposed to a quadratic function. If the rate of change of saturation is compared for a condition where approximately the same mass of wetting phase has entered the domain, a distinct difference in the minimum of approx. an order of magnitude from the reference case to the extended cases can be observed (see Fig. 6.6, right). As shown in the Fig 6.5, right, the saturation has a more pronounced front in the reference case. This effect is reflected in the rate of change of saturation (see Fig. 6.6, right). At the same time, the saturation rate near the boundary is slightly smaller for

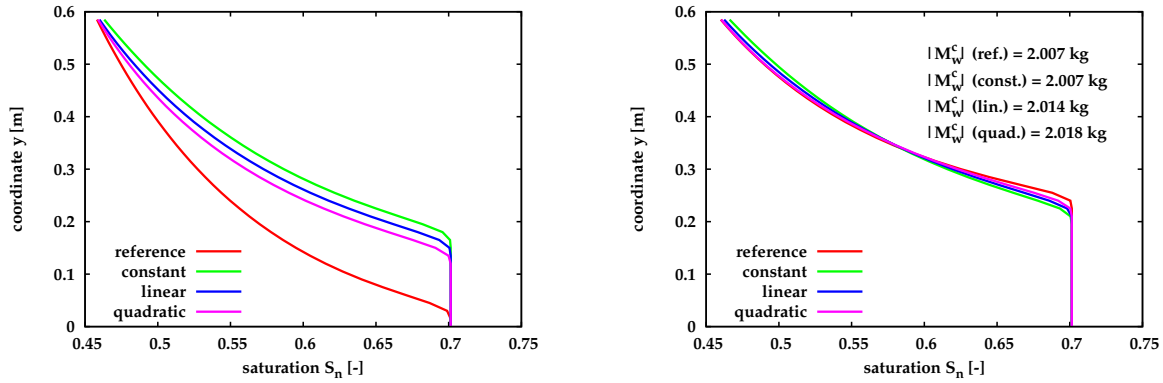

Figure 6.5: $S_n(y)$ for the first imbibition example applying varying $\tau(Se)$ at time $t = 1000\,s$ (left) and at a cumulative mass of $|M_W^c| \sim 2\,kg$ (right). For the exact values of the cumulative mass see Fig. 6.3

the reference case.

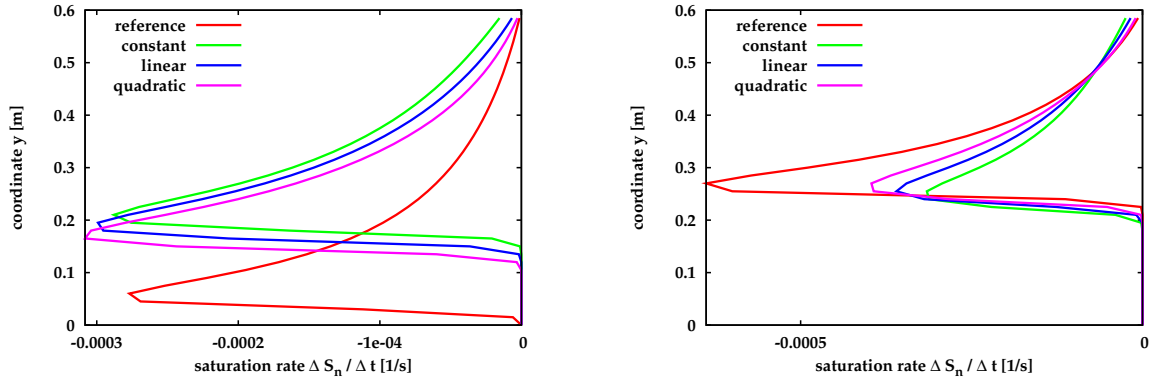

Figure 6.6: $^{\Delta S_n}/_{\Delta t}(y)$ for the first imbibition example at time $t = 1000\,s$ (left) and at a cumulative mass of $|M_W^c| \simeq 2\,kg$ (right). For the exact values of the cumulative mass see Fig. 6.3

For the derivative in the y-direction after Eqn. 6.2, the difference in the coordinates is always positive. Thus for a with depth decreasing rate of change of saturation (meaning in absolute values the magnitude increases) the gradient is positive. If on the other hand, the rate increases (meaning here that it goes back to zero) the gradient becomes negative. In all cases, one maximum and one minimum in the gradient of the rate of change of saturation are observable (see Fig. 6.7). From the top boundary downwards, the gradient increases up to a maximum, which corresponds to reaching the wetting phase front, where the rate of change of saturation has a minimum and thus in absolute terms the highest rates of change of saturation occur. Then the gradient decreases steeply to a minimum and increases again to zero. The run of the curve reflects the inflection points of the rate of change of saturation near the front.

When the profiles of a given time are compared, neither the shape nor the magnitude of the gradients differ much (see Fig. 6.7, left). However, for the same M_w^c, the reference case produces more pronounced extrema (see Fig. 6.7, right).

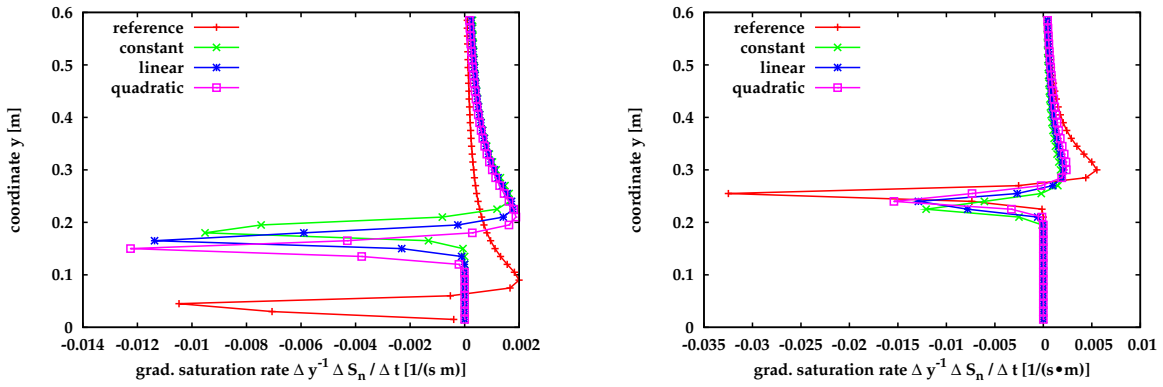

Figure 6.7: $\Delta y^{-1}\Delta S_n/\Delta t(y)$ for the first imbibition example at time $t = 1000\,\mathrm{s}$ (left) and at a cumulative mass of $|M_w^c| \sim 2\,\mathrm{kg}$ (right)

Plots of the rate of change of saturation and its gradient at $y = 0.3\,\mathrm{m}$ as a function of time illustrate the whole range of these quantities for a location in the middle of the domain (see Fig. 6.8). In absolute values the minimum of the saturation rate for the reference case is approx. twice as high as for the cases including the extended $P_c(S_w)$ relationship. Moreover, the minimum is also reached about twice as fast (see Fig. 6.8, left). Consequently, the same holds true for the gradient of the saturation rate (see Fig. 6.8, right). Both the minimum and the maximum are approx. twice as large and are reached about twice as fast for the reference case compared to the extended cases.

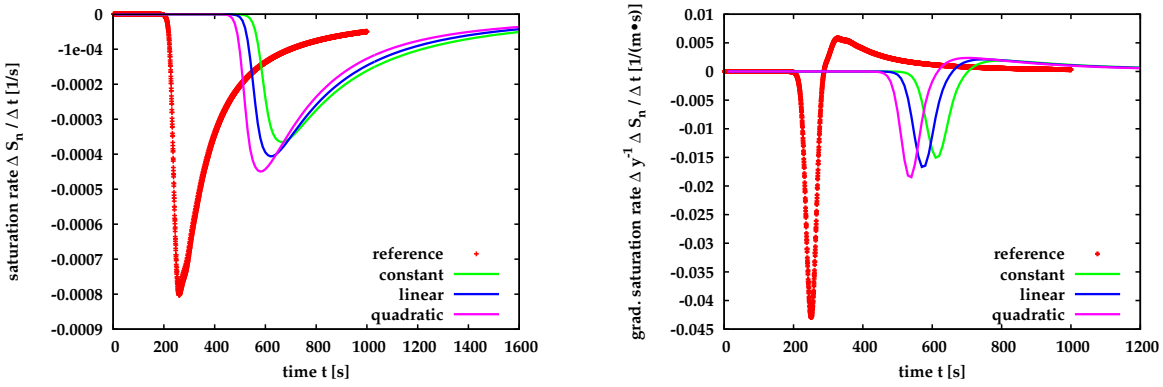

Figure 6.8: $\Delta S_n/\Delta t(t)$ (left) and $\Delta y^{-1}\Delta S_n/\Delta t$ (right) at $y = 0.3\,\mathrm{m}$ for the first imbibition example

Similar to the preliminary investigation, the sensitivity of $M_w^c(t)$ and of $S_w(x,t)$ w.r.t. to the parameters τ and K are investigated, applying again the log-values (see Fig. 6.9). The parameters have opposing effects on the $M_w^c(t)$ and $S_w(x,t)$ functions.

The sensitivities for the coefficient are again smaller than the ones for the permeability, but the difference is reduced to approx. one order of magnitude. Moreover, the temporal distribution patterns differ. While the sensitivity of $M_{\mathrm{w}}^{\mathrm{c}}(t)$ for the permeability has a pronounced extremum at $t \sim 1070\,\mathrm{s}$ when the boundary conditions clearly influence the flow behaviour, the sensitivity for τ is more evenly distributed. Moreover, the sensitivity of $S_{\mathrm{w}}(x,t)$ w.r.t. the permeability increase with increasing depth, whereas w.r.t. to the coefficient they decrease. While the sensitivities' different orders of magnitude would still pose a problem, at least the different temporal distribution patterns of the sensitivities would be of advantage for an inverse parameter identification. Moreover, the results imply that local measurements of the saturation yield more distinct sensitivity patterns than the integral measure of the cumulative mass.

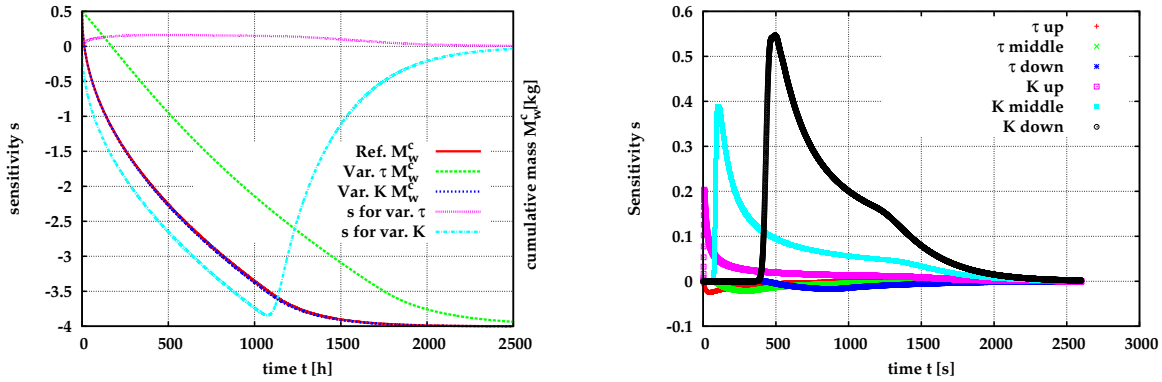

Figure 6.9: Sensitivity of $M_{\mathrm{w}}^{\mathrm{c}}(t)$ (left) and of $S_{\mathrm{w}}(x,t)$ (right) w.r.t. $\log(K)$ and $\log(\tau)$ for the first imbibition example

6.2.3 Calculation and interpretation of the dimensionless numbers

The dimensionless numbers Dy after Eqn. (3.24) and DyC after Eqn. (3.26) as appearing in the dimensionless analysis in Sec. 3.6 aid to assess the influence of dynamic in relation to viscous and capillary equilibrium effects. On the basis of the simulation results, it will be analysed whether these dimensionless numbers aid to predict an influence on the solution stemming from the inclusion of the extended $P_{\mathrm{c}}(S_{\mathrm{w}})$ relationship. It is inherently assumed, that the coefficient is a known constant not depending on the saturation.

Dy as well as DyC can be calculated for the example above (see Tab. 6.2). For the characteristic length scale either the system length, the grid spacing in the y-direction or the front width are applied. The front width is estimated using the gradient of the saturation rate at $t = 1000\,\mathrm{s}$. The part of the domain where the gradient runs through a maximum and minimum is assumed to correlate with the front width. Note, that the front width should relate to a transient process and will therefore change in time. Thus a characteristic front width needs to be identified. The

characteristic capillary pressure is obtained from the equilibrium $P_c(S_w)$ relationship at $P_c(S_e = 0.5)$. Applying the grid spacing as the characteristic length scale leads to

Table 6.2: Dimensionless numbers Dy and DyC for the first imbibition example. For the calculation of DyC $u_c = 10^{-5}\,\mathrm{m/s}$ and $P_{cc} = P_c^e(S_e = 0.5) = 5.1 \cdot 10^3\,\mathrm{Pa}$

Number	system length $l_c = 0.6\,\mathrm{m}$	front width $l_c = 0.2\,\mathrm{m}$	grid spacing $l_c = 0.015\,\mathrm{m}$
Dy [-]	70.9	638.5	$1.1 \cdot 10^5$
Dy [-] for $K = 10^{-12}\,\mathrm{m}^2$	0.08	0.68	120.8
Dy [-] for $\tau = 10^5\,\mathrm{Pa\,s}$	0.71	6.38	1135.1
DyC [-]	0.09	0.27	3.55
Ca [-]	$1.3 \cdot 10^{-3}$	$4.2 \cdot 10^{-4}$	$3.1 \cdot 10^{-5}$

an overestimation of the dynamic in relation to the viscous effects, the value for Dy seems unrealistically high. When a coefficient of $\tau = 10^5\,\mathrm{Pa\,s}$ is applied (for which Dy then also would predict a dominance of the dynamic over the viscous effects), the cumulative mass over time does not show an influence on the solution (see Fig. 6.4), even though PAPAFOTIOU, 2004 [90] showed that the saturation distribution is slightly affected. Thus, applying the grid spacing as the characteristic system length is not considered appropriate and will not be pursued in the following.
The front width as the characteristic system length yields fairly satisfying results. The calculated Dy numbers give the correct estimate, that a clear influence on the results can be observed for the applied parameters of the first example and a coefficient of $10^7\,\mathrm{Pa\,s}$, but not for changing the permeability to $K = 10^{-12}\,\mathrm{m}^2$ as shown in an additional simulation. It would also predict that for a coefficient of $\tau = 10^5\,\mathrm{Pa\,s}$ a slight influence on the results can be observed. Applying the front width can be interpreted in a physical sense. Assuming that steep fronts are encountered in fast processes and broad fronts in slow processes, the number Dy would then predict correctly that for slow processes the dynamic effects do not need to be taken into account. As a consequence also the flow velocity enters indirectly into the calculation of the dimensionless number Dy. A dominance of dynamic to viscous effects suffices to show an effect on the simulation results.
In addition, the capillary number Ca is calculated, which is much smaller than one for any of the applied characteristic lengths.
In summary, the following aspects deserve attention.

- The sensitivity of the cumulative mass or of the saturation $S_w(x,t)$ w.r.t. the coefficient τ remains by two orders of magnitude smaller than w.r.t. to all other parameters applied in the model. Consequently, the chosen initial and boundary conditions are not considered appropriate to evaluate the coefficient τ with an inverse procedure. A set of different boundary conditions is applied in the second imbibition example.

- The inclusion of the extended $P_c(S_w)$ relationship in the conservation equations effects a retardation of the imbibition process simulated here when quantities such as the cumulative mass or the saturation distribution at a given time are compared to a reference case.

- When examining the saturation profile at a given mass in the system, the inclusion of the extended relationship has resulted in a flattening of the front. Thus, when rather than the mass in the system the characteristic time is considered, the inclusion of the extended $P_c(S_w)$ relationship can have the opposite effect; at the front the infiltration is faster and behind the front (and the inflection point in the saturation distribution) the infiltration is retarded.

- Assessing the influence of the dynamic to the viscous effects confirms, that for the chosen set-up and the coefficient τ equalling $\tau = 10^7\,\mathrm{Pa\,s}$ the dynamic dominate the viscous effects. However, the definition of the characteristic length plays a critical role in the computation of the dimensionless numbers. The front width is considered an appropriate choice. The capillary equilibrium effects dominate the dynamic effects if either the system length or the front width are applied to calculate DyC.

In the following, an imbibition process is analysed, where instead of Dirichlet boundary conditions a Neumann boundary condition for the wetting phase should ensure that at a given time the same mass has infiltrated into the domain.

6.3 Second imbibition example

In comparison to the first example the porous media properties are slightly altered (compare Tab. 6.3). Gravity is neglected. Atmospheric pressure equals $P_{atm} = 10^5\,\mathrm{Pa}$. Initially, a wetting phase pressure of $P_w = 89439.9\,\mathrm{Pa}$, which corresponds to $P_n - P_c(1.056 \cdot 10^4\,\mathrm{Pa}$ is prescribed, assuming that the pressure of the non-wetting phase is constant at atmospheric pressure for $t = 0$ (see Fig. 6.10). The saturation of the non-wetting phase equals $S_n = 1.0 - S_w(P_c) = 0.85$, which corresponds to a wetting phase saturation that is higher than the residual saturation. The initial conditions are also assigned to the lower boundary. Instead of applying only Dirichlet boundary conditions as in the first example, a Neumann boundary condition is prescribed at the upper boundary in order to induce an influx of wetting phase into the domain. The Neumann boundary condition should ensure that the cumulative mass over time is equal for the reference and the extended cases. Thus, also the characteristic time scale should not differ. Consequently, if the inclusion of the extended $P_c(S_w)$ relationship has an influence on the simulation results it should be noticeable in the saturation profile, and thus the distribution of the rate of change of saturation and its gradient.
PAPAFOTIOU, 2004 [90] shows for this example that the rate of change of saturation is small for an influx of $q_w = -0.001\,\mathrm{kg/(m^2\,s)}$. Consequently no influence of the

Table 6.3: Fluid and porous medium properties for the second example

Property	Value
Viscosity wetting phase μ_w	$1.0 \cdot 10^{-3}$ Pa s
Viscosity non-wetting phase μ_n	$1.65 \cdot 10^{-5}$ Pa s
Residual saturation wetting phase S_{wr}	0.1
Residual saturation non-wetting phase S_{nr}	0.0
Porosity ϕ	0.4
Intrinsic permeability K	$1.0 \cdot 10^{-11}$ m^2
VAN GENUCHTEN α	0.0004 1/Pa
VAN GENUCHTEN n	3.0

extended relationship on the simulation results for magnitudes of the τ coefficient of up to $\tau = 10^7$ Pa s can be observed.

6.3.1 Simulation results

First the cumulative mass of water inside the domain as a function of time for the reference case is compared to cases where the extended $P_c(S_w)$ relationship is applied for a Neumann boundary condition of $q_w = -0.01\,\mathrm{kg}/(\mathrm{m}^2\,\mathrm{s})$ at the top (see Fig. 6.11). The Neumann boundary condition has effected a characteristic time to attain a steady state of $t_c \simeq 2.25 \cdot 10^4$ s for all cases. As in the first example, applying a constant coefficient of $\tau = 10^6$ Pa s does not affect the results. Again, a threshold value needs to be reached for the given boundary conditions and thus induced flow conditions to show an effect on the solution. In the following, this case is neglected. When the term 'constant' is applied, it refers to a constant coefficient of $\tau = 10^7$ Pa s from now on.
Up to a time of $t \sim 1.4 \cdot 10^4$ s the results are 'expected'. As a consequence of the Neumann boundary condition the cumulative mass over time does not differ from the reference case to the ones including the extended $P_c(S_w)$ relationship.
Up to that time, the same wetting phase mass has infiltrated into the domain. In the integral measure of the cumulative mass no difference can be observed. However, at $t = 1.38 \cdot 10^4$ s the wetting, and thus non-wetting phase, is distributed differently inside the domain (see $S_n(y)$ in Fig. 6.12, left). In the reference case, the non-wetting phase saturation is still higher in the upper (left) part of the domain compared to the extended cases, whereas in the lower part of the domain the non-wetting phase saturation is smaller. At the front, the highest rates of change of saturation occur (see Fig. 6.12, right), thus the influence from the extended $P_c(S_w)$ relationship is high in comparison to the reference case.
Coming back to the cumulative mass of wetting phase over time, at times larger than $t \sim 1.4 \cdot 10^4$ s the behaviour of the extended cases is unexpected. The data from the constant case exhibit a non-monotonic behaviour. The mass of wetting phase in the domain increases to nearly $|M_w^c| \simeq 16$ kg to decrease again and approach the

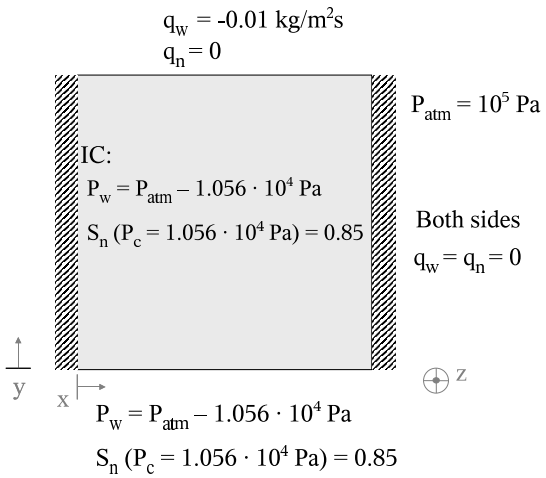

Figure 6.10: Initial and boundary conditions for the second example

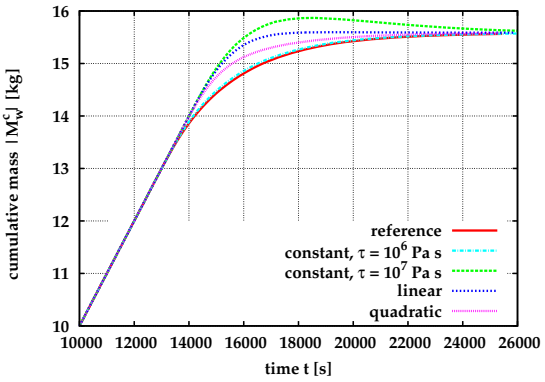

Figure 6.11: Norm of $M_w^c(t)$ for $10^4\,\mathrm{s} < t < 2.6 \cdot 10^4\,\mathrm{s}$ for the second imbibition example with $q_w = -0.01\,\mathrm{kg/(m^2\,s)}$ at the top boundary

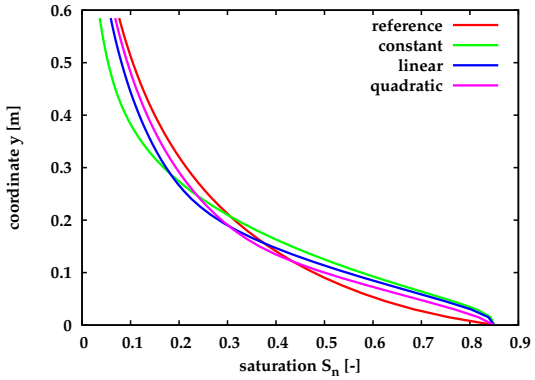

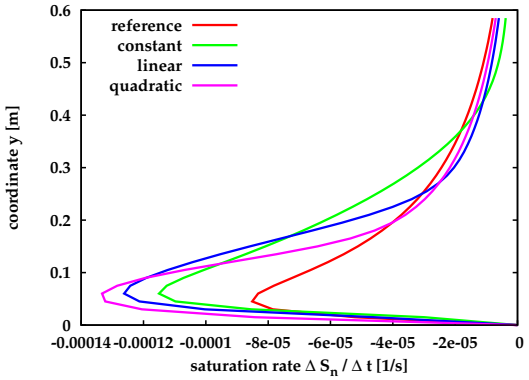

Figure 6.12: $S_n(y)$ (left) and $^{\Delta S_n}/_{\Delta t}(y)$ (right) at time $t = 1.38 \cdot 10^4\,\mathrm{s}$ for the second imbibition example

same equilibrium value also observed in the other cases. This effect deserves special attention. In order to get a better insight the non-wetting phase saturation as a function of time and of space for the constant case are plotted (see Fig. 6.13). Moreover the flow velocity of the wetting phase in the y-direction is compared at two times (see Fig. 6.14). First, the saturation developments with time for the upper part of the domain at $y = 0.51\,\mathrm{m}$ are compared (see Fig. 6.13, left). While until $t \sim 3500\,\mathrm{s}$ the saturation $S_n(t)$ of the reference and the constant case hardly differ, at later times the saturation of the reference case changes slower and behaves monotonically. The saturation of the constant case changes quicker in comparison to the reference case and shows a non-monotonic run. For the location $y = 0.225\,\mathrm{m}$ the saturation of the

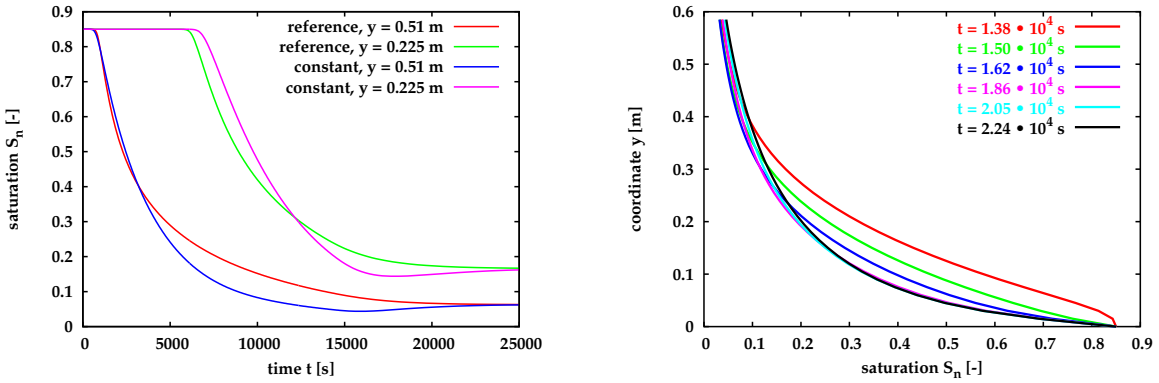

Figure 6.13: $S_n(t)$ at $y = 0.51\,\mathrm{m}$ and $y = 0.225\,\mathrm{m}$ (left) and at selected times for the constant case (right)

reference case starts to change noticeably at $t \sim 6000\,\mathrm{s}$, while the set-off of the constant case is approx. 500 s later. Until $t \sim 1.2 \cdot 10^4\,\mathrm{s}$ the saturation at a given time has changed quicker in the reference case compared to the constant case. From then on, the same effect as for the upper location can be observed, namely a non-monotonic behaviour of the $S_n(t)$ data of the constant case.
This non-monotonic run of $S_n(t)$ indicates an accumulation of wetting phase and as well a reversal of the process. The velocity profiles v_{wy} of the reference and the constant case illustrate how this process reversal is caused (see Fig. 6.14).

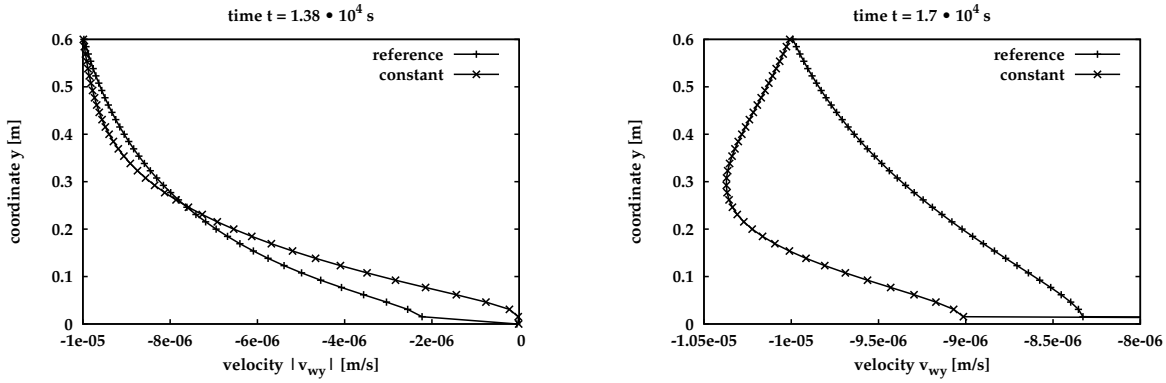

Figure 6.14: Wetting phase velocity v_{wy} at selected times for reference and constant case of second imbibition example

While at $t = 1.38 \cdot 10^4\,\mathrm{s}$ both velocity profiles decrease monotonously with depth until they both have an order of magnitude of $\sim 10^{-8}\,\mathrm{m/s}$ at the lower boundary, but they show a different behaviour. The velocities v_{wy} from the constant case are higher in the upper part and smaller in the lower part of the domain in comparison to the reference case. This is reflected in the saturation profile of the non-wetting phase, where the front has not propagated into the domain as far in the constant compared

to the reference case (see above). At $t = 1.7 \cdot 10^4$ s the velocities of the reference case show a local maximum (in absolute values) at 0.3 m. The retardation of the front and the necessity to obey the influx boundary condition at the top boundary have caused a higher flow velocity in the middle of the domain. Wetting phase mass is accumulated because the front is damped and the wetting phase cannot exfiltrate as it would be necessary to prevent this accumulation. Thus, especially in the lower part of the domain, an increase and subsequent decrease of the wetting phase saturation can be observed. From imbibition the process changes to drainage when the system tries to attain equilibrium. Thus, in contrast to the first example, also positive rates of change can be observed in the constant case (see Fig. 6.15, left). The gradient of the rate of change of saturation at given locations in the sample also changes, here from initially negative values to positive ones before approaching a steady state and thus zero (see Fig. 6.15, right). Although a process reversal occurs, the wetting phase flow is uniquely oriented into the opposite y-direction.

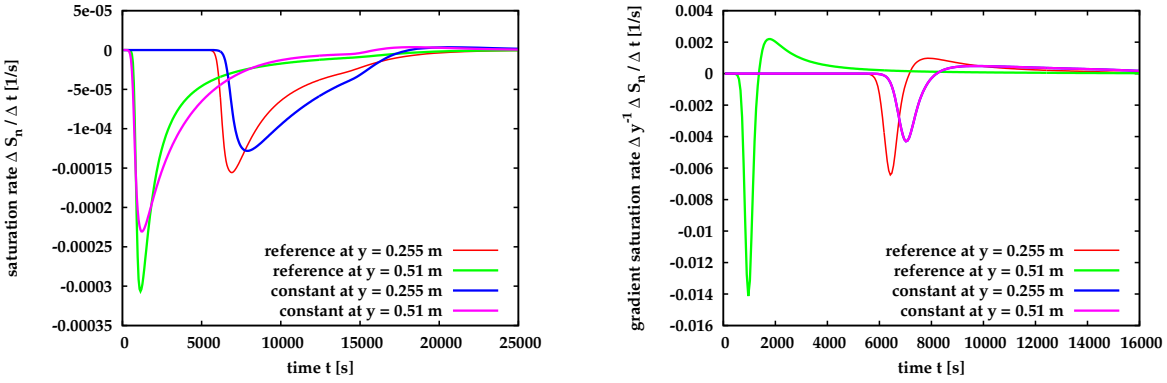

Figure 6.15: ${}^{\Delta S_n}/_{\Delta t}(t)$ (left) and $\Delta y^{-1} {}^{\Delta S_n}/_{\Delta t}(t)$ (right) at two locations (second imbibition example)

6.3.2 Sensitivity analysis

As for the previous example, the sensitivity for the system response, $M_w^c(t)$ and $S_w(x,t)$ w.r.t. to permeability and the τ coefficient are determined (see Fig. 6.16). For this example, the sensitivities of the $S_w(x,t)$ functions w.r.t. the coefficient τ are approx. one order of magnitude smaller than the ones for the permeability. For both parameters the extrema become larger with increasing depth. While for the permeability also the width of the positive peaks increase with depth, the peaks for the coefficient τ become sharper with increasing depth. Another difference can be noted towards the end of the simulation time. The sensitivity for the permeability does not reduce to zero. As a Neumann boundary condition is applied, at equilibrium the same flux is observed for the reference compared to the case of the parameter variation. As the permeability is constant only a different saturation and thus relative permeability distribution, can ensure the same effective permeability compared

to the reference case. Near the steady state the sensitivity for the coefficient τ decreases to zero, as is to be expected for vanishing saturation rates. The saturation distribution then equals the one of the reference case.

Another difference relates to the cumulative mass $M_w^c(t)$. For the variation of the permeability, obviously, the cumulative mass is not sensitive as a Neumann boundary condition is applied. However, the cumulative mass is sensitive w.r.t. a variation in the coefficient τ as soon as the lower boundary condition influences the flow behaviour. For the determination of parameters the influence of the boundary conditions should be prevented as the parameters might become non-unique. Nevertheless, the sensitivity of the cumulative outflow w.r.t. the coefficient τ for this example applying a Neumann boundary condition is the only case, where a system response shows a sensitivity exclusively for the coefficient.

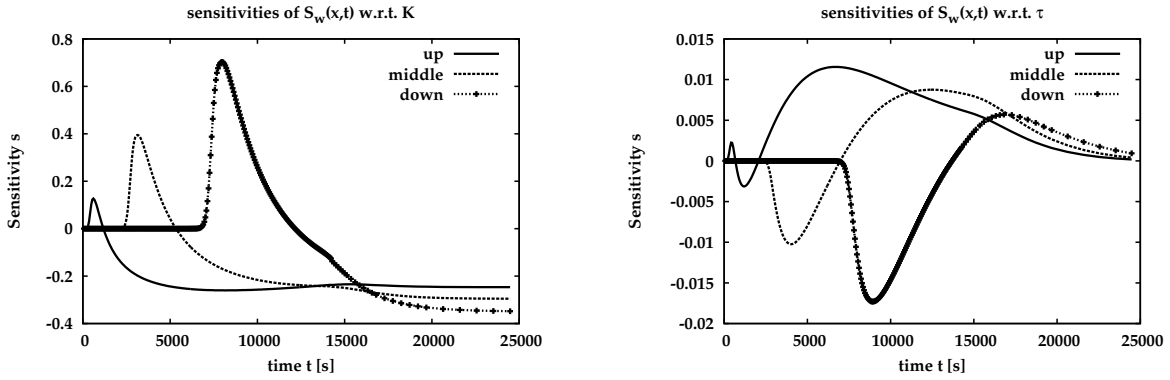

Figure 6.16: Sensitivity of $S_w(y,t)$ w.r.t. the intrinsic permeability $\log(K)$ (left) and w.r.t. the coefficient $\log(\tau)$

6.3.3 Calculation and interpretation of dimensionless numbers

Similar to the first case, the dimensionless numbers Dy and DyC are calculated (see Tab. 6.4). For the characteristic length scale either the system length or the front width are applied. The front width is again estimated on the basis of the gradient of the saturation rate, here at $t = 1.38 \cdot 10^4$ s.

In order to assess the influence of the dynamic to the viscous effects, applying the front width predicts an influence on the results. The number DyC is of the same order of magnitude as for the first example, but the magnitudes of the capillary number are higher. The magnitudes of Ca reflect that the viscous effects are larger compared to the first example. In the next example, the parameters are chosen such that the number Dy as well as DyC exceed one. For the calculation of the numbers it is assumed, that the front width can be predicted.

Table 6.4: Dimensionless numbers Dy and DyC for the second imbibition example applying for the calculation of DyC $u_c = 10^{-5}$ m/s and $P_{cc} = P_c^e(S_e = 0.5) = 3.1 \cdot 10^3$ Pa

Number	system length $l = 0.6$ m	front width $l = 0.2$ m
Dy [-]	0.69	6.25
Dy [-] for $\tau = 10^6$ Pa s	0.07	0.63
DyC [-]	0.13	0.40
Ca [-]	0.19	0.06

6.4 Third imbibition example

In comparison to the second example, all parameters except the VAN GENUCHTEN α and the coefficient τ remain the same. The coefficient τ is increased by an order of magnitude to $\tau = 10^8$ Pa s and treated as a constant. At the same time the VAN GENUCHTEN parameter is increased by an order of magnitude, which reduces the characteristic capillary pressure $P_c(S_e = 0.5)$ by an order of magnitude. The boundary and initial conditions for the wetting phase pressure are adapted accordingly to $P_w = P_{atm} - 1056$ Pa.

Applying the front width as the characteristic length ($l_c = 0.2$ m), for $P_{cc} = 310$ Pa the number DyC amounts to DyC $= 4.0$, while Dy equals 62.

First, again the cumulative mass over time is analysed (see Fig. 6.17, left). Similar to the first example, the data from the reference and the constant case do not differ up to a time $t \sim 1.7 \cdot 10^4$ s. For later times the steady-state distribution is approached faster in the reference case compared to the extended case. The observed effect is different to the second example where an overshoot in the cumulative mass occurs.

The saturation distributions over height at $t = 1.8 \cdot 10^3$ s show that the inclusion of the extended relationship has effected a smearing of the front and an almost linear run of the curve from the upper boundary to the front where $S_n \to 0.85$ (see Fig. 6.17, right). At later times, the saturation profile of the constant case shows oscillations at non-wetting phase saturations near zero. These oscillations lead to negative non-wetting phase saturations which influence the cumulative mass of wetting phase. For a linear case, the resulting $S_n(y)$ also show pronounced negative non-wetting phase saturations near the transition $S_n \to 0$. Moreover, the saturation profile follows a convex shape for $y \sim 0.37$ m, which is a different behaviour from the reference as well as the constant case. If oscillations in the saturation occur, the cumulative mass is no longer a good measure to assess the process, as the mass balance is affected by the oscillations.

Two additional simulations assist to examine possible reasons for the oscillations. First the non-wetting phase saturation is fixed at the upper boundary to a value larger than zero. Thus the upper boundary condition of the non-wetting phase is changed from a no-flux Neumann condition to a Dirichlet boundary condition of

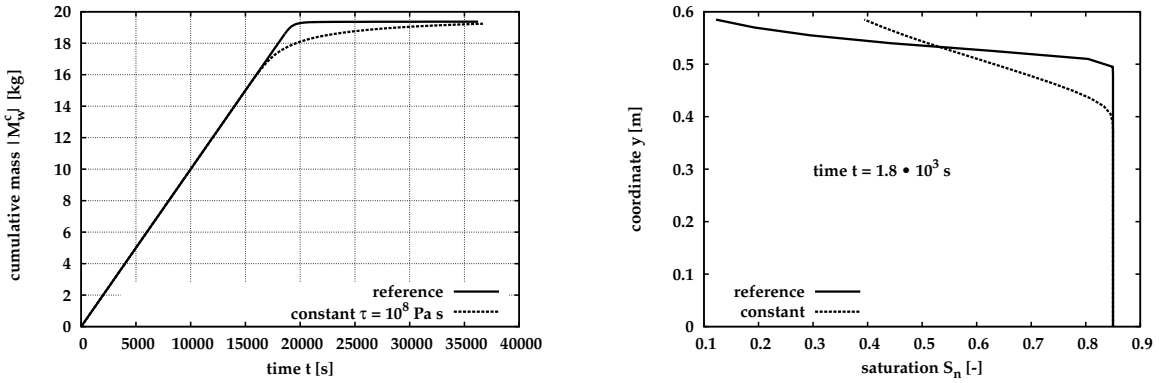

Figure 6.17: $M_w^c(t)$ (left) and $S_n(y)$ at selected times (right) for third example

$S_n = 0.05$, but the results illustrate that the oscillations also occur in this case (see Fig. 6.18, left). If the viscosity ratio is changed from that of water-air ($\mu_w/\mu_n = 61$) to a ratio of one ($\mu_w = \mu_n = 10^{-3}$ Pa s) the oscillations do not arise (see Fig. 6.18, right). Thus, it is assumed that the oscillations are not caused by the regularisation of the $P_c(S_w)$ relationship with $S_w \to 1.0$. Oscillations in the solution of the two-phase balance equations including the extended $P_c(S_w)$ relationship are expected for unfavourable ratios of the advective to the capillary influence (e.g. [29]). For the case presented here, this may be interpreted in terms of the dimensionless number DyC. If the dynamic influence (where with the characteristic flow velocity u_c also viscous forces are inherent) is much larger than the diffusive forces stemming from the equilibrium capillary pressure, then oscillations might occur. It should be noted in this context, that the in Sec. 3.6 defined dimensionless numbers can only be consulted for an estimation of the dominating forces. The influence from the viscosity ratio is not captured.

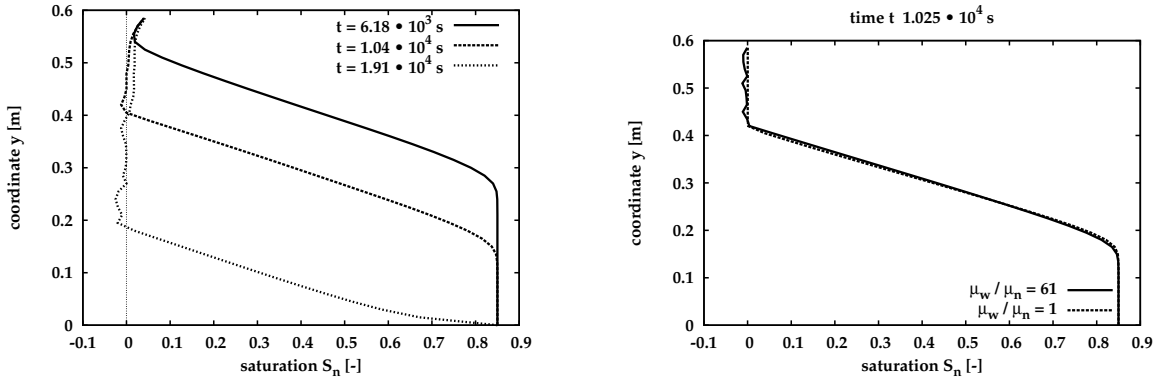

Figure 6.18: $S_n(y)$ for a Dirichlet boundary condition of $S_n = 0.05$ at the upper boundary (left) and various viscosity ratios (right)

In summary, the following aspects deserve attention.

- For the second example, the sensitivities of $M_{\mathrm{w}}^{\mathrm{c}}(t)$ and $S_{\mathrm{w}}(x,t)$ w.r.t. to the coefficient τ are increased compared to the first example. However, they are still approx. one order of magnitude smaller than with respect to e.g. the intrinsic permeability. It is therefore suggested that for inverse parameter identification all other parameters should be determined independently first in an equilibrium experiment (see Sec. 3.1). For the subsequent determination of the coefficient τ it needs to be assumed that the residual saturations and the relative permeabilities do not depend on the dynamics of the flow process. This assumption requires verification.

- In the second example a Neumann boundary condition is applied. The inclusion of the coefficient τ may lead to a process reversal. From an imbibition process, locally a change to drainage and then back to imbibition can be observed.

- In a last example, the set-up is altered with the aim to have a dominance of dynamic over viscous as well as a dominance of the dynamic over the capillary equilibrium force. The simulation results for the inclusion of τ show then oscillations for a viscosity ratio $\mu_{\mathrm{w}}/\mu_{\mathrm{n}} = 61$, but disappear for a ratio of one. Consequently, the dimensionless numbers Dy and DyC do not suffice to assess the influence of the forces, the viscosity ratio also needs to be considered. For the dominance of dynamic forces and a large viscosity ratio the character of the solution might change. It should be stressed here that the parameter combination was chosen only with a view to have a dominance of dynamic over capillary equilibrium forces. A porous medium with such properties might not exist. The observed oscillations are not physical, as negative saturations cannot occur. Still, it should be noticed, that for unfavourable conditions these oscillations can occur in the solution of the two-phase flow equations including the extended $P_{\mathrm{c}}(S_{\mathrm{w}})$ relationship.

6.5 Summary

In this chapter, the influence of including the extended $P_{\mathrm{c}}(S_{\mathrm{w}})$ relationship on simulation results is discussed with respect to the cumulative mass of wetting phase in the domain over time, profiles of non-wetting phase saturation, the rate of change of non-wetting phase saturation and its spatial gradient. Boundary conditions and the parameters of the porous medium are chosen to represent varying magnitudes of the dimensionless numbers Dy and DyC. The results of the analysis can be summarised as follows.
In order to design laboratory experiments a sensitivity analysis can be carried out to ensure large sensitivities for the model parameters. Assuming that all parameters of the two-phase model would be estimated together in an inverse approach the sensitivities of the cumulative mass $M_{\mathrm{w}}^{\mathrm{c}}(t)$ and saturations $S_{\mathrm{w}}(x,t)$ w.r.t. to all parameters have been determined. The sensitivities w.r.t. the coefficient τ remain at least one

order of magnitude smaller than to the other parameters except in one example for the cumulative mass applying a Neumann boundary condition. It is therefore suggested to determine all other parameters first in an equilibrium experiment (see Sec. 3.1). For the subsequent quantification of the coefficient τ, the residual saturations and the relative permeabilities should not depend on the dynamics of the flow process. This assumptions requires verification with laboratory experiments. Furthermore, a more detailed sensitivity analysis should also identify correlations between the parameters.

The inclusion of the extended $P_c(S_w)$ relationship in the conservation equations effects the simulation results if the influence of the dynamic over the viscous forces is large enough. This ratio can be measured by the dimensionless number Dy applying e.g. the front width as a characteristic length scale. However, the nature of the effect on the solution cannot be predicted on the basis of this ratio. Depending on the boundary conditions, the inclusion of the extended $P_c(S_w)$ relationship can have a dampening effect on the rate of change of saturation and thus a retardation effect with respect to the cumulative mass. It can flatten the front by accelerating and slowing down the displacement locally. It can induce a process reversal from imbibition to drainage and back. If additionally the dynamic dominate the equilibrium capillary forces oscillations in the solution might occur for a large viscosity ratio $M = \mu_w/\mu_n$. For the considered saturation ranges the choice of the function $\tau(S_e)$ influences the simulation results quantitatively. However, a difference in the characteristics of the solutions could not be identified. Rather than the functional relationship the magnitude of $\tau(Se = 0.5)$ effects the solution.

7 Conclusions and outlook

7.1 Conclusions

The here presented thesis focuses on two-phase flow processes on the local to macroscale, while accounting for dynamic effects, that is to say a rate-dependence, in the capillary pressure-saturation relationship. Dynamic effects have been observed for example in laboratory experiments reported in the literature. Several authors have proposed an extended $P_c(S_w)$ relationship which can be applied instead of the traditional function that relates the wetting phase saturation to the equilibrium capillary pressure. In a general form, the extended $P_c(S_w)$ relationship can be given as

$$P_n - P_w - P_c^e(S_w) = P_c^d - P_c^e(S_w) = -\tau \frac{\partial S_w}{\partial t} \,. \tag{7.1}$$

The difference of the phase pressures equals thus the equilibrium capillary pressure under static or steady-state conditions. Under transient conditions, the difference $P_c^d - P_c^e$ is assumed to be a linear function of the rate of change of saturation. As a consequence, the factor of proportionality, τ is introduced, here denoted as coefficient τ. This coefficient is shown to be a function of the water saturation. Moreover, it depends on the properties of the porous medium.
The extended $P_c(S_w)$ relationship is analysed under three main aspects.

1. In order to assess the relevance of dynamic effects, a dimensional analysis on the basis of the two-phase balance equations being closed with the extended $P_c(S_w)$ has been carried out. The arising dimensionless numbers facilitate to characterise flow processes which necessitate the inclusion of an extended $P_c(S_w)$ relationship in simulations.

2. The coefficient τ is quantified using laboratory experiments performed by GeoDelft, The Netherlands and numerical experiments.

3. Finally, the impact on the numerical solution of the balance equations being closed with an extended $P_c(S_w)$ relationship is assessed with simulations of imbibition processes in various porous media with varying initial and boundary conditions.

Apart from the well-known capillary and gravitational number, Ca and Gr, additionally, the dimensionless number Dy evolves through the dimensional analysis.

Dy quantifies the ratio of forces due to dynamic effects to forces due to viscous effects. Relating Dy to Ca and Gr yields DyC, the ratio of 'dynamic forces' to capillary equilibrium forces, and DyG, the ratio of 'dynamic forces' to gravitational forces. If the coefficient τ is assumed to be a constant, the importance of dynamic forces diminishes with increasing characteristic length scale with relation to equilibrium capillary, viscous and gravitational forces. On the basis of simulations, the front width of the invading phase was found to be an appropriate interpretation of the characteristic length scale. With increasing transient flow velocity, the influence of the dynamic forces augments.

Furthermore, the coefficient τ is calculated on the basis of laboratory and numerical experiments. The laboratory experiments performed by GeoDelft, The Netherlands, with a sand ($K = 3.06 \cdot 10^{-12}\,\mathrm{m}^2$, $P_\mathrm{d} = 5587\,\mathrm{Pa}$) yield values for the coefficient τ ranging between $\tau = 11.0\,\mathrm{kPa\,s}$ to $\tau = 154.7\,\mathrm{kPa\,s}$ depending on the water saturation. An inversely proportional linear dependence of the coefficient τ on the water saturation is found. A test of the linearity of the extended $P_\mathrm{c}(S_\mathrm{w})$ relationship suggests that at small rates of change of saturation a non-linear relation might be required. If a regression of the extended $P_\mathrm{c}(S_\mathrm{w})$ relationship to the experimental data of each of the three dynamic experiments is performed, the coefficient increases with decreasing influx. This implies that for capillary-dominated flow the coefficient reaches a maximum or tends to infinity. Theoretically, the extended $P_\mathrm{c}(S_\mathrm{w})$ relationship is not required for capillary-dominated flow as then the equilibration between the dynamic and the equilibrium capillary pressure should always be given. Thus, a dynamic $P_\mathrm{c}(S_\mathrm{w})$ and the coefficient τ could not be determined for such flow processes. It is therefore suggested to either perform the fitting on the basis of several dynamic experiments with different boundary conditions or to use an experimental set-up which facilitates to determine τ by inverse parameter identification (see O'CARROLL ET AL., 2005 [86]).

In addition to the analysis of the laboratory experiments, numerical experiments are performed. First, the equilibrium $P_\mathrm{c}(S_\mathrm{w})$ relationship is determined for a coarse sand with two embedded fine sand lenses to test the approach to the averaging of the phase pressures, whose difference yields the capillary pressure for the upscaled $P_\mathrm{c}^\mathrm{e}(S_\mathrm{w})$ relationship. The phase volume-weighted average phase pressures ensure a good agreement with the analytically calculated average $P_\mathrm{c}^\mathrm{e}(S_\mathrm{w})$ relationship. Choosing the boundary capillary pressure for the average $P_\mathrm{c}(S_\mathrm{w})$ might conceal that the average capillary pressure within the domain might exceed the boundary capillary pressure due to pooling effects of the non-wetting phase on the fine sand lenses. This effect vanishes for small pressure gradients within the phases. For high boundary capillary pressures, the average capillary pressure remains significantly smaller than the boundary capillary pressure although equilibrium criteria suggest that a steady state is reached. The equilibrium criteria influence thus the magnitude of the upscaled residual water saturation. The application of very strict equilibrium criteria results in unacceptable large execution times for calculating the equilibrium $P_\mathrm{c}(S_\mathrm{w})$ relationship. The numerical simulation is thus not as efficient as e.g. a percolation model. However, percolation models are based on the assumption of capillary

equilibrium and can therefore not capture effects from viscous influences as e.g. the pooling of non-wetting phase as shown by ATAIE-ASHTIANI ET AL., 2002 [2].
In a second step, dynamic numerical experiments are carried out first for homogeneous domains to test the averaging approach. This test facilitates to distinguish between effects arising from heterogeneities and influences from the averaging length scale, the boundary conditions, and porous medium as well as fluid properties. A dynamic effect in the $P_c(S_w)$ relationship can only be detected if averaged phase pressures in contrast to a nodal value alone are applied for the calculation of the capillary pressure. At one node, the difference in phase pressures equals the capillary pressure as prescribed by the mathematical-numerical model.
The coefficient τ determined in numerical experiments scales proportionally to the porosity, the (saturation-weighted average) viscosity, and the squared averaging length, as well as inversely proportional to the intrinsic permeability for viscosity ratios μ_w/μ_n of one and smaller at medium water saturations $S_{wr} << S_w < 1.0$. The scaling confirms results by DAHLE ET AL., 2005 [30] who applied a bundle of capillary tubes model in order to estimate the coefficient τ. The parameters of the equilibrium $P_c(S_w)$ relationship have a minor influence on the coefficient τ. The empirical formula for the coefficient τ by STAUFFER, 1978 [108] could not be confirmed on the basis of the numerical experiments. If the coefficient τ correlates positively with the averaging length, its magnitude is not clearly bounded and an REV can not be defined. Consequently, either the averaging length needs to be related to a bounded property (e.g. the inverse of the distance of a characteristic pressure drop) or the averaging of the phase pressures has to be re-defined.
An influence resulting from the simple heterogeneity pattern on the coefficient is only noticeable in case the fine sand lenses are drained. The heterogeneity stemming from the spatially-correlated random field does not affect $\tau(S_w)$. The continuous distribution of the parameters ensures that the average behaviour of the system dominates. Considering the spatially-correlated random field of K and P_d as a continuously distributed sub-scale heterogeneity, such patterns do not need to be taken into account for the determination of the coefficient τ derived from numerical experiments. It should be stressed, that for periodic heterogeneities with a clear separation of the small to the large scale as applied in homogenisation theory, dynamic effects have been identified (e.g. BOURGEAT & PANFILOV, 1998 [16], LEWANDOWSKA ET AL., 2004, 2005 [75, 76]).
In the last part of this thesis, a numerical model is applied with which the two-phase balance equations including the extended $P_c(S_w)$ relationship are solved. A sensitivity analysis reveals that neither the integral cumulative mass nor local measures of the saturation possess a sufficient sensitivity w.r.t. the coefficient τ when compared to the other model parameters. It is therefore suggested, that for an inverse parameter identification on the basis of laboratory experiments, all parameters of the traditional two-phase flow model should be determined independently first before quantifying the coefficient on the basis of an additional experiment, which should be specifically designed for the determination of the coefficient. This procedure assumes, that neither the residual saturations nor the relative permeabilities depend

on the dynamics of the flow process.
The dimensionless numbers Dy and DyC can be consulted to assess an impact on the solution when the extended $P_c(S_w)$ relationship is included in the balance equations. The front width should be applied as the characteristic length scale when calculating these numbers. In the simulation of imbibition examples, it is observed that for a dominance of the dynamic over the viscous forces (Dy $>>$ 1), the rate of change of saturation is dampened and thus a retardation effect with respect to the cumulative mass occurs. Locally, accelerating and slowing down of the displacement can flatten a front in comparison to a reference case. Applying a Neumann boundary condition, a process reversal from imbibition to drainage and back occurred. If additionally the equilibrium capillary forces are diminished (DyC $>>$ 1), oscillations in the solution might occur for a large viscosity ratio M. The choice of the function $\tau(S_e)$ influences the simulation results quantitatively, but a different characteristic of the solution could not be clearly identified. However, it should be noted, that in most simulations the wetting phase saturation did not approach $S_w \rightarrow 1.0$, where the highest difference to a constant coefficient would occur. Summarising all the simulations, it should be emphasised that an influence from the extended $P_c(S_w)$ relationship can only be shown for sufficiently high saturation rates and at the same time high coefficients τ. The dimensionless numbers Dy and DyC can give an estimate whether the solution is influenced, in addition also the viscosity ratio needs to be considered.

7.2 Outlook

Although many laboratory experiments have been presented in the literature which examine dynamic effects in the $P_c(S_w)$ relationship, the application of an extended $P_c(S_w)$ relationship in simulations is not widely established. Many fundamental questions are still open in this field of research.
The dependence of the coefficient τ determined in numerical experiments on the averaging volume is an unresolved problem. It needs to be established whether a different averaging of the phase pressures could overcome the scale dependence. It also needs to be assessed whether the coefficient τ relating to a heterogeneous domain on the local scale, can still be interpreted as an effective parameter on the macroscale. If this is not the case, averaging related to the scale transition from the local scale to the macroscale would be obsolete. It is also not clear, whether a scale dependence might be observable in laboratory experiments as it has not been attempted up to now to examine this aspect in the laboratory.
In order to apply the coefficient τ determined in the numerical experiments, other properties need to be upscaled at the same time. While for the upscaling of intrinsic permeability many approaches exist and a rate-dependence is not expected, the relative permeability-saturation relationship might show dynamic effects. It is unclear yet, how to determine the dynamic relative permeabilities together with the dynamic capillary pressure in numerical experiments. But only a consistent averaging

of all the properties would facilitate a comparison to laboratory experiments.
The issue of dynamic relative permeability-saturation relationships also relates to the laboratory experiments. STAUFFER, 1978 [108] has proposed such a relation on the basis of laboratory experiments with fine sands and water-gas fluid systems, but his relation has not been verified in other studies up to now. Moreover, it needs to be investigated whether the residual saturations of both fluid phases are altered under dynamic conditions.
Furthermore, a more detailed study of the influence resulting from the inclusion of the extended $P_c(S_w)$ relationship in the balance equations needs to be performed. The discretisation presented here cannot be applied to heterogeneous domains because the gradient of the saturation needs to be determined. The saturation might be discontinuous at the interface of heterogeneities. In order to correctly include the interfaces, an interface condition similar to the one proposed by DE NEEF, 2000 [35] to represent the entry pressure conditions, is called for.
Generally speaking, dynamic and hysteretic effects influence the constitutive relationships applied for two-phase flow processes on the local and macroscale. The processes leading to these effects and their interaction are yet not fully understood. This prevents a sound assessment of their relevance on different spatial or temporal scales. This study contributes to the understanding of dynamic effects in the capillary pressure-saturation relationship on the local scale and macroscale as well as giving an assessment as to when these effects might need to be taken into account for the evaluation of two-phase flow processes.

Bibliography

[1] L. Anton and R. Hilfer. Trapping and mobilisation of residual fluid during capillary desaturation in porous media. *Physical Review E*, 59(6):6819 – 6823, 1999.

[2] B. Ataie-Ashtiani, S. M. Hassanizadeh, and M. A. Celia. Effects of heterogeneities on capillary pressure-saturation-relative permeability relationships. *Journal of Contaminant Hydrology*, 56:175 – 192, 2002.

[3] B. Ataie-Ashtiani, S. M. Hassanizadeh, M. Oostrom, M. A. Celia, and M. D. White. Effective parameters for two-phase flow in a porous medium with periodic heterogeneities. *Journal of Contaminant Hydrology*, 49:87 – 109, 2001.

[4] Y. Bachmat and J. Bear. Macroscopic modeling of transport phenomena in porous media. 1: The continuum approach. *Transport in Porous Media*, 1:213 – 240, 1986.

[5] G. I. Barenblatt, J. G. Azorero, A. De Pablo, and J. L. Vazquez. Mathematical model of non-equilibrium water-oil displacement in porous strata. *Applicable Analysis*, 65:19 – 45, 1997.

[6] G. I. Barenblatt and A. A. Gilman. Nonequilibrium counterflow capillary impregnation. *J. of Eng. Phys.*, 52:335 – 339, 1987.

[7] G. I. Barenblatt, T. W. Patzek, and D. B. Silin. The mathematical model of non-equilibrium effects in water-oil displacement. In *SPE/DOE 13th Symposium on improved oil recovery*, volume SPE 75169, Tulsa, USA, 2002.

[8] P. Bastian. Numerical computation of multiphase flows in porous media, 1999. Habilitation thesis, Christian-Albrechts-Universität Kiel.

[9] P. Bastian and R. Helmig. Efficient Fully-Coupled Solution Techniques for Two Phase Flow in Porous Media. Parallel Multigrid Solution and Large Scale Computations. *Advances in Water Resources*, 23:199 – 216, 1999.

[10] J. Bear. *Dynamics of Fluids in Porous Media*. Dover Publications, Inc, New York, 1972.

[11] J. Bear and J. J. Nitao. On equilibrium and primary variables in transport in porous media. *Transport in Porous Media*, 18:151 – 184, 1995.

[12] A. Yu. Beliaev and S. M. Hassanizadeh. A theoretical model of hysteresis and dynamic effects in the capillary relation for two-phase flow in porous media. *Transport in Porous Media*, 43:487 – 510, 2001.

[13] A. Yu. Beliaev and R.J. Schotting. Analysis of a new model for unsaturated flow in porous media including hysteresis and dynamic effects. *Computational Geosciences*, 5:345 – 368, 2001.

[14] R. G. Bentsen and M. Muskat. Effect of hydrodynamic forces on capillary pressure and relative permeability. *Transport in Porous Media*, 17:121 – 132, 1994.

[15] T. D. Blake, M. Bracke, and Y. D. Shikhmurzaev. Experimental evidence of nonlocal hydrodynamic influence on the dynamic contact angle. *Physics of Fluids*, 11(8):1995 – 2007, 1999.

[16] A. Bourgeat and M. Panfilov. Effective two-phase flow through highly heterogeneous porous media: Capillary nonequilibrium effects. *Computational Geosciences*, 2:191 – 215, 1998.

[17] C. Braun. *Ein Upscaling-Verfahren für Mehrphasenströmungen in porösen Medien*. PhD thesis, Institut für Wasserbau, Universität Stuttgart, Stuttgart, Germany, 2000.

[18] C. Braun, R. Helmig, and S. Manthey. Determination of constitutive relationships for two-phase flow processes in heterogeneous porous media with emphasis on the relative permeability-saturation-relationship. *Journal of Contaminant Hydrology*, 76(1-2):47 – 85, 2005.

[19] R. H. Brooks and A. T. Corey. Hydraulic properties of porous media. In *Hydrology Papers*, volume 3. Colorado State University, Fort Collins, 1964.

[20] R. H. Brooks and A. T. Corey. Properties of porous media affecting fluid flow. *Journal of the Irrigation and Drainage Division*, pages 61 – 88, 1966.

[21] N. T. Burdine. Relative permeability calculations from pore-size distribution data. Technical report, Research Report, Petroleum Transactions, AIME, 1953.

[22] H.-J. Butt, K. Graf, and M. Kappl. *Physics and chemistry of interfaces*. Wiley-VCH, 2003.

[23] R. F. Carsel and R. S. Parrish. Developing joint probability distributions of soil water retention characteristics. *Water Resources Research*, 24:755 – 769, 1988.

[24] R. J. Charbeneau. *Groundwater hydraulics and pollutant transport*. Prentice Hall, Upper Saddle River, 2000.

[25] I. Chatzis and F. A. Dullien. Dynamic immiscible displacement mechanisms in pore doublets: theory versus experiment. *Journal of Colloid and Interface Science*, 91(1):199 – 222, 1983.

[26] E. C. Childs and N. Collis-George. The permeability of porous materials. *Proc. Roy. Soc.*, A 201:392 – 405, 1950.

[27] B. D. Coleman and W. Noll. The thermodynamics of elastic materials with heat conduction and viscosity. *Arch. Ra. Mech. Anal.*, 13:168 – 178, 1963.

[28] A. T. Corey and R. H. Brooks. The Brooks-Corey relationship. Characterization and measurement of the hydraulic properties of unsaturated porous media. In M. Th. van Genuchten, F. J. Leija, and L. Wu, editors, *Proc. Int. Workshop on Characterization and Measurement of the Hydraulic Properties of Unsaturated Porous Media, October 22 – 24, 1997*, volume 1, pages 13 – 18, Riverside, CA, U.S.A., 1999.

[29] C. Cuesta, C. J. van Duijn, and J. Hulshof. Infiltration in porous media with dynamic capillary pressure: travelling waves. *Euro. Journal of Applied Mathematics*, 11:381 – 397, 2000.

[30] H. K. Dahle, M. A. Celia, and S. M. Hassanizadeh. Bundle of tubes model for calculating dynamic effects in the capillary pressure-saturation relationship. In D. B. Das and S. M. Hassanizadeh, editors, *Upscaling Multiphase Flow in Porous Media*, pages 5 – 22. Springer, 2005.

[31] H. Darcy. *Les fontaines de la ville Dijon*. Dalmont, Paris, 1856.

[32] D. B. Das, S. M. Hassanizadeh, B. Rotter, and B. Ataie-Ashtiani. A numerical study of micro-heterogeneity effects on upscaled properties of two-phase flow in porous media. *Transport in Porous Media*, 56:329 – 350, 2004.

[33] J. M. Davidson, D. R. Nielsen, and J. W. Biggar. The dependence of soil water uptake and release upon the applied pressure increment. *Soil Science Society of America, Proceedings*, 30:298 – 304, 1966.

[34] P. G. de Gennes. Wetting: statics and dynamics. *Reviews of Modern Physics*, 57(3):827 – 863, 1985.

[35] M. J. de Neef. *Modeling Capillary Effects in Heterogeneous Porous Media*. PhD thesis, Technische Universiteit Delft, Delft, The Netherlands, 2000.

[36] W. Durner, B. Schultze, and T. Zurmühl. Transient flow experiments for the determination of the soil hydraulic properties – an evaluation of different experimental boundary conditions. In W. Durner, J. Halbertsma, and M. Cislerova, editors, *European Workshop on Advanced Methods to Determine Hydraulic Properties of Soils*, pages 85 – 88. University of Bayreuth, June 10 – 12, 1996.

[37] W. Durner, B. Schultze, and T. Zurmühl. State-of-the-art in inverse modeling of inflow/outflow experiments. In M. Th. van Genuchten, F. J. Leija, and L. Wu, editors, *Proc. Int. Workshop on Characterization and Measurement of the Hydraulic Properties of Unsaturated Porous Media*, pages 661 – 681, October 22 – 24, 1997.

[38] B. B. Dykaar and P. K. Kitanidis. Determination of the effective hydraulic conductivity for heterogeneous porous media using a numerical spectral approach: 1. method. *Water Resources Research*, 28 No.4:1155 – 1166, 1992.

[39] D. E. Elrick. Unsaturated flow properties of soils. *Australian Journal of Soil Research*, 1:1 – 8, 1963.

[40] A. Elzeftawy and R. S. Mansell. Hydraulic conductivity calculations for unsaturated steady-state and transient-state flow in sand. *Soil Science Society of America, Proceedings*, 39:599 – 603, 1975.

[41] M. Fermigier and P. Jenffer. Experimental investigation of the dynamic contact angle in liquid-liquid systems. *Journal of Colloid Interface Science*, 146:226 – 241, 1991.

[42] A. S. Fokas and Y. C. Yortsos. On the exactly solvable equation $s_t = [(\beta s + \gamma)^{-2} s_x]_x + \alpha(\beta s + \gamma)^{-2} s_x$ occuring in two-phase flow in porous media. *SIAM Journal of Applied Mathematics*, 42:318 – 332, 1982.

[43] S. P. Friedman. Dynamic contact angle explanation of flow rate-dependent saturation-pressure relationships during transient liquid flow in unsaturated porous media. *Journal of Adhesion Science Technology*, 13(12):1495 – 1518, 1999.

[44] L.W. Gelhar, C. Welty, and K.R. Rehfeldt. A critical review of data on field-scale dispersion in aquifers. *Water Resources Research*, 28(7):1954 – 1974, 1992.

[45] T. Gielen, S. M. Hassanizadeh, M. A. Celia, H. K. Dahle, and A. Leijnse. A pore-scale network approach to investigate dynamic effects in multiphase flow. In Casss T. Miller, M. W. Farthing, W. G. Gray, and G. F. Pinder, editors, *Proceedings of the XV International Conference on 'Computational Methods in Water Resources'*, volume I, pages 83 – 94, Chapel Hill, North Carolina, USA, June 13 – 17, 2004.

[46] T. Gielen, S. M. Hassanizadeh, A. Leijnse, and H. F. Nordhaug. Dynamic effects in multiphase flow: a porscale network approach. In D. B. Das and S. M. Hassanizadeh, editors, *Upscaling Multiphase Flow in Porous Media*, pages 217 – 236. Springer, 2005.

[47] H. Graf. *Experimental investigations on multiphase phenomena in porous media*. PhD thesis, Rupertus Carola University of Heidelberg, Heidelberg, Germany, 2004.

[48] W. G. Gray and S. M. Hassanizadeh. Averaging theorems and averaged equations for transport of interface properties in multiphase systems. *International Journal of Multiphase Flow*, 15(1):81 – 95, 1989.

[49] T. R. Green, J. E. Constanz, and D. L. Freyberg. Upscaled soil-water retention using van Genuchten's function. *Journal of Hydrologic Engineering*, 1(3), 1996.

[50] W. Hackbusch. *Multi-grid methods and applications*. Springer, Berlin, 1985.

[51] S. M. Hassanizadeh. Derivation of basic equations mass transport in porous media, part 2, Generalized Darcy's and Fick's laws. *Advances in Water Resources*, 9:208 –222, 1986.

[52] S. M. Hassanizadeh, M. A. Celia, and H. K. Dahle. Dynamic effect in the capillary pressure - saturation relationship and its impact on unsaturated flow. *Vadose Zone Hydrology*, 1:38 – 57, 2002.

[53] S. M. Hassanizadeh and W. G. Gray. General conservation equations for multiphase systems: 1. Averaging procedure. *Advances in Water Resources*, 2:131 – 144, 1979.

[54] S. M. Hassanizadeh and W. G. Gray. General conservation equations for multiphase systems: 2. mass, momenta, energy, and entropy equations. *Advances in Water Resources*, 2:191 – 203, 1979.

[55] S. M. Hassanizadeh and W. G. Gray. Mechanics and thermodynamics of multiphase flow in porous media including interphase boundaries. *Advances in Water Resources*, 13(4):169 – 186, 1990.

[56] S. M. Hassanizadeh and W. G. Gray. Thermodynamic basis of capillary pressure in porous media. *Water Resources Research*, 29(10):3389 – 3405, 1993.

[57] S. M. Hassanizadeh, O. Oung, and S. Manthey. Laboratory experiments and simulations on the significance of non-equilibrium effect in capillary pressure-saturation relationship. In T. Schanz, editor, *Unsaturated Soils: Experimental Studies, Proceedings of the International Conference 'From Experimental Evidence towards Numerical Modeling of Unsaturated Soils' in Weimar, Germany, September 18 – 19, 2003*, volume I of *Springer Proceedings in Physics, Vol. 93*, pages 3 – 14. Springer, 2005.

[58] R. Helmig. *Theorie und Numerik der Mehrphasenströmungen in geklüftet-porösen Medien*. PhD thesis, Institut für Strömungsmechanik und Elektronisches Rechnen im Bauwesen, Universität Hannover, Hannover, Germany, 1993.

[59] R. Helmig. *Multiphase Flow and Transport Processes in the Subsurface*. Springer, 1997.

[60] R. Helmig and R. Huber. Comparison of galerkin-type discretization techniques for two-phase flow in heterogeneous porous media. *Advances in Water Resources*, 21(8):697 – 711, 1998.

[61] R. Hilfer. Transport and relaxation phenomena in porous media. *Advances in Chemical Physics*, XCII:299 – 424, 1996.

[62] R. Hilfer and P. E. Øren. Dimensional analysis of pore scale and field scale immiscible displacement. *Transport in Porous Media*, 22:53 – 72, 1996.

[63] R. L. Hoffman. Study of advancing interface, 1. Interface shape in liquid-gas systems. *Journal of Colloid Interface Science*, 50:228 – 241, 1975.

[64] K. J. Hollenbeck and K. H. Jensen. Experimental evidence of randomness and non-uniqueness in unsaturated outflow experiments designed for hydraulic parameter estimation. *Advances in Water Resources*, 34(4):595 – 602, 1998.

[65] S. I. Hwang and S. E. Powers. Estimating unique soil hydraulic parameters for sandy media from multi-step outflow experiemnts. *Advances in Water Resources*, 26:445 – 456, 2003.

[66] H. Jakobs. *Simulation nicht-isothermer Gas-Wasser-Prozesse in komplexen Kluft-Matrix-Systemen*. PhD thesis, Institut für Wasserbau, Universität Stuttgart, Stuttgart, Germany, 2004.

[67] F. Kalaydjian. A macroscopic description of multiphase flow in porous media involving spacetime evolution of fluid/fluid interface. *Transport in Porous Media*, 2:537 – 552, 1987.

[68] F. Kalaydjian. Dynamic capillary pressure curve for water/oil displacement in porous media: Theory vs. experiment. *Society of Petroleum Engineers*, SPE 24813:491 – 506, 1992.

[69] W. R. Kneale. Observations of the behaviour of large cores of soil during drainage, and the calculation of hydraulic conductivity. *Journal of Soil Science*, 36:163 – 171, 1985.

[70] H. Kobus. Prognoseinstrumente und Meßdatenrealität in der Grundwasserwirtschaft. *Perspektiven der Wasserforschung, Mitteilung 14 der Senatskommission für Wasserforschung der Deutschen Forschungsgemeinschaft*, 1995.

[71] L. W. Lake. *Enhanced Oil Recovery*. Prentice Hall, New Jersey, 1989.

[72] S. Lang. *Parallele numerische Simulation instationärer Probleme mit adaptiven Methoden auf unstrukturierten Gittern*. PhD thesis, Institut für Wasserbau, Universität Stuttgart, Stuttgart, Germany, 2001.

[73] P. S. Laplace. *Traité de Mécanique Céleste; Supplement au Dixième Livre, Sur l'Action Capillaire*. Courcier, Paris, 1806.

[74] M. C. Leverett. Capillary behaviour in porous solids. *Transaction of the AIME*, 142:152 – 169, 1941.

[75] J. Lewandowska, A. Szymkiewicz, K. Burzyski, and M. Vauclin. Modeling of unsaturated water flow in double-porosity soils by the homogenization approach. *Advances in Water Resources*, 27(3):283 – 296, 2004.

[76] J. Lewandowska, A. Szymkiewicz, W. Gorczewska, and M. Vauclin. Infiltration in a double-porosity medium: Experiments and comparison with a theoretical model. *Water Resources Research*, 41:W02022, 2005.

[77] S. Manthey, S.M. Hassanizadeh, and R. Helmig. Macro-scale dynamic effects in homogeneous and heterogenous porous media. *Transport in Porous Media*, 58:121 – 145, 2005.

[78] S. Manthey, S.M. Hassanizadeh, O. Oung, and R. Helmig. Dynamic capillary pressure effects in two-phase flow through heterogeneous porous media. In Cass T. Miller, M. W. Farthing, W. G. Gray, and G. F. Pinder, editors, *Proceedings of the XV International Conference on 'Computational Methods in Water Resources'*, volume I, pages 631 – 644, Chapel Hill, North Carolina, USA, June 13 – 17, 2004. Elsevier.

[79] J. Middendorf. *Zur Beschreibung des kapillaren Flüssigkeitstransportes in Papier*. PhD thesis, Fakultät für Maschinenbau und Verfahrenstechnik, Technische Universität Chemnitz, 2000.

[80] E. E. Miller and R. D. Miller. Physical theory for capillary flow phenomena. *Journal of Applied Physics*, 27(4):324 – 332, 1956.

[81] R. S. Mokady and P. F. Low. The tension-moisture content relationship under static and dynamic conditions. *Soil Sci. Amer. Proc.*, 28:583 – 584, 1964.

[82] Y. Mualem. A new model for predicting the hydraulic conductivity of unsaturated porous media. *Water Resources Research*, 12(3):513 – 522, 1976.

[83] C. G. Ngan and E. B. Dussan. On the nature of the dynamic contact angle: an experimental study. *Journal of Fluid Mechancis*, 118:27 – 40, 1982.

[84] J. L. Nieber, R. Z. Dautov, and A. G. Egorov. Dynamic capillary pressure mechanism for instability in gravity-driven flows: Review and extension to very dry conditions. In D. B. Das and S. M. Hassanizadeh, editors, *Upscaling Multiphase Flow in Porous Media*, pages 147 – 172. Springer, 2005.

[85] G. Nützmann, H. Moser, and H. Handke. Inverse parameter identification of soil hydraulic properties – results of a new soil column experiment. In A. Peters, G. Wittum, B. Herrling, U. Meissner, C. A. Brebbia, W. G. Gray, and G. F. Pinder, editors, *Proceedings of Computational Methods in Water Resources X*

held in Heidelberg, volume I, pages 785 – 792, Dordrecht, NL, July 1994. Kluwer Academic Publishers.

[86] D. M. O'Carroll, T. J. Phelan, and L. M. Abriola. Exploring dynamic effects in capillary pressure in multistep outflow experiments. *Water Resources Research*, 41, 2005.

[87] A. Ostermann. Sensitivity analysis. In W. Fellin, H. Lessmann, M. Oberguggenberger, and R. Vieider, editors, *Uncertainty in Civil Engineering*, pages 100 – 114. Springer, 2005.

[88] O. Oung and A. Bezuijen. Selective pore pressure transducers for use in model tests to study two-phase flow in porous media. *Int. J. Physical Modelling in Geotechnics*, 4:31 – 42, 2003.

[89] O. Oung, S. M. Hassanizadeh, and A. Bezuijen. Two-phase flow experiments in a geocentrifuge and the significance of dynamic capillary pressure effect. *Journal of Porous Media*, 8(3):247 – 257, 2005.

[90] A. Papafotiou. Interpretation of simulation results including a dynamic capillary pressure relationship. Master's thesis, Institut für Wasserbau, Universität Stuttgart, Stuttgart, Germany, 2004.

[91] J. R. Philip. Horizontal redistribution with capillary hysteresis. *Water Resources Research*, 27(7):1459 – 1469, 1991.

[92] G. E. Pickup and K. D. Stephen. An assessment of steady-state scale-up for small-scale geological models. *Petroleum Geoscience*, 6:203 – 210, 2000.

[93] R. Plagge, P. Häupl, and M. Renger. Transient effects on the hydraulic properties of porous media. In M. Th. van Genuchten, F. J. Leija, and L. Wu, editors, *Proc. Int. Workshop on Characterization and Measurement of the Hydraulic Properties of Unsaturated Porous Media, October 22 – 24, 1997*, volume 2, pages 905 – 912, Riverside, CA, U.S.A., 1999.

[94] A. Poulovassilis. The uniqueness of the moisture characteristics. *Journal of Soil Science*, 25(1):27 – 33, 1974.

[95] L. A. Richards. Capillary conduction of liquids through porous medium. *Physics*, pages 318 – 333, 1931.

[96] A. E. Scheidegger. *The Physics of Flow Through Porous Media*. University of Toronto Press, Toronto and Buffalo, 3rd edition edition, 1974.

[97] M. Schroth, J. D. Istok, S. J. Ahearn, and J. S. Selker. Geometry and position of light nonaqueous-phase liquid lenses in water-wetted porous-media. *Journal of Contaminant Hydrology*, 19:269 – 287, 1995.

[98] H. Schubert. *Kapillarität in porösen Feststoffsystemen*. Springer Verlag, 1982.

[99] B. Schultze and W. Durner. Bestimmung der hydraulischen eigenschaften von bodenproben durch inverser simulation instationärer fließexperimente: Dynamische effekte. *Mitteilungen der Deutschen Bodenkundlichen Gesellschaft*, 85/I:163 – 166, 1997.

[100] B. Schultze, O. Ippisch, B. Huwe, and W. Durner. Dynamic nonequilibrium during unsaturated water flow. In F. J. Leija M. Th. van Genuchten and L. Wu, editors, *Proc. Int. Workshop on Characterization and Measurement of the Hydraulic Properties of Unsaturated Porous Media*, volume 2, pages 877 – 892, Riverside, CA, U.S.A., October 22 – 24, 1997. University of California.

[101] D. Schulze-Makuch. Longitudinal dispersivity data and implications for scaling behavior. *Groundwater*, 43(3):443 – 456, 2005. 10.1111/j.1745-6584.2005.0051.x.

[102] Y. D. Shikhmurzaev. Dynamic contact angles in gas/liquid/solid systems and flow in vicinity of moving contact line. *AIChE Journal*, 42:601 – 612, 1997.

[103] Y. D. Shikhmurzaev. Spreading of drops on solid surfaces in a quasi-static regime. *Physics of Fluids*, 9(2):266 – 275, 1997.

[104] D. Silin and T. Patzek. On the Barenblatt model of spontaneous countercurrent imbibition. *Transport in Porous Media*, 54:297 – 322, 2004.

[105] J. Simùnek, O. Wendroth, N. Wypler, and M. Th. van Genuchten. Non-equilibrium water flow characterized by means of upward infiltration experiments. *European Journal of Soil Science*, 52:13 – 24, 2001.

[106] D. E. Smiles, G. Vachaud, and M. Vauclin. A test of the uniqueness of the soil moisture characteristic during transient, nonhysteretic flow of water in a rigid soil. *Soil Sci. Soc. Amer. Proc.*, 35:534 – 539, 1971.

[107] F. Stauffer. *Einfluss der kapillaren Zone auf instationäre Drainagevorgänge*. PhD thesis, Eidgenössische Technische Hochschule Zürich, Zürich, Switzerland, 1977.

[108] F. Stauffer. Time dependence of the relations between capillary pressure, water content and conductivity during drainage of porous media. In *On scale effects in porous media*, Thessaloniki, Greece, 1978. IAHR.

[109] G. C. Topp, A. Klute, and D. B. Peters. Comparison of water content-pressure head data obtained by equilibrium, steady-state, and unsteady-state methods. *Soil Science Society of America, Proceedings*, 31:312 – 314, 1967.

[110] C. D. Tsakiroglou, M. A. Theodoropoulou, and V. Karoutsos. Nonequilibrium capillary pressure and relative permeability curves of porous media. *AIChE Journal*, 49(10):2472 – 2486, 2003.

[111] N. Ursino and T. Gimmi. Combined effect of heterogeneity, anisotropy and saturation on steady state flow and transport: Structure recognition and numerical simulation. *Water Resources Research*, 40:W01514, 2004.

[112] G. Vachaud, M. Vauclin, D. Khanji, and M. Wakil. Effects of air pressure on water flow in an unsaturated stratified vertical column of sand. *Water Resources Research*, 9(1):160 – 173, 1973.

[113] G. Vachaud, M. Vauclin, and M. Wakil. A study of the uniqueness of the soil moisture characteristic during desorption by vertical drainage. *Soil Science Society of America, Proceedings*, 36:531 – 532, 1972.

[114] M. T. Van Genuchten. A closed-form equation for predicting the hydraulic conductivity of unsaturated soils. *Soil Sci. Soc. Am. J.*, 44:892 – 898, 1980.

[115] M. T. Van Genuchten, M. G. Schaap, B. P. Mohanty, J. Simunek, and F. J. Leij. Modeling flow and transport processes at the local scale. In J. Feyen and K. Wiyo, editors, *Modelling of transport processes in soils*, pages 23 – 45, Leuven, Belgium, 1999.

[116] H.-J. Vogel, P. Bastian, and K. Roth. Downscaling hydraulischer eigenschaften zur schätzung von transportparametern. *Mitteilungen der Deutschen Bodenkundlichen Gesellschaft*, pages 278 – 281, 1999.

[117] H.-J. Vogel, J. Tölke, V. P. Schulz, M. Krafczyk, and K. Roth. Comparison of a lattice-boltzmann model, a full-morphology model, and a pore network model for determining capillary pressure-saturation relationships. *Vadoze Zone Journal*, 4:380 – 388, 2005.

[118] C. Wana-Etyem. *Static and dynamic water content-pressure head relations of porous media*. Phd-thesis, Civil Engineering Department, Colorado State University, Fort Collins, Colorado, U.S.A., 1982.

[119] E. Washburn. The dynamics of capillary flow. *Physcal Review*, 17:273 – 283, 1921.

[120] K. K. Watson. Non-continuous porous media flow. Technical Report 84, Water Research Laboratory, The University of New South Wales, Manly Vale, Australia, 1965.

[121] K. K. Watson. Water content-pressure head relationship. *Soil Science Society of America, Proceedings*, 32:892, 1968.

[122] K. K. Watson and F. D. Whisler. System dependence of the water content-pressure head relationship. *Soil Science Society of America, Proceedings*, 32:121 – 123, 1968.

[123] K. K. Watson and F. D. Whisler. The use of dynamic soil water characteristics in a numerical model. *Soil Science*, 125:83 – 91, 1978.

[124] M. M. Weislogel. Steady spontaneous capillary flow in partially coated tubes. *AIChE Journal*, 43(3):645 – 654, 1997.

[125] D. A. Weitz, J. P. Stokes, R. C. Ball, and A. P. Kushnick. Dynamic capillary pressure in porous media: Origin of the viscous-fingering length scale. *Physical Review Letters*, 59(26):2967, 1987.

[126] S. Whitaker. The transport equations for multi-phase systems. *Chemical Engineering Science*, 28:139 – 147, 1973.

[127] S. Whitaker. Flow in porous media I: A theoretical derivation of Darcy's law. *Transport in Porous Media*, 1:3 – 25, 1986.

[128] S. Whitaker. Flow in porous media II: The governing equations for immiscible two-phase flow. *Transport in Porous Media*, 1:105 – 125, 1986.

[129] D. Wildenschild, J. W. Hopmanns, and J. Simunek. Flow rate dependence of soil hydraulic characteristics. *Soil Science Society of America, Journal*, 65:35 – 48, 2001.

[130] T. Young. An essay on the cohesion of fluids. *Philosophilcal Trans. Royal Society of London*, 95:65 – 87, 1805.

[131] M.-Y. Zhou and P. Sheng. Dynamics of immiscible fluid displacement in a capillary tube. *Physical Review Letters*, 64(8):882 – 885, 1990.

[132] E. Zimmermann. *Ein Beitrag zur Bestimmung des statischen und dynamischen Randwinkels*. PhD thesis, Universität-GH-Essen, Germany, 1986.

A Two-phase flow processes in a multi-step outflow experiment

In the framework of the project MUSKAT ('Multi-Skalen Transport', funded by the German Research Foundation, DFG, project number He-2531/2-2) two-phase flow processes were examined by the three project partners from the Universität Heidelberg (sub-project 'A'), the Technische Universität München (and later the Technische Universität Braunschweig, sub-project 'B') and the Universität Stuttgart. In the following, some of the investigations performed in Stuttgart are presented. Parts of them can be found in the appendix to the project report.
Within the sub-project 'C' the following aspects were examined.

- A multi-step outflow laboratory experiment with a soil column performed by sub-project 'A' before the start of the MUSKAT project was simulated and analysed. The simulations repeat the ones performed by VOGEL ET AL., 1999 [116].
- A parameter variation served to analyse the influence of the different parameters on the drainage flow behaviour.
- Furthermore, the influence of heterogeneities on the local scale on the two-phase flow processes during multi-step outflow experiments were assessed.
- Finally, the model concepts underlying the simulations were examined.

In the following, the results of these steps will be presented.

Analysis of a multi-step outflow experiment

A multi-step outflow experiment with a natural soil performed by the group in Heidelberg served as a pre-investigation subject before sub-project 'A' carried out experiments with artificial columns performed within the MUSKAT project (see GRAF, 2004 [47]). First the experiment with the natural soil is simulated applying the two-phase module of MUFTE-UG (see Sec. 4). As primary variables the pressures of the wetting and non-wetting phase are chosen. The P_w-P_n formulation necessitates a $P_c(S_w)$ relationship that can be inverted (compare HELMIG, 1997 [59]), as e.g. the VAN GENUCHTEN parametrisation. The parameters of the two fluids represent the ones of water and gas (air, see Tab. 2.1). Repeating the simulations of VOGEL ET AL., 1999 [116] the soil column is first assumed to be homogeneous applying effective parameters determined by VOGEL ET AL., 1999 (see Tab. A.1) and then, in a second

approach, structural information about the soil column gained by computer tomography (also performed in Heidelberg, see VOGEL ET AL., 1999 [116]) is included as information. From the 3D computer tomography scan a distribution of grey levels was obtained, where 256 levels are distinguished (for a distribution of the grey values please consult Fig. A.1). On the basis of independent measurements of the porosity as well as the density of the soil matrix and water, one grey level can be correlated to a density and thus a porosity. For the simulations, it is furthermore assumed that the soil parameters are correlated, for example a small porosity would correspond to a small intrinsic permeability.

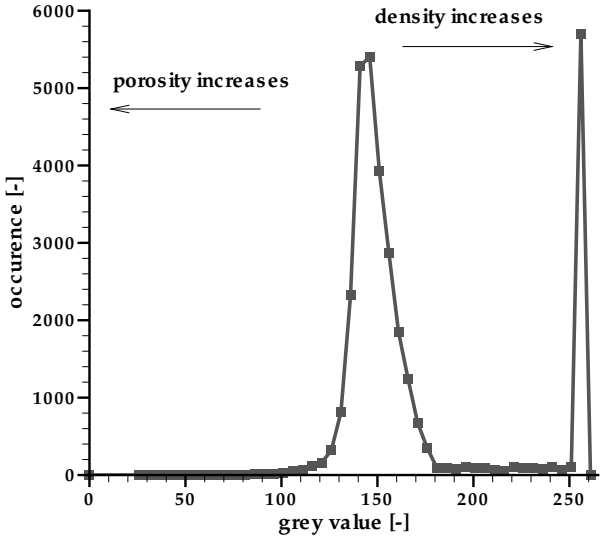

Figure A.1: Occurrence of the grey values from a scan of the soil column for classes of five levels each (0-21, 26, 31,..). The peak at the highest class is caused by the tensiometer installed in the column.

Table A.1: Effective soil parameters for the natural soil column (height 0.1 m, radius 0.08 m), determined with inverse parameter identification applying the RICHARDS' equation by VOGEL ET AL., 1999 [116]

Parameter	K [m^2]	ϕ [-]	VG α [1/Pa]	VG n [-]	S_{wr} [-]	S_{nr} [-]
	$2.63 \cdot 10^{-12}$	0.5027	$4.5 \cdot 10^{-4}$	1.7386	0.497	0.0

The initial and boundary conditions mimic the ones applied in the laboratory experiment (see Tab. A.2). The domain is initially fully water-saturated, thus at the beginning a hydrostatic pressure distribution is assumed. At the lower boundary

the pressure (corresponding to the potential in the laboratory experiments) is lowered in steps over defined time intervals. At the upper boundary gas can infiltrate into the column. The gas pressure is assumed to remain at atmospheric pressure at the upper boundary during the whole experiment.

Table A.2: Boundary conditions for the simulation of a multi-step outflow experiment (NEU = Neumann, DIR = Dirichlet)

Variable	upper boundary		sides		lower boundary	
P_w	NEU	$q_w = 0.0$	NEU	$q_w = 0.0$	DIR	$P_w = P_w(t)$
P_n	DIR	$P_n = P_{atm}$	NEU	$q_n = 0.0$	NEU	$q_n = 0.0$

The cumulative outflow of water related to the radius of the soil column h_c [L] for the homogeneous case („homogeneous, VG“ in Fig. A.2, left) applying the parametrisation of VAN GENUCHTEN /MUALEM (see Secs. 2.2.1 and 2.2.2) is compared to the cumulative outflow gained from a simulation including the structural information about the soil column from the computer tomography („heterogeneous“ in Fig. A.2, left). VOGEL ET. AL., 1999 [116] weighted the effective parameters on the porosity distribution such that their arithmetic average represented the effective parameters. In order to obtain a quantitative measure for the quality of the simulations, the residuals r, quantifying the difference between the measurement and the simulation at a given measurement time, are calculated (see Fig. A.2, right). High values of the residual at the beginning of the steps might be attributed to a slight time lag in the pressure reduction from experiment to simulation. Nevertheless, the plot of the residuals reveals that

- the residuals both for the homogeneous as well as the heterogeneous case diminish with decreasing water saturation in the column (global trend),
- for each pressure step the residuals show local trends from high to low (heterogeneous) or low to high (homogeneous) values, and that
- the inclusion of the heterogeneity could not enhance the agreement between simulation and measurement.

Moreover, neither the homogeneous nor the heterogeneous case reproduce the characteristics of the second to fifth step, where in the laboratory experiment initially a high outflow occurs as a direct response to the pressure decrease, followed by a slow approach to equilibrium. This behaviour was also observed in other laboratory experiments with an artificial porous medium. It will in the following be denoted relaxation effect in the outflow curve.
The local (and global) trend in the residuals (as opposed to a random distribution of the errors) can have the following causes.

- The higher volume of outflow in the first pressure step in the simulations opposed to the measurement may be attributed to differing initial conditions. In

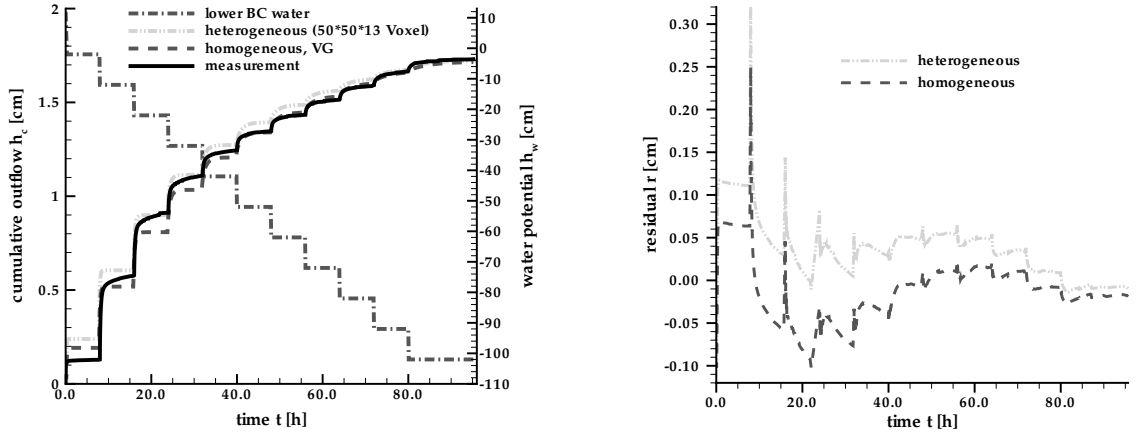

Figure A.2: Cumulative outflow of water from laboratory experiment („measurement“) and simulations (left) as repeated from VOGEL ET AL., 1999 [116] and difference (residual r) between measurement and simulations (right)

the simulation a fully water-saturated column is assumed. The same initial condition is aimed at in the laboratory experiments. However, it is very difficult to achieve in natural soil columns.

- The parameters might need to be verified in additional measurements, maybe independent measurements of for example the $P_c(S_w)$ relationship are desirable. Also, additional measurements during the multi-step outflow experiment such as saturation measurements might improve the parameters gained by inverse parameter identification. It was not possible to undertake any of these steps for the soil column investigated here, as it had been destroyed in the meantime. Within the MUSKAT project, the parameters porosity and permeability were determined independently and the constitutive relationships were computed on the basis of direct simulations on the pore scale (see VOGEL ET AL., 2005 [117]).

- With the applied parametrisation of the $P_c(S_w)$ relationship after VAN GENUCHTEN, 1980 [114], and (based on the VAN GENUCHTEN $P_c(S_w)$ relation) of the $k_{r\alpha}(S_\alpha)$ relationships after MUALEM, 1976 [82] the observed outflow behaviour cannot be reproduced exactly. As especially the flow behaviour cannot be represented the relative permeabilities might need to be handled differently. Approaches exist for example by DURNER ET AL., 1997 [36, 37] or SCHULTZE ET AL., 1997, 1999 [99, 100], who allow for different $k_{r\alpha}(S_\alpha)$ relationships for each pressure step and thus for different effective saturations. In the framework of the MUSKAT project, the constitutive relationships were determined independently on the pore scale (compare VOGEL ET AL., 2005 [117]), thus additional parameter identifications using alternative parametrisations of the

constitutive relationships did not encompass the aims of the project.

- The physical-mathematical model underlying the numerical model (see Secs. 2 and 4) is based on the conservation of mass of the two fluid phases, applying the extended DARCY's law for the approximation of the velocity. Perhaps the outflow behaviour cannot be represented with this model. One explanation might be that its inherent assumptions are not valid for the simulated experiment.

Although inverse parameter estimation did not belong to the aims of the MUSKAT project a sensitivity analysis is carried out in order to assess whether a variation of one of the parameters entering into the discretised balance equation could effect the observed outflow behaviour if only quantitatively. The parametrisations itself are not questioned. Although the inclusion of heterogeneity did not result in a better agreement between simulation and measurement the influence of heterogeneity on the outflow behaviour is investigated applying spatially correlated random fields. The last item of the list is examined in the last section of this appendix.

Parameter variation

In contrast to the MUSKAT project report, where parameters of an artificial porous medium were applied in the parameter variation, the sensitivity of the cumulative outflow is here examined on the basis of the multi-step outflow experiment described above. The primary aim of this analysis was to identify one or more parameters to which the (simulated) cumulative outflow shows a sensitivity when in the laboratory measurement the relaxation behaviour can be observed (see especially second to fourth pressure step in Fig. A.3). The sensitivity of the parameter should be high in this range of the experiment and low especially towards the end of the experiment as there the measurement is reproduced with an acceptable accuracy.
As solely a primary drainage process is considered, the residual (or entrapped) nonwetting phase saturation S_{nr} is assumed to equal zero in all cases. All parameters are varied by plus one percent of their reference value. The reference values are listed in Tab. A.1. This parameter set for the reference simulation was gained with an inverse approach on the basis of the RICHARDS equation. For the RICHARDS equation an infinite mobility of the gas phase is assumed and thus a $k_{\mathrm{rn}}(S_{\mathrm{n}})$ relationship is not accounted for. Moreover, the VG-n and the residual saturation S_{wr} were not treated independently in the $P_{\mathrm{c}}(S_{\mathrm{w}})$ and the $k_{\mathrm{rw}}(S_{\mathrm{w}})$ relationship. For the reference simulation it is assumed, that both parameters can furthermore be transfered to the $k_{\mathrm{rn}}(S_{\mathrm{n}})$ relationship. The parameters in the constitutive relationships that enter more than one relation, for example the residual water saturation, are varied independently for this sensitivity analysis.
The cumulative outflow does not show pronounced differences for the range of variation in the parameters (see Fig. A.4). The sensitivity of the outflow w.r.t. the parameters can nevertheless be determined applying Eqn. 6.4. Possible correlations

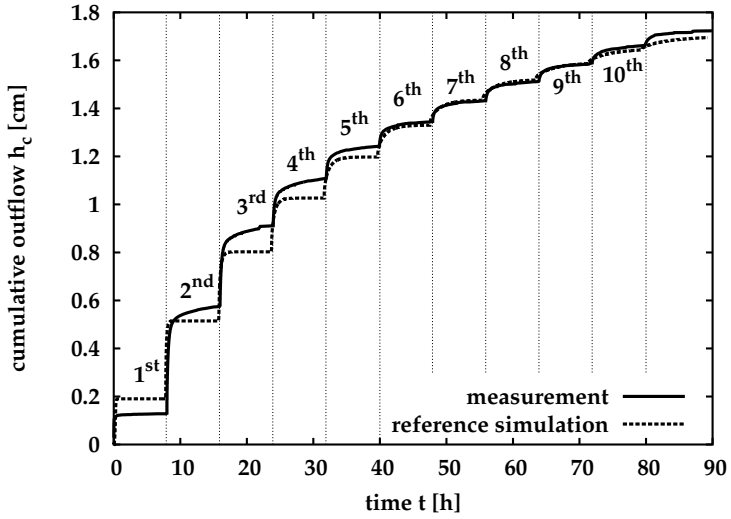

Figure A.3: Cumulative outflow, measured and simulated, including enumeration of steps

between the parameters are not examined here as the parameter sensitivity is not applied to enhance an inverse parameter estimation procedure.
In order to facilitate a comparison of the magnitude of the sensitivities for the various parameters, the logarithm of the intrinsic permeability and the VG-α enter Eqn. 6.4. In the following, the sensitivities of the cumulative outflow w.r.t. the parameters applied in the physical-mathematical model are described.
First, the influence of the structural parameters, the intrinsic permeability and the porosity are considered (see Fig. A.5). The sensitivity of the cumulative outflow w.r.t. the intrinsic permeability is expected to be positive. As the parameter is increased, the flow velocities should be larger inducing thus a larger cumulative outflow. The sensitivity of the cumulative outflow w.r.t. the intrinsic permeability is high at the onset of a pressure step. The sensitivity then decreases. During the first part of the numerical experiment the sensitivity diminishes rapidly to zero, but towards the end decreases slower and does not reach zero, indicating that static conditions are not attained. As here the focus is on the parts of the experiment where the sensitivity w.r.t. to the parameter decreases to zero the intrinsic permeability is not considered an appropriate quantity to be altered in order to mimic the behaviour observed in the laboratory.
The sensitivity of the cumulative outflow w.r.t. the porosity shows a different behaviour. First the general trend, the increase of the sensitivity is remarkable. The porosity occurs in the accumulation terms of the conservation equations. As the porous medium is assumed to be rigid, the porosity can be extricated from the partial time derivative and thus acts as a coefficient in the accumulation term. A variation of the porosity thus does not influence the flow behaviour but mainly the magnitude of the cumulative outflow for a given pressure step. If the porosity is increased also the cumulative outflow is increased. The sensitivity increases towards

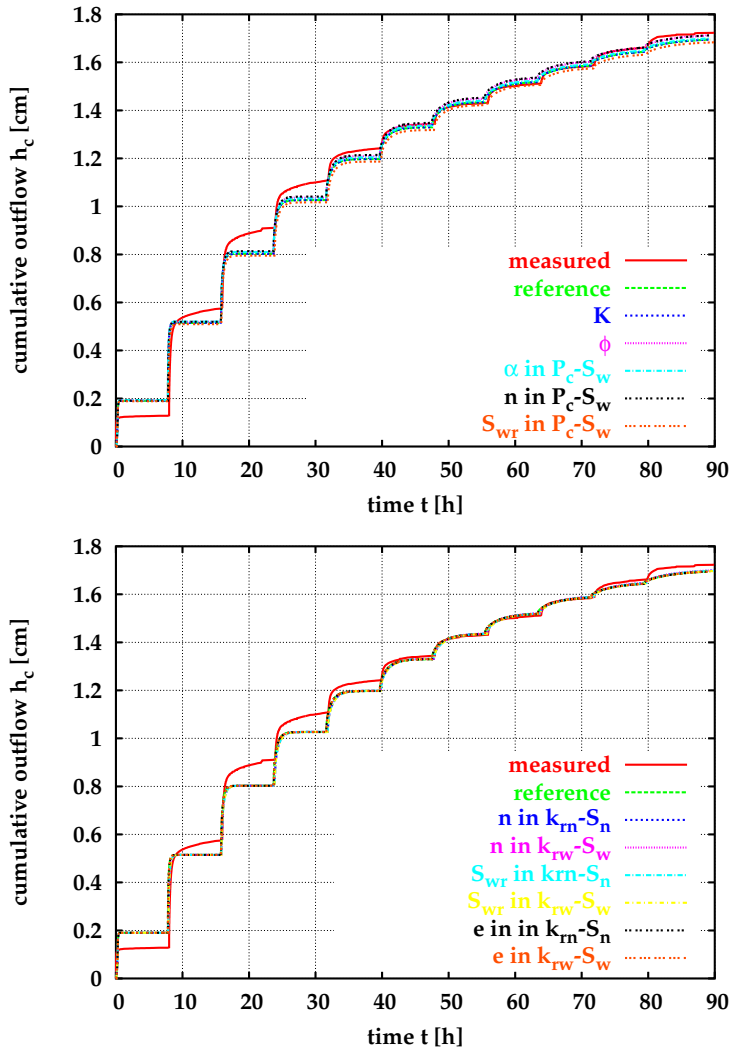

Figure A.4: Cumulative outflow h_c for the parameter variation on the basis of the multi-step outflow experiment with the soil column

the end of the experiment as the saturation of the wetting phase and thus the outflow decreases. The relative influence of the porosity variation is thus higher. Also the sensitivity cumulates with increasing time. Similar to the intrinsic permeability the porosity does not induce the desired sensitivity pattern.
Now, the sensitivity of the outflow w.r.t. the parameters VG-α and VG-n in the $P_c(S_w)$ relationship will be examined. The parameter α in the $P_c(S_w)$ relationship determines the capillary pressure at $S_e = 0.5$, thus an increase of α results in a lower capillary pressure for water saturations between $S_{wr} < S_w < 1.0$ (see Fig. A.6, left). Consequently, the magnitude of outflow for a given pressure step is increased compared to the reference case and the sensitivity of the outflow is positive (see Fig. A.7, left). The cumulative outflow has a maximum in sensitivity w.r.t. α at the mid-

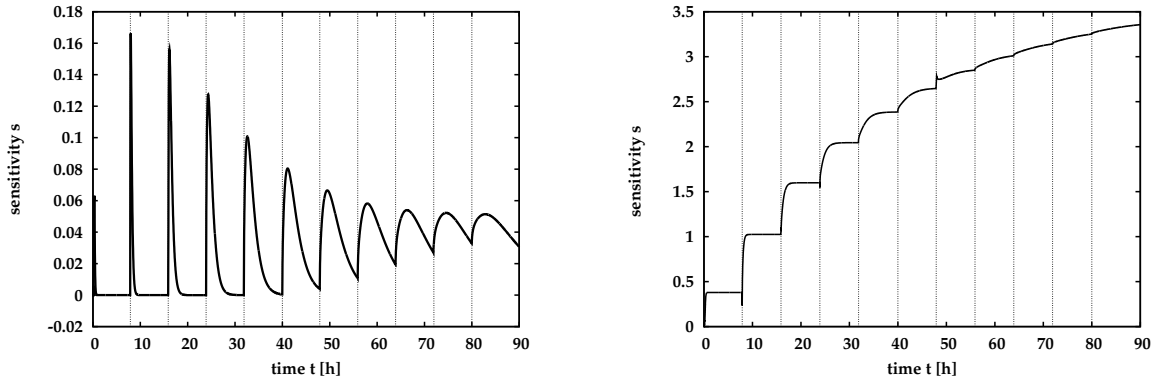

Figure A.5: Sensitivity of the cumulative outflow w.r.t. the intrinsic permeability K (left) and the porosity ϕ (right)

dle part of the numerical experiment. The largest difference between the reference $P_c(S_w)$ and the varied $P_c(S_w)$ relationship occurs at medium saturations. Thus, in the domain the highest difference between the reference and the varied case can be noticed also at medium saturations. Towards the end of the experiment, the saturations in the domain approach the residual water saturation. As the residual saturation S_{wr} is not altered by the variation of α the sensitivity of the outflow w.r.t. α decreases. Apart from the global trend, a trend for each step can be noticed. From on the third pressure step, the sensitivity of the cumulative outflow w.r.t. α decreases first and then increases again. The direct response to the outflow is mainly influenced by the mobility and the intrinsic permeability, but not by the more quantitative measures of the $P_c(S_w)$ relationship.

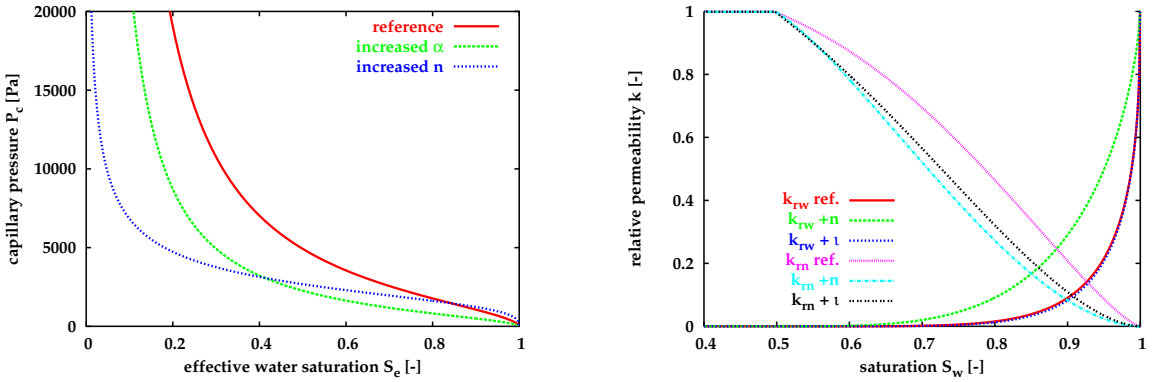

Figure A.6: $P_c(S_w)$ (left) and $k_{r\alpha}(S_\alpha)$ (right) relationships illustrating the influence of the parameter variation with VG-α = 0.001, VG-n = 3.0, and ι = 0.9

A similar behaviour can be noted in the sensitivity of the cumulative outflow w.r.t. the VG-n varied only in the $P_c(S_w)$ relationship (see Fig. A.7, left). As a global trend an increase with increasing time can be detected. The VG-n determines the

slope of the $P_c(S_w)$ relationship. If n is augmented, then the $P_c(S_w)$ relationship gets a flatter slope for saturations of $S_{wr} < S_w < 1.0$ (see Fig. A.6, left). At the first pressure step thus a negative sensitivity of the cumulative outflow can be observed. The capillary pressure at high water saturations is larger in the varied compared to the reference case, thus less outflow occurs in the varied case. The influence of the n variation on the outflow is especially high at the second and third step, where high to medium water saturations occur in the domain. The capillary pressure of a given water saturation gained from the $P_c(S_w)$ relationship is then smaller in the variation case compared to the reference $P_c(S_w)$ relationship. Consequently, for a given applied capillary pressure, induced through the pressure decrease of the water phase at the lower boundary, more water exfiltrates the domain compared to the reference case. The magnitude of the sensitivity remains approx. constant towards the end of the experiment, indicating a quantitative difference from the different $P_c(S_w)$ relationships but not a large influence on the flow behaviour.
The sensitivity of the cumulative outflow w.r.t. the VG-n varied in the $P_c(S_w)$ relationship also shows local trends within each of the pressure steps. For the first three steps the sensitivity increases up to a given value and then remains constant, indicating that this parameter has mainly a quantitative influence on the cumulative outflow behaviour. From on the fourth step, the sensitivity first decreases as the direct response to the pressure step occurs and then increases again, as quantitative aspects gain in importance. However, at the interesting parts the sensitivity remains constant, implying only a quantitative difference to the reference case but not a qualitative one.

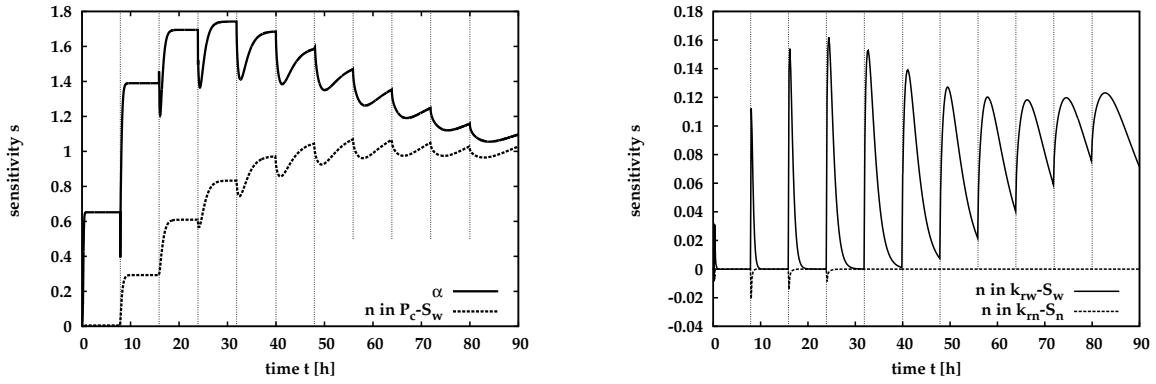

Figure A.7: Sensitivity of the cumulative outflow w.r.t. VG-α as well as VG-n in the $P_c(S_w)$ relationship (left) and VG-n in the $k_{r\alpha}(S_\alpha)$ relationships (right)

Variations of the VG-n in one of the $k_{r\alpha}(S_\alpha)$ relationships (see Fig. A.6, right) influence the mobility of the respective phase. Thus mainly an effect on the flow behaviour but not on the attained magnitude of the outflow after one step is noticeable (presuming equilibrium can be reached, see Fig. A.7, right). The increase of this parameter in the $k_{rn}(S_n)$ relationship results in a smaller relative permeability of the non-wetting phase at $S_{nr} < S_n < (1.0 - S_{wr})$. Consequently an influence on the

outflow behaviour is to be expected at high non-wetting phase saturations. As k_{rn} is decreased at a given S_n that is smaller than $(1.0 - S_{wr})$ compared to the reference $k_{rn}(S_n)$ relationship, the direct response to the early pressure steps is retarded, as the inflow of gas occurs slower (the sensitivity is thus negative). In general it might be stated, that the influence of the parameter n in the $k_{rn}(S_n)$ is small compared to the one in the $k_{rw}(S_w)$ relationship. This may be attributed to the fact that the mobility is the ratio of relative permeability to viscosity. The viscosity of the non-wetting phase, here air, is sixty times smaller than that of the wetting phase. Consequently, the influence of the relative permeability on the mobility is small compared to the influence of the n variation in the $k_{rw}(S_w)$ relationship.

If n is increased in the $k_{rw}(S_w)$ relationship, the relative permeability of the water phase at a given saturation $S_{wr} < S_w < 1.0$ is larger compared to the reference case (see Fig. A.6, right). The variation in n here mainly influences the direct response to the pressure decrease, but diminishes after that. As the relative permeability is larger, the outflow occurs faster. At least for the first steps the saturation distribution in the domain is the same. During the first five pressure steps the sensitivity diminishes to zero at the end of the steps. Only in the later steps, when equilibrium between applied pressure and saturation distribution is not attained and the relative permeability of the wetting phase has decreased distinctly, the sensitivity of the outflow w.r.t. n in the $k_{rw}(S_w)$ relationship remains larger than zero. As the the sensitivity decreases to zero at the steps of interest, the variation of n in the $k_{rw}(S_w)$ relationship is not considered an appropriate choice to improve the agreement between simulation and measurement.

Moreover, the residual wetting phase saturation S_{wr} was varied in the constitutive relationships. The influence on the outflow from the variation of S_{wr} in the $k_{rn}(S_n)$ relationship is distinctly exceeded by the sensitivity of the outflow w.r.t. to the S_{wr} variation in the $k_{rw}(S_w)$ relationship (see Fig. A.8, left). Obviously, the influence becomes more pronounced with increasing time and thus decreasing water saturations in the domain. At the beginning of the numerical experiment the outflow behaviour is affected, because with augmenting S_{wr} the relative permeability of the water phase at high water saturations is decreased compared to the reference case. Thus, the sensitivity is negative. Apart from the global trend a local trend shows an increase of sensitivity for the direct response to a new pressure decrease at the lower boundary followed by a decrease in the sensitivity towards the end of the steps. Despite the impact on the flow behaviour, no influence can be observed in the ranges of interest.

The most pronounced effect on the outflow behaviour originates from the variation of S_{wr} in the $P_c(S_w)$ relationship (see Fig. A.8, left). This variable has produced the sensitivity pattern of a quantity that mainly has an influence on the quantitative behaviour of the outflow. It shows a global trend of increasingly negative sensitivity. Additionally, it shows a local trend of decreasing sensitivity as the direct response to the pressure decrease occurs to then increase again towards the end of the pressure steps.

Finally, the parameter ι (compare Eqns. (2.20) and (2.21)) in the $k_{r\alpha}(S_\alpha)$ relationships

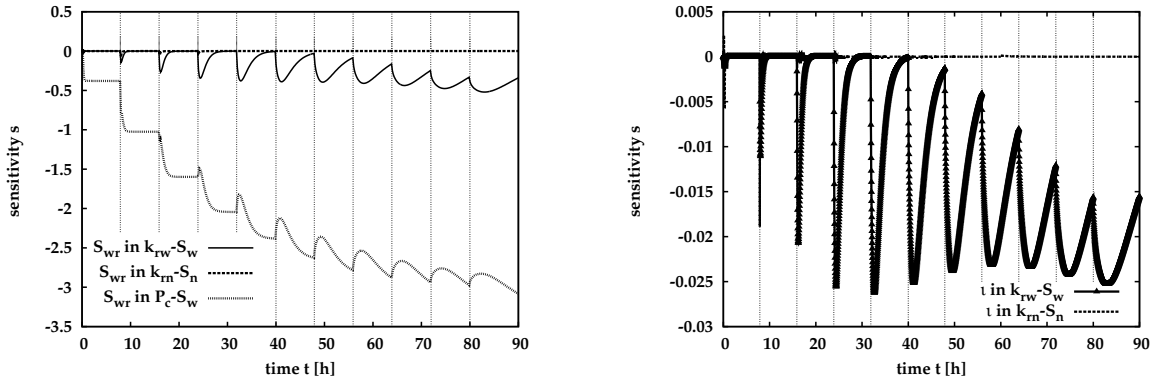

Figure A.8: Sensitivity of the cumulative outflow w.r.t. S_{wr} (left) and the exponent ι in the $k_{\mathrm{r}\alpha}(S_\alpha)$ relationships (right)

is altered. As a default value, $\iota = 0.5$ is set, because it proved to be appropriate for a large number of soils. Nevertheless, an exponent unequal to 0.5 is possible, thus also this parameter is varied by plus one percent. The influence on the respective $k_{\mathrm{r}\alpha}(S_\alpha)$ relationship is depicted in Fig. A.6, right, where ι is $\iota = 0.9$ for illustration purposes. Even for this high variation hardly any influence can be observed on the $k_{\mathrm{rw}}(S_{\mathrm{w}})$ relationship, though $k_{\mathrm{rw}}(S_{\mathrm{w}})$ is decreased for a given saturation larger than S_{wr}. The influence on the $k_{\mathrm{rn}}(S_{\mathrm{n}})$ relationship is more pronounced. There, at a given saturation of the non-wetting phase larger than $(1.0 - S_{\mathrm{wr}})$ the relative permeability of the phase is decreased compared to the reference case.
As the mobilities of the phases are altered, the sensitivities are large at the responses to the pressure decreases and diminish thereafter within one pressure step. This holds true for both phases, although on different orders of magnitude. The sensitivity of the cumulative outflow w.r.t. the exponent ι in the $k_{\mathrm{rw}}(S_{\mathrm{w}})$ relationship is by several orders of magnitude larger than the one w.r.t. the variation in $k_{\mathrm{rn}}(S_{\mathrm{n}})$. A sensitivity w.r.t. the ranges of the experiment of interest here is not observable.
In summary, the following aspects deserve attention:

- As the cumulative outflow shows a distinct sensitivity w.r.t. many of the parameters towards the end of the experiment, this part of the experiment is reproduced best (compare Fig. A.2).

- The parameters in the balance equations may be classified into quantitative and qualitative parameters w.r.t. a multi-step outflow simulation. While the qualitative parameters influence the flow behaviour and thus show a distinct influence on the outflow at the direct response to a pressure decrease, the quantitative parameters determine the quasi-static distribution of the fluids at the end of a pressure step. Towards the end of the experiment, when the mobility of the water phase is small and a quasi-static distribution is not attained at the end of a step, the qualitative parameters gain importance also for the later parts of each pressure step. The intrinsic permeability, and the param-

eters entering into the $k_{r\alpha}(S_\alpha)$ relationships are here classified as qualitative parameters. The porosity as well as the parameters of the $P_c(S_w)$ relationship are classified as quantitative parameters.

- For the reproduction of the outflow behaviour observed in step 2 to 4 in the measurement an alteration of a qualitative parameter seems to be necessary. If however, one of those is altered, also the direct response to the pressure decrease is influenced. If, for example, the permeability is decreased noticeably, the outflow is flatter also at the beginning of pressure step 2 to 4, which is not desirable.

Consequently, it has not been possible to clearly identify a parameter which might effect the observed relaxation process in the simulations.

The influence of local-scale heterogeneity

The grey values from the 3D computer tomography scan of a soil column show a unimodal distribution (the second peak at the largest grey value class is caused by the tensiometer, see Fig. A.1). Although inclusion of the heterogeneous distribution of soil parameters did not enhance the agreement between simulation and measurement, another attempt is made to perhaps identify sub-scale heterogeneity patterns that might induce the observed outflow behaviour.
Local-scale heterogeneity of subsurface systems is often characterised with geostatistical approaches, e.g. variogrammes, which are based on the correlation length, the variance of the distribution and an anisotropy factor.
These geostatistical approaches also allow to generate spatially correlated random fields of e.g. the logarithm of intrinsic permeability which possess the properties of a prescribed variogramme.
The following questions will be tackled on the basis of simulations of multi-step outflow experiments applying spatially correlated random fields with different anisotropy ratios:

- Does a spatial correlation of the intrinsic permeability have an influence on the drainage behaviour?

- If, additionally to the spatially correlated random field of intrinsic permeability, a field of $P_c(S_w)$ relationships is obtained, does this influence the drainage behaviour?

- Is it possible to reproduce with simulations the tailing behaviour of the cumulative outflow observed in laboratory experiments if spatially correlated random fields of permeability (and $P_c(S_w)$ relationships) are applied? Might it thus be an option to apply multi-continua approaches (e.g. double continuum approach in analogy to fracture-matrix systems) in order to reproduce the tailing?

First, three two-dimensional spatially correlated random fields of the logarithm of intrinsic permeability were generated for a domain of 0.1 m by 0.1 m following the approach of DYKAAR & KITANIDIS, 1992 [38]. For the variogramme $\gamma(h)$ an exponentiell model was chosen, namely

$$\gamma(h) = s^2(1 - \exp(-h/a)) \,, \tag{A.1}$$

where h defines the distance between two locations, s^2 the variance and a the correlation length. The correlation length may be defined direction-dependent in horizontal (a_h) and in vertical (a_v) direction. The back-transformation of the $\ln K$, which follow a lognormal distribution necessitates to cut-off very large values because otherwise undesirably high permeability values might evolve. For the back-transformation the following equation was applied

$$K = \frac{\exp(\ln K) \cdot (K_\mathrm{max} - K_\mathrm{min})}{1 + \exp(\ln K)} \,, \tag{A.2}$$

where the maximum intrinsic permeability K_max needs to be chosen, while the minimum can be gained from the distribution or might otherwise be chosen too. For the homogeneous reference case, effective parameters would need to be identified with an appropriate upscaling approach. This was not attempted as the main interest is on the influence on the flow behaviour induced by heterogeneity.
The fields of intrinsic permeability will in the following be denoted 'isotropic' ($a_\mathrm{h} = a_\mathrm{v}$), 'horizontal' ($a_\mathrm{h} > a_\mathrm{v}$) and 'vertical' ($a_\mathrm{h} < a_\mathrm{v}$) (see Fig. A.9). For $a = 0.01$ m, ten correlation lengths occur in one direction. For $a = 0.03$ m only about three correlation lengths can occur in the 0.1 m long and broad domain. Three correlation lengths might not suffice to prevent boundary effects or effects from the interaction to gravity. But as a natural soil should be mimicked where the exact distribution of heterogeneity might be unknown these possible effects are accepted for the moment.

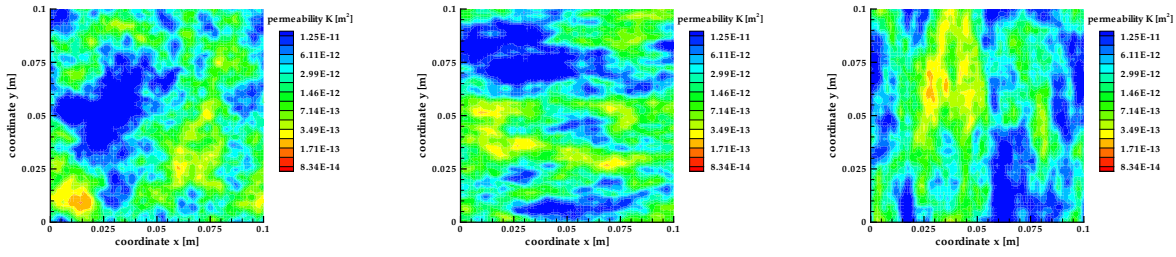

Figure A.9: Spatially correlated random fields of intrinsic permeability: isotropic (left, $a_\mathrm{h} = a_\mathrm{v} = 0.015$ m), horizontal (middle, $a_\mathrm{h} = 0.03$ m, $a_\mathrm{v} = 0.01$ m) and vertical (right, $a_\mathrm{h} = 0.01$ m, $a_\mathrm{v} = 0.03$ m). All were generated with a mean of $\ln K = -26.66$ and a variance of $s^2 = 1.0$

Capillary pressure-saturation relationships can be scaled with the distribution of

$\ln K$ values following the LEVERETT approach [74] after

$$P_c^{scaled} = P_c^{ref} \sqrt{\frac{\ln K}{\ln K^{ref}}}\ , \tag{A.3}$$

where the superscript 'ref' refers to a reference, that is a average quantity. The parameters for the porous medium follow the ones of the natural soil listed in Tab. A.1. The initial and boundary conditions adhere to the ones used in the laboratory experiment (see Tab. A.2 and Fig. A.2, left)
In a first step, only a heterogenous distribution of intrinsic permeability was applied in the simulation mimicking a multi-step outflow experiment. The resulting three outflow curves do not differ and thus not show a discernable influence from the different anisotropies in the correlation lengths (see Fig. A.10, left). Consequently, further random fields with varying distributions of K were not tested as no additional information was expected.
In a second step, heterogeneous distributions of $P_c(S_w)$ relationships were generated following the LEVERETT approach. The simulation was then carried out with the heterogeneous K and $P_c(S_w)$ fields. The resulting outflow curves of the the isotropic and vertical case differ only slightly (see Fig. A.10, right). The cumulative outflow of the horizontal case is slightly retarded from on the third step. Also, the system has not attained equilibrium at the end of a step from on the fifth pressure step. The reason for this behaviour might be found in the spatial distribution (see Fig. A.9, middle). In the upper part of the domain a large area of high intrinsic permeability can be detected. As gravity is included in the simulation, the upper part of the domain is drained earlier than the lower part in case a single $P_c(S_w)$ relationship is applied. Here, additionally the large K values effect a smaller capillary pressure at a given saturation compared to the reference $P_c(S_w)$ relationship. Thus, these areas drained quickly which reduces the effective permeability. Together with the smaller intrinsic permeabilities in the lower part of the domain the average effective permeability of the domain becomes smaller compared to the other cases. Consequently, the effect on the outflow curve is caused by the interplay with gravity and the ratio of correlation length to domain length.
However, none of the outflow curves from the random fields exhibited the typical outflow behaviour measured in the laboratory, which show a high initial outflow followed by a slow approach to equilibrium between applied pressure and the saturation distribution. The flattening of the curve for the various pressure steps might also be attained by a parameter variation as described earlier in this appendix.
In summary, it may be stated that a continuous distribution of heterogeneity does not result in the desired effect in the cumulative outflow behaviour. The applied spatially correlated random fields were generated for a unimodal distribution of lnK. In a second approach a bimodal distribution is tested for its ability to effect the observed outflow behaviour. This procedure is followed despite the fact that for the natural soil column a bimodal distribution could not be identified while the column experiment showed the outflow behaviour of initially high outflow followed by a slow transition to equilibrium. It is thus assumed here, that in order to effect a tailing

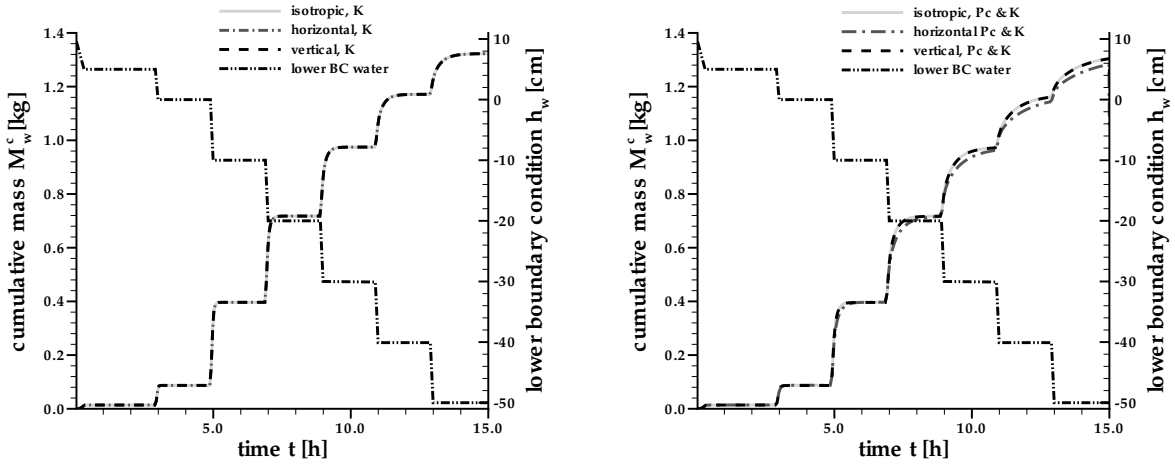

Figure A.10: Cumulative outflow over time for the random fields, using distribution of K only (left) and using distribution of K and $P_c(S_w)$ relationships (right)

in the outflow a clear bimodal distribution would be required. However, the plot of the distribution does not reveal if within a soil there might be a clustering of the different permeability values which might result in coarse and fine areas within a sample.
The bimodal distribution can be seen in analogy to fracture-matrix systems which can be modelled with a double-continuum approach. In order to obtain a bimodal field first an indicator field $i(\mathbf{x})$ with a mean of zero and given correlation lengths was generated. From the indicator field a binary field is deduced after

$$I(\mathbf{x}) = \begin{cases} 0 & \text{if} \quad i(\mathbf{x}) \leq 0 \\ 1 & \text{if} \quad i(\mathbf{x}) > 0\,. \end{cases} \tag{A.4}$$

Subsequently two independent spatially correlated random fields „coarse“ and „fine“ were generated following the approach described above for the unimodal fields. Then the entries of the indicator field were overwritten as

$$\ln K(\mathbf{x}) = \begin{cases} \ln K(\mathbf{x}) \subset \text{coarse} & \text{if} \quad I(\mathbf{x}) = 1 \\ \ln K(\mathbf{x}) \subset \text{fine} & \text{if} \quad I(\mathbf{x}) = 0\,. \end{cases} \tag{A.5}$$

The parameter of the fields are listed in Tab. A.3, the generated fields of the intermediate steps are plotted in Figs. A.11 to A.13. The resulting fields (see Fig. A.14) possess a bimodal distribution of the $\ln K$ values (see Fig. A.15).
An upscaling procedure to obtain effective parameters for the fields is not attempted here. In the first step, only the heterogeneous distribution of intrinsic permeability is applied. The resulting outflow curves do not show a dependence on the anisotropy of the field (see Fig. A.16, left). Moreover, the expected tailing of the cumulative outflow curves is also not observed.

Table A.3: Geostatistical parameters for the generation of the bimodal permeability fields, with star marked values denote the average and mean that were calculated despite the bimodal distribution

	mean μ	variance s^2	a_h	a_v
permeability field, coarse	-24.0	1.0	0.05 m	0.05 m
permeability field, fine	-28.0	1.0	0.05 m	0.05 m
indicator field, vertical	0.0	0.5	0.01 m	0.03 m
indicator field, horizontal	0.0	0.5	0.03 m	0.01 m
bimodal permeability field*, „bimodal vertical“	-25.99	3.81		
bimodal permeability field*, „bimodal horizontal“	-26.0429	4.10		

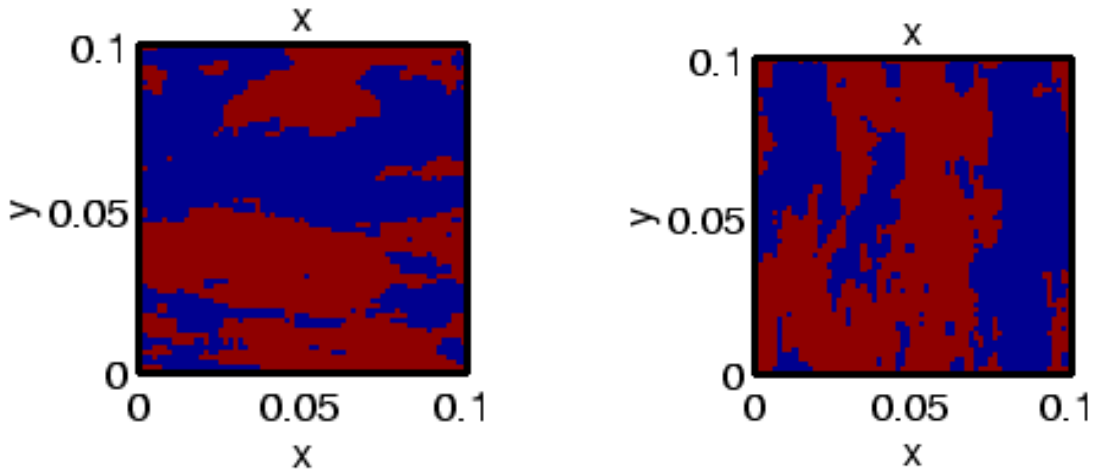

Figure A.11: Indicator random fields: horizontal (left) and vertical (right)

In the second step also the $P_c(S_w)$ relationship was considered as heterogeneous applying the LEVERETT scaling as given in Eqn. A.3. As the final field did not possess the information any longer whether it was derived from the fine or the coarse random field, the average permeability is based on the average of the bimodal field. As these values differ (see Tab. A.3), the two bimodal cases cannot be compared quantitatively. The simulation of the field 'bimodal horizontal' showed problems in the time stepping behaviour. Convergence could only be reached for small time steps of less than a 10^{-5} s, the simulation was thus stopped at $t \sim 5$ h. The cumulative outflow behaviour over time of the 'bimodal horizontal' case until $t \sim 5$ h and the one from the 'bimodal vertical' case do not show a pronounced influence on the flow behaviour from the additional inclusion of the $P_c(S_w)$ field (see Fig. A.16, right). The attained magnitude after a pressure step differs to the case where only the intrinsic permeability distribution is considered. However, the expected tailing again is not observable.

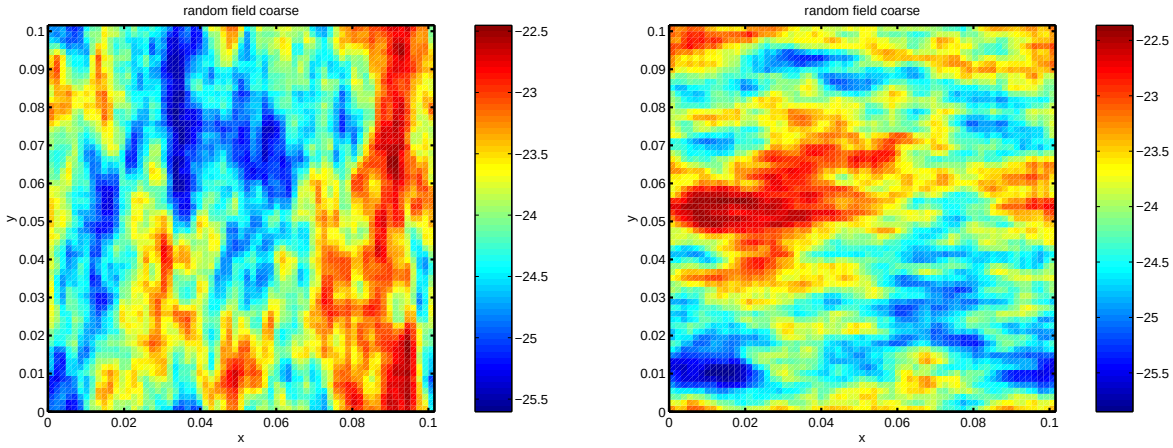

Figure A.12: Spatially correlated random fields: „horizontal coarse“ (left) and „vertical coarse“ (right)

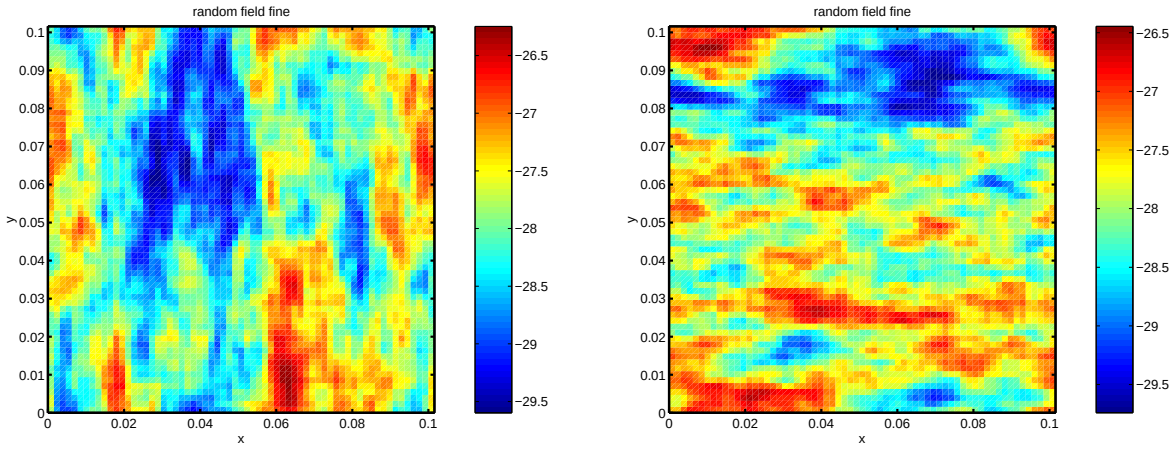

Figure A.13: Spatially correlated random fields: „horizontal fine“ (left) and „vertical fine“ (right)

SIMUNEK ET AL., 2001 [105] applied a double porosity approach to capture relaxation processes. LEWANDOWSKA ET AL., 2004 [75] used homogenisation theory for a double porosity approach and were able to reproduce relaxation effects, there denoted 'tailing' with the upscaled model. A similar kind of tailing could not be reproduced with the here chosen approach and parameter combination. LEWANDOWSKA ET AL., 2004 defined the ratio of the characteristic dimensionless hydraulic diffusivities (the ratio of dimensionless hydraulic conductivity to the specific water capacity) of the fine to the coarse material of the double porosity medium. In order to see a tailing effect, this ratio needs to be of the order of magnitude of ε^2. The scale separation parameter ε is defined as $\varepsilon = {}^{l}/_{L}$, where l is the length scale of the heterogeneity and L is the system length. In general, ε needs to be small, in order to apply the homogenisation approach.

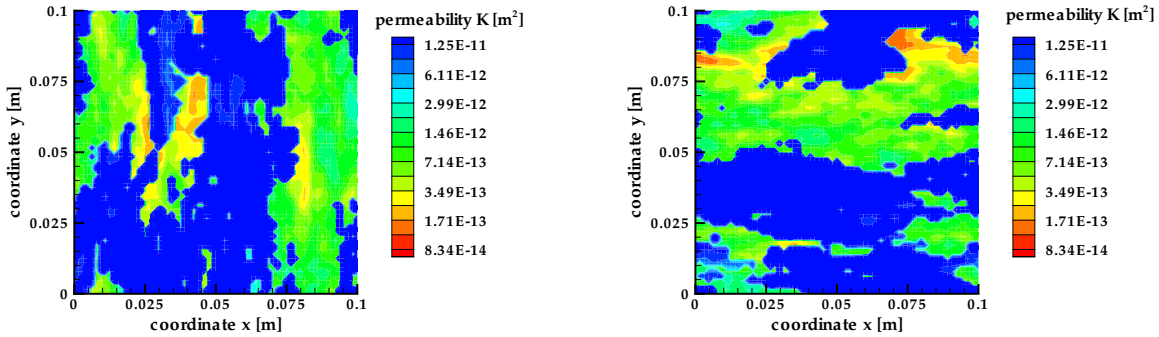

Figure A.14: Bimodal spatially correlated random fields, with vertically (left) and horizontally (right) oriented anisotropy

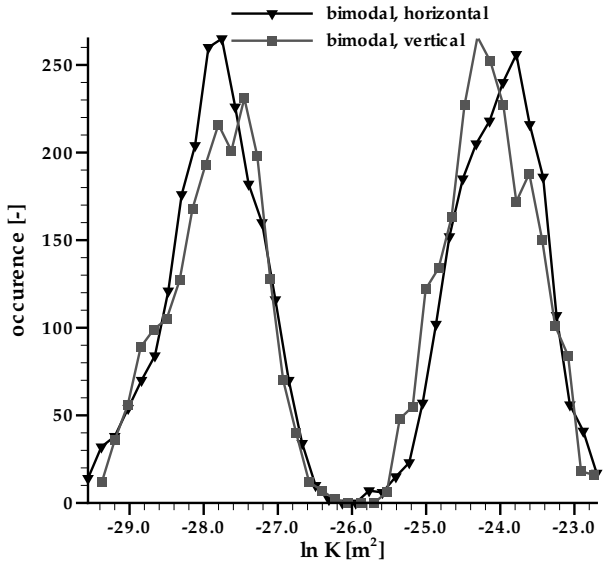

Figure A.15: Discrete frequency distribution of $\ln K$ for the fields „bimodal vertical“ and „bimodal horizontal“

Here, neither a clear scale separation was attempted nor were the parameters chosen to fulfil the requirements found by LEWANDOWSKA ET AL., 2004. If the correlation length is inserted as the small-scale length l and the domain dimension for the system length, ε can be computed for the presented bimodal fields. For a correlation length of $a = 0.01\,\mathrm{m}$ a scale separation might be assumed to hold for a domain of 0.1 m length, but not for one of $a = 0.03\,\mathrm{m}$. The parameters of the refer-

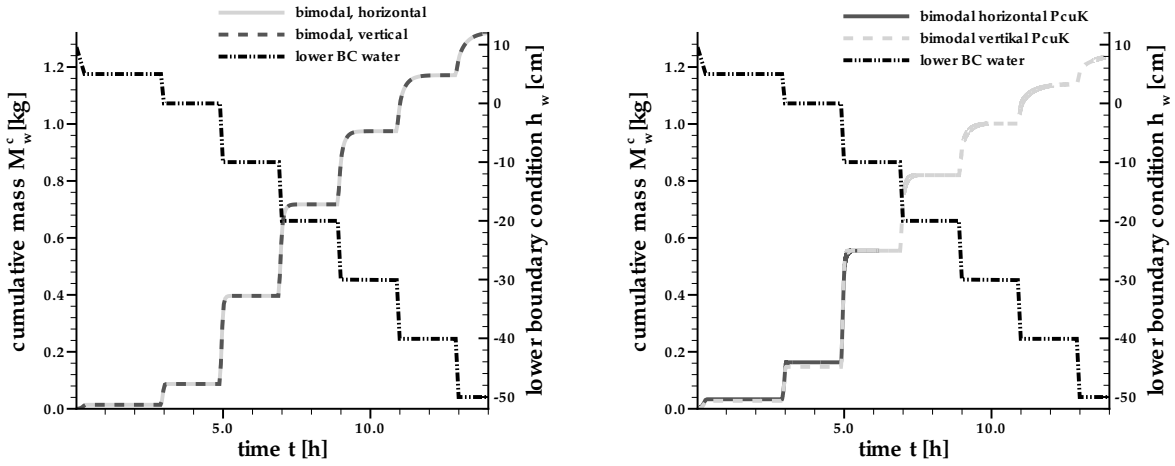

Figure A.16: Cumulative outflow for bimodal distributions, for heterogeneity in intrinsic permeability only (left) and for in heterogeneity in intrinsic permeability and the $P_c(S_w)$ relationship (right)

ence $P_c(S_w)$ relationship (from which the specific water capacity might be derived) follow the ones determined for the natural soil column.
In the following, the above described findings are summarised.

- The inclusion of heterogeneity on the local scale did not result in a relaxation behaviour as observed in certain outflow steps in a laboratory measurement. Neither the information gained from computer tomography nor the generated random fields could clearly effect simulations in the desired direction.

- According to LEWANDOWSKA ET AL., 2004 the ratio of the dimensionless hydraulic diffusivities needs to be of a given order to obtain a relaxation process. Obviously, many assumptions about the porous medium enter into the homogenisation approach chosen by them that were not fulfilled in the simulations presented here. However, the simulations were based on parameters determined for the soil column. If the relaxation behaviour cannot be reproduced with the underlying model applying these parameters while accounting for local-scale heterogeneity, pore-scale processes, not captured by the underlying model, suggest themselves as a cause for the observed relaxation behaviour. As a consequence, the physical-mathematical model needs to be analysed with a view to short-comings.

Review of the model concepts and assumptions

The analysis of the difference between measurement and simulation for each measurement has shown that deviations between measurement and simulation were

not distributed randomly but showed a local and a global trend. Trends may indicate that the physical-mathematical model is built on assumptions that do not apply in the considered case. Also, the simulations using local-scale heterogeneities did not effect the observed outflow behaviour, also suggesting shortcomings in the physical-mathematical model. Thus, the assumptions underlying DARCY's law and the constitutive relationships will be shortly summarised in the following.
The flow velocity in the balance equation for a fluid in a two-phase system for the local and higher scales is described by the extended DARCY's law (see Sec. 2.3.2). The following assumptions need to be made to apply this law.

- Any inertial terms may be neglected as only slow flow velocities occur. Calculation of the REYNOLDS number given in Eqn. (2.26) for the above described examples showed that it always remained less than four. The linearity of DARCY's law should hold within this range of REYNOLDS numbers. Neglecting inertial terms is justified because laminar flow dominates.

- It is common practice to neglect the coupling effects due to viscous shear stresses between two fluids. WHITAKER, 1986A, 1986B [127, 128] postulates that the disregard of these coupling terms is especially justified for water-gas systems with a high difference in the dynamic viscosities. BENTSEN, 1994 [14] proved experimentally that neglecting the coupling term only leads to very small errors. Consequently, disregarding the coupling term is assumed to be justified.

- Gravity is the only body force and acts only in the vertical direction.

- The viscous shear stresses within one fluid can be described by NEWTON's law. The fluids applied in this study, water and gas, both behave as Newtonian fluids.

- At the boundary between a fluid and the solid matrix a no-slip condition holds.

Whether the last requirement is fulfilled in the flow processes observed in the laboratory, cannot be answered in the frame of this study as simulations on the pore scale are necessary to assess the influence of slip as opposed to no-slip conditions. Apart from the last aspect the assumptions to allow an application of DARCY's are fulfilled. It should be noted however, that all of these assumptions except the second one already apply for single phase flow and thus do not account for the additional problems encountered in two-phase flow. The interaction of the two fluids with each other and the porous matrix are captured by the constitutive relationships, namely the capillary pressure-saturation relationship and the relative permeability-saturation relationships. The conservation equations for the two fluid phases are coupled through these constitutive relationships. It is common practice to apply a parametrisation for these relationships and to calculate the relative permeabilities using the $P_c(S_w)$ relationship parameters. Most often, the same parameters for the $k_{rw}(S_w)$ as for the $k_{rn}(S_n)$ relationship are used. The parameter variation

has shown, that it is advisable to treat the parameters of the $k_{r\alpha}(S_\alpha)$ relationships independently. Furthermore, it is assumed for the constitutive relationships, that they are determined under static or steady-state conditions. Strictly speaking, they should also only be applied to describe such conditions. Nevertheless, they are commonly applied to simulate transient processes. Laboratory and theoretical studies questioning the uniqueness of the $P_c(S_w)$ relationship under transient conditions are described in Sec. 3 of this study.
The presence of dynamic effects in the $P_c(S_w)$ relationship and resulting consequences for the simulation of multi-step outflow experiments cannot be precluded. For a water-DNAPL fluid system O'CARROLL ET AL., 2005 [86] improved the performance of a simulation of a multi-step outflow experiment when they included an extended $P_c(S_w)$ relationship as opposed to a traditional, unique one.
However, the attempt to simulate the multi-step outflow experiment using the implementation of the extended $P_c(S_w)$ outlined in Sec. 4.3 did not effect the desired results. Depending on the magnitude of the coefficient τ or the $\tau(S_e)$ function the cumulative outflow of the wetting phase shows an overshoot at the initial pressure step(s). The occurrence of the overshoot seems to be related to the occurrence of fully water saturated parts in the column. The overshoot also occurred if a quadratic $\tau(Se)$ function was used that diminishes to zero at $S_w = 1.0$.
In Sec. 6.4 it was shown that oscillations occurred for certain magnitudes of the dimensionless numbers Dy and DyC and a high viscosity ratio. It is assumed here, that a similar effect occurs. Due to personal communication with A. Weiss, Stuttgart it is furthermore assumed that a dampening of the flow process cannot be expected for all combinations of porous media parameters, values of the coefficient τ and viscosity ratios. Further investigations on the behaviour of the balance equations being closed by the extended $P_c(S_w)$ relationship are necessary.

B Laboratory experiments from GeoDelft, The Netherlands

GeoDelft, Delft, The Netherlands carried out laboratory experiments to examine the influence of dynamic effects in the capillary pressure-saturation relationship. Following the see Eqn. (3.13) required data is the equilibrium $P_c^e(S_w)$ relationship, at least one dynamic $P_c^d(S_w)$ relationship and pertaining to that the rate of change of saturation. In the following the approach taken by GeoDelft to determine these data is described because the results are applied in this thesis. The experiments are described to some extend in HASSANIZADEH ET AL., 2005 [57] and MANTHEY ET AL., 2004 [78]. Although GeoDelft performed a full cycle of primary drainage, main imbibition and main drainage experiments, here the focus is on the primary drainage $P_c(S_w)$ relationships.

Experimental set-up and measurements

Experimental set-up The experimental set-up consists of three parts from top to bottom: the upper chamber, the sand sample chamber, and the lower chamber (see Fig. B.1). The upper chamber consists of an air chamber and the reservoir of the non-wetting fluid, here Perchlorethylen (PCE). The pressure of the PCE in the upper reservoir is adjusted via the pressurised air. The upper reservoir can contain 170 ml of PCE, which is more than five times the pore volume of the sand of 32.3 ml, thus a complete drainage of the sample could be achieved. The lower chamber acts as a water (flow-through) reservoir. The water is then collected in the burette, where the height of the water table can be related to the water saturation in the sand sample.
The sand sample is placed in a cylindrical chamber, which has a height of $\Delta z = 0.03$ m and an innner diameter of $d = 0.06$ m. The sample is supported by two membrane filters, a hydrophobic membrane on the top and a hydrophilic lower membrane. These membranes prevent the infiltration of one fluid into the reservoir of the other. Both membranes need to be stabilised by holders possessing a height of $\Delta z = 0.01$ m. The properties of the membranes and their holders are listed in Tab. 5.3 in Sec. 5.4.1. On top of the upper filter a weight is placed by means of a rod. Thus the matrix of the packed sand is stabilised.

Measurements OUONG & BEZUIJEN, 2003 [88] give a detailed description of the selective pore pressure transducers applied in the experiements. These pressure transducers are installed at opposing sides at middle-height of the sand column.

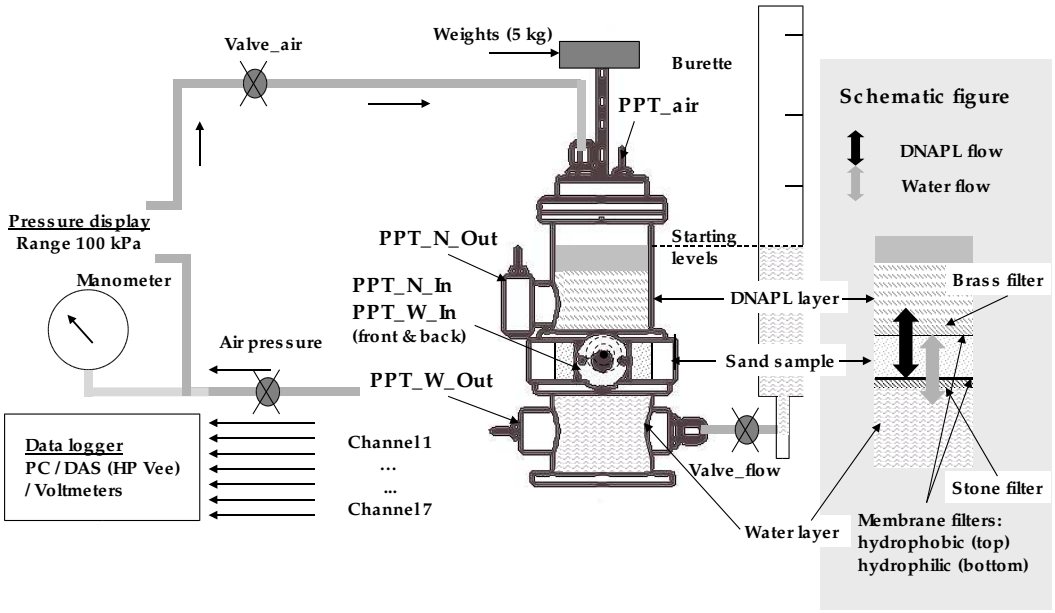

Figure B.1: Schematic representation of the experimental set-up as used by GeoDelft laboratories [78]

They measure the phase pressure of the water or the PCE pressure in the sand sample during the experiments. The hydrophilic pore pressure transducer (indicated by 'PPT_W_IN' in Figure B.1) measures the pressure of the water phase P_w within the sample and the hydrophobic pore pressure transducer ('PPT_N_IN' in Figure B.1) monitors the pressure P_n of the non-wetting phase. For both the measurements the phase needs to be continuous to be representative. From the difference between P_n and P_w the capillary pressure within the sand sample can be derived assuming that the flow processes in the sample are mainly one-dimensional. It is assumed that both phase pressures are measured for a finite area, thus the capillary pressure is denoted local capillary pressure $P_c(\mathbf{x})$. Furthermore, pressure gauges in the lower and upper reservoir ('PPT_W_OUT' and 'PPT_N_OUT'in Figure B.1) monitor the phase pressures outside the sand column. All pressure measurements are performed continuously in each of the experiments.

The volume of water flowing out of the sand sample is derived from two measurements. On the one hand, the water level in the burette indicates the water volume that has left the sample. On the other hand, the outflowing water volume can be deduced from the water pressure in the water reservoir ('PPT_W_IN'). The burette measurement is mainly applied as reference value to deduce the water volume from the pressure measurements. In contrast to the pressure measurements, the saturation can only be deduced as an average over the whole sample.

Properties of the sand sample and the membranes

The experimentally determined values for the intrinsic permeability K and the porosity ϕ are listed in Tab. 5.3. In addition the properties of the membranes are given as they are applied in the simulation of the dynamic experiment described in Sec. 5.4.1. Porosity values for the membranes and membrane holders are taken from the manufacturer's data. Because the membranes are only $\Delta z = 4.5 \cdot 10^{-7}\,\mathrm{m}$ high, their intrinsic permeability could only be determined together with the membrane holders. The coarse filter supporting the lower membrane and its holder is neglected because of its high permeability of $K > 1.0 \cdot 10^{-8}\,\mathrm{m}^2$. For the BROOKS & COREY parameters of the $P_c(S_w)$ relationships of the membranes reasonable values are assumed for the numerical simulations (see Sec. 5.4.1).

Initial and boundary conditions

All laboratory experiments were carried out under isothermal conditions at 20°C. Initially, the sand sample is fully saturated with water to facilitate primary drainage experiments. Two kinds of primary drainage experiments were carried out. In the equilibrium experiment the equilibrium $P_c^e(S_w)$ relationship is determined for quasi-static states, and in the dynamic experiments the dynamic $P_c^d(S_w)$ is measured during transient flow processes.

Equilibrium $P_c^e(S_w)$ To determine the equilibrium primary drainage $P_c(S_w)$ the capillary pressure is increased stepwise by raising the air and thus the PCE pressure in the upper reservoir. This induces the non-wetting phase to infiltrate into the sand sample once the entry pressure of the sand is overcome. Before the next increase of non-wetting phase pressure, an equilibrium criterion needs to be matched, that is to say the water saturation should not change by more than $0.05\,\mathrm{ml/h}$. The then measured local phase pressure difference and the average water saturation yield one data pair for the equilibrium $P_c^e(S_w)$ relationship. This procedure is repeated until a given maximum non-wetting phase pressure is reached. All data pairs then yield the equilibrium $P_c^e(S_w)$ relationship (see Figure 5.8).

Dynamic $P_c^d(S_w)$ Furthermore, dynamic primary drainage experiments were performed, where the PCE pressure is increased to a large value in one step. In the primary drainage experiments presented here the pressure of the non-wetting phase in the upper reservoir P_n^T was increased to 16 kPa, 20 kPa, and 25 kPa within xx seconds. Continuous measurement of the phase pressures and the water saturation then yields dynamic primary drainage $P_c^d(S_w)$ relationships (see Figure 5.8).
The analysis of the experimental results with a view to determining the material coefficient τ after HASSANIZADEH & GRAY, 1993 is described in Sec. 5.3.

C Additional figures related to Chapter 5

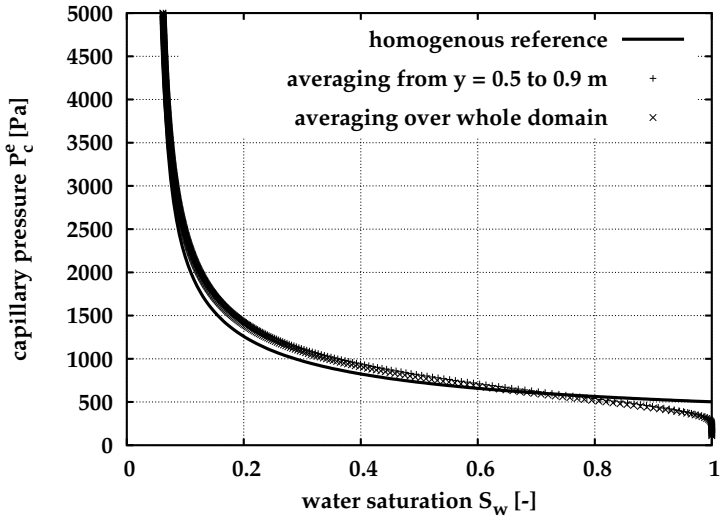

Figure C.1: Equilibrium $P_c^e(S_w)$ for the spatially correlated random field

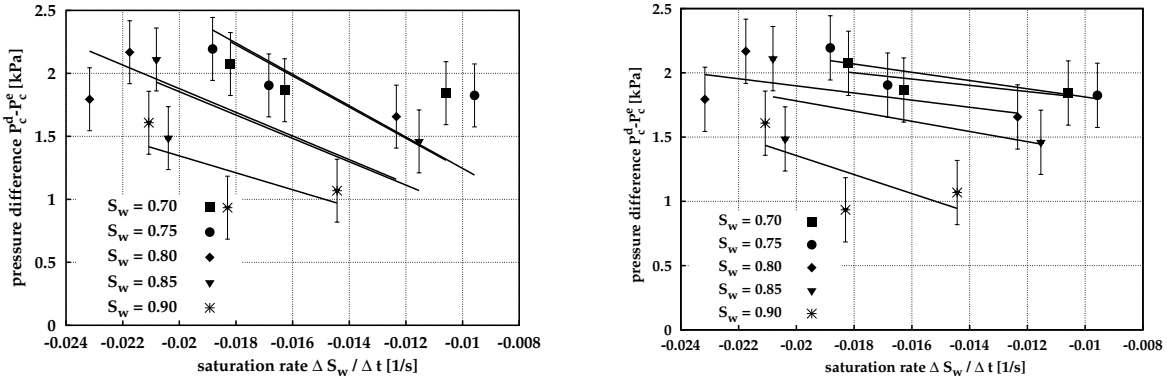

Figure C.2: Plot of $\Delta P_c(^{\Delta S_w}/_{\Delta t})$ at various water saturations and linear regressions for case 1 for τ_0 (left) and τ_b (right)

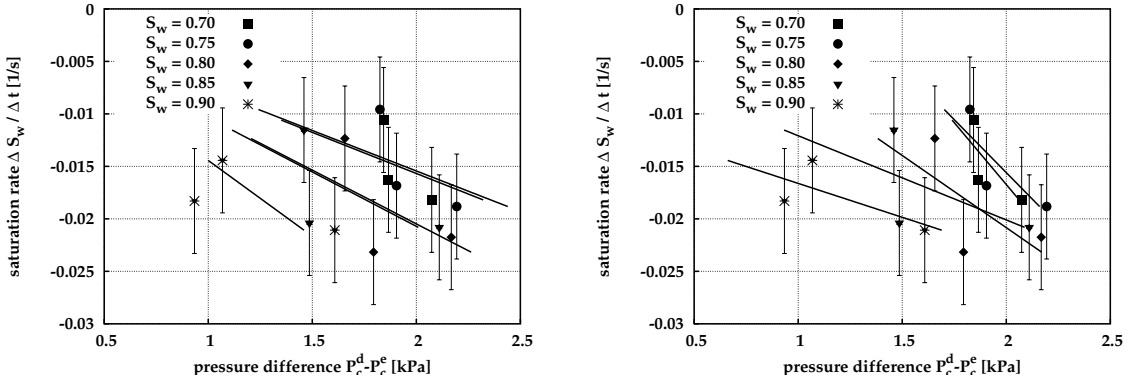

Figure C.3: Plot of $^{\Delta S_w}/_{\Delta t}(\Delta P_c)$ at various water saturations and linear regressions for case 2 for τ_0 (left) and τ_b (right)

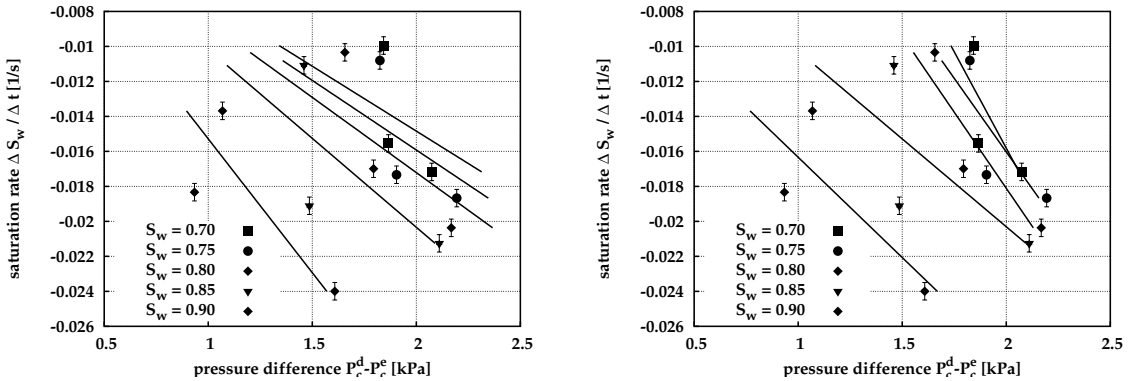

Figure C.4: Plot of $^{\Delta S_w}/_{\Delta t}(\Delta P_c)$ (smoothed $^{\Delta S_w}/_{\Delta t}$) at various water saturations and linear regressions for case 3 for τ_0 (left) and τ_b (right)

Table C.1: Values of τ and b for selected water saturations gained from regression with Eqn. (5.14) and from regression with Eqn. (3.13), confidence intervalls for the τ values are plotted in Fig. 5.20

For $\Delta P_c(\frac{\Delta S_w}{\Delta t})$ allowing for error in ΔP_c of +/- 0.25 Pa					
S_w	b [kPa]	error b [+/- %]	τ_b [kPas]	τ_0 [kPas]	$\tau_0 - \tau_b$ [kPas]
0.70	1.56	20.6	24.33	123.72	99.39
0.75	1.49	24.77	32.11	124.51	92.40
0.80	1.34	51.8	27.78	93.93	66.15
0.85	0.99	106.2	39.65	92.73	53.08
0.90	−0.12	1153.	73.89	67.25	−6.64

For $\frac{\Delta S_w}{\Delta t}(\Delta P_c)$ allowing for error in $\frac{\Delta S_w}{\Delta t}$ of +/- 0.005 1/s					
S_w	b [kPa]	error b [+/- %]	τ_b [kPas]	τ_0 [kPas]	$\tau_0 - \tau_b$ [kPas]
0.70	1.29	43.12	42.41	127.58	85.17
0.75	1.23	45.89	49.56	129.57	80.01
0.80	0.48	368.4	72.72	97.68	24.96
0.85	−0.51	640.7	124.62	96.56	−28.06
0.90	−1.57	185.7	154.72	69.27	−85.45
For $\frac{\Delta S_w}{\Delta t}(\Delta P_c)$ allowing for error in smoothed $\frac{\Delta S_w}{\Delta t}$ of +/- 0.0005 1/s					
S_w	b [kPa]	error b [+/- %]	τ_b [kPas]	τ_0 [kPas]	$\tau_0 - \tau_b$ [kPas]
0.70	1.28	46.5	45.41	134.76	89.35
0.75	1.05	72.8	59.40	125.64	66.24
0.80	0.96	46.9	57.49	116.20	58.71
0.85	−0.02	8208.	99.58	98.33	−1.25
0.90	−0.43	299.7	87.28	65.41	−21.87

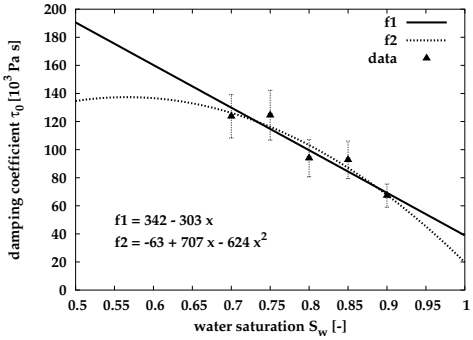

Figure C.5: Regressions to $\tau_0(S_w)$ (from regression to experimental data with Eqn.(3.13)) using functions of different order

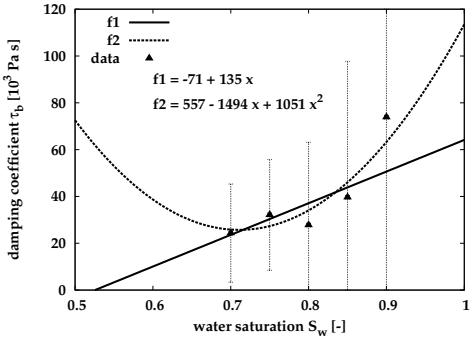

Figure C.6: Regressions to $\tau_b(S_w)$ (from regression to experimental data with Eqn. (5.14))

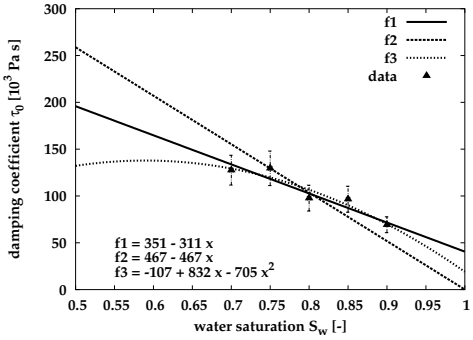

Figure C.7: Regressions to $\tau_0(S_w)$ (from regression to experimental data with the inverse of Eqn.(3.13)) using functions of different order

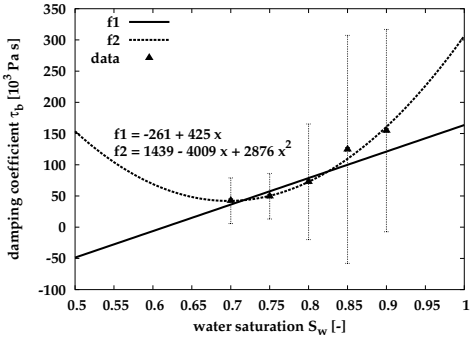

Figure C.8: Regressions to $\tau_b(S_w)$ (from regression to experimental data with the inverse of Eqn. (5.14))

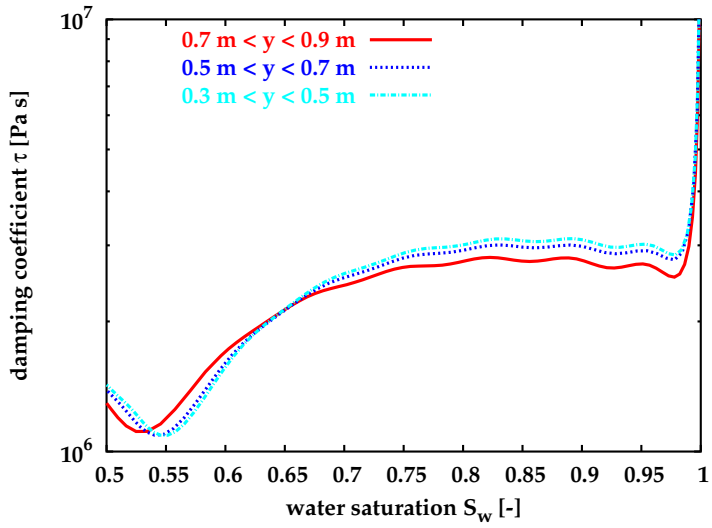

Figure C.9: $\tau(S_w)$ for different averaging locations for the homogeneous reference sand

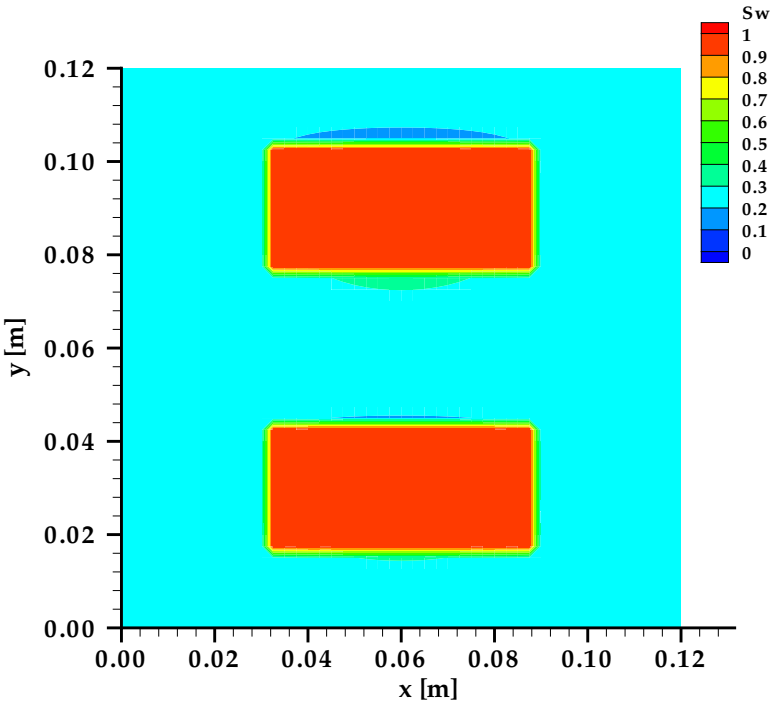

Figure C.10: Distribution of wetting phase at $P_c^B = 607\,\text{Pa}$

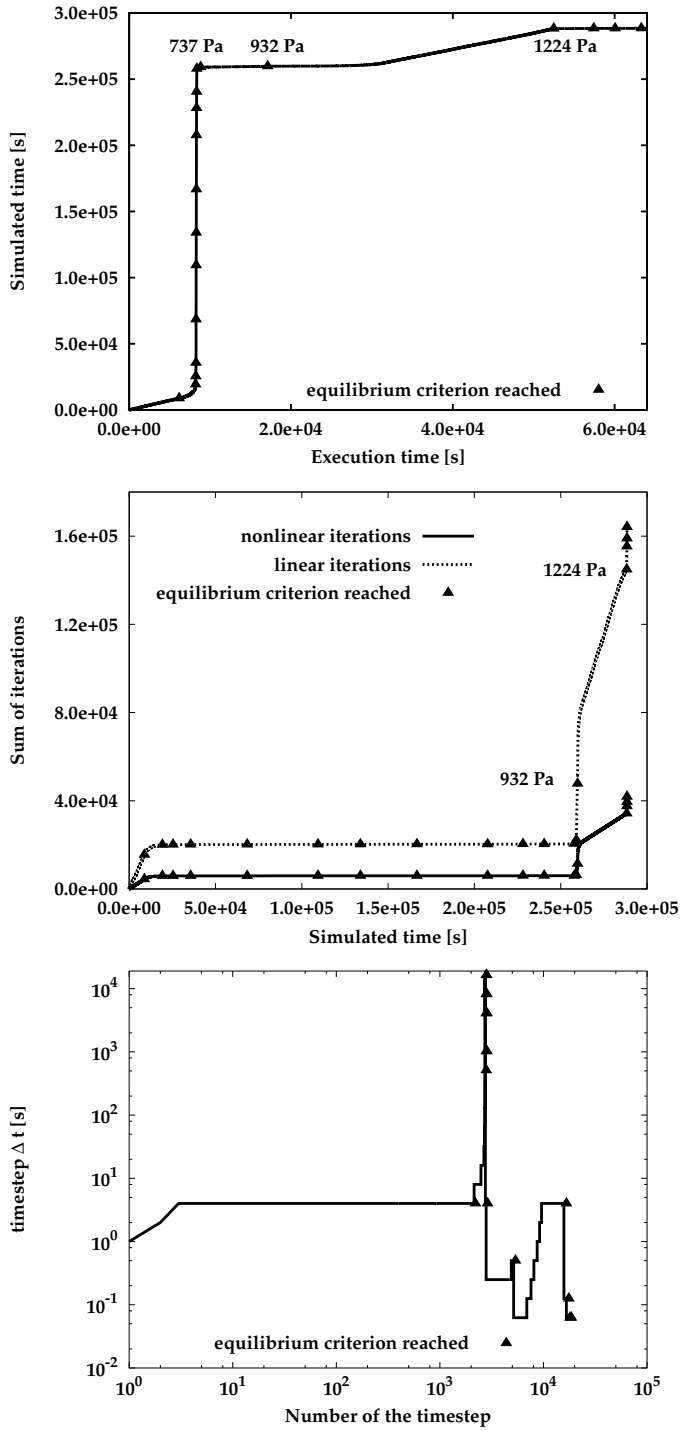

Figure C.11: Execution to simulated time, number of linear and non-linear iterations and the time step size for the numerical drainage experiment applying $\varepsilon_S = 10^{-6}$ & $\varepsilon_P = 10^{-2}$ Pa as the equilibrium criteria

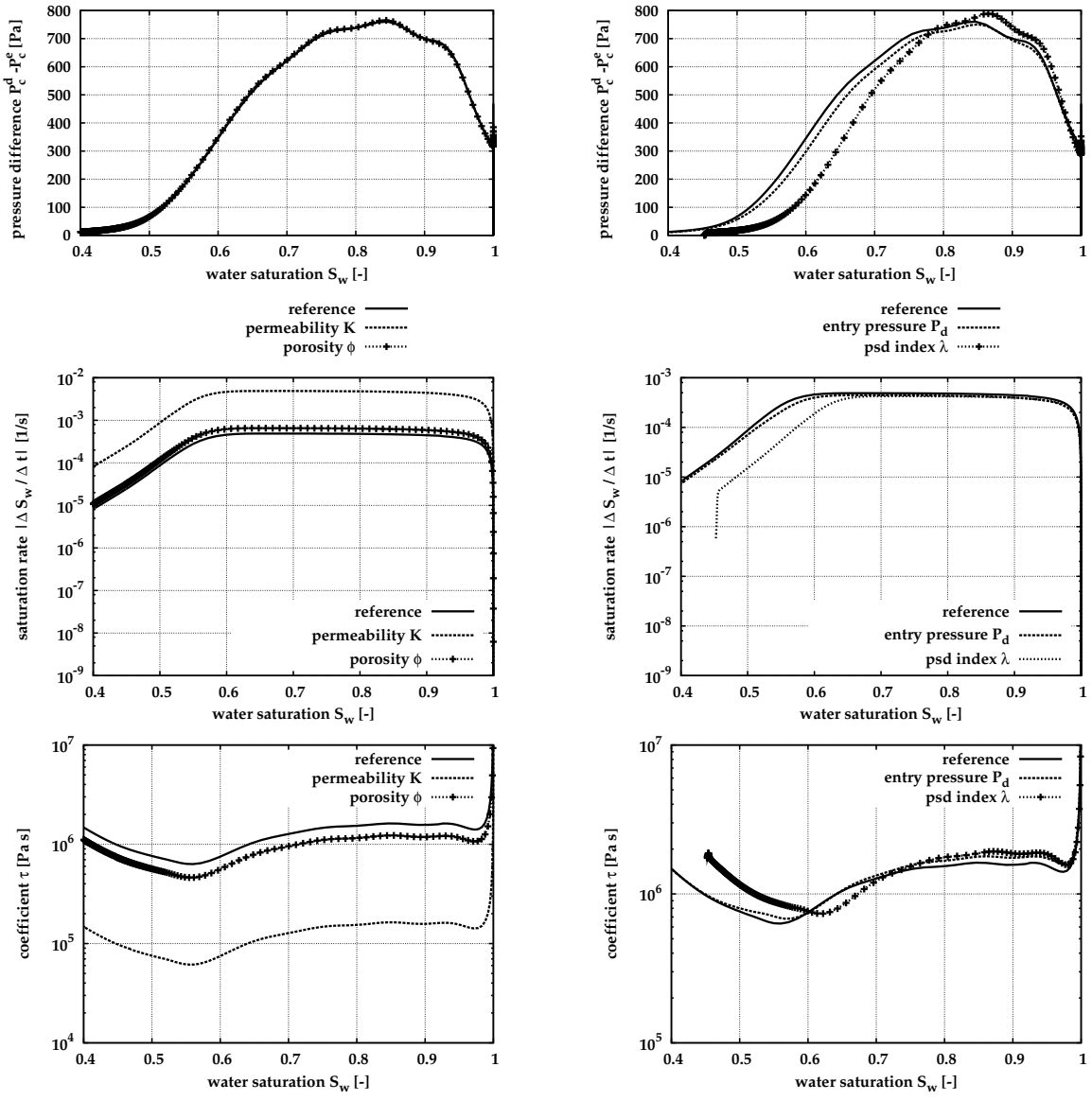

Figure C.12: Results for the parameter variation for the homogeneous sand ($\Delta P_c(S_w)$, $\Delta S_w/\Delta t(S_w)$ and $\tau(S_w)$)

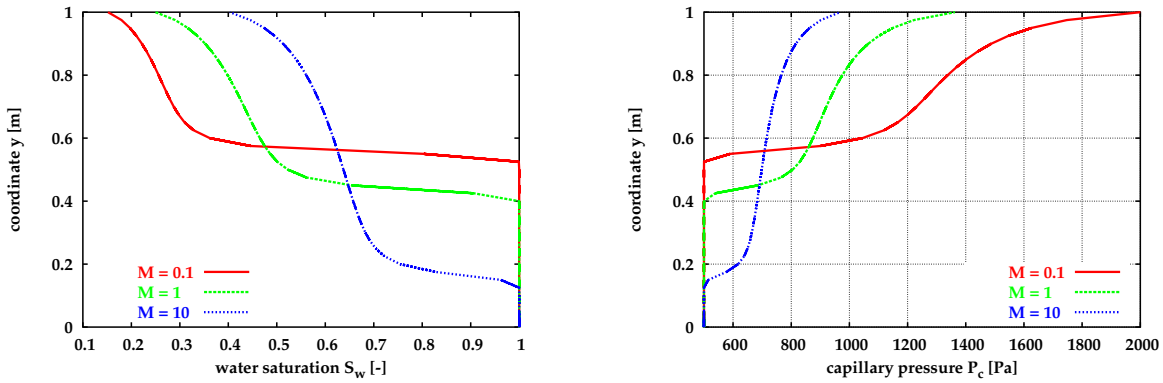

Figure C.13: $S_w(y)$ (left) and $P_c(y)$ (right) for different viscosity ratios (for M = 1: $\mu = 0.001\,\mathrm{Pa\,s}$)

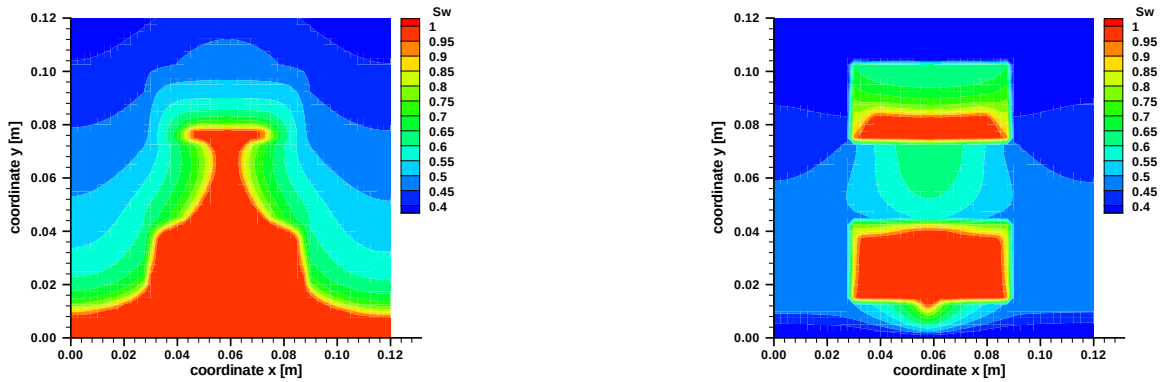

Figure C.14: Wetting phase saturation for simple heterogeneity example varying permeability (left, $t = 100\,\mathrm{s}$) and varying permeability plus entry pressure (right, $t = 150\,\mathrm{s}$)

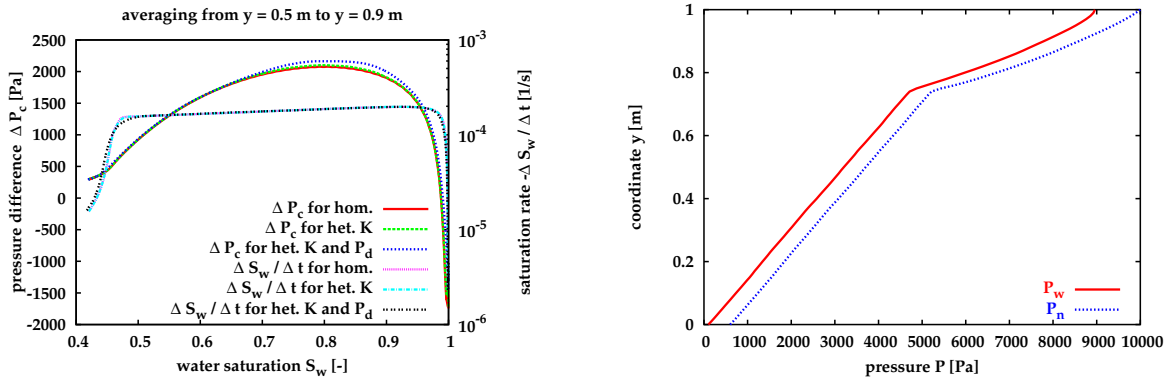

Figure C.15: $\Delta P_c(S_w)$ and $^{\Delta S_w}/_{\Delta t}(S_w)$ (left) and $P_n(y)$ as well as $P_w(y)$ at $t = 1500\,\mathrm{s}$ (right) for the spatially correlated random field